November 19, 2019 Docket No. PROJ0769

U.S. Nuclear Regulatory Commission
ATTN: Document Control Desk
One White Flint North
11555 Rockville Pike
Rockville, MD 20852-2738

SUBJECT: NuScale Power, LLC Submittal of "Improvements in Frequency Domain Soil-Structure-Fluid Interaction Analysis," TR-0118-58005, Revision 1

REFERENCES:
1. Letter from NuScale Power, LLC to the Nuclear Regulatory Commission, "NuScale Power, LLC Submittal of 'Improvements in Frequency Domain Soil-Structure-Fluid Interactions Analysis' Topical Report,TR-0118-58005, Revision 0," dated July 26, 2018 (ML18208A362)
2. U.S. Nuclear Regulatory Commission, "Request for Additional Information no. 9676 (eRAI No. 9676), dated April 17, 2019 (ML19107A498)
3. NuScale Power, LLC Response to NRC "Request for Additional Information No. 9676 (eRAI No. 9676), dated June 17, 2019 (ML19168A249)

NuScale Power, LLC (NuScale) hereby submits Revision 1 of the "Improvements in Frequency Domain Soil-Structure-Fluid Interactions Analysis," topical report (TR-0118-58005). The initial issue of this topical report was submitted for Nuclear Regulatory Commission review by Reference 1. Request for Additional Information (RAI) 9676 (Reference 2) was responded to via Reference 3. This submittal of Revision 1 incorporates the RAI 9676 responses and additional review requested clarifications. The purpose of this submittal is to request that the NRC continue its review and approval of the frequency domain soil-structure-fluid interaction seismic analysis methodology using the Soil Library concept.

Enclosure 1 contains the proprietary version of the report titled "Improvements in Frequency Domain Soil-Structure-Fluid Interaction Analysis." NuScale requests that the proprietary version be withheld from public disclosure in accordance with the requirements of 10 CFR § 2.390. The enclosed affidavit (Enclosure 3) supports this request. Enclosure 2 contains the nonproprietary version of the report.

This letter makes no regulatory commitments and no revisions to any existing regulatory commitments.

If you have any questions, please feel free to contact Marty Bryan at 541-457-7172 or at mbryan@nuscalepower.com if you have any questions.

Sincerely,

Zackary W. Rad
Director, Regulatory Affairs
NuScale Power, LLC

Distribution: Samuel Lee, NRC, OWFN-8H12
Gregory Cranston, NRC, OWFN-8H12
Michael Dudek, NRC, OWFN-8H12
William Ward, NRC, OWFN-8G9A

Enclosure 1: “Improvements in Frequency Domain Soil-Structure-Fluid Interaction Analysis,” TR-0118-58005-P, Revision 1, proprietary version
Enclosure 2: “Improvements in Frequency Domain Soil-Structure-Fluid Interaction Analysis,” TR-0118-58005-NP, nonproprietary version
Enclosure 3: Affidavit of Zackary W. Rad, AF-1119-67982

Enclosure 1:

"Improvements in Frequency Domain Soil-Structure-Fluid Interaction Analysis," TR-0118-58005-P, Revision 1, proprietary version

NuScale Power, LLC
1100 NE Circle Blvd., Suite 200 Corvallis, Oregon 97330 Office 541.360-0500 Fax 541.207.3928
www.nuscalepower.com

Enclosure 2:

"Improvements in Frequency Domain Soil-Structure-Fluid Interaction Analysis," TR-0118-58005-NP, Revision 1, nonproprietary version

Licensing Topical Report

Improvements in Frequency Domain Soil-Structure-Fluid Interaction Analysis

November 2019

Revision 1

Docket: PROJ0769

NuScale Power, LLC

1100 NE Circle Blvd., Suite 200

Corvallis, Oregon 97330

www.nuscalepower.com

© Copyright 2019 by NuScale Power, LLC

© Copyright 2019 by NuScale Power, LLC

Licensing Topical Report

COPYRIGHT NOTICE

This report has been prepared by NuScale Power, LLC and bears a NuScale Power, LLC, copyright notice. No right to disclose, use, or copy any of the information in this report, other than by the U.S. Nuclear Regulatory Commission (NRC), is authorized without the express, written permission of NuScale Power, LLC.

The NRC is permitted to make the number of copies of the information contained in this report that is necessary for its internal use in connection with generic and plant-specific reviews and approvals, as well as the issuance, denial, amendment, transfer, renewal, modification, suspension, revocation, or violation of a license, permit, order, or regulation subject to the requirements of 10 CFR 2.390 regarding restrictions on public disclosure to the extent such information has been identified as proprietary by NuScale Power, LLC, copyright protection notwithstanding. Regarding nonproprietary versions of these reports, the NRC is permitted to make the number of copies necessary for public viewing in appropriate docket files in public document rooms in Washington, DC, and elsewhere as may be required by NRC regulations. Copies made by the NRC must include this copyright notice and contain the proprietary marking if the original was identified as proprietary.

Department of Energy Acknowledgement and Disclaimer

This material is based upon work supported by the Department of Energy under Award Number DE-NE0008820.

This report was prepared as an account of work sponsored by an agency of the United States Government. Neither the United States Government nor any agency thereof, nor any of their employees, makes any warranty, express or implied, or assumes any legal liability or responsibility for the accuracy, completeness, or usefulness of any information, apparatus, product, or process disclosed, or represents that its use would not infringe privately owned rights. Reference herein to any specific commercial product, process, or service by trade name, trademark, manufacturer, or otherwise does not necessarily constitute or imply its endorsement, recommendation, or favoring by the United States Government or any agency thereof. The views and opinions of authors expressed herein do not necessarily state or reflect those of the United States Government or any agency thereof.

© Copyright 2019 by NuScale Power, LLC

CONTENTS

Abstract **1**

Executive Summary of Topical Report TR-0118-58005 ..... **2**

1.0 Introduction **4**

1.1 Purpose 4

1.2 Scope 4

1.3 Abbreviations and Definitions 5

2.0 Background **8**

2.1 Regulatory Requirements 9

3.0 Assumptions and Software **10**

3.1 Assumptions 10

3.2 Software 10

4.0 Solution Strategy **11**

4.1 Substructuring 11

4.2 Frequency Domain Solution 12

4.3 Soil Library 12

4.4 Analysis Tools 12

5.0 Theoretical Basis **23**

5.1 Analysis Background 23

5.2 Soil Library 34

5.3 SASSI Enhancements 37

6.0 Demonstation Problems **41**

6.1 Example 1: Surface Reactor Problem from SASSI User's Manual 41

6.2 Example 2: Embedded Building with Soil-Structure Interaction 54

6.3 Example 3: Embedded Building with Soil-Structure-Fluid Interaction 81

6.4 Representative Reactor Building with Soil-Structure-Fluid Interaction 106

7.0 Soil Library Implementation **130**

7.1 Soil Library Organization 130

7.2 Reduced Impedance and Load Vectors 132

8.0 Summary and Conclusions **133**

9.0 References **134**

© Copyright 2019 by NuScale Power, LLC

9.1 Referenced Documents 134
Appendix A. Response of a Single Degree of Freedom System with Base Motion 137
Appendix B. Effect of Mass Formulations on Response 145
Appendix C. Structural Meshing for High Frequency Response 149
Appendix D. Influence of Halfspace Depth 155
Appendix E. Example 2, SASSI vs ANSYS Results 164
Appendix F. Example 3, SASSI vs ANSYS Results 180
Appendix G. Fixed Base Response for Examples 2 and 3 220
Appendix H. SSI Response for Examples 2 and 3 227
Appendix I. Example 4, Acceleration Transfer Functions 243
Appendix J. Example 4, Acceleration Time Histories 340
Appendix K. Example 4, In-Structure Response Spectra 437
Appendix L. Example 4, Fluid Pressure Transfer Functions 534
Appendix M. Example 4, Fluid Pressure Time Histories 541
Appendix N. Example 4, Relative Displacement Transfer Functions 548
Appendix O. Example 4, Relative Displacement Time Histories 645
Appendix P. Example 4, RXM Lug Force Transfer Functions 742
Appendix Q. Example 4, RXM Lug Force Time Histories 749
Appendix R. Example 4, RXM Support Transfer Functions 756
Appendix S. Example 4, RXM Support Time Histories 769

© Copyright 2019 by NuScale Power, LLC

TABLES

Table 1-1 Abbreviations....5
Table 1-2 Definitions....6
Table 6-1 Frequencies, modal mass, and cumulative mass for Example 1....44
Table 6-2 Comparison of SASSI and ANSYS peak accelerations (g)....46
Table 6-3 Comparison of SASSI and ANSYS peak overturning moments (ft-kip)....46
Table 6-4 Example 2, low frequency lumped parameter impedance....58
Table 6-5 Frequencies, modal mass, and cumulative mass for Example 2....62
Table 6-6 Example 3 low frequency acoustic pressure....87
Table 6-7 Frequencies, modal mass, and cumulative mass for Example 3....89
Table 6-8 Analysis Frequency Numbers....109
Table 6-9 Nodes for Acceleration Comparisons....111
Table 6-10 Nodes for Fluid Pressure Comparisons....116
Table 6-11 RXM Lug Nodes....124
Table B-1 Soil column modes....145
Table C-1 Natural frequency (Hz)....150

FIGURES

Figure 4-1 Idealized soil, structure, and fluid Substructures....15
Figure 4-2 Reduced excavated soil impedance....16
Figure 4-3 Soil impedance library....17
Figure 4-4 SASSI solution for soil impedance and load vector at frequency *i*....18
Figure 4-5 ANSYS frequency domain solution....19
Figure 4-6 SASSI frequency domain solution using Soil Library and ANSYS building model....20
Figure 4-7 SASSI frequency domain solution using Soil Library and HOUSE building model....21
Figure 4-8 Traditional SASSI frequency domain solution....22
Figure 5-1 SASSI axisymmetric model for impedance analysis (Reference 9.1.11)....38
Figure 5-2 SASSI flexible volume substructuring (Reference 9.1.11)....39
Figure 5-3 Schematic of transfer function interpolation....39
Figure 5-4 Example partition for impedance matrix reduction....40
Figure 6-1 Stick model of PWR containment and internals (Reference 9.1.15)....47
Figure 6-2 Example 1 model (Reference 9.1.15)....48
Figure 6-3 Comparison of real translational impedance, example 1....49
Figure 6-4 Comparison of imaginary translational impedance, example 1....49
Figure 6-5 Comparison of real rotational impedance, example 1....50
Figure 6-6 Comparison of imaginary rotational impedance, example 1....50
Figure 6-7 Comparison of transfer functions, top of containment, example 1....51
Figure 6-8 Comparison of transfer functions, top of internals, example 1....51
Figure 6-9 Comparison of 2% damped ISRS, top of containment, example 1....52
Figure 6-10 Comparison of 2% damped ISRS, top of internals, example 1....52
Figure 6-11 Comparison of overturning moment, base of containment, example 1....53
Figure 6-12 Comparison of overturning moment, base of internals, example 1....53

© Copyright 2019 by NuScale Power, LLC

Figure 6-13 Example 2, building model, +Y is north and +X is east 67
Figure 6-14 Example 2, excavated soil model, +Y is north and +X is east 68
Figure 6-15 Example problem 2 soil site 69
Figure 6-16 Translation soil impedance, example 2 70
Figure 6-17 Translation-rocking soil impedance, example 2 70
Figure 6-18 Rocking, torsion soil impedance, example 2 71
Figure 6-19 Soil impedance phase angle, example 2 71
Figure 6-20 Soil impedance center of rotation, example 2 72
Figure 6-21 Comparison of *Kxx* lumped parameter soil impedance 73
Figure 6-22 Node locations with reported seismic response 74
Figure 6-23 Comparison of SASSI and soil library solutions, center roof response, layer 1 input 75
Figure 6-24 Comparison of SASSI and soil library solutions, center roof response, layer 4 input 76
Figure 6-25 Comparison of SASSI and ANSYS plate element formulations, center roof response, layer 1 input 77
Figure 6-26 Comparison of SASSI and ANYSYS plate element formulations, center roof response, layer 4 input 78
Figure 6-27 Comparison of SASSI and ANSYS solution, center roof response, layer 1 input 79
Figure 6-28 Comparison of SASSI and ANSYS solution, center roof response, layer 4 input 80
Figure 6-29 Example 3, surface input time histories 95
Figure 6-30 5% damped response spectra for example 3 surface input time histories 96
Figure 6-31 Comparison of SASSI and ANSYS solutions, center roof structural response, layer 1 input 97
Figure 6-32 Comparison of SASSI and ANSYS solutions, center roof structural response, layer 4 input 98
Figure 6-33 Comparison of SASSI and ANSYS 5% damped ISRS, center roof structural response 99
Figure 6-34 Comparison of SASSI and ANSYS solutions, fluid pressure, layer 1 input 100
Figure 6-35 Comparison of SASSI and ANSYS solutions, fluid pressure, layer 4 input 101
Figure 6-36 Comparison of SASSI and ANSYS acoustic fluid pressure (ksf sec^2/ft) time histories 102
Figure 6-37 Comparison of fixed base response for example problems 2 and 3 103
Figure 6-38 Comparison of SSI response for example problems 2 and 3 104
Figure 6-39 Comparison of SSI response for example problems 2 and 3 105
Figure 6-40a Isometric view 107
Figure 6-40b Longitudinal section 107
Figure 6-40c Reactor pool with 12 RXM 108
Figure 6-41 Input Motion Response Spectra, 5% Damping 110
Figure 6-42 Transfer Functions for Node 1900, Top of RXM-1 113
Figure 6-43 Acceleration Time Histories for Node 1900, Top of RXM-1 114
Figure 6-44 In-Structure Response Spectra for Node 1900, Top of RXM-1 115

© Copyright 2019 by NuScale Power, LLC

Figure 6-45 Location of Fluid Pressure Nodes on Near Side of Wall, Additional Nodes are on the Far Side 117
Figure 6-46 Pressure Transfer Functions for Node 87499 118
Figure 6-47 Pressure Time Histories for Node 87499 119
Figure 6-48 Relative Displacement Transfer Functions for Node 1900, Top of RXM-1 121
Figure 6-49 Relative Displacement Time Histories for Node 1900, Top of RXM-1 122
Figure 6-50 Force Transfer Functions for RXM-1, West Lug 125
Figure 6-51 Force Time Histories for RXM-1, West Lug 126
Figure 6-52 Base Reaction Transfer Functions for RXM-1 127
Figure 6-53 Base Reaction Time Histories for RXM-1 128
Figure A-1 Simple mass-spring-dashpot system 140
Figure A-2 Transfer function amplitude for 1 Hz SDOF systems with 10% structural, simplified structural, or viscous damping 140
Figure A-3 Transfer function amplitude for 1 Hz SDOF systems with 10% structural, simplified structural, or viscous damping, expanded scale 141
Figure A-4 Transfer function phase angle for 1 Hz SDOF systems with 10% structural, simplified structural, or viscous damping 141
Figure A-5 Combined spring and dashpot forces for SDOF systems with 10% structural, simplified structural, or viscous damping, cycled at 1 Hz 142
Figure A-6 Combined spring and dashpot forces for SDOF systems with 10% structural, simplified structural, or viscous damping, cycled at 1 Hz, expanded scale 142
Figure A-7 Combined spring and dashpot forces for SDOF systems with 10% structural, simplified structural, or viscous damping, cycled at 1 Hz 143
Figure A-8 Combined spring and dashpot forces for SDOF systems with 10% structural, simplified structural, or viscous damping, cycled at 0.5 Hz 143
Figure A-9 Combined spring and dashpot forces for SDOF systems with 10% structural, simplified structural, or viscous damping, cycled at 2 Hz 144
Figure B-1 Lumped mass (LM), consistent mass (CM), and lumped-consistent mass (LCM) transfer function comparison with wave equation benchmark, Vs/5L = 32 Hz 148
Figure C-1 Rectangular plate model 10, 1 151
Figure C-2 Rectangular plate model 9, 2 152
Figure C-3 Rectangular plate model 8, 3 152
Figure C-4 Rectangular plate model 7, 4 153
Figure C-5 Rectangular plate model 3, 5 153
Figure C-6 Rectangular plate model 4, 2 154
Figure D-1 Comparison of *Kxx* lumped parameter soil impedance 156
Figure D-2 Comparison of $K_{X\theta Y}$ lumped parameter soil impedance 157
Figure D-3 Comparison of K_{YY} lumped parameter soil impedance 158
Figure D-4 Comparison of $K_{Y\theta X}$ lumped parameter soil impedance 159
Figure D-5 Comparison of K_{ZZ} lumped parameter soil impedance 160
Figure D-6 Comparison of $K_{\theta X\theta X}$ lumped parameter soil impedance 161
Figure D-7 Comparison of $K_{\theta Y\theta Y}$ lumped parameter soil impedance 162
Figure D-8 Comparison of $K_{\theta Z\theta Z}$ lumped parameter soil impedance 163

© Copyright 2019 by NuScale Power, LLC

Figure E-1 Center roof, *X* response to layer 1 *X* seismic input, example 2 165
Figure E-2 SW corner roof, *X* response to layer 1 *X* seismic input, example 2 165
Figure E-3 SW corner roof, *Z* response to layer 1 *X* seismic input, example 2 166
Figure E-4 Center basemat, *X* response to layer 1 *X* seismic input, example 2 166
Figure E-5 West wall, *X* response to layer 1 *X* seismic input, example 2 167
Figure E-6 West wall, *Z* response to layer 1 *X* seismic input, example 2 167
Figure E-7 Center roof, *Y* response to layer 1 *Y* seismic input, example 2 168
Figure E-8 SW corner roof, *Y* response to layer 1 *Y* seismic input, example 2 168
Figure E-9 SW corner roof, *Z* response to layer 1 *Y* seismic input, example 2 169
Figure E-10 Center basemat, *Y* response to layer 1 *Y* seismic input, example 2 169
Figure E-11 South wall, *Y* response to layer 1 *Y* seismic input, example 2 170
Figure E-12 South wall, *Z* response to layer 1 *Y* seismic input, example 2 170
Figure E-13 Center roof, *Z* response to layer 1 *Z* seismic input, example 2 171
Figure E-14 SW corner roof, *Z* response to layer 1 *Z* seismic input, example 2 171
Figure E-15 Center basemat, *Z* response to layer 1 *Z* seismic input, example 2 172
Figure E-16 Center roof, *X* response to layer 4 *X* seismic input, example 2 172
Figure E-17 SW corner roof, *X* response to layer 4 *X* seismic input, example 2 173
Figure E-18 SW corner roof, *Z* response to layer 4 *X* seismic input, example 2 173
Figure E-19 Center basemat, *X* response to layer 4 *X* seismic input, example 2 174
Figure E-20 West wall, *X* response to layer 4 *X* seismic input, example 2 174
Figure E-21 West wall, *Z* response to layer 4 *X* seismic input, example 2 175
Figure E-22 Center roof, *Y* response to layer 4 *Y* seismic input, example 2 175
Figure E-23 SW corner roof, *Y* response to layer 4 *Y* seismic input, example 2 176
Figure E-24 SW corner roof, *Z* response to layer 4 *Y* seismic input, example 2 176
Figure E-25 Center basemat, *Y* response to layer 4 *Y* seismic input, example 2 177
Figure E-26 South wall, *Y* response to layer 4 *Y* seismic input, example 2 177
Figure E-27 South wall, *Z* response to layer 4 *Y* seismic input, example 2 178
Figure E-28 Center roof, *Z* response to layer 4 *Z* seismic input, example 2 178
Figure E-29 SW corner roof, *Z* response to layer 4 *Z* seismic input, example 2 179
Figure E-30 Center basemat, *Z* response to layer 4 *Z* seismic input, example 2 179
Figure F-1 Center roof, *X* response to layer 1 *X* seismic input, example 3 182
Figure F-2 SW corner roof, *X* response to layer 1 *X* seismic input, example 3 182
Figure F-3 SW corner roof, *Z* response to layer 1 *X* seismic input, example 3 183
Figure F-4 Center basemat, *X* response to layer 1 *X* seismic input, example 3 183
Figure F-5 West wall, *X* response to layer 1 *X* seismic input, example 3 184
Figure F-6 West wall, *Z* response to layer 1 *X* seismic input, example 3 184
Figure F-7 Center roof, *Y* response to layer 1 *Y* seismic input, example 3 185
Figure F-8 SW corner roof, *Y* response to layer 1 *Y* seismic input, example 3 185
Figure F-9 SW corner roof, *Z* response to layer 1 *Y* seismic input, example 3 186
Figure F-10 Center basemat, *Y* response to layer 1 *Y* seismic input, example 3 186
Figure F-11 South wall, *Y* response to layer 1 *Y* seismic input, example 3 187
Figure F-12 South wall, *Z* response to layer 1 *Y* seismic input, example 3 187
Figure F-13 Center roof, *Z* response to layer 1 *Z* seismic input, example 3 188
Figure F-14 SW corner roof, *Z* response to layer 1 *Z* seismic input, example 3 188
Figure F-15 Center basemat, *Z* response to layer 1 *Z* seismic input, example 3 189

© Copyright 2019 by NuScale Power, LLC

Figure F-16 Center roof, *X* response to layer 4 *X* seismic input, example 3 189
Figure F-17 SW corner roof, *X* response to layer 4 *X* seismic input, example 3 190
Figure F-18 SW corner roof, *Z* response to layer 4 *X* seismic input, example 3 190
Figure F-19 Center basemat, *X* response to layer 4 *X* seismic input, example 3 191
Figure F-20 West wall, *X* response to layer 4 *X* seismic input, example 3 191
Figure F-21 West wall, *Z* response to layer 4 *X* seismic input, example 3 192
Figure F-22 Center roof, *Y* response to layer 4 *Y* seismic input, example 3 192
Figure F-23 SW corner roof, *Y* response to layer 4 *Y* seismic input, example 3 193
Figure F-24 SW corner roof, *Z* response to layer 4 *Y* seismic input, example 3 193
Figure F-25 Center basemat, *Y* response to layer 4 *Y* seismic input, example 3 194
Figure F-26 South wall, *Y* response to layer 4 *Y* seismic input, example 3 194
Figure F-27 South wall, *Z* response to layer 4 *Y* seismic input, example 3 195
Figure F-28 Center roof, *Z* response to layer 4 *Z* seismic input, example 3 195
Figure F-29 SW corner roof, *Z* response to layer 4 *Z* seismic input, example 3 196
Figure F-30 Center basemat, *Z* response to layer 4 *Z* seismic input, example 3 196
Figure F-31 Comparison of SASSI and ANSYS 5% damped ISRS, center roof structural response 197
Figure F-32 Comparison of SASSI and ANSYS 5% damped ISRS, roof SW corner 198
Figure F-33 Comparison of SASSI and ANSYS 5% damped ISRS, center of west wall at grade elevation 199
Figure F-34 Comparison of SASSI and ANSYS 5% damped ISRS, center of south wall at grade elevation 200
Figure F-35 Comparison of SASSI and ANSYS 5% damped ISRS, center of basemat 201
Figure F-36 West wall, 6.25 ft deep, pressure response to layer 1 *X* seismic input, example 3 202
Figure F-37 West wall, 12.5 ft deep, pressure response to layer 1 *X* seismic input, example 3 202
Figure F-38 West wall, 18.75 ft deep, pressure response to layer 1 *X* seismic input, example 3 203
Figure F-39 South wall, 6.25 ft deep, pressure response to layer 1 *Y* seismic input, example 3 203
Figure F-40 South wall, 12.5 ft deep, pressure response to layer 1 *Y* seismic input, example 3 204
Figure F-41 South wall, 18.75 ft deep, pressure response to layer 1 *Y* seismic input, example 3 204
Figure F-42 West wall, 6.25 ft deep, pressure response to layer 1 Z seismic input, example 3 205
Figure F-43 West wall, 12.5 ft deep, pressure response to layer 1 *Z* seismic input, example 3 205
Figure F-44 West wall, 18.75 ft deep, pressure response to layer 1 *Z* seismic input, example 3 206
Figure F-45 South wall, 6.25 ft deep, pressure response to layer 1 *Z* seismic input, example 3 206
Figure F-46 South wall, 12.5 ft deep, pressure response to layer 1 *Z* seismic input, example 3 207

© Copyright 2019 by NuScale Power, LLC

Figure F-47 South wall, 18.75 ft Deep, pressure response to layer 1 *Z* seismic input, example 3 207
Figure F-48 Center basemat, 18.75 ft deep, pressure response to layer 1 *Z* seismic input, example 3 208
Figure F-49 West wall, 6.25 ft deep, pressure response to layer 4 *X* seismic input, example 3 208
Figure F-50 West wall, 12.5 ft deep, pressure response to layer 4 *X* seismic input, example 3 209
Figure F-51 West wall, 18.75 ft deep, pressure response to layer 4 *X* seismic input, example 3 209
Figure F-52 South wall, 6.25 ft deep, pressure response to layer 4 *Y* seismic input, example 3 210
Figure F-53 South wall, 12.5 ft deep, pressure response to layer 4 *Y* seismic input, example 3 210
Figure F-54 South wall, 18.75 ft deep, pressure response to layer 4 *Y* seismic input, example 3 211
Figure F-55 West wall, 6.25 ft deep, pressure response to layer 4 *Z* seismic input, example 3 211
Figure F-56 West wall, 12.5 ft deep, pressure response to layer 4 *Z* seismic input, example 3 212
Figure F-57 West wall, 18.75 ft deep, pressure response to layer 4 *Z* seismic input, example 3 212
Figure F-58 South wall, 6.25 ft deep, pressure response to layer 4 *Z* seismic input, example 3 213
Figure F-59 South wall, 12.5 ft deep, pressure response to layer 4 *Z* seismic input, example 3 213
Figure F-60 South wall, 18.75 ft deep, pressure response to layer 4 *Z* seismic input, example 3 214
Figure F-61 Center basemat, 18.75 ft deep, pressure response to layer 4 *Z* seismic input, example 3 214
Figure F-62 Comparison of SASSI and ANSYS acoustic fluid pressure (ksf sec^2/ft) time histories, center of west wall 215
Figure F-63 Comparison of SASSI and ANSYS acoustic fluid pressure (ksf sec^2/ft) time histories, center of south wall 216
Figure F-64 Comparison of SASSI and ANSYS acoustic fluid pressure (ksf sec^2/ft) time histories, center of west wall 217
Figure F-65 Comparison of SASSI and ANSYS acoustic fluid pressure (ksf sec^2/ft) time histories, center of south wall 218
Figure F-66 Comparison of SASSI and ANSYS acoustic fluid pressure (ksf sec^2/ft) time histories, center of basemat 219
Figure G-1 Center roof, *X* response to *X* seismic input, example 3 221
Figure G-2 SW corner roof, *X* response to *X* seismic input, example 3 221
Figure G-3 SW corner roof, *Z* response to *X* seismic input, example 3 222
Figure G-4 West wall, *X* response to *X* seismic input, example 3 222
Figure G-5 West wall, *Z* response to *X* seismic input, example 3 223

© Copyright 2019 by NuScale Power, LLC

Figure G-6 Center roof, *Y* response to *Y* seismic input, example 3....223
Figure G-7 SW corner roof, *Y* response to *Y* seismic input, example 3....224
Figure G-8 SW corner roof, *Z* response to *Y* seismic input, example 3....224
Figure G-9 South wall, *Y* response to *Y* seismic input, example 3....225
Figure G-10 South wall, *Z* response to *Y* seismic input, example 3....225
Figure G-11 Center roof, *Z* response to *Z* seismic input, example 3....226
Figure G-12 SW corner roof, *Z* response to *Z* seismic input, example 3....226
Figure H-1 Center roof, *X* response to layer 1 *X* seismic input, example 3....228
Figure H-2 SW corner roof, *X* response to layer 1 *X* seismic input, example 3....228
Figure H-3 SW corner roof, *Z* response to layer 1 *X* seismic input, example 3....229
Figure H-4 Center basemat, *X* response to layer 1 *X* seismic input, example 3....229
Figure H-5 West wall, *X* response to layer 1 *X* seismic input, example 3....230
Figure H-6 West wall, *Z* response to layer 1 *X* seismic input, example 3....230
Figure H-7 Center roof, *Y* response to layer 1 *Y* seismic input, example 3....231
Figure H-8 SW corner roof, *Y* response to layer 1 *Y* seismic input, example 3....231
Figure H-9 SW corner roof, *Z* response to layer 1 *Y* seismic input, example 3....232
Figure H-10 Center basemat, *Y* response to layer 1 *Y* seismic input, example 3....232
Figure H-11 South wall, *Y* response to layer 1 *Y* seismic input, example 3....233
Figure H-12 South wall, *Z* response to layer 1 *Y* seismic input, example 3....233
Figure H-13 Center roof, *Z* response to layer 1 *Z* seismic input, example 3....234
Figure H-14 SW corner roof, *Z* response to layer 1 *Z* seismic input, example 3....234
Figure H-15 Center basemat, *Z* response to layer 1 *Z* seismic input, example 3....235
Figure H-16 Center roof, *X* response to layer 4 *X* seismic input, example 3....235
Figure H-17 SW corner roof, *X* response to layer 4 *X* seismic input, example 3....236
Figure H-18 SW corner roof, *Z* response to layer 4 *X* seismic input, example 3....236
Figure H-19 Center basemat, *X* response to layer 4 *X* seismic input, example 3....237
Figure H-20 West wall, *X* response to layer 4 *X* seismic input, example 3....237
Figure H-21 West wall, *Z* response to layer 4 *X* seismic input, example 3....238
Figure H-22 Center roof, *Y* response to layer 4 *Y* seismic input, example 3....238
Figure H-23 SW corner roof, *Y* response to layer 4 *Y* seismic input, example 3....239
Figure H-24 SW corner roof, *Z* response to layer 4 *Y* seismic input, example 3....239
Figure H-25 Center basemat, *Y* response to layer 4 *Y* seismic input, example 3....240
Figure H-26 South wall, *Y* response to layer 4 *Y* seismic input, example 3....240
Figure H-27 South wall, *Z* response to layer 4 *Y* seismic input, example 3....241
Figure H-28 Center roof, *Z* response to layer 4 *Z* seismic input, example 3....241
Figure H-29 SW corner roof, *Z* response to layer 4 *Z* seismic input, example 3....242
Figure H-30 Center basemat, *Z* response to layer 4 *Z* seismic input, example 3....242
Figure I-1 Transfer Function, X Input, Node 120933, Northwest Corner on Top of Basemat....244
Figure I-2 Transfer Function, Y Input, Node 120933, Northwest Corner on Top of Basemat....245
Figure I-3 Transfer Function, Z Input, Node 120933, Northwest Corner on Top of Basemat....246
Figure I-4 Transfer Function, X Input, Node 120978, Mid-Span of North Exterior Wall on Top of Basemat....247

© Copyright 2019 by NuScale Power, LLC

Figure I-5 Transfer Function, Y Input, Node 120978, Mid-Span of North Exterior Wall on Top of Basemat....248
Figure I-6 Transfer Function, Z Input, Node 120978, Mid-Span of North Exterior Wall on Top of Basemat....249
Figure I-7 Transfer Function, X Input, Node 121053, Northeast Corner on Top of Basemat....250
Figure I-8 Transfer Function, Y Input, Node 121053, Northeast Corner on Top of Basemat....251
Figure I-9 Transfer Function, Z Input, Node 121053, Northeast Corner on Top of Basemat....252
Figure I-10 Transfer Function, X Input, Node 4914, RXM 1 Floor Node under Module....253
Figure I-11 Transfer Function, Y Input, Node 4914, RXM 1 Floor Node under Module....254
Figure I-12 Transfer Function, Z Input, Node 4914, RXM 1 Floor Node under Module....255
Figure I-13 Transfer Function, X Input, Node 46054, RXM 6 Floor Node under Module....256
Figure I-14 Transfer Function, Y Input, Node 46054, RXM 6 Floor Node under Module....257
Figure I-15 Transfer Function, Z Input, Node 46054, RXM 6 Floor Node under Module....258
Figure I-16 Transfer Function, X Input, Node 185505, Northwest Corner at El. 50’....259
Figure I-17 Transfer Function, Y Input, Node 185505, Northwest Corner at El. 50’....260
Figure I-18 Transfer Function, Z Input, Node 185505, Northwest Corner at El. 50’....261
Figure I-19 Transfer Function, X Input, Node 182529, Mid-Span of West Slab along Grid Line RX-C at El. 50’....262
Figure I-20 Transfer Function, Y Input, Node 182529, Mid-Span of West Slab along Grid Line RX-C at El. 50’....263
Figure I-21 Transfer Function, Z Input, Node 182529, Mid-Span of West Slab along Grid Line RX-C at El. 50’....264
Figure I-22 Transfer Function, X Input, Node 184359, Edge of Slab at Grid Line RX-4 at El. 50’....265
Figure I-23 Transfer Function, Y Input, Node 184359, Edge of Slab at Grid Line RX-4 at El. 50’....266
Figure I-24 Transfer Function, Z Input, Node 184359, Edge of Slab at Grid Line RX-4 at El. 50’....267
Figure I-25 Transfer Function, X Input, Node 185174, Mid-Span of North Slab between Grid Lines RX-4 and RX-5 at El. 50’....268
Figure I-26 Transfer Function, Y Input, Node 185174, Mid-Span of North Slab between Grid Lines RX-4 and RX-5 at El. 50’....269
Figure I-27 Transfer Function, Z Input, Node 185174, Mid-Span of North Slab between Grid Lines RX-4 and RX-5 at El. 50’....270
Figure I-28 Transfer Function, X Input, Node 185623, Northeast Corner at El. 50’....271
Figure I-29 Transfer Function, Y Input, Node 185623, Northeast Corner at El. 50’....272
Figure I-30 Transfer Function, Z Input, Node 185623, Northeast Corner at El. 50’....273
Figure I-31 Transfer Function, X Input, Node 255527, Northwest Corner at El. 75’....274
Figure I-32 Transfer Function, Y Input, Node 255527, Northwest Corner at El. 75’....275
Figure I-33 Transfer Function, Z Input, Node 255527, Northwest Corner at El. 75’....276
Figure I-34 Transfer Function, X Input, Node 255195, Mid-Span of North Slab between Grid Lines RX-4 and RX-5 at El. 75’....277

© Copyright 2019 by NuScale Power, LLC

Figure I-35 Transfer Function, Y Input, Node 255195, Mid-Span of North Slab between Grid Lines RX-4 and RX-5 at El. 75’ 278
Figure I-36 Transfer Function, Z Input, Node 255195, Mid-Span of North Slab between Grid Lines RX-4 and RX-5 at El. 75’ 279
Figure I-37 Transfer Function, X Input, Node 254481, Edge of East Slab along Grid Line RX-6 at El. 75’ 280
Figure I-38 Transfer Function, Y Input, Node 254481, Edge of East Slab along Grid Line RX-6 at El. 75’ 281
Figure I-39 Transfer Function, Z Input, Node 254481, Edge of East Slab along Grid Line RX-6 at El. 75’ 282
Figure I-40 Transfer Function, X Input, Node 332235, Northwest Corner of Exterior Wall at El 100’ 283
Figure I-41 Transfer Function, Y Input, Node 332235, Northwest Corner of Exterior Wall at El 100’ 284
Figure I-42 Transfer Function, Z Input, Node 332235, Northwest Corner of Exterior Wall at El 100’ 285
Figure I-43 Transfer Function, X Input, Node 331936, Mid-Span of North Slab between Grid Lines RX-4 and RX-5 at El 100’ 286
Figure I-44 Transfer Function, Y Input, Node 331936, Mid-Span of North Slab between Grid Lines RX-4 and RX-5 at El 100’ 287
Figure I-45 Transfer Function, Z Input, Node 331936, Mid-Span of North Slab between Grid Lines RX-4 and RX-5 at El 100’ 288
Figure I-46 Transfer Function, X Input, Node 331222, Edge of North Slab along Grid Line RX-4 at El 100’ 289
Figure I-47 Transfer Function, Y Input, Node 331222, Edge of North Slab along Grid Line RX-4 at El 100’ 290
Figure I-48 Transfer Function, Z Input, Node 331222, Edge of North Slab along Grid Line RX-4 at El 100’ 291
Figure I-49 Transfer Function, X Input, Node 331292, Edge of East Slab along Grid Line RX-6 at El 100’ 292
Figure I-50 Transfer Function, Y Input, Node 331292, Edge of East Slab along Grid Line RX-6 at El 100’ 293
Figure I-51 Transfer Function, Z Input, Node 331292, Edge of East Slab along Grid Line RX-6 at El 100’ 294
Figure I-52 Transfer Function, X Input, Node 352669, Northwest Corner of Exterior Wall at El 125’ 295
Figure I-53 Transfer Function, Y Input, Node 352669, Northwest Corner of Exterior Wall at El 125’ 296
Figure I-54 Transfer Function, Z Input, Node 352669, Northwest Corner of Exterior Wall at El 125’ 297
Figure I-55 Transfer Function, X Input, Node 351629, Northwest Corner of Bio Shield 298
Figure I-56 Transfer Function, Y Input, Node 351629, Northwest Corner of Bio Shield 299
Figure I-57 Transfer Function, Z Input, Node 351629, Northwest Corner of Bio Shield 300
Figure I-58 Transfer Function, X Input, Node 352370, Mid-Span of North Slab at between Grid Lines RX-4 and RX-5 at El 125’ 301

© Copyright 2019 by NuScale Power, LLC

Figure I-59 Transfer Function, Y Input, Node 352370, Mid-Span of North Slab at between Grid Lines RX-4 and RX-5 at El 125' 302
Figure I-60 Transfer Function, Z Input, Node 352370, Mid-Span of North Slab at between Grid Lines RX-4 and RX-5 at El 125' 303
Figure I-61 Transfer Function, X Input, Node 351696, Northeast Corner of Bio Shield 304
Figure I-62 Transfer Function, Y Input, Node 351696, Northeast Corner of Bio Shield 305
Figure I-63 Transfer Function, Z Input, Node 351696, Northeast Corner of Bio Shield 306
Figure I-64 Transfer Function, X Input, Node 392329, Top of Roof at Grid Line RX-1 307
Figure I-65 Transfer Function, Y Input, Node 392329, Top of Roof at Grid Line RX-1 308
Figure I-66 Transfer Function, Z Input, Node 392329, Top of Roof at Grid Line RX-1 309
Figure I-67 Transfer Function, X Input, Node 392378, Roof Slab between Grid Lines RX-4 and RX-5 310
Figure I-68 Transfer Function, Y Input, Node 392378, Roof Slab between Grid Lines RX-4 and RX-5 311
Figure I-69 Transfer Function, Z Input, Node 392378, Roof Slab between Grid Lines RX-4 and RX-5 312
Figure I-70 Transfer Function, X Input, Node 394770, Northeast Corner of Roof Slab 313
Figure I-71 Transfer Function, Y Input, Node 394770, Northeast Corner of Roof Slab 314
Figure I-72 Transfer Function, Z Input, Node 394770, Northeast Corner of Roof Slab 315
Figure I-73 Transfer Function, X Input, Node 8216, RXM-1 West Lug 316
Figure I-74 Transfer Function, Y Input, Node 8216, RXM-1 West Lug 317
Figure I-75 Transfer Function, Z Input, Node 8216, RXM-1 West Lug 318
Figure I-76 Transfer Function, X Input, Node 8215, RXM-1 North Lug 319
Figure I-77 Transfer Function, Y Input, Node 8215, RXM-1 North Lug 320
Figure I-78 Transfer Function, Z Input, Node 8215, RXM-1 North Lug 321
Figure I-79 Transfer Function, X Input, Node 8214, RXM-1 East Lug 322
Figure I-80 Transfer Function, Y Input, Node 8214, RXM-1 East Lug 323
Figure I-81 Transfer Function, Z Input, Node 8214, RXM-1 East Lug 324
Figure I-82 Transfer Function, X Input, Node 1900, RXM-1 Top 325
Figure I-83 Transfer Function, Y Input, Node 1900, RXM-1 Top 326
Figure I-84 Transfer Function, Z Input, Node 1900, RXM-1 Top 327
Figure I-85 Transfer Function, X Input, Node 49356, RXM-6 West Lug 328
Figure I-86 Transfer Function, Y Input, Node 49356, RXM-6 West Lug 329
Figure I-87 Transfer Function, Z Input, Node 49356, RXM-6 West Lug 330
Figure I-88 Transfer Function, X Input, Node 49355, RXM-6 North Lug 331
Figure I-89 Transfer Function, Y Input, Node 49355, RXM-6 North Lug 332
Figure I-90 Transfer Function, Z Input, Node 49355, RXM-6 North Lug 333
Figure I-91 Transfer Function, X Input, Node 49354, RXM-6 East Lug 334
Figure I-92 Transfer Function, Y Input, Node 49354, RXM-6 East Lug 335
Figure I-93 Transfer Function, Z Input, Node 49354, RXM-6 East Lug 336
Figure I-94 Transfer Function, X Input, Node 43040, RXM-6 Top 337
Figure I-95 Transfer Function, Y Input, Node 43040, RXM-6 Top 338
Figure I-96 Transfer Function, Z Input, Node 43040, RXM-6 Top 339
Figure J-1 Acceleration Time History, X Input, Node 120933, Northwest Corner on Top of Basemat 341

© Copyright 2019 by NuScale Power, LLC

Figure J-2 Acceleration Time History, Y Input, Node 120933, Northwest Corner on Top of Basemat 342
Figure J-3 Acceleration Time History, Z Input, Node 120933, Northwest Corner on Top of Basemat 343
Figure J-4 Acceleration Time History, X Input, Node 120978, Mid-Span of North Exterior Wall on Top of Basemat 344
Figure J-5 Acceleration Time History, Y Input, Node 120978, Mid-Span of North Exterior Wall on Top of Basemat 345
Figure J-6 Acceleration Time History, Z Input, Node 120978, Mid-Span of North Exterior Wall on Top of Basemat 346
Figure J-7 Acceleration Time History, X Input, Node 121053, Northeast Corner on Top of Basemat 347
Figure J-8 Acceleration Time History, Y Input, Node 121053, Northeast Corner on Top of Basemat 348
Figure J-9 Acceleration Time History, Z Input, Node 121053, Northeast Corner on Top of Basemat 349
Figure J-10 Acceleration Time History, X Input, Node 4914, RXM 1 Floor Node under Module 350
Figure J-11 Acceleration Time History, Y Input, Node 4914, RXM 1 Floor Node under Module 351
Figure J-12 Acceleration Time History, Z Input, Node 4914, RXM 1 Floor Node under Module 352
Figure J-13 Acceleration Time History, X Input, Node 46054, RXM 6 Floor Node under Module 353
Figure J-14 Acceleration Time History, Y Input, Node 46054, RXM 6 Floor Node under Module 354
Figure J-15 Acceleration Time History, Z Input, Node 46054, RXM 6 Floor Node under Module 355
Figure J-16 Acceleration Time History, X Input, Node 185505, Northwest Corner at El. 50’ 356
Figure J-17 Acceleration Time History, Y Input, Node 185505, Northwest Corner at El. 50’ 357
Figure J-18 Acceleration Time History, Z Input, Node 185505, Northwest Corner at El. 50’ 358
Figure J-19 Acceleration Time History, X Input, Node 182529, Mid-Span of West Slab along Grid Line RX-C at El. 50’ 359
Figure J-20 Acceleration Time History, Y Input, Node 182529, Mid-Span of West Slab along Grid Line RX-C at El. 50’ 360
Figure J-21 Acceleration Time History, Z Input, Node 182529, Mid-Span of West Slab along Grid Line RX-C at El. 50’ 361
Figure J-22 Acceleration Time History, X Input, Node 184359, Edge of Slab at Grid Line RX-4 at El. 50’ 362
Figure J-23 Acceleration Time History, Y Input, Node 184359, Edge of Slab at Grid Line RX-4 at El. 50’ 363

© Copyright 2019 by NuScale Power, LLC

Figure J-24 Acceleration Time History, Z Input, Node 184359, Edge of Slab at Grid Line RX-4 at El. 50' 364
Figure J-25 Acceleration Time History, X Input, Node 185174, Mid-Span of North Slab between Grid Lines RX-4 and RX-5 at El. 50' 365
Figure J-26 Acceleration Time History, Y Input, Node 185174, Mid-Span of North Slab between Grid Lines RX-4 and RX-5 at El. 50' 366
Figure J-27 Acceleration Time History, Z Input, Node 185174, Mid-Span of North Slab between Grid Lines RX-4 and RX-5 at El. 50' 367
Figure J-28 Acceleration Time History, X Input, Node 185623, Northeast Corner at El. 50' 368
Figure J-29 Acceleration Time History, Y Input, Node 185623, Northeast Corner at El. 50' 369
Figure J-30 Acceleration Time History, Z Input, Node 185623, Northeast Corner at El. 50' 370
Figure J-31 Acceleration Time History, X Input, Node 255527, Northwest Corner at El. 75' 371
Figure J-32 Acceleration Time History, Y Input, Node 255527, Northwest Corner at El. 75' 372
Figure J-33 Acceleration Time History, Z Input, Node 255527, Northwest Corner at El. 75' 373
Figure J-34 Acceleration Time History, X Input, Node 255195, Mid-Span of North Slab between Grid Lines RX-4 and RX-5 at El. 75' 374
Figure J-35 Acceleration Time History, Y Input, Node 255195, Mid-Span of North Slab between Grid Lines RX-4 and RX-5 at El. 75' 375
Figure J-36 Acceleration Time History, Z Input, Node 255195, Mid-Span of North Slab between Grid Lines RX-4 and RX-5 at El. 75' 376
Figure J-37 Acceleration Time History, X Input, Node 254481, Edge of East Slab along Grid Line RX-6 at El. 75' 377
Figure J-38 Acceleration Time History, Y Input, Node 254481, Edge of East Slab along Grid Line RX-6 at El. 75' 378
Figure J-39 Acceleration Time History, Z Input, Node 254481, Edge of East Slab along Grid Line RX-6 at El. 75' 379
Figure J-40 Acceleration Time History, X Input, Node 332235, Northwest Corner of Exterior Wall at El 100' 380
Figure J-41 Acceleration Time History, Y Input, Node 332235, Northwest Corner of Exterior Wall at El 100' 381
Figure J-42 Acceleration Time History, Z Input, Node 332235, Northwest Corner of Exterior Wall at El 100' 382
Figure J-43 Acceleration Time History, X Input, Node 331936, Mid-Span of North Slab between Grid Lines RX-4 and RX-5 at El 100' 383
Figure J-44 Acceleration Time History, Y Input, Node 331936, Mid-Span of North Slab between Grid Lines RX-4 and RX-5 at El 100' 384
Figure J-45 Acceleration Time History, Z Input, Node 331936, Mid-Span of North Slab between Grid Lines RX-4 and RX-5 at El 100' 385

© Copyright 2019 by NuScale Power, LLC

Figure J-46 Acceleration Time History, X Input, Node 331222, Edge of North Slab along Grid Line RX-4 at El 100’ 386
Figure J-47 Acceleration Time History, Y Input, Node 331222, Edge of North Slab along Grid Line RX-4 at El 100’ 387
Figure J-48 Acceleration Time History, Z Input, Node 331222, Edge of North Slab along Grid Line RX-4 at El 100’ 388
Figure J-49 Acceleration Time History, X Input, Node 331292, Edge of East Slab along Grid Line RX-6 at El 100’ 389
Figure J-50 Acceleration Time History, Y Input, Node 331292, Edge of East Slab along Grid Line RX-6 at El 100’ 390
Figure J-51 Acceleration Time History, Z Input, Node 331292, Edge of East Slab along Grid Line RX-6 at El 100’ 391
Figure J-52 Acceleration Time History, X Input, Node 352669, Northwest Corner of Exterior Wall at El 125’ 392
Figure J-53 Acceleration Time History, Y Input, Node 352669, Northwest Corner of Exterior Wall at El 125’ 393
Figure J-54 Acceleration Time History, Z Input, Node 352669, Northwest Corner of Exterior Wall at El 125’ 394
Figure J-55 Acceleration Time History, X Input, Node 351629, Northwest Corner of Bio Shield 395
Figure J-56 Acceleration Time History, Y Input, Node 351629, Northwest Corner of Bio Shield 396
Figure J-57 Acceleration Time History, Z Input, Node 351629, Northwest Corner of Bio Shield 397
Figure J-58 Acceleration Time History, X Input, Node 352370, Mid-Span of North Slab at between Grid Lines RX-4 and RX-5 at El 125’ 398
Figure J-59 Acceleration Time History, Y Input, Node 352370, Mid-Span of North Slab at between Grid Lines RX-4 and RX-5 at El 125’ 399
Figure J-60 Acceleration Time History, Z Input, Node 352370, Mid-Span of North Slab at between Grid Lines RX-4 and RX-5 at El 125’ 400
Figure J-61 Acceleration Time History, X Input, Node 351696, Northeast Corner of Bio Shield 401
Figure J-62 Acceleration Time History, Y Input, Node 351696, Northeast Corner of Bio Shield 402
Figure J-63 Acceleration Time History, Z Input, Node 351696, Northeast Corner of Bio Shield 403
Figure J-64 Acceleration Time History, X Input, Node 392329, Top of Roof at Grid Line RX-1 404
Figure J-65 Acceleration Time History, Y Input, Node 392329, Top of Roof at Grid Line RX-1 405
Figure J-66 Acceleration Time History, Z Input, Node 392329, Top of Roof at Grid Line RX-1 406
Figure J-67 Acceleration Time History, X Input, Node 392378, Roof Slab between Grid Lines RX-4 and RX-5 407

© Copyright 2019 by NuScale Power, LLC

Figure J-68 Acceleration Time History, Y Input, Node 392378, Roof Slab between Grid Lines RX-4 and RX-5 408
Figure J-69 Acceleration Time History, Z Input, Node 392378, Roof Slab between Grid Lines RX-4 and RX-5 409
Figure J-70 Acceleration Time History, X Input, Node 394770, Northeast Corner of Roof Slab 410
Figure J-71 Acceleration Time History, Y Input, Node 394770, Northeast Corner of Roof Slab 411
Figure J-72 Acceleration Time History, Z Input, Node 394770, Northeast Corner of Roof Slab 412
Figure J-73 Acceleration Time History, X Input, Node 8216, RXM-1 West Lug 413
Figure J-74 Acceleration Time History, Y Input, Node 8216, RXM-1 West Lug 414
Figure J-75 Acceleration Time History, Z Input, Node 8216, RXM-1 West Lug 415
Figure J-76 Acceleration Time History, X Input, Node 8215, RXM-1 North Lug 416
Figure J-77 Acceleration Time History, Y Input, Node 8215, RXM-1 North Lug 417
Figure J-78 Acceleration Time History, Z Input, Node 8215, RXM-1 North Lug 418
Figure J-79 Acceleration Time History, X Input, Node 8214, RXM-1 East Lug 419
Figure J-80 Acceleration Time History, Y Input, Node 8214, RXM-1 East Lug 420
Figure J-81 Acceleration Time History, Z Input, Node 8214, RXM-1 East Lug 421
Figure J-82 Acceleration Time History, X Input, Node 1900, RXM-1 Top 422
Figure J-83 Acceleration Time History, Y Input, Node 1900, RXM-1 Top 423
Figure J-84 Acceleration Time History, Z Input, Node 1900, RXM-1 Top 424
Figure J-85 Acceleration Time History, X Input, Node 49356, RXM-6 West Lug 425
Figure J-86 Acceleration Time History, Y Input, Node 49356, RXM-6 West Lug 426
Figure J-87 Acceleration Time History, Z Input, Node 49356, RXM-6 West Lug 427
Figure J-88 Acceleration Time History, X Input, Node 49355, RXM-6 North Lug 428
Figure J-89 Acceleration Time History, Y Input, Node 49355, RXM-6 North Lug 429
Figure J-90 Acceleration Time History, Z Input, Node 49355, RXM-6 North Lug 430
Figure J-91 Acceleration Time History, X Input, Node 49354, RXM-6 East Lug 431
Figure J-92 Acceleration Time History, Y Input, Node 49354, RXM-6 East Lug 432
Figure J-93 Acceleration Time History, Z Input, Node 49354, RXM-6 East Lug 433
Figure J-94 Acceleration Time History, X Input, Node 43040, RXM-6 Top 434
Figure J-95 Acceleration Time History, Y Input, Node 43040, RXM-6 Top 435
Figure J-96 Acceleration Time History, Z Input, Node 43040, RXM-6 Top 436
Figure K-1 In-Structure Response Spectra, X Input, Node 120933, Northwest Corner on Top of Basemat 438
Figure K-2 In-Structure Response Spectra, Y Input, Node 120933, Northwest Corner on Top of Basemat 439
Figure K-3 In-Structure Response Spectra, Z Input, Node 120933, Northwest Corner on Top of Basemat 440
Figure K-4 In-Structure Response Spectra, X Input, Node 120978, Mid-Span of North Exterior Wall on Top of Basemat 441
Figure K-5 In-Structure Response Spectra, Y Input, Node 120978, Mid-Span of North Exterior Wall on Top of Basemat 442

© Copyright 2019 by NuScale Power, LLC

Figure K-6 In-Structure Response Spectra, Z Input, Node 120978, Mid-Span of North Exterior Wall on Top of Basemat 443
Figure K-7 In-Structure Response Spectra, X Input, Node 121053, Northeast Corner on Top of Basemat 444
Figure K-8 In-Structure Response Spectra, Y Input, Node 121053, Northeast Corner on Top of Basemat 445
Figure K-9 In-Structure Response Spectra, Z Input, Node 121053, Northeast Corner on Top of Basemat 446
Figure K-10 In-Structure Response Spectra, X Input, Node 4914, RXM 1 Floor Node under Module 447
Figure K-11 In-Structure Response Spectra, Y Input, Node 4914, RXM 1 Floor Node under Module 448
Figure K-12 In-Structure Response Spectra, Z Input, Node 4914, RXM 1 Floor Node under Module 449
Figure K-13 In-Structure Response Spectra, X Input, Node 46054, RXM 6 Floor Node under Module 450
Figure K-14 In-Structure Response Spectra, Y Input, Node 46054, RXM 6 Floor Node under Module 451
Figure K-15 In-Structure Response Spectra, Z Input, Node 46054, RXM 6 Floor Node under Module 452
Figure K-16 In-Structure Response Spectra, X Input, Node 185505, Northwest Corner at El. 50’ 453
Figure K-17 In-Structure Response Spectra, Y Input, Node 185505, Northwest Corner at El. 50’ 454
Figure K-18 In-Structure Response Spectra, Z Input, Node 185505, Northwest Corner at El. 50’ 455
Figure K-19 In-Structure Response Spectra, X Input, Node 182529, Mid-Span of West Slab along Grid Line RX-C at El. 50’ 456
Figure K-20 In-Structure Response Spectra, Y Input, Node 182529, Mid-Span of West Slab along Grid Line RX-C at El. 50’ 457
Figure K-21 In-Structure Response Spectra, Z Input, Node 182529, Mid-Span of West Slab along Grid Line RX-C at El. 50’ 458
Figure K-22 In-Structure Response Spectra, X Input, Node 184359, Edge of Slab at Grid Line RX-4 at El. 50’ 459
Figure K-23 In-Structure Response Spectra, Y Input, Node 184359, Edge of Slab at Grid Line RX-4 at El. 50’ 460
Figure K-24 In-Structure Response Spectra, Z Input, Node 184359, Edge of Slab at Grid Line RX-4 at El. 50’ 461
Figure K-25 In-Structure Response Spectra, X Input, Node 185174, Mid-Span of North Slab between Grid Lines RX-4 and RX-5 at El. 50’ 462
Figure K-26 In-Structure Response Spectra, Y Input, Node 185174, Mid-Span of North Slab between Grid Lines RX-4 and RX-5 at El. 50’ 463
Figure K-27 In-Structure Response Spectra, Z Input, Node 185174, Mid-Span of North Slab between Grid Lines RX-4 and RX-5 at El. 50’ 464

© Copyright 2019 by NuScale Power, LLC

Figure K-28 In-Structure Response Spectra, X Input, Node 185623, Northeast Corner at El. 50’ 465
Figure K-29 In-Structure Response Spectra, Y Input, Node 185623, Northeast Corner at El. 50’ 466
Figure K-30 In-Structure Response Spectra, Z Input, Node 185623, Northeast Corner at El. 50’ 467
Figure K-31 In-Structure Response Spectra, X Input, Node 255527, Northwest Corner at El. 75’ 468
Figure K-32 In-Structure Response Spectra, Y Input, Node 255527, Northwest Corner at El. 75’ 469
Figure K-33 In-Structure Response Spectra, Z Input, Node 255527, Northwest Corner at El. 75’ 470
Figure K-34 In-Structure Response Spectra, X Input, Node 255195, Mid-Span of North Slab between Grid Lines RX-4 and RX-5 at El. 75’ 471
Figure K-35 In-Structure Response Spectra, Y Input, Node 255195, Mid-Span of North Slab between Grid Lines RX-4 and RX-5 at El. 75’ 472
Figure K-36 In-Structure Response Spectra, Z Input, Node 255195, Mid-Span of North Slab between Grid Lines RX-4 and RX-5 at El. 75’ 473
Figure K-37 In-Structure Response Spectra, X Input, Node 254481, Edge of East Slab along Grid Line RX-6 at El. 75’ 474
Figure K-38 In-Structure Response Spectra, Y Input, Node 254481, Edge of East Slab along Grid Line RX-6 at El. 75’ 475
Figure K-39 In-Structure Response Spectra, Z Input, Node 254481, Edge of East Slab along Grid Line RX-6 at El. 75’ 476
Figure K-40 In-Structure Response Spectra, X Input, Node 332235, Northwest Corner of Exterior Wall at El 100’ 477
Figure K-41 In-Structure Response Spectra, Y Input, Node 332235, Northwest Corner of Exterior Wall at El 100’ 478
Figure K-42 In-Structure Response Spectra, Z Input, Node 332235, Northwest Corner of Exterior Wall at El 100’ 479
Figure K-43 In-Structure Response Spectra, X Input, Node 331936, Mid-Span of North Slab between Grid Lines RX-4 and RX-5 at El 100’ 480
Figure K-44 In-Structure Response Spectra, Y Input, Node 331936, Mid-Span of North Slab between Grid Lines RX-4 and RX-5 at El 100’ 481
Figure K-45 In-Structure Response Spectra, Z Input, Node 331936, Mid-Span of North Slab between Grid Lines RX-4 and RX-5 at El 100’ 482
Figure K-46 In-Structure Response Spectra, X Input, Node 331222, Edge of North Slab along Grid Line RX-4 at El 100’ 483
Figure K-47 In-Structure Response Spectra, Y Input, Node 331222, Edge of North Slab along Grid Line RX-4 at El 100’ 484
Figure K-48 In-Structure Response Spectra, Z Input, Node 331222, Edge of North Slab along Grid Line RX-4 at El 100’ 485
Figure K-49 In-Structure Response Spectra, X Input, Node 331292, Edge of East Slab along Grid Line RX-6 at El 100’ 486

© Copyright 2019 by NuScale Power, LLC

Figure K-50 In-Structure Response Spectra, Y Input, Node 331292, Edge of East Slab along Grid Line RX-6 at El 100’ 487
Figure K-51 In-Structure Response Spectra, Z Input, Node 331292, Edge of East Slab along Grid Line RX-6 at El 100’ 488
Figure K-52 In-Structure Response Spectra, X Input, Node 352669, Northwest Corner of Exterior Wall at El 125’ 489
Figure K-53 In-Structure Response Spectra, Y Input, Node 352669, Northwest Corner of Exterior Wall at El 125’ 490
Figure K-54 In-Structure Response Spectra, Z Input, Node 352669, Northwest Corner of Exterior Wall at El 125’ 491
Figure K-55 In-Structure Response Spectra, X Input, Node 351629, Northwest Corner of Bio Shield 492
Figure K-56 In-Structure Response Spectra, Y Input, Node 351629, Northwest Corner of Bio Shield 493
Figure K-57 In-Structure Response Spectra, Z Input, Node 351629, Northwest Corner of Bio Shield 494
Figure K-58 In-Structure Response Spectra, X Input, Node 352370, Mid-Span of North Slab at between Grid Lines RX-4 and RX-5 at El 125’ 495
Figure K-59 In-Structure Response Spectra, Y Input, Node 352370, Mid-Span of North Slab at between Grid Lines RX-4 and RX-5 at El 125’ 496
Figure K-60 In-Structure Response Spectra, Z Input, Node 352370, Mid-Span of North Slab at between Grid Lines RX-4 and RX-5 at El 125’ 497
Figure K-61 In-Structure Response Spectra, X Input, Node 351696, Northeast Corner of Bio Shield 498
Figure K-62 In-Structure Response Spectra, Y Input, Node 351696, Northeast Corner of Bio Shield 499
Figure K-63 In-Structure Response Spectra, Z Input, Node 351696, Northeast Corner of Bio Shield 500
Figure K-64 In-Structure Response Spectra, X Input, Node 392329, Top of Roof at Grid Line RX-1 501
Figure K-65 In-Structure Response Spectra, Y Input, Node 392329, Top of Roof at Grid Line RX-1 502
Figure K-66 In-Structure Response Spectra, Z Input, Node 392329, Top of Roof at Grid Line RX-1 503
Figure K-67 In-Structure Response Spectra, X Input, Node 392378, Roof Slab between Grid Lines RX-4 and RX-5 504
Figure K-68 In-Structure Response Spectra, Y Input, Node 392378, Roof Slab between Grid Lines RX-4 and RX-5 505
Figure K-69 In-Structure Response Spectra, Z Input, Node 392378, Roof Slab between Grid Lines RX-4 and RX-5 506
Figure K-70 In-Structure Response Spectra, X Input, Node 394770, Northeast Corner of Roof Slab 507
Figure K-71 In-Structure Response Spectra, Y Input, Node 394770, Northeast Corner of Roof Slab 508

© Copyright 2019 by NuScale Power, LLC

Figure K-72 In-Structure Response Spectra, Z Input, Node 394770, Northeast Corner of Roof Slab....509
Figure K-73 In-Structure Response Spectra, X Input, Node 8216, RXM-1 West Lug....510
Figure K-74 In-Structure Response Spectra, Y Input, Node 8216, RXM-1 West Lug....511
Figure K-75 In-Structure Response Spectra, Z Input, Node 8216, RXM-1 West Lug....512
Figure K-76 In-Structure Response Spectra, X Input, Node 8215, RXM-1 North Lug....513
Figure K-77 In-Structure Response Spectra, Y Input, Node 8215, RXM-1 North Lug....514
Figure K-78 In-Structure Response Spectra, Z Input, Node 8215, RXM-1 North Lug....515
Figure K-79 In-Structure Response Spectra, X Input, Node 8214, RXM-1 East Lug....516
Figure K-80 In-Structure Response Spectra, Y Input, Node 8214, RXM-1 East Lug....517
Figure K-81 In-Structure Response Spectra, Z Input, Node 8214, RXM-1 East Lug....518
Figure K-82 In-Structure Response Spectra, X Input, Node 1900, RXM-1 Top....519
Figure K-83 In-Structure Response Spectra, Y Input, Node 1900, RXM-1 Top....520
Figure K-84 In-Structure Response Spectra, Z Input, Node 1900, RXM-1 Top....521
Figure K-85 In-Structure Response Spectra, X Input, Node 49356, RXM-6 West Lug....522
Figure K-86 In-Structure Response Spectra, Y Input, Node 49356, RXM-6 West Lug....523
Figure K-87 In-Structure Response Spectra, Z Input, Node 49356, RXM-6 West Lug....524
Figure K-88 In-Structure Response Spectra, X Input, Node 49355, RXM-6 North Lug....525
Figure K-89 In-Structure Response Spectra, Y Input, Node 49355, RXM-6 North Lug....526
Figure K-90 In-Structure Response Spectra, Z Input, Node 49355, RXM-6 North Lug....527
Figure K-91 In-Structure Response Spectra, X Input, Node 49354, RXM-6 East Lug....528
Figure K-92 In-Structure Response Spectra, Y Input, Node 49354, RXM-6 East Lug....529
Figure K-93 In-Structure Response Spectra, Z Input, Node 49354, RXM-6 East Lug....530
Figure K-94 In-Structure Response Spectra, X Input, Node 43040, RXM-6 Top....531
Figure K-95 In-Structure Response Spectra, Y Input, Node 43040, RXM-6 Top....532
Figure K-96 In-Structure Response Spectra, Z Input, Node 43040, RXM-6 Top....533
Figure L-1 Wingwall Pressure Transfer Functions at Node 87499....535
Figure L-2 Wingwall Pressure Transfer Functions at Node 95777....536
Figure L-3 Wingwall Pressure Transfer Functions at Node 87960....537
Figure L-4 Wingwall Pressure Transfer Functions at Node 96376....538
Figure L-5 Wingwall Pressure Transfer Functions at Node 89399....539
Figure L-6 Wingwall Pressure Transfer Functions at Node 97727....540
Figure M-1 Wingwall Pressure Time Histories at Node 87499....542
Figure M-2 Wingwall Pressure Time Histories at Node 95777....543
Figure M-3 Wingwall Pressure Time Histories at Node 87960....544
Figure M-4 Wingwall Pressure Time Histories at Node 96376....545
Figure M-5 Wingwall Pressure Time Histories at Node 89399....546
Figure M-6 Wingwall Pressure Time Histories at Node 97727....547
Figure N-1 Relative Displacement TF, X Input, Node 120933, Northwest Corner on Top of Basemat....549
Figure N-2 Relative Displacement TF, Y Input, Node 120933, Northwest Corner on Top of Basemat....550
Figure N-3 Relative Displacement TF, Z Input, Node 120933, Northwest Corner on Top of Basemat....551

© Copyright 2019 by NuScale Power, LLC

Figure N-4 Relative Displacement TF, X Input, Node 120978, Mid-Span of North Exterior Wall on Top of Basemat 552
Figure N-5 Relative Displacement TF, Y Input, Node 120978, Mid-Span of North Exterior Wall on Top of Basemat 553
Figure N-6 Relative Displacement TF, Z Input, Node 120978, Mid-Span of North Exterior Wall on Top of Basemat 554
Figure N-7 Relative Displacement TF, X Input, Node 121053, Northeast Corner on Top of Basemat 555
Figure N-8 Relative Displacement TF, Y Input, Node 121053, Northeast Corner on Top of Basemat 556
Figure N-9 Relative Displacement TF, Z Input, Node 121053, Northeast Corner on Top of Basemat 557
Figure N-10 Relative Displacement TF, X Input, Node 4914, RXM 1 Floor Node under Module 558
Figure N-11 Relative Displacement TF, Y Input, Node 4914, RXM 1 Floor Node under Module 559
Figure N-12 Relative Displacement TF, Z Input, Node 4914, RXM 1 Floor Node under Module 560
Figure N-13 Relative Displacement TF, X Input, Node 46054, RXM 6 Floor Node under Module 561
Figure N-14 Relative Displacement TF, Y Input, Node 46054, RXM 6 Floor Node under Module 562
Figure N-15 Relative Displacement TF, Z Input, Node 46054, RXM 6 Floor Node under Module 563
Figure N-16 Relative Displacement TF, X Input, Node 185505, Northwest Corner at El. 50’ 564
Figure N-17 Relative Displacement TF, Y Input, Node 185505, Northwest Corner at El. 50’ 565
Figure N-18 Relative Displacement TF, Z Input, Node 185505, Northwest Corner at El. 50’ 566
Figure N-19 Relative Displacement TF, X Input, Node 182529, Mid-Span of West Slab along Grid Line RX-C at El. 50’ 567
Figure N-20 Relative Displacement TF, Y Input, Node 182529, Mid-Span of West Slab along Grid Line RX-C at El. 50’ 568
Figure N-21 Relative Displacement TF, Z Input, Node 182529, Mid-Span of West Slab along Grid Line RX-C at El. 50’ 569
Figure N-22 Relative Displacement TF, X Input, Node 184359, Edge of Slab at Grid Line RX-4 at El. 50’ 570
Figure N-23 Relative Displacement TF, Y Input, Node 184359, Edge of Slab at Grid Line RX-4 at El. 50’ 571
Figure N-24 Relative Displacement TF, Z Input, Node 184359, Edge of Slab at Grid Line RX-4 at El. 50’ 572
Figure N-25 Relative Displacement TF, X Input, Node 185174, Mid-Span of North Slab between Grid Lines RX-4 and RX-5 at El. 50’ 573

© Copyright 2019 by NuScale Power, LLC

Figure N-26 Relative Displacement TF, Y Input, Node 185174, Mid-Span of North Slab between Grid Lines RX-4 and RX-5 at El. 50' 574
Figure N-27 Relative Displacement TF, Z Input, Node 185174, Mid-Span of North Slab between Grid Lines RX-4 and RX-5 at El. 50' 575
Figure N-28 Relative Displacement TF, X Input, Node 185623, Northeast Corner at El. 50' 576
Figure N-29 Relative Displacement TF, Y Input, Node 185623, Northeast Corner at El. 50' 577
Figure N-30 Relative Displacement TF, Z Input, Node 185623, Northeast Corner at El. 50' 578
Figure N-31 Relative Displacement TF, X Input, Node 255527, Northwest Corner at El. 75' 579
Figure N-32 Relative Displacement TF, Y Input, Node 255527, Northwest Corner at El. 75' 580
Figure N-33 Relative Displacement TF, Z Input, Node 255527, Northwest Corner at El. 75' 581
Figure N-34 Relative Displacement TF, X Input, Node 255195, Mid-Span of North Slab between Grid Lines RX-4 and RX-5 at El. 75' 582
Figure N-35 Relative Displacement TF, Y Input, Node 255195, Mid-Span of North Slab between Grid Lines RX-4 and RX-5 at El. 75' 583
Figure N-36 Relative Displacement TF, Z Input, Node 255195, Mid-Span of North Slab between Grid Lines RX-4 and RX-5 at El. 75' 584
Figure N-37 Relative Displacement TF, X Input, Node 254481, Edge of East Slab along Grid Line RX-6 at El. 75' 585
Figure N-38 Relative Displacement TF, Y Input, Node 254481, Edge of East Slab along Grid Line RX-6 at El. 75' 586
Figure N-39 Relative Displacement TF, Z Input, Node 254481, Edge of East Slab along Grid Line RX-6 at El. 75' 587
Figure N-40 Relative Displacement TF, X Input, Node 332235, Northwest Corner of Exterior Wall at El 100' 588
Figure N-41 Relative Displacement TF, Y Input, Node 332235, Northwest Corner of Exterior Wall at El 100' 589
Figure N-42 Relative Displacement TF, Z Input, Node 332235, Northwest Corner of Exterior Wall at El 100' 590
Figure N-43 Relative Displacement TF, X Input, Node 331936, Mid-Span of North Slab between Grid Lines RX-4 and RX-5 at El 100' 591
Figure N-44 Relative Displacement TF, Y Input, Node 331936, Mid-Span of North Slab between Grid Lines RX-4 and RX-5 at El 100' 592
Figure N-45 Relative Displacement TF, Z Input, Node 331936, Mid-Span of North Slab between Grid Lines RX-4 and RX-5 at El 100' 593
Figure N-46 Relative Displacement TF, X Input, Node 331222, Edge of North Slab along Grid Line RX-4 at El 100' 594
Figure N-47 Relative Displacement TF, Y Input, Node 331222, Edge of North Slab along Grid Line RX-4 at El 100' 595
Figure N-48 Relative Displacement TF, Z Input, Node 331222, Edge of North Slab along Grid Line RX-4 at El 100' 596

© Copyright 2019 by NuScale Power, LLC

Figure N-49 Relative Displacement TF, X Input, Node 331292, Edge of East Slab along Grid Line RX-6 at El 100’ 597
Figure N-50 Relative Displacement TF, Y Input, Node 331292, Edge of East Slab along Grid Line RX-6 at El 100’ 598
Figure N-51 Relative Displacement TF, Z Input, Node 331292, Edge of East Slab along Grid Line RX-6 at El 100’ 599
Figure N-52 Relative Displacement TF, X Input, Node 352669, Northwest Corner of Exterior Wall at El 125’ 600
Figure N-53 Relative Displacement TF, Y Input, Node 352669, Northwest Corner of Exterior Wall at El 125’ 601
Figure N-54 Relative Displacement TF, Z Input, Node 352669, Northwest Corner of Exterior Wall at El 125’ 602
Figure N-55 Relative Displacement TF, X Input, Node 351629, Northwest Corner of Bio Shield 603
Figure N-56 Relative Displacement TF, Y Input, Node 351629, Northwest Corner of Bio Shield 604
Figure N-57 Relative Displacement TF, Z Input, Node 351629, Northwest Corner of Bio Shield 605
Figure N-58 Relative Displacement TF, X Input, Node 352370, Mid-Span of North Slab at between Grid Lines RX-4 and RX-5 at El 125’ 606
Figure N-59 Relative Displacement TF, Y Input, Node 352370, Mid-Span of North Slab at between Grid Lines RX-4 and RX-5 at El 125’ 607
Figure N-60 Relative Displacement TF, Z Input, Node 352370, Mid-Span of North Slab at between Grid Lines RX-4 and RX-5 at El 125’ 608
Figure N-61 Relative Displacement TF, X Input, Node 351696, Northeast Corner of Bio Shield 609
Figure N-62 Relative Displacement TF, Y Input, Node 351696, Northeast Corner of Bio Shield 610
Figure N-63 Relative Displacement TF, Z Input, Node 351696, Northeast Corner of Bio Shield 611
Figure N-64 Relative Displacement TF, X Input, Node 392329, Top of Roof at Grid Line RX-1 612
Figure N-65 Relative Displacement TF, Y Input, Node 392329, Top of Roof at Grid Line RX-1 613
Figure N-66 Relative Displacement TF, Z Input, Node 392329, Top of Roof at Grid Line RX-1 614
Figure N-67 Relative Displacement TF, X Input, Node 392378, Roof Slab between Grid Lines RX-4 and RX-5 615
Figure N-68 Relative Displacement TF, Y Input, Node 392378, Roof Slab between Grid Lines RX-4 and RX-5 616
Figure N-69 Relative Displacement TF, Z Input, Node 392378, Roof Slab between Grid Lines RX-4 and RX-5 617
Figure N-70 Relative Displacement TF, X Input, Node 394770, Northeast Corner of Roof Slab 618

© Copyright 2019 by NuScale Power, LLC

Figure N-71 Relative Displacement TF, Y Input, Node 394770, Northeast Corner of Roof Slab 619
Figure N-72 Relative Displacement TF, Z Input, Node 394770, Northeast Corner of Roof Slab 620
Figure N-73 Relative Displacement TF, X Input, Node 8216, RXM-1 West Lug 621
Figure N-74 Relative Displacement TF, Y Input, Node 8216, RXM-1 West Lug 622
Figure N-75 Relative Displacement TF, Z Input, Node 8216, RXM-1 West Lug 623
Figure N-76 Relative Displacement TF, X Input, Node 8215, RXM-1 North Lug 624
Figure N-77 Relative Displacement TF, Y Input, Node 8215, RXM-1 North Lug 625
Figure N-78 Relative Displacement TF, Z Input, Node 8215, RXM-1 North Lug 626
Figure N-79 Relative Displacement TF, X Input, Node 8214, RXM-1 East Lug 627
Figure N-80 Relative Displacement TF, Y Input, Node 8214, RXM-1 East Lug 628
Figure N-81 Relative Displacement TF, Z Input, Node 8214, RXM-1 East Lug 629
Figure N-82 Relative Displacement TF, X Input, Node 1900, RXM-1 Top 630
Figure N-83 Relative Displacement TF, Y Input, Node 1900, RXM-1 Top 631
Figure N-84 Relative Displacement TF, Z Input, Node 1900, RXM-1 Top 632
Figure N-85 Relative Displacement TF, X Input, Node 49356, RXM-6 West Lug 633
Figure N-86 Relative Displacement TF, Y Input, Node 49356, RXM-6 West Lug 634
Figure N-87 Relative Displacement TF, Z Input, Node 49356, RXM-6 West Lug 635
Figure N-88 Relative Displacement TF, X Input, Node 49355, RXM-6 North Lug 636
Figure N-89 Relative Displacement TF, Y Input, Node 49355, RXM-6 North Lug 637
Figure N-90 Relative Displacement TF, Z Input, Node 49355, RXM-6 North Lug 638
Figure N-91 Relative Displacement TF, X Input, Node 49354, RXM-6 East Lug 639
Figure N-92 Relative Displacement TF, Y Input, Node 49354, RXM-6 East Lug 640
Figure N-93 Relative Displacement TF, Z Input, Node 49354, RXM-6 East Lug 641
Figure N-94 Relative Displacement TF, X Input, Node 43040, RXM-6 Top 642
Figure N-95 Relative Displacement TF, Y Input, Node 43040, RXM-6 Top 643
Figure N-96 Relative Displacement TF, Z Input, Node 43040, RXM-6 Top 644
Figure O-1 Relative Displacement TH, X Input, Node 120933, Northwest Corner on Top of Basemat 646
Figure O-2 Relative Displacement TH, Y Input, Node 120933, Northwest Corner on Top of Basemat 647
Figure O-3 Relative Displacement TH, Z Input, Node 120933, Northwest Corner on Top of Basemat 648
Figure O-4 Relative Displacement TH, X Input, Node 120978, Mid-Span of North Exterior Wall on Top of Basemat 649
Figure O-5 Relative Displacement TH, Y Input, Node 120978, Mid-Span of North Exterior Wall on Top of Basemat 650
Figure O-6 Relative Displacement TH, Z Input, Node 120978, Mid-Span of North Exterior Wall on Top of Basemat 651
Figure O-7 Relative Displacement TH, X Input, Node 121053, Northeast Corner on Top of Basemat 652
Figure O-8 Relative Displacement TH, Y Input, Node 121053, Northeast Corner on Top of Basemat 653

© Copyright 2019 by NuScale Power, LLC

Figure O-9 Relative Displacement TH, Z Input, Node 121053, Northeast Corner on Top of Basemat 654
Figure O-10 Relative Displacement TH, X Input, Node 4914, RXM 1 Floor Node under Module 655
Figure O-11 Relative Displacement TH, Y Input, Node 4914, RXM 1 Floor Node under Module 656
Figure O-12 Relative Displacement TH, Z Input, Node 4914, RXM 1 Floor Node under Module 657
Figure O-13 Relative Displacement TH, X Input, Node 46054, RXM 6 Floor Node under Module 658
Figure O-14 Relative Displacement TH, Y Input, Node 46054, RXM 6 Floor Node under Module 659
Figure O-15 Relative Displacement TH, Z Input, Node 46054, RXM 6 Floor Node under Module 660
Figure O-16 Relative Displacement TH, X Input, Node 185505, Northwest Corner at El. 50’ 661
Figure O-17 Relative Displacement TH, Y Input, Node 185505, Northwest Corner at El. 50’ 662
Figure O-18 Relative Displacement TH, Z Input, Node 185505, Northwest Corner at El. 50’ 663
Figure O-19 Relative Displacement TH, X Input, Node 182529, Mid-Span of West Slab along Grid Line RX-C at El. 50’ 664
Figure O-20 Relative Displacement TH, Y Input, Node 182529, Mid-Span of West Slab along Grid Line RX-C at El. 50’ 665
Figure O-21 Relative Displacement TH, Z Input, Node 182529, Mid-Span of West Slab along Grid Line RX-C at El. 50’ 666
Figure O-22 Relative Displacement TH, X Input, Node 184359, Edge of Slab at Grid Line RX-4 at El. 50’ 667
Figure O-23 Relative Displacement TH, Y Input, Node 184359, Edge of Slab at Grid Line RX-4 at El. 50’ 668
Figure O-24 Relative Displacement TH, Z Input, Node 184359, Edge of Slab at Grid Line RX-4 at El. 50’ 669
Figure O-25 Relative Displacement TH, X Input, Node 185174, Mid-Span of North Slab between Grid Lines RX-4 and RX-5 at El. 50’ 670
Figure O-26 Relative Displacement TH, Y Input, Node 185174, Mid-Span of North Slab between Grid Lines RX-4 and RX-5 at El. 50’ 671
Figure O-27 Relative Displacement TH, Z Input, Node 185174, Mid-Span of North Slab between Grid Lines RX-4 and RX-5 at El. 50’ 672
Figure O-28 Relative Displacement TH, X Input, Node 185623, Northeast Corner at El. 50’ 673
Figure O-29 Relative Displacement TH, Y Input, Node 185623, Northeast Corner at El. 50’ 674
Figure O-30 Relative Displacement TH, Z Input, Node 185623, Northeast Corner at El. 50’ 675

© Copyright 2019 by NuScale Power, LLC

Figure O-31 Relative Displacement TH, X Input, Node 255527, Northwest Corner at El. 75’....676
Figure O-32 Relative Displacement TH, Y Input, Node 255527, Northwest Corner at El. 75’....677
Figure O-33 Relative Displacement TH, Z Input, Node 255527, Northwest Corner at El. 75’....678
Figure O-34 Relative Displacement TH, X Input, Node 255195, Mid-Span of North Slab between Grid Lines RX-4 and RX-5 at El. 75’....679
Figure O-35 Relative Displacement TH, Y Input, Node 255195, Mid-Span of North Slab between Grid Lines RX-4 and RX-5 at El. 75’....680
Figure O-36 Relative Displacement TH, Z Input, Node 255195, Mid-Span of North Slab between Grid Lines RX-4 and RX-5 at El. 75’....681
Figure O-37 Relative Displacement TH, X Input, Node 254481, Edge of East Slab along Grid Line RX-6 at El. 75’....682
Figure O-38 Relative Displacement TH, Y Input, Node 254481, Edge of East Slab along Grid Line RX-6 at El. 75’....683
Figure O-39 Relative Displacement TH, Z Input, Node 254481, Edge of East Slab along Grid Line RX-6 at El. 75’....684
Figure O-40 Relative Displacement TH, X Input, Node 332235, Northwest Corner of Exterior Wall at El 100’....685
Figure O-41 Relative Displacement TH, Y Input, Node 332235, Northwest Corner of Exterior Wall at El 100’....686
Figure O-42 Relative Displacement TH, Z Input, Node 332235, Northwest Corner of Exterior Wall at El 100’....687
Figure O-43 Relative Displacement TH, X Input, Node 331936, Mid-Span of North Slab between Grid Lines RX-4 and RX-5 at El 100’....688
Figure O-44 Relative Displacement TH, Y Input, Node 331936, Mid-Span of North Slab between Grid Lines RX-4 and RX-5 at El 100’....689
Figure O-45 Relative Displacement TH, Z Input, Node 331936, Mid-Span of North Slab between Grid Lines RX-4 and RX-5 at El 100’....690
Figure O-46 Relative Displacement TH, X Input, Node 331222, Edge of North Slab along Grid Line RX-4 at El 100’....691
Figure O-47 Relative Displacement TH, Y Input, Node 331222, Edge of North Slab along Grid Line RX-4 at El 100’....692
Figure O-48 Relative Displacement TH, Z Input, Node 331222, Edge of North Slab along Grid Line RX-4 at El 100’....693
Figure O-49 Relative Displacement TH, X Input, Node 331292, Edge of East Slab along Grid Line RX-6 at El 100’....694
Figure O-50 Relative Displacement TH, Y Input, Node 331292, Edge of East Slab along Grid Line RX-6 at El 100’....695
Figure O-51 Relative Displacement TH, Z Input, Node 331292, Edge of East Slab along Grid Line RX-6 at El 100’....696
Figure O-52 Relative Displacement TH, X Input, Node 352669, Northwest Corner of Exterior Wall at El 125’....697

© Copyright 2019 by NuScale Power, LLC

Figure O-53 Relative Displacement TH, Y Input, Node 352669, Northwest Corner of Exterior Wall at El 125' 698
Figure O-54 Relative Displacement TH, Z Input, Node 352669, Northwest Corner of Exterior Wall at El 125' 699
Figure O-55 Relative Displacement TH, X Input, Node 351629, Northwest Corner of Bio Shield 700
Figure O-56 Relative Displacement TH, Y Input, Node 351629, Northwest Corner of Bio Shield 701
Figure O-57 Relative Displacement TH, Z Input, Node 351629, Northwest Corner of Bio Shield 702
Figure O-58 Relative Displacement TH, X Input, Node 352370, Mid-Span of North Slab at between Grid Lines RX-4 and RX-5 at El 125' 703
Figure O-59 Relative Displacement TH, Y Input, Node 352370, Mid-Span of North Slab at between Grid Lines RX-4 and RX-5 at El 125' 704
Figure O-60 Relative Displacement TH, Z Input, Node 352370, Mid-Span of North Slab at between Grid Lines RX-4 and RX-5 at El 125' 705
Figure O-61 Relative Displacement TH, X Input, Node 351696, Northeast Corner of Bio Shield 706
Figure O-62 Relative Displacement TH, Y Input, Node 351696, Northeast Corner of Bio Shield 707
Figure O-63 Relative Displacement TH, Z Input, Node 351696, Northeast Corner of Bio Shield 708
Figure O-64 Relative Displacement TH, X Input, Node 392329, Top of Roof at Grid Line RX-1 709
Figure O-65 Relative Displacement TH, Y Input, Node 392329, Top of Roof at Grid Line RX-1 710
Figure O-66 Relative Displacement TH, Z Input, Node 392329, Top of Roof at Grid Line RX-1 711
Figure O-67 Relative Displacement TH, X Input, Node 392378, Roof Slab between Grid Lines RX-4 and RX-5 712
Figure O-68 Relative Displacement TH, Y Input, Node 392378, Roof Slab between Grid Lines RX-4 and RX-5 713
Figure O-69 Relative Displacement TH, Z Input, Node 392378, Roof Slab between Grid Lines RX-4 and RX-5 714
Figure O-70 Relative Displacement TH, X Input, Node 394770, Northeast Corner of Roof Slab 715
Figure O-71 Relative Displacement TH, Y Input, Node 394770, Northeast Corner of Roof Slab 716
Figure O-72 Relative Displacement TH, Z Input, Node 394770, Northeast Corner of Roof Slab 717
Figure O-73 Relative Displacement TH, X Input, Node 8216, RXM-1 West Lug 718
Figure O-74 Relative Displacement TH, Y Input, Node 8216, RXM-1 West Lug 719
Figure O-75 Relative Displacement TH, Z Input, Node 8216, RXM-1 West Lug 720
Figure O-76 Relative Displacement TH, X Input, Node 8215, RXM-1 North Lug 721
Figure O-77 Relative Displacement TH, Y Input, Node 8215, RXM-1 North Lug 722

© Copyright 2019 by NuScale Power, LLC

Figure O-78 Relative Displacement TH, Z Input, Node 8215, RXM-1 North Lug 723
Figure O-79 Relative Displacement TH, X Input, Node 8214, RXM-1 East Lug..... 724
Figure O-80 Relative Displacement TH, Y Input, Node 8214, RXM-1 East Lug..... 725
Figure O-81 Relative Displacement TH, Z Input, Node 8214, RXM-1 East Lug..... 726
Figure O-82 Relative Displacement TH, X Input, Node 1900, RXM-1 Top 727
Figure O-83 Relative Displacement TH, Y Input, Node 1900, RXM-1 Top 728
Figure O-84 Relative Displacement TH, Z Input, Node 1900, RXM-1 Top 729
Figure O-85 Relative Displacement TH, X Input, Node 49356, RXM-6 West Lug..... 730
Figure O-86 Relative Displacement TH, Y Input, Node 49356, RXM-6 West Lug..... 731
Figure O-87 Relative Displacement TH, Z Input, Node 49356, RXM-6 West Lug..... 732
Figure O-88 Relative Displacement TH, X Input, Node 49355, RXM-6 North Lug 733
Figure O-89 Relative Displacement TH, Y Input, Node 49355, RXM-6 North Lug 734
Figure O-90 Relative Displacement TH, Z Input, Node 49355, RXM-6 North Lug 735
Figure O-91 Relative Displacement TH, X Input, Node 49354, RXM-6 East Lug..... 736
Figure O-92 Relative Displacement TH, Y Input, Node 49354, RXM-6 East Lug..... 737
Figure O-93 Relative Displacement TH, Z Input, Node 49354, RXM-6 East Lug..... 738
Figure O-94 Relative Displacement TH, X Input, Node 43040, RXM-6 Top 739
Figure O-95 Relative Displacement TH, Y Input, Node 43040, RXM-6 Top 740
Figure O-96 Relative Displacement TH, Z Input, Node 43040, RXM-6 Top 741
Figure P-1 RXM #1 West Lug, Force Transfer Functions 743
Figure P-2 RXM #1 North Lug, Force Transfer Functions..... 744
Figure P-3 RXM #1 East Lug, Force Transfer Functions 745
Figure P-4 RXM #6 West Lug, Force Transfer Functions 746
Figure P-5 RXM #6 North Lug, Force Transfer Functions..... 747
Figure P-6 RXM #6 East Lug, Force Transfer Functions 748
Figure Q-1 RXM #1 West Lug, Force Time Histories 750
Figure Q-2 RXM #1 North Lug, Force Time Histories..... 751
Figure Q-3 RXM #1 East Lug, Force Time Histories 752
Figure Q-4 RXM #6 West Lug, Force Time Histories 753
Figure Q-5 RXM #6 North Lug, Force Time Histories..... 754
Figure Q-6 RXM #6 East Lug, Force Time Histories 755
Figure R-1 Base Support for RXM 1, Force Fx TF 757
Figure R-2 Base Support for RXM 1, Force Fy TF 758
Figure R-3 Base Support for RXM 1, Force Fz TF 759
Figure R-4 Base Support for RXM 1, Moment Mx TF 760
Figure R-5 Base Support for RXM 1, Moment My TF 761
Figure R-6 Base Support for RXM 1, Moment Mz TF 762
Figure R-7 Base Support for RXM 6, Force Fx TF 763
Figure R-8 Base Support for RXM 6, Force Fy TF 764
Figure R-9 Base Support for RXM 6, Force Fz TF 765
Figure R-10 Base Support for RXM 6, Moment Mx TF 766
Figure R-11 Base Support for RXM 6, Moment My TF 767
Figure R-12 Base Support for RXM 6, Moment Mz TF 768
Figure S-1 Base Support for RXM 1, Force Fx Time Histories..... 770
Figure S-2 Base Support for RXM 1, Force Fy Time Histories..... 771

© Copyright 2019 by NuScale Power, LLC

Figure S-3 Base Support for RXM 1, Force Fz Time Histories....772
Figure S-4 Base Support for RXM 1, Moment Mx Time Histories....773
Figure S-5 Base Support for RXM 1, Moment My Time Histories....774
Figure S-6 Base Support for RXM 1, Moment Mz Time Histories....775
Figure S-7 Base Support for RXM 6, Force Fx Time Histories....776
Figure S-8 Base Support for RXM 6, Force Fy Time Histories....777
Figure S-9 Base Support for RXM 6, Force Fz Time Histories....778
Figure S-10 Base Support for RXM 6, Moment Mx Time Histories....779
Figure S-11 Base Support for RXM 6, Moment My Time Histories....780
Figure S-12 Base Support for RXM 6, Moment Mz Time Histories....781

© Copyright 2019 by NuScale Power, LLC

Abstract

This report describes a frequency domain soil-structure-fluid interaction seismic analysis methodology using the Soil Library concept. A Soil Library consists of a pre-calculated soil substructure that is used to perform coupled soil-structure-fluid interaction analyses of nuclear structures using commercial finite element software.

Nuclear power plants include structures with coupled soil, structure and fluid interaction behaviors. A single analysis tool that is capable of evaluating soil structure interaction (SSI) while incorporating structure fluid interaction along with operating load analyses, is not currently available. Thus, the analysis of these structures is often performed piecewise in labor-intensive steps.

The seismic analysis (Soil Library) methodology described in this report considers an alternate work flow. “SASSI” (the System for Analysis of Soil-Structure Interaction) is used to generate soil impedances and seismic load vectors. The impedances and load vectors are imported to a commercial finite element method (FEM) code as a soil substructure. The commercial FEM code then combines the soil substructure with a building substructure, a fluid substructure and equipment substructures, as needed. The commercial FEM code analyzes the integrated soil-structure-fluid-equipment system.

There are efficiencies to be gained from this integrated analysis work flow as described herein.

© Copyright 2019 by NuScale Power, LLC

Executive Summary of Topical Report TR-0118-58005

This NuScale topical report presents a methodology for performing the seismic analysis for nuclear power plant structures, systems, and components (SSC), to demonstrate compliance with 10 CFR 50 General Design Criteria (GDC) 2, and NUREG-0800 Standard Review Plan Section 3.7.2 “Seismic System Analysis.”

The purpose of this report is to provide an alternate seismic methodology for use by an applicant or licensee to perform seismic analyses of complex, interacting structures, soils, fluid systems, and major mechanical components.

Typically, structural analyses of buildings and major mechanical components are performed using a commercial Finite Element Method (FEM) code, such as ANSYS. Commercial general purpose finite element codes have element and material libraries which include the ability to consider structural, thermal and fluid loadings. However, commercial FEM codes do not have the ability to effectively perform to the level of soil-structure interaction analyses required for seismic evaluation of complex interacting structures.

Nuclear power plants include large, detailed structures with coupled soil, structure and fluid interaction behaviors. A single analysis tool that is capable of evaluating soil structure interaction (SSI), while incorporating structure fluid interaction along with operating load analyses, is not available. Thus, the analysis of these structures is typically performed piecewise in labor-intensive steps.

SSI is required per NUREG-0800, Standard Review Plan Section 3.7.2 “Seismic System Analysis” and is typically performed using System for Analysis of Soil-Structure Interaction (SASSI). While SASSI has capabilities for developing soil impedances, it has a limited collection of structural elements and does not have an integrated environment for considering operating loads, thermal loads, or detailed fluid interaction. Furthermore, most versions of SASSI have size limitations which require the use of simplified analysis models.

The traditional analysis work flow is to develop and analyze a simplified seismic model for SSI analyses and to export response parameters to a detailed building model, which is then analyzed using a commercial FEM code. Building response parameters are then exported to equipment analyses. Thus, multiple separate models must be maintained as the seismic design evolves.

The seismic analysis methodology described is this report simplifies this process by utilizing a single analysis model rather than multiple separate models, thus eliminating assumptions/boundary conditions at individual model interfaces. SASSI is used to generate soil impedances and seismic load vectors. The impedances and load vectors are imported to a commercial FEM code as a soil substructure. The FEM code then combines the soil substructure with the building substructure, a fluid substructure, and equipment substructures,

© Copyright 2019 by NuScale Power, LLC

as needed. The commercial FEM code then performs the analysis of the integrated soil-structure-fluid equipment system. As a result, analysis run times are reduced and flexibility is improved to generate seismic evaluation results.

The proposed methodology extends the capability to analyze complex structural dynamic behavior beyond the capability provided by the SASSI computer code. For example, the ANSYS acoustic element permits a more accurate representation of fluid-structure interaction phenomena than that obtained using the library of structural element types provided by SASSI.

Using the element library and sub-structuring capabilities of the ANSYS computer code, more detailed and realistic models are practical, resulting in increased accuracy.

Several example problems are used to demonstrate the improved analysis work flow using ANSYS with the Soil Library and results are compared to a typical SSI solution developed using SASSI.

© Copyright 2019 by NuScale Power, LLC

1.0 Introduction

1.1 Purpose

The purpose of this topical report is to develop a frequency domain soil-structure-fluid interaction seismic analysis methodology that can be used with a commercially available finite element program to perform seismic analyses of a coupled soil-structure-fluid system. A second purpose is to validate the application of this Soil Library methodology using several example problems. The example problems validate the Soil Library methodology by demonstrating that it is functionally equivalent to a SASSI analysis.

The results of this analytical procedure provide design parameters for the seismic qualification of nuclear safety-related systems, structures and components.

1.2 Scope

The frequency domain soil-structure-fluid interaction seismic analysis methodology discussed in this report has the following attributes:

Equivalent linear-elastic analysis: Material properties are assumed to be linear-elastic during the analysis. Nonlinear material properties are considered by using equivalent linear stiffness and an effective damping. This applies to both soil and structural properties. Equivalent linear soil properties are discussed in ASCE 4-2016 (Reference 9.1.2). They consist of degraded elastic stiffness and an effective damping ratio, and are typically developed using SHAKE (Reference 9.1.18). Similarly, structural materials such as reinforced concrete may use an effective cracked stiffness and effective damping per ASCE 43-05 (Reference 9.1.3).

The behavior of boundary conditions and constraints is linear. Thus, contact, liftoff, and sliding are not directly modeled. ASCE 4-2016 considers contact in a linear system by running elastic bounding cases and enveloping results. Similarly, sliding between an embedded structure and adjacent soil is addressed by enveloping analyses with the soil degree-of-freedom (DOF) parallel to the wall plane either free or constrained to the wall.

Superposition of elastically computed responses in different directions along with elastically computed gravity loadings is used. Thus, the seismic response in the X, Y and Z directions is developed independently and combined with gravity loads using linear load combinations.

Frequency domain analysis: The soil impedance is frequency dependent, thus the seismic analyses are performed in the frequency domain. Complex frequency dependent transfer functions are developed to describe the response of both structures and acoustic fluids.

© Copyright 2019 by NuScale Power, LLC

The energy dissipation of structural elements is considered using structural or complex damping. Viscous damping of the fluid is also included.

Complex response analysis is used to obtain time domain response to transient loadings such as seismic ground motion.

Functionally equivalent to SASSI: This analysis approach is designed to be functionally equivalent to a SASSI analysis. Thus, the soil impedance is developed using SASSI. The seismic load vectors representing vertically propagating shear and P-waves with a control motion at different layers are also developed using SASSI. The transfer function interpolation methodology used in SASSI is incorporated in the ANSYS solution.

1.3 Abbreviations and Definitions

The abbreviations used in this report are shown in Table 1-1. Definitions of common terms used in the report are shown in Table 1-2.

Table 1-1 Abbreviations

Term	Definition
ASME	American Society of Mechanical Engineers
DOF	Degree-of-Freedom
FEM	Finite Element Method
FFT	Fast Fourier Transform
FSI	Fluid Structure Interaction
GDC	General Design Criteria
ISRS	In-Structure Response Spectra
LWR	Light Water Reactor
NRC	Nuclear Regulatory Commission
RG	Regulatory Guide
RPV	Reactor Pressure Vessel
RXM	reactor power module
SASSI	System for Analysis of Soil-Structure Interaction
SSI	Soil-Structure Interaction
TF	Transfer Functions

© Copyright 2019 by NuScale Power, LLC

Table 1-2 Definitions

Term	Definition
Building Substructure	Model representing the building mass and stiffness
Control Point	Location where the seismic input is defined. Typically the surface of the free field or the free-field layer at the elevation of the building foundation.
Dynamic Stiffness	The frequency-dependent resistance of a linear elastic system to a harmonic (sinusoidal) input motion. It is represented using complex notation to describe the amplitude and phase calculated from the ratio of force to displacement.
Equipment Substructure	Model representing the mass and stiffness of a particular component. There may be multiple equipment substructures that interact with each other, fluid substructures, and the building substructure.
Excavated (Soil) Impedance	Soil impedance at the interaction nodes minus the dynamic stiffness of the excavated soil volume.
Fluid Substructure	Model representing the mass, viscous damping, stiffness, and fluid-structure coupling terms of the acoustic fluid elements. There may be multiple fluid substructures that interact with each other, equipment substructures, and the building substructure.
Reduced Excavated (Soil) Impedance	Excavated Impedance in which the degrees of freedom of the interaction nodes not in the basement boundary are condensed out.
Soil Impedance	The dynamic stiffness of soil supporting a foundation. Impedance includes stiffness, inertial effects, radiation damping, and material damping. Soil impedance is usually frequency dependent and has a complex value.
Soil Library	A collection of soil impedance and seismic load vectors for a soil substructure computed at different frequencies and different soil layered halfspace properties.
Soil Substructure	Model representing the soil impedance of a layered elastic halfspace with an excavation.

© Copyright 2019 by NuScale Power, LLC

Term	Definition
Substructure	Submodel that can be combined with other submodels. The term substructure does not imply that an ANSYS superelement is utilized.
Transfer Function	Mathematical relationship that describes the response of one part of a structure given the input at a control point.
Tape1, Tape2, Tape3, Tape4	SASSI data files
Tape8	SASSI data file that is used to store transfer functions

© Copyright 2019 by NuScale Power, LLC

2.0 Background

Nuclear power plants include structures with coupled soil, structure and fluid interaction behaviors. A single analysis tool that is capable of performing SSI while incorporating structure fluid interaction along with operating load analyses is not currently available. Thus, the analysis of these structures is often performed piecewise in the following labor-intensive steps.

Soil structure interaction is required and is typically performed using SASSI. While SASSI has capabilities for developing soil impedances, it has a limited collection of structural elements and does not have an integrated environment for considering operating loads, thermal loads, nor detailed fluid interaction. Furthermore, most versions of SASSI have significant size limitations which require the use of simplified analysis models.

Seismic analyses of the safety-related nuclear structures and major mechanical components are often performed using a commercial FEM code, such as ANSYS. Commercial general purpose finite element codes have element and material libraries which include the ability to consider structural, thermal and fluid loadings. However, commercial FEM codes do not have the ability to perform the same level of soil-structure interaction analyses as SASSI.

Thus, the traditional seismic analysis workflow is to develop and analyze a simplified seismic model for SSI analyses and to export response parameters to a detailed building model that is then analyzed using a commercial FEM code. Building response parameters are then exported to equipment analyses. Thus, multiple separate models must be maintained as the design evolves.

The Soil Library proposed in this report considers an alternate work flow. SASSI is used to generate soil impedances and seismic load vectors. The impedances and load vectors are imported to a commercial FEM code as a soil substructure. The commercial FEM code combines the soil substructure with a building substructure, a fluid substructure and equipment substructures, as needed. The commercial FEM code then analyzes the integrated soil-structure-fluid-equipment system.

There are significant efficiencies to be gained from this integrated analysis workflow such as:

- It extends analysis capabilities by allowing the full suite of modern FEM elements, materials and constraints to be used in the analysis. As an example, acoustic elements can be included which allows coupled soil-structure-fluid interaction analysis. Another example is that major equipment can be included in the analysis by using substructuring.

© Copyright 2019 by NuScale Power, LLC

- It reduces SSI analysis costs. Soil impedance and seismic load vectors are calculated once for a soil type, while the structure may be subject to multiple modifications. Additionally, the library can contain impedances at different soil sites simplifying the design of standard plants.

- It streamlines the analysis process by using the same model for both operational and seismic loads. This eliminates the need to develop, maintain, and properly document, simplified SSI analysis models in an environment with an evolving design.

Section 4.0 presents the Soil Library solution strategy. The theoretical basis for the seismic analysis is discussed in Section 5.0. Section 6.0 contains example problems that demonstrate the application of the Soil Library. Section 7.0 discusses the Soil Library implementation. Summary and conclusions are contained in Section 8.0.

The appendices contain a discussion of ancillary analysis issues and detailed responses for the analyses performed for the example problems.

2.1 Regulatory Requirements

2.1.1 10 CFR 50 Appendix A GDC 2

In accordance with General Design Criterion (GDC) 2, nuclear power unit structures, systems, and components important to safety shall be designed to withstand the effects of natural phenomena such as earthquakes, tornadoes, hurricanes, floods, tsunami, and seiches without loss of capability to perform their safety functions.

2.1.2 10 CFR 50 Appendix S

10 CFR 50 Appendix S requires applicants to design nuclear power plant structures, systems, and components important to safety to withstand the effects of natural phenomena, such as earthquakes, without the loss of capability to perform their safety function.

© Copyright 2019 by NuScale Power, LLC

3.0 Assumptions and Software

3.1 Assumptions

The analysis methodology is based on the assumptions listed below. These are typical assumptions for a seismic analysis of nuclear structures and are discussed in ASCE 4. These general assumptions do not require validation.

1. Material properties are linear-elastic during the analysis.

2. The behavior of boundary conditions and constraints is linear.

3. The seismic load is represented by vertically propagating shear and compression waves.

3.2 Software

The following safety-significant software is used in this evaluation:

- SDE-SASSI v2.1 by Carl J. Costantino and Associates, LLC (Reference 9.1.6)

- The general purpose finite element program ANSYS, Version 18.1 (Reference 9.1.26) was used in this evaluation.

The following nonsafety-significant software is used in this evaluation:

- Mathematica v11 by Wolfram Research Inc. (Reference 9.1.12)

  Mathematica was used to perform the numerical studies contained in Appendix A through Appendix C. Mathematica was not used to calculate structural responses discussed in Section 6.0.

© Copyright 2019 by NuScale Power, LLC

4.0 Solution Strategy

This section presents an overview of the solution strategy. The coupled soil-structure-fluid interaction problem consists of a single model assembled from building-fluid sub-models and soil substructure and is solved in the frequency domain. The solution for a given structural configuration uses pre-calculated soil impedance and load vectors, stored in a Soil Library, to facilitate multiple efficient structural evaluations for a given soil site.

SASSI is used to develop the soil impedances and load vectors in the Soil Library and is used to solve seismic responses. An ANSYS frequency domain solver, which is functionally equivalent to SASSI, is also presented. Given the rich element library, post-processing capability and the ability to integrate with other load cases, the ANSYS solver is the analysis tool selected for structure and equipment evaluations.

4.1 Substructuring

The coupled soil-structure-fluid interaction problem is composed of the following four substructures and is shown schematically in Figure 4-1.

Soil substructure: The soil substructure is the impedance of an elastic half-space including the effects of an excavation. The soil substructure is developed in SASSI and the soil impedance matrix and load vector, at predetermined frequencies, are stored, as substructures, in a Soil Library for later use.

Building substructure: The building substructure consists of the building model and may also include soil backfill between the soil substructure and the building walls. The building model is developed in ANSYS utilizing a modern finite element library.

Equipment substructure(s): Major equipment substructures with sufficient mass to interact with the building response is included in the analysis. The equipment substructures are developed in ANSYS.

Fluid substructure: The fluid substructure consists of acoustic elements representing the fluid coupling between the building and equipment. The fluid substructure is also developed in ANSYS.

This evaluation focuses on the soil substructure. The building, equipment, and fluid substructures are lumped together for convenience.

© Copyright 2019 by NuScale Power, LLC

4.2 Frequency Domain Solution

Elastic soil impedances are frequency dependent; thus, soil structure interaction (SSI) problems are typically solved in the frequency domain. Fluid-structure interaction analyses using acoustic elements are viscoelastic and can be solved in either the time or the frequency domain. Thus, the coupled soil-structure-fluid interaction problem is solved in the frequency domain and incorporates frequency dependent soil impedances.

The quality of a frequency domain analysis is dependent on which frequencies are computed and which are interpolated. A complex building-fluid system, with interacting structures, equipment and fluid requires a large number of computed frequencies representing structural, equipment and fluid natural frequencies. On the other hand, the soil impedance of a relatively uniform site varies slowly with frequency.

4.3 Soil Library

SASSI develops the excavated soil impedance by assembling the soil flexibility matrix for a layered half-space, inverting the flexibility matrix to obtain soil impedance for the layered half-space, and deducting the excavated soil volume as shown in Figure 4-2.

The numerical process of inverting the layered half-space flexibility matrix represents much of the SASSI computational effort. In a typical analysis, there are numerous building model iterations performed while the excavated soil impedance remains constant. The Soil Library consist of a series of pre-calculated excavated soil impedance super-elements that can be used with different building models, as shown schematically in Figure 4-3.

As discussed above, the soil impedance and seismic load vectors are frequency dependent. At a given analysis frequency, the soil impedance and load vectors are calculated directly using SASSI.

4.4 Analysis Tools

The analysis tools used to develop the Soil Library and to solve the dynamic response in the frequency domain are discussed below.

4.4.1 Soil Library Development

The soil impedance matrices and load vectors are calculated using SDE-SASSI Version 2.1 (Reference 9.1.6) as shown in Figure 4-4. SASSI HOUSE is used to generate the stiffness of the excavated soil model. Note that HOUSE uses a mixed lumped and consistent mass formulation that has better convergence characteristics than either the

© Copyright 2019 by NuScale Power, LLC

lumped or consistent mass formulations alone. The response of the layered halfspace is solved using SASSI SITE. SASSI POINT3 is used to develop flexibilities for the axisymmetric/asymmetric point response model.

The flexibilities are assembled and inverted in SASSI ANALYS yielding a soil impedance for the layered half space. The excavated soil stiffness is removed from the layered halfspace impedance using the SASSI Direct Method[1]. Internal soil impedance degrees of freedom (DOF) which do not interact with the building are condensed out of the impedance matrix and load vectors to reduce the impedance library file size. The condensation occurs at each frequency and does not affect the results. The reduced impedance matrix and load vectors are stored in the Soil Library.

4.4.2 ANSYS Solver

A substructure containing the building, fluid substructure, and any equipment substructures is developed in ANSYS. In Figure 4-5 this substructure is referred to as the *Building Substructure*. For a given frequency *i*, the impedance matrix and load vector are obtained from the Soil Library and combined with the dynamic stiffness of the building substructure. ANSYS is then used to solve for the frequency domain transfer function at frequency *i*. When sufficient calculated frequencies are developed, ANSYS is used to assemble and interpolate the transfer functions using the same interpolation algorithm as SASSI. The time domain solution is obtained by Complex Response Analysis using the same method that SASSI uses. ANSYS has a suite of post-processing tools which are then used to evaluate the time domain results. Note that the ANSYS frequency domain solution, using the Soil Library, is functionally equivalent to the SASSI frequency domain solution.

Implementation of the ANSYS solver is included in the current discussion to demonstrate how the soil impedance library is ultimately used. Results from the ANSYS solver are included in the example problems discussed in Section 6.0 to demonstrate functional equivalency between the ANSYS and SASSI solvers.

[1] Each node in the excavated soil model is attached to the corresponding interaction node and the excavated soil model does not have any free nodes. The SASSI Subtraction, Extended Subtraction, or Modified Subtraction methods are not used.

© Copyright 2019 by NuScale Power, LLC

4.4.3 SASSI Solver

ANSYS is used to export the building substructure, discussed in the preceding section, in the form of mass, damping and stiffness matrices. These matrices are combined with the soil impedance matrix and seismic load vectors at a given frequency, and are used in the solution of the transfer function using SDE-SASSI Anal16, as shown in Figure 4-6. The transfer functions are stored on a series of Tape8s and the individual frequency Tape 8s are combined together and post-processed as in traditional SASSI analysis.

Alternately, the building model can be assembled using the SASSI HOUSE Module as shown in Figure 4-7. The building stiffness is combined with the soil impedance matrix and seismic load vectors, and the analysis proceeds as discussed above. Note that many of the elements available in ANSYS are considered to be superior to the elements implemented in SASSI.

The SASSI solver is used in this study to provide a check on the ANSYS solver. In production, either the ANSYS or SASSI solver could be used. The extensive ANSYS tools for model assembly and post-processing makes ANSYS the preferred solver.

Traditional SASSI Solution

The traditional SASSI solution is shown schematically in Figure 4-8. The building and excavated soil models are contained in a single model and input to HOUSE. This is in contrast with the Soil Library development in Figure 4-4, where only the excavated soil is input to HOUSE. The soil impedance is developed at each analysis frequency and combined with the excavated soil and building models. Transfer functions are computed and stored on Tape8. The SASSI MOTION module, and others, are used to provide time domain results.

© Copyright 2019 by NuScale Power, LLC

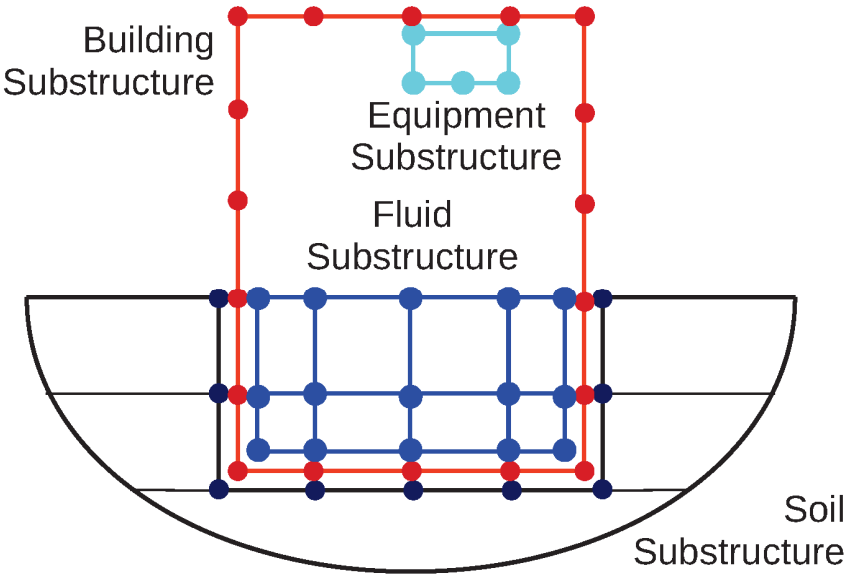

Figure 4-1 Idealized soil, structure, and fluid Substructures

© Copyright 2019 by NuScale Power, LLC

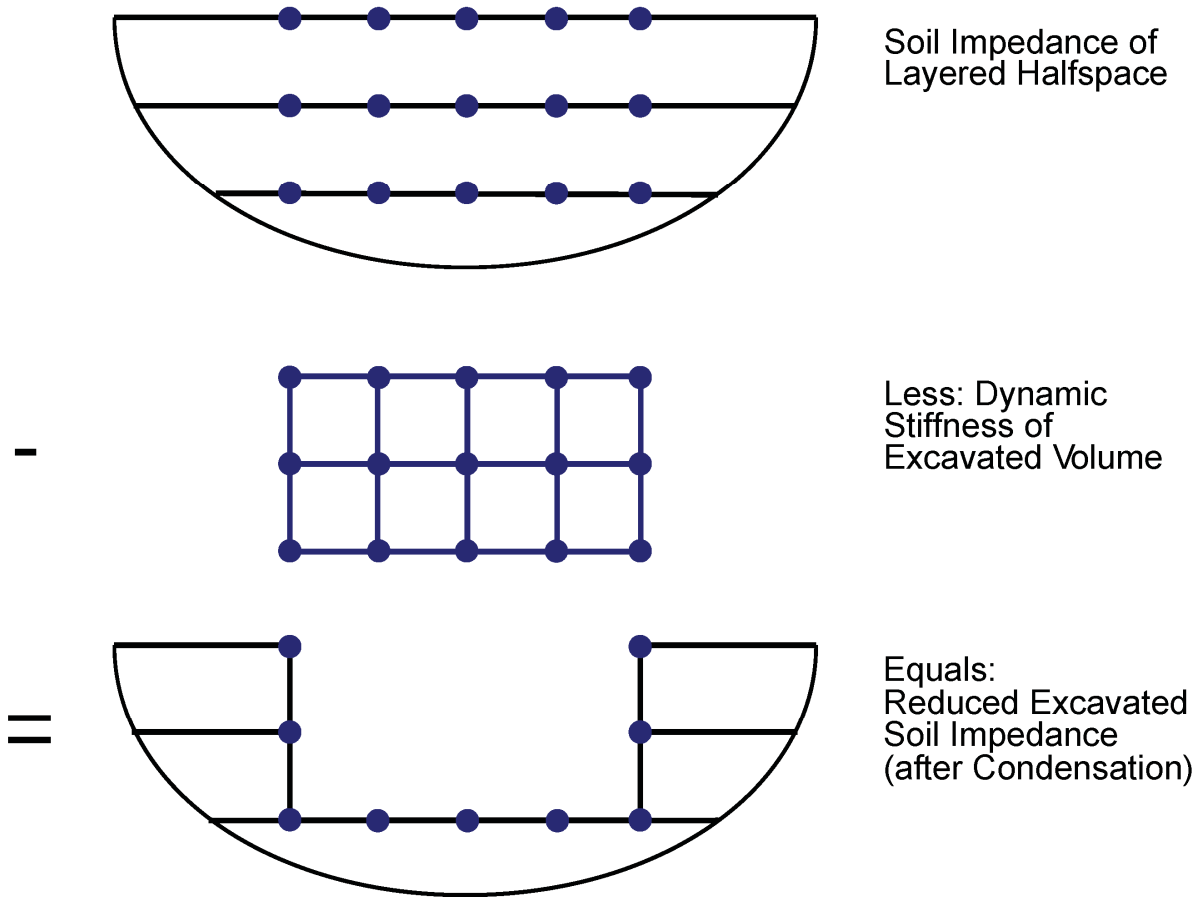

Figure 4-2 Reduced excavated soil impedance

© Copyright 2019 by NuScale Power, LLC

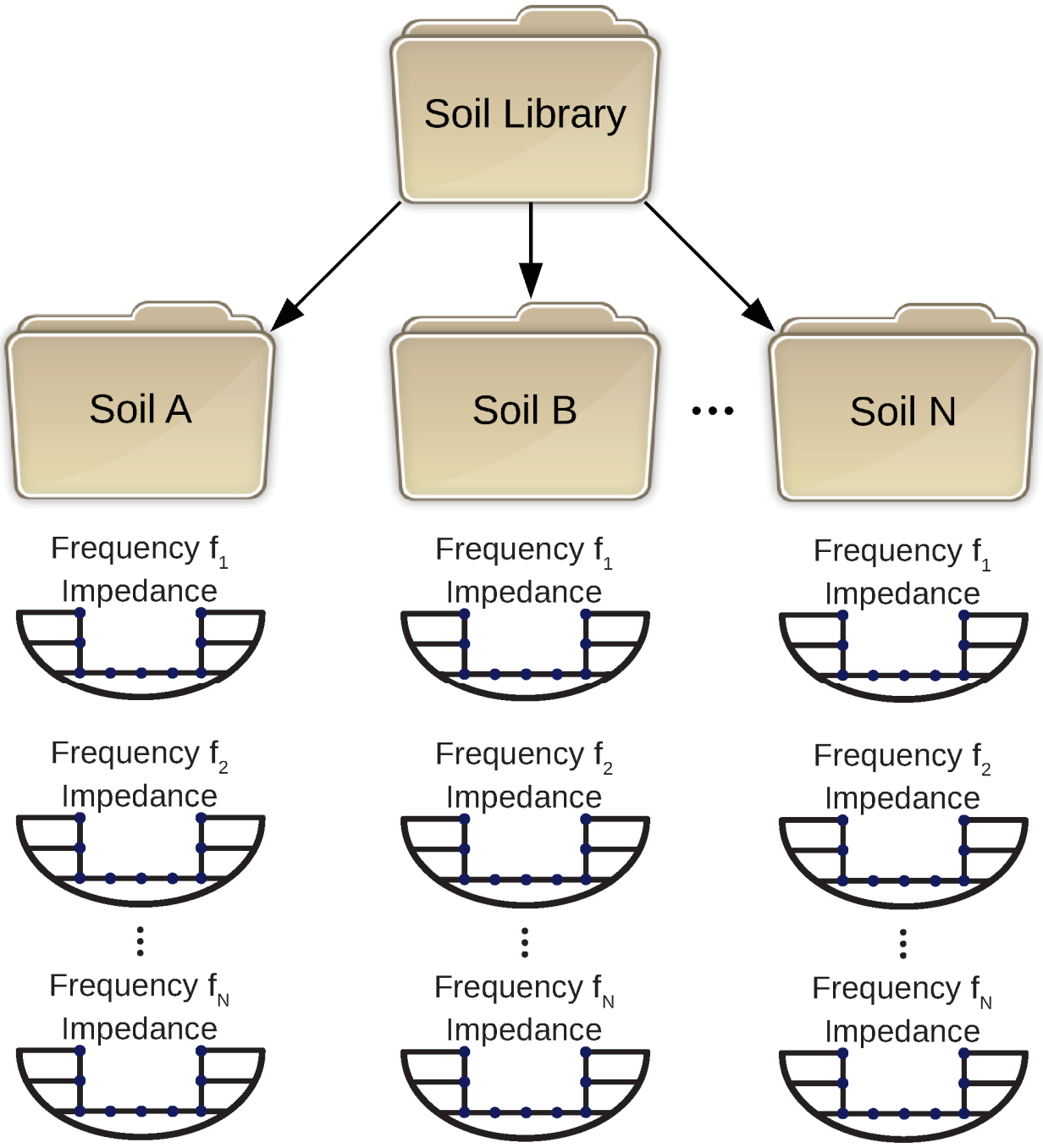

Figure 4-3 Soil impedance library

© Copyright 2019 by NuScale Power, LLC

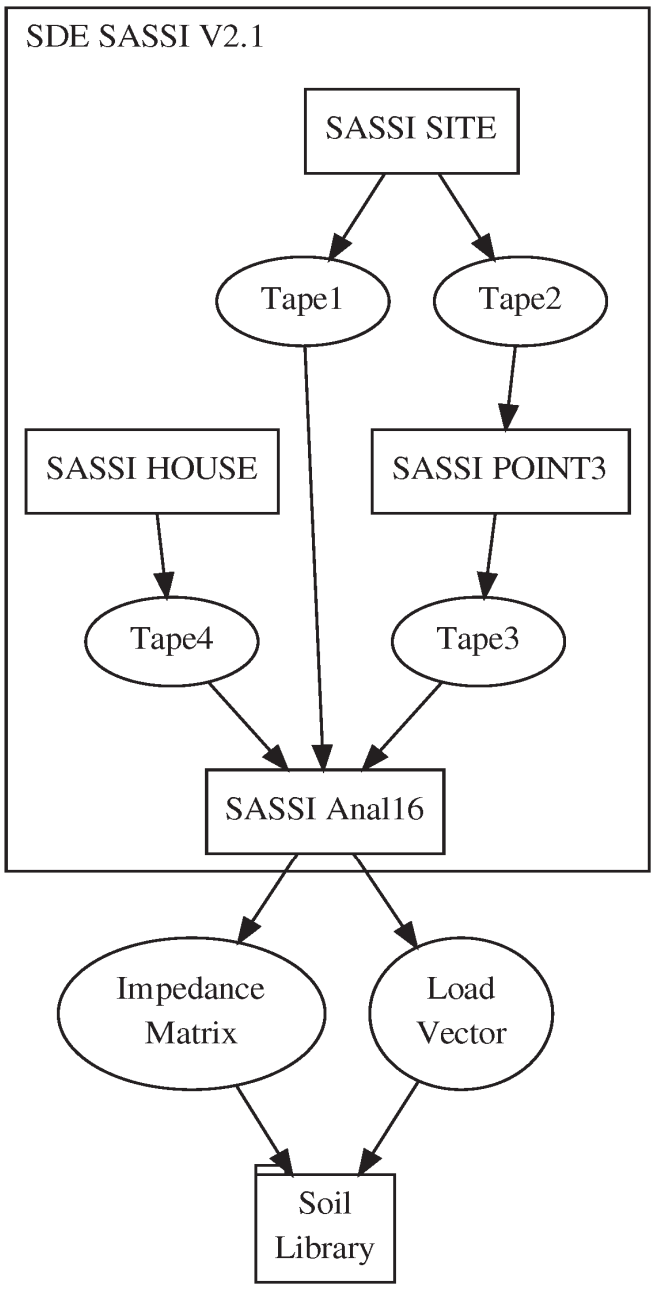

Figure 4-4 SASSI solution for soil impedance and load vector at frequency *i*

© Copyright 2019 by NuScale Power, LLC

{{

}}2(a),(c)

Figure 4-5 ANSYS frequency domain solution

© Copyright 2019 by NuScale Power, LLC

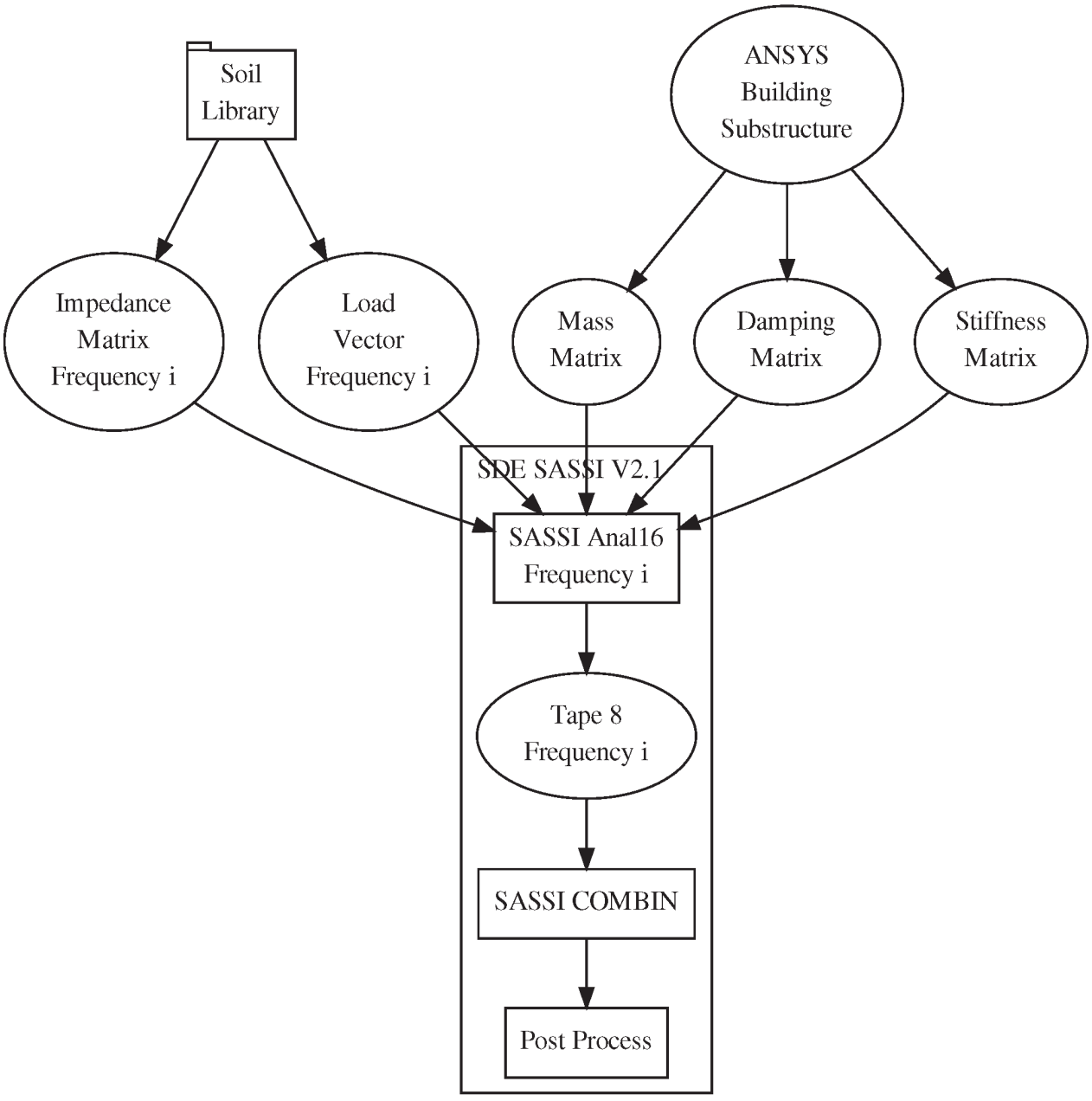

Figure 4-6 SASSI frequency domain solution using Soil Library and ANSYS building model

© Copyright 2019 by NuScale Power, LLC

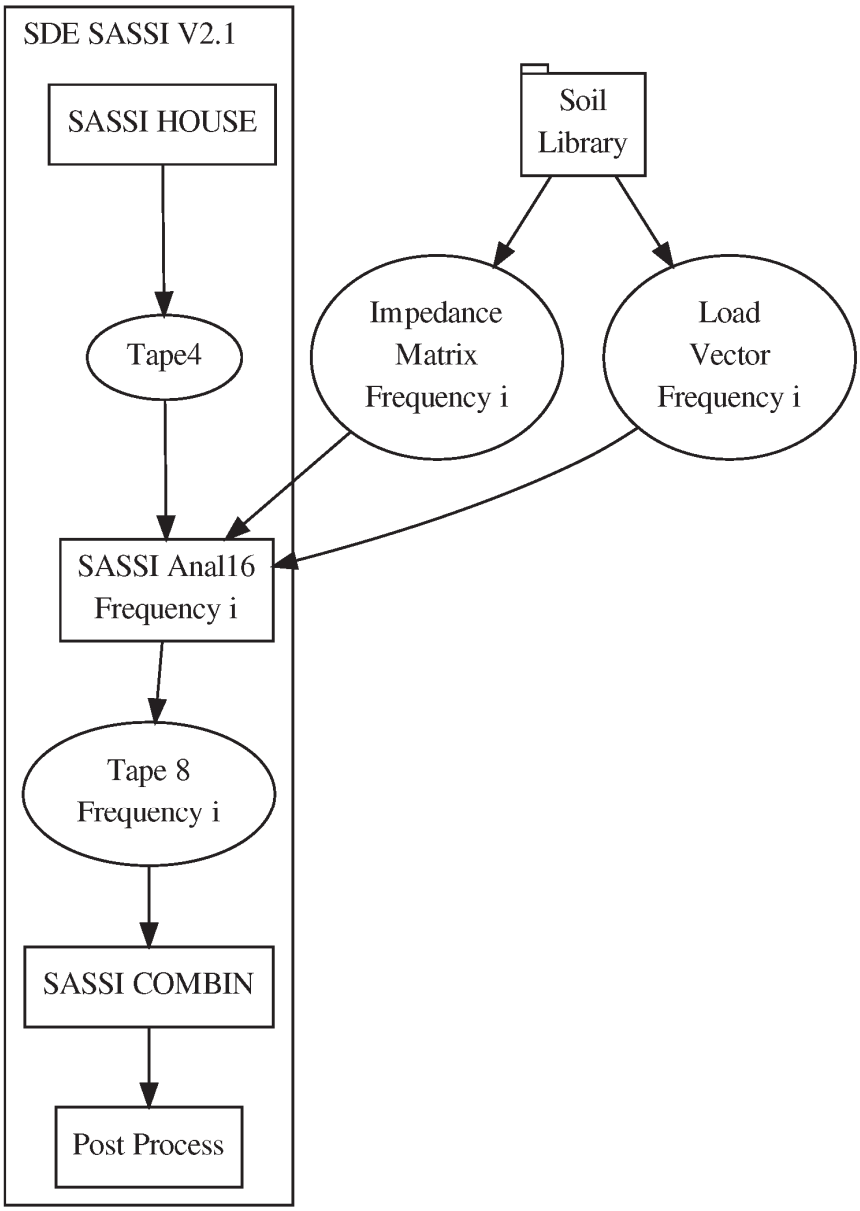

Figure 4-7 SASSI frequency domain solution using Soil Library and HOUSE building model

© Copyright 2019 by NuScale Power, LLC

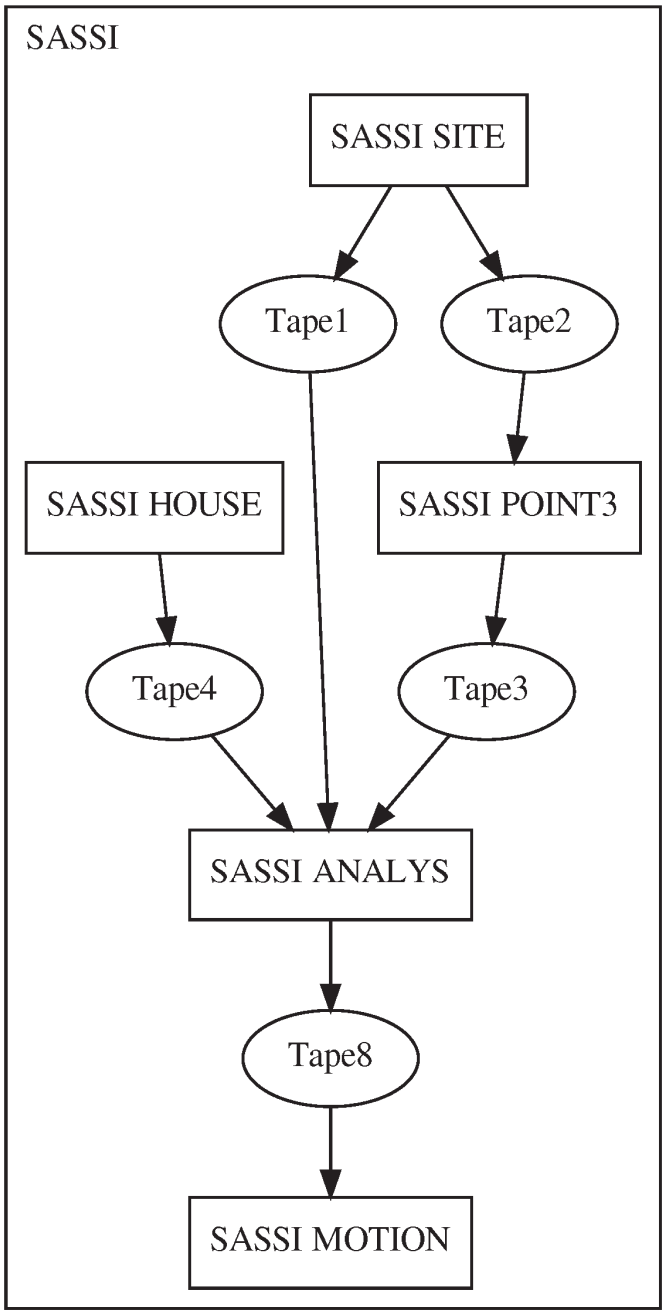

Figure 4-8 Traditional SASSI frequency domain solution

© Copyright 2019 by NuScale Power, LLC

5.0 Theoretical Basis

The theoretical basis for frequency domain analysis is discussed below to provide a framework to describe the proposed analysis.

5.1 Analysis Background

The following describe portions of the SASSI frequency domain solution required to implement the Soil Library in ANSYS. Enhancements to the SASSI analysis methodology are discussed in Section 5.2 and 5.3.

5.1.1 Equation of Motion

The equation of motion in the time domain for a damped linear elastic system is typically expressed as:

$$M\ddot{X}(t) + C\dot{X}(t) + KX(t) = F(t) \qquad \text{Equation 5-1}$$

where M , C, and K are the mass, viscous damping and stiffness matrices, t is time, $X(t)$ is a vector of absolute displacements, $\dot{X}(t)$ is a vector of absolute velocities, $\ddot{X}(t)$ is a vector of absolute accelerations, and $F(t)$ is a vector of applied forces. For steady state harmonic motion, let:

$$\begin{aligned} X(t) &= X(\omega)e^{i\omega t} \\ F(t) &= F(\omega)e^{i\omega t} \end{aligned} \qquad \text{Equation 5-2}$$

Substituting Equation 5-2 into Equation 5-1 yields:

$$(-\omega^2 M + i\omega C + K)\ X(\omega)e^{i\omega t} = F(\omega)e^{i\omega t} \qquad \text{Equation 5-3}$$

© Copyright 2019 by NuScale Power, LLC

Dividing this equation by $e^{i\omega t}$ yields:

$$S(\omega)X(\omega) = F(\omega) \quad \text{Equation 5-4}$$

Where S is the dynamic stiffness at frequency ω,

$$S(\omega) = (-\omega^2 M + i\omega C + K) \quad \text{Equation 5-5}$$

$X(\omega)$ is the absolute displacement at frequency ω, $F(\omega)$ is the applied load at frequency ω, ω is the frequency in radians per second, and $i = \sqrt{-1}$.

5.1.2 Complex Response Analysis

One definition of the Fourier transform from the frequency to the time domain is:

$$X(t) = \Re\left(\sum_{s=0}^{N/2} a_s\, e^{i\omega_s t}\right) \quad \text{Equation 5-6}$$

where $\Re$ is the real part, N is the number of points, $\omega_s = 2\pi s/(N\Delta t)$, s is the frequency number, and a_s is a complex Fourier coefficient in the frequency domain. The Fourier coefficient a_s is:

$$a_s = \begin{cases} \dfrac{1}{N}\displaystyle\sum_{k=0}^{N-1}\left(a_k\, e^{-i\omega_s k\Delta t}\right) & \text{for } s = 0, s = \dfrac{N}{2} \\ \dfrac{2}{N}\displaystyle\sum_{k=0}^{N-1}\left(a_k\, e^{-i\omega_s k\Delta t}\right) & \text{for } 1 \le s \le \dfrac{N}{2} - 1 \end{cases} \quad \text{Equation 5-7}$$

© Copyright 2019 by NuScale Power, LLC

where a_k is the time history magnitude at each time step, the a_k are real numbers, Δt is the time step and the remaining terms have been previously defined. Note that there are 1+N/2 unique frequency domain coefficients. Frequency domain coefficients a_0 and $a_{N/2}$ are real while a_1 through $a_{(N/2)-1}$ are complex. Note that N is assumed to be an integer power of 2, $N = 2^n$.

The definition of a transfer function for a linear system, is (Reference 9.1.21):

$$TF(\omega) = \frac{\mathscr{F}(Output)}{\mathscr{F}(Input)} \qquad \text{Equation 5-8}$$

Where $\mathscr{F}(a)$ is a Fourier transform of a. The Fourier transform of an acceleration or displacement time history with N points are the 1+N/2 unique Fourier coefficients calculated with Equation 5-7.

As discussed in 5.1.6 the seismic load vector is based on a unit free-field ground displacement of the control layer. Thus, the solution of Equation 5-4 is the output $X(\omega)$, due to a unit control layer input, and the transfer function is:

$$TF(\omega) = \frac{X(\omega)}{1} = S(\omega)^{-1}F(\omega) \qquad \text{Equation 5-9}$$

If the ground motion is described as a displacement time history, then the displacement response is:

$$TF(\omega) \cdot \mathscr{F}(X_{Input}) = \mathscr{F}(X_{Output}) \qquad \text{Equation 5-10}$$

Taking the second derivative of both sides with respect to time yields an acceleration response for an acceleration input:

$$TF(\omega) \cdot \mathscr{F}(\ddot{X}_{Input}) = \mathscr{F}(\ddot{X}_{Output}) \qquad \text{Equation 5-11}$$

© Copyright 2019 by NuScale Power, LLC

The input acceleration time history is transformed to the frequency domain using Equation 5-7. An acceleration response Fourier coefficient for each input Fourier coefficient is calculated using Equation 5-11. The acceleration response time history is calculated from the Fourier coefficients using Equation 5-6.

Note that the analysis can be truncated in the frequency domain and that less than *N*/2 non-zero Fourier coefficients may be considered.

Calculation of the transfer function can be computationally extensive and the transfer function is often effectively interpolated using the procedures in Section 5.1.7.

Equation 5-6 and Equation 5-7 were not calculated as written. These equations are more efficiently computed using a Fast-Fourier Transform (FFT) found in most software libraries.

The FFT represents a periodic infinite sequence of earthquake events. Sufficient time is included to allow the response to be damped out between each event. If the number of non-zero time history data approaches *N*, the Fourier transform can generate spurious results through a process called aliasing.

5.1.3 Damping in Frequency Domain Analyses

In frequency domain analysis, the damping is represented as a viscous damping term, *C*, or as structural damping by using a complex stiffness, k^*:

$$k^* = k(1 - 2\xi^2 + 2i\xi\sqrt{1-\xi^2})$$

Equation 5-12

where ξ is the damping ratio and k is the stiffness. Structural damping can be used as a multiplier on stiffness or elastic modulus. Structural damping is also referred to as viscoelastic damping, frequency independent damping and complex stiffness.

A simplified structural damping formulation in literature (Reference 9.1.18) and in the ANSYS methodology is:

$$k^* = k(1 + 2i\xi)$$

Equation 5-13

The damping formulation in Equation 5-12 is used in SASSI and is incorporated in the SASSI analyses in this report.

© Copyright 2019 by NuScale Power, LLC

Appendix A compares the response of a single degree of freedom system, subject to base motion, with structural damping, simplified structural damping, and viscous damping.

Figure A-7 through Figure A-9 demonstrate that the energy dissipation with structural damping and simplified structural damping is frequency independent while the energy dissipation with viscous damping is frequency dependent.

In the soil-structure-fluid interaction problem, material damping in the soil and structural elements are represented with structural damping while fluid viscosity is represented with viscous damping.

5.1.4 Mass Matrices and Element Size for Soil Dynamics

J. Lysmer, "Analytical Procedures in Soil Dynamics," in Reference 9.1.10, provides convergence criterion that targets less than 10% error on wave amplitude:

$$f_{cutoff} = \frac{V_s}{8L} \text{ for lumped mass}$$

$$f_{cutoff} = \frac{V_s}{8L} \text{ for consistent mass} \qquad \text{Equation 5-14}$$

$$f_{cutoff} = \frac{V_s}{5L} \text{ for mixed mass}$$

where f_{cutoff} is the analysis cutoff frequency, or the highest frequency with less than 10% error. Alternately, Lysmer's criterion can be stated as $\lambda/8$ for lumped or consistent mass and $\lambda/5$ for mixed mass where λ is a wave length. The wave length for a shear wave is $\lambda = V_s/f$, where V_s is the shear wave velocity and f is the frequency in Hz.

This criterion is demonstrated in Appendix B which considers the free field response of a soil column that is approximated using simple shear beam elements. Lumped, consistent, and mixed lumped-consistent mass matrices are considered. The resulting transfer functions are compared to the 1D wave equation solution implemented in SHAKE (Reference 9.1.18).

Near the cutoff frequency, the lumped mass formulation underestimates the natural frequency while the consistent mass formulation overestimates the natural frequency. Combining the two formulations therefore provides a reasonable estimate of the true natural frequency. The response using the mixed lumped-consistent mass formulation

© Copyright 2019 by NuScale Power, LLC

has less error than the response based on either the lumped mass or the consistent mass formulations.

The SASSI HOUSE Module has an eight node brick element that incorporates the mixed lumped-consistent mass formulation. The SASSI HOUSE brick elements are used to represent the excavated soil in the development of the Soil Library and the $\lambda/5$ mesh size criterion is used to develop the Soil Library.

5.1.5 Layered Halfspace Soil Impedance

The layered halfspace soil impedance matrix, [*Z*], of the interaction nodes is developed at each calculated frequency by inverting a complex soil flexibility matrix:

$$[Z] = [Flexibility]^{-1}$$

Equation 5-15

The flexibility matrix is full and the numerical inversion process is the single most computationally expensive step in a SASSI analysis.

Each row of the flexibility matrix is assembled by applying a unit load at an interaction DOF and calculating the resulting displacement at each DOF (Reference 9.1.11) as shown schematically in Figure 5-1. Displacements of the layered halfspace are calculated using a special axisymmetric model with asymmetric loading and transmitting boundaries. Additional details of this process are presented in Reference 9.1.16.

5.1.6 Seismic Load Vector

SASSI uses the flexible volume substructuring method (Reference 9.1.11) where the structure, foundation and soil are partitioned as shown in Figure 5-2. Figure 5-2a represents the total system, Figure 5-2b represents the free field soil and Figure 5-2c represents the building and excavated soil. The following subscripts represent different parts of the structure:

Subscript	Nodes
s	Superstructure
t	Basement Boundary
i	Excavated Soil of Interaction Nodes
j	Interaction node not on basement boundary, *j* = *i* - *t*
b	External Boundary
g	Remaining Soil

© Copyright 2019 by NuScale Power, LLC

where the basement boundary nodes, *t*, are at the external basement surface.

The equation of motion, Equation 5-4, for the free-field foundation substructure, Figure 5-2(b) is:

$$\begin{bmatrix} S_{ii} & S_{ig} & S_{ib} \\ S_{gi} & S_{gg} & S_{gb} \\ S_{bi} & S_{bg} & S_{bb} \end{bmatrix} \begin{Bmatrix} X_i \\ X_g \\ X_b \end{Bmatrix} = \begin{Bmatrix} F_i \\ 0 \\ F_b \end{Bmatrix} \qquad \text{Equation 5-16}$$

where F_b are forces acting on the boundary and F_i are interaction forces from the structure and excavated soil acting on the free field.

The equation of motion, Equation 5-4, for the building and excavated soil part of the substructure in Figure 5-2(c) is:

$$\begin{bmatrix} S_{ss} & S_{st} \\ S_{ts} & S_{tt} - S'_{ii} \end{bmatrix} \begin{Bmatrix} X_s \\ X_i \end{Bmatrix} = \begin{Bmatrix} 0 \\ -F_i \end{Bmatrix} \qquad \text{Equation 5-17}$$

where the term S'_{ii} represents the dynamic stiffness of the excavated soil volume. At common locations, the interaction and boundary deformations are equivalent ($X_i = X_t$). When the internal interaction DOF are considered, the dimensions for interaction DOF are larger than the basement boundary DOF and S_{tt} is adjusted to have the same dimensions as S'_{ii}.

Assuming that the external boundary is far from the structure, and substituting in the free field motion, X', the motion for the free field substructure, Equation 5-16, can be written

$$\begin{bmatrix} S_{ii} & S_{ig} & S_{ib} \\ S_{gi} & S_{gg} & S_{gb} \\ S_{bi} & S_{bg} & S_{bb} \end{bmatrix} \begin{Bmatrix} X'_i \\ X'_g \\ X'_b \end{Bmatrix} = \begin{Bmatrix} 0 \\ 0 \\ F_b \end{Bmatrix} \qquad \text{Equation 5-18}$$

Note that the free field motion X' consists of a unit in-layer displacement of the control layer propagated to the remaining layers by a site response analysis.

© Copyright 2019 by NuScale Power, LLC

Subtracting Equation 5-18 from Equation 5-16 yields:

$$\left[\begin{array}{c|cc} S_{ii} & S_{ig} & S_{ib} \\ \hline S_{gi} & S_{gg} & S_{gb} \\ S_{bi} & S_{bg} & S_{bb} \end{array}\right] \left\{\begin{array}{c} X_i - X_i' \\ \hline X_g - X_g' \\ X_b - X_b' \end{array}\right\} = \left\{\begin{array}{c} F_i \\ \hline 0 \\ 0 \end{array}\right\} \qquad \text{Equation 5-19}$$

Partitioning the matrix as shown, solving for $X_g - X_g'$ and $X_b - X_b'$ and back substituting into Equation 5-19 yields

$$\{F_i\} = [Z]\{X_i - X_i'\} \qquad \text{Equation 5-20}$$

where [*Z*] is the layered halfspace soil impedance of the excavated soil nodes (interaction nodes). Equation 5-19 could be used to develop [*Z*], but the assumption that the external boundary is far from the structure causes the solution to Equation 5-19 to become more extensive than the solution in Section 5.1.5.

Substituting Equation 5-20 into Equation 5-17 yields:

$$\left[\begin{array}{cc} S_{ss} & S_{st} \\ S_{ts} & S_{tt} + Z - S_{ii}' \end{array}\right] \left\{\begin{array}{c} X_s \\ X_i \end{array}\right\} = \left\{\begin{array}{c} 0 \\ F_{EQ} \end{array}\right\} \qquad \text{Equation 5-21}$$

Where F_{EQ} is the seismic load vector that is the product of the layered halfspace soil impedance, *Z*, and the free field ground motion X'_i:

$$\{F_{EQ}\} = [Z]\{X_i'\} \qquad \text{Equation 5-22}$$

Both the soil impedance and free field ground motion vary with frequency, thus the seismic load vector also varies with soil frequency. The free field ground motion is developed by a site response analysis and represents vertically propagating horizontal shear waves or vertically propagating compression waves (P-waves).

The free field response for a vertically propagating shear and P-wave is a function of the layer where a unit motion is defined, referred to as the control layer.

© Copyright 2019 by NuScale Power, LLC

5.1.7 SASSI Transfer Function Interpolation

The transfer function for a two degree of freedom system can be written as a rational fraction[2]:

$$TF = \frac{c_1 + c_2\omega^2}{c_3 + c_4\omega^2 + \omega^4} \qquad \text{Equation 5-23}$$

where c_i are coefficients and ω is the frequency in radians per second. Similarly, the transfer function for a N degree of freedom system can be written as:

$$TF = \frac{b_0 + b_1\omega^2 + b_2\omega^4 + \cdots}{d_0 + d_1\omega^2 + d_2\omega^4 + d_3\omega^6 + \cdots} = \frac{\sum_{k=0}^{N-1} b_k\omega^{2k}}{\sum_{k=0}^{N} d_k\omega^{2k}} \qquad \text{Equation 5-24}$$

This equation could be used to interpolate transfer functions but experience has shown that attempting to fit a large number of terms can be problematic.

Fredrick F. Tajirian, “Impedance Matrices and Interpolation Techniques for 3-D Interaction Analysis of the Flexible Volume Method,” (Reference 9.1.20) proposed the following interpolation function:

$$tf = \frac{c_1\,\omega^4 + c_2\,\omega^2 + c_3}{\omega^4 + c_4\,\omega^2 + c_5} \qquad \text{Equation 5-25}$$

which is based on a two degree of freedom system with an extra ω^4 term in the numerator. Note that the coefficients c_1 to c_5 are complex coefficients, the frequency ω is a real number, and the resulting transfer function has a complex value.

[2] Both numerator and denominator are polynomials.

© Copyright 2019 by NuScale Power, LLC

Rearranging terms yields:

$$(\omega^4)\, c_1 + (\omega^2)\, c_2 + c_3 - (tf\,\omega^2)\, c_4 - tf\, c_5 = tf\,\omega^4 \qquad \text{Equation 5-26}$$

Expanding to five simultaneous equations yields:

$$\begin{pmatrix} \omega_1^4 & \omega_1^2 & 1 & -tf_1\,\omega_1^2 & -tf_1 \\ \omega_2^4 & \omega_2^2 & 1 & -tf_2\,\omega_2^2 & -tf_2 \\ \omega_3^4 & \omega_3^2 & 1 & -tf_3\,\omega_3^2 & -tf_3 \\ \omega_4^4 & \omega_4^2 & 1 & -tf_4\,\omega_4^2 & -tf_4 \\ \omega_5^4 & \omega_5^2 & 1 & -tf_5\,\omega_5^2 & -tf_5 \end{pmatrix} \begin{Bmatrix} c_1 \\ c_2 \\ c_3 \\ c_4 \\ c_5 \end{Bmatrix} = \begin{Bmatrix} tf_1\,\omega_1^4 \\ tf_2\,\omega_2^4 \\ tf_3\,\omega_3^4 \\ tf_4\,\omega_4^4 \\ tf_5\,\omega_5^4 \end{Bmatrix} \qquad \text{Equation 5-27}$$

Equation 5-27 is solved numerically. However, it should be noted that this equation may be ill-conditioned. For some cases the determinant of the array on the left side of Equation 5-27 is zero and there is not a unique solution for the constants. An example is a constant transfer function at various frequencies, which occurs when extracting a transfer function at the control motion in the free field and the transfer function is 1.0 regardless of the frequency. Older versions of SASSI do not check for numerical problems in the solution of Equation 5-27 and the behavior of the program is dependent on how, or if, the compiler handles runtime errors[3].

One current implementation (Reference 9.1.6) solves Equation 5-27 using a robust LAPACK (Reference 9.1.1) routine which detects singular matrices and illegal arguments. If an error solving Equation 5-27 is detected, then linear interpolation of the transfer function is substituted.

In practice, there are an arbitrary number of frequencies. SASSI computes the interpolated transfer functions based on the first five computed frequencies, f_1, f_2, . . . f_5. For simplicity, label this interpolation as *A*, as shown in Figure 5-3. Second, SASSI

[3] Some compilers flag erroneous results with *NaN* for “Not a Number.”

© Copyright 2019 by NuScale Power, LLC

computes interpolated transfer functions based on computed frequencies, f_2, f_3, . . . f_6, called *B*, and then averages the transfer functions due to interpolation *A* and *B*, for the frequencies where two different transfer functions are computed. Thus, between frequencies f_2 and f_5, the interpolated transfer function is $TF = (TF_A + TF_B)/2$. This process is repeated until interpolated transfer functions have been computed across the entire range of computed frequencies.

The resulting interpolated transfer functions are based on a weighted average that is biased towards high frequencies. For example, the interpolated transfer function for frequencies between f_4 and f_5 are:

$$TF_{f4:f5} = \frac{\frac{\frac{TF_A+TF_B}{2}+TF_C}{2} + TF_D}{2} = \frac{TF_A + TF_B}{8} + \frac{TF_C}{4} + \frac{TF_D}{2} \qquad \text{Equation 5-28}$$

Thus, the behavior of the transfer function for a frequency near f_4 is dominated by an interpolation that ranges between f_4 and f_8. Neither the interpolation scheme nor its basis are discussed by Tajirian. It is suspected that this approach was selected because of programming expediency. The weighted averaging scheme in Equation 5-28 is used in the current implementation to retain fidelity with SASSI.

5.1.8 Interpretation of Complex Results

Note that the values of *S*, *X* and *F are* complex numbers. A complex number, z, can be considered to have a magnitude |*z*| and a phase angle of $\varphi = atan2(\Im(z),\Re(z))$. The value atan2(y,x) is the principal value of the arc tangent of y/x, expressed in radians. This will be between - pi and + pi. The time domain response of the complex value *z* is:

$$z(t) = |z|e^{i\phi} \cdot e^{i\omega t} = |z|\ e^{i(\phi+\omega t)} \qquad \text{Equation 5-29}$$

where the phase angle represents a difference, or lag, in response time. The physical displacement, at time *t*, is the real part of *z(t)*, or:

$$\Re(z(t)) = |z|\ \cos(\omega t + \phi) \qquad \text{Equation 5-30}$$

© Copyright 2019 by NuScale Power, LLC

If z represents a transfer function[4], then the response z lags the input by $t_o = \varphi/\omega$ if φ is negative. For positive φ, the response lags the input by $t_o = (\varphi - 2\pi)/\omega$.

5.2 Soil Library

This section discusses enhancements to the traditional SASSI methodology that are necessary to support the proposed analysis.

5.2.1 Reduction of Impedance Matrix and Seismic Load Vectors

The soil impedance matrix, Equation 5-15, and the seismic load vector, Equation 5-22, are defined at each interaction DOF but only contact the structure at the basemat boundary DOF, *t*, where the t DOF are identified in Section 5.1.6. Storing the full impedance matrix for moderately sized problems can be resource intensive, thus the internal DOF, *i-t*, are condensed out of both the impedance and load vectors. This condensation is performed at each frequency and does not alter the solution.

Omitting the structure stiffness terms from Equation 5-21, gives:

$$([Z] - [S'_{ii}])\{X_i\} = [C_{ii}]\{X_i\} = \{F_{EQ}\} \qquad \text{Equation 5-31}$$

where $[C_{ii}] = [Z - S'_{ii}]$ is the soil impedance less the excavated soil (i.e., excavated soil impedance). Equation 5-31 is partitioned

$$\begin{bmatrix} C_{jj} & C_{jt} \\ C_{tj} & C_{tt} \end{bmatrix} \begin{Bmatrix} X_j \\ X_t \end{Bmatrix} = \begin{Bmatrix} F_{EQ\ j} \\ F_{EQ\ t} \end{Bmatrix} \qquad \text{Equation 5-32}$$

[4] Assumes that the input control motion has zero phase. If the input motion has a non-zero phase, the time lag is calculated using the difference between φ and the input motion phase.

© Copyright 2019 by NuScale Power, LLC

where j are the interaction DOF not on the basement boundary, $j = i - t$. Condensing out the *jth*DOF yields:

$$[Z_{Red}]\{X_t\} = \{F_{EQ\ Red}\} \quad \text{Equation 5-33}$$

where the reduced excavated impedance is:

$$[Z_{Red}] = [C_{tt}] - [C_{tj}] \cdot [C_{jj}]^{-1} \cdot [C_{jt}] \quad \text{Equation 5-34}$$

and the reduced seismic load vector is:

$$\{F_{EQ\ Red}\} = \{F_{EQ\ t}\} - [C_{tj}] \cdot [C_{jj}]^{-1} \cdot \{F_{EQ\ j}\} \quad \text{Equation 5-35}$$

The reduced excavated soil impedances for the layered halfspace with excavation and the reduced load vector, Equation 5-34 and Equation 5-35 are computed and stored in the Soil Library. Note that the term $[C_{jj}]^{-1} \bullet [C_{tj}]$ in Equation 5-34 is equal to $[D]$ in $[C_{jj}][D] = [C_{tj}]$, which can be obtained using a linear solver instead of a matrix inversion[5]. A similar term in Equation 5-35 is also obtained using a linear solver.

An example soil volume with 28,830 interaction nodes has 4,471 interaction nodes on the perimeter of the excavation that are common with the basement shell (*t* nodes) and 24,359 interaction nodes interior to the basement shell (*j* nodes), as shown schematically in Figure 5-4. The storage size for a symmetric excavated impedance matrix, where each complex number is represented by (2) 64 bit numbers, is provided below. For the example problem, the condensation in Equation 5-34 reduces the memory, and file size required to store the excavated impedance matrix, by a reduction factor of 42. Note that the reduction factor is analogous to the ratio between the volume and surface of a sphere, squared, and can be approximated with $N_i^{2/3}/22$, where N_i is the total number of interaction (*i*) nodes.

[5] The linear solver is more efficient when $t < j$. As seen in the example, *t* is often smaller than *j* for moderately sized problems.

© Copyright 2019 by NuScale Power, LLC

Case	Nodes	DOF	Memory[6]
Full	28,830	86,490	55.7 GB
Reduced	4,471	13,413	1.3 GB

5.2.2

5.2.2 Lumped Parameter Soil Impedance

The reduced excavated soil impedance in Equation 5-34 represents the impedance of *N* interaction nodes that are attached to a building. If the building is replaced by a rigid massless structure, then the deformations of the rigid massless structure represent flexibilities and these flexibilities can be used to develop the impedance for the rigid massless structure. The impedance of the rigid massless structure is also called lumped parameter impedance. This method is discussed in the SASSI User's Manual (Reference 9.1.15) and is used in Example 1.

Alternately, rigid body constraints can be used to transform the reduced excavated impedance matrix to a single node with six degrees of freedom, which represents a lumped parameter soil impedance. The rigid body force transformation matrix for a six DOF (Reference 9.1.25) is:

$$[T_i] = \begin{bmatrix} 1 & 0 & 0 & 0 & 0 & 0 \\ 0 & 1 & 0 & 0 & 0 & 0 \\ 0 & 0 & 1 & 0 & 0 & 0 \\ 0 & -z & y & 1 & 0 & 0 \\ z & 0 & -x & 0 & 1 & 0 \\ -y & x & 0 & 0 & 0 & 1 \end{bmatrix} \qquad \text{Equation 5-36}$$

where *x*, *y*, and *z* are the coordinate of Node *i* less the control node coordinate, the columns represent the three translational and three rotational DOFs of Node *i* and the rows represent the six degrees of freedom of the control node. If Node *i* only has translational DOF then the last three columns of the transformation matrix are omitted.

[6] Ideal symmetric memory, without overhead. Minimum size for a binary file.

© Copyright 2019 by NuScale Power, LLC

The transformation for *N* nodes is:

$$[T] = [T_1, T_2, \cdots T_N] \qquad \text{Equation 5-37}$$

and the lumped parameter impedance is:

$$[Z_{Lumped\ Parameter}] = [T] \cdot [Z_{Red}] \cdot [T]^T \qquad \text{Equation 5-38}$$

The lumped parameter impedance is typically a 6x6 matrix which describes the impedance of a rigid massless foundation attached to each of the *t* DOF. Note, this transformation is not applied to the *j* DOF in Equation 5-32 as it artificially constrains *{Xj}*.

5.3 SASSI Enhancements

ANSYS, and other commercially available finite element programs, have libraries of structural elements, acoustic elements, and constraint equations that can be implemented in SASSI analyses. Elements and constraints are described mathematically in the substructure mass, stiffness, and viscous damping matrices, which are exported from the commercial FEM program, along with a table identifying the degrees of freedom.

SDE-SASSI (Reference 9.1.6) has the ability to import mass, stiffness, viscous damping, and load matrices and sub matrices, and assemble these matrices with internal matrices from the SASSI HOUSE Module. Thus, SDE-SASSI has the ability to solve a SSI problem using an ANSYS substructure containing fluid-structure interaction.

Some formulations of fluid structure interaction problems have unsymmetric mass and stiffness matrices. SDE-SASSI implements an unsymmetric solver that is used to solve these fluid-structure interaction problems.

SDE-SASSI utilizes a split solver employing a sparse solver for the structural portion of the dynamic stiffness and a dense solver for the soil impedance interaction degrees of freedom. SDE-SASSI takes advantage of parallel distributed memory computing to solve various problem sizes.

SDE-SASSI also has the ability to write intermediate results such as the soil flexibility matrix, the free-field impedance matrix, and the combined impedance and excavated soil matrix. Additionally, SDE-SASSI has the ability to reduce the impedance and seismic load vectors using the transformation discussed in Section 5.2.1. The soil library is composed of reduced impedance and seismic load vectors calculated by SDE-SASSI.

© Copyright 2019 by NuScale Power, LLC

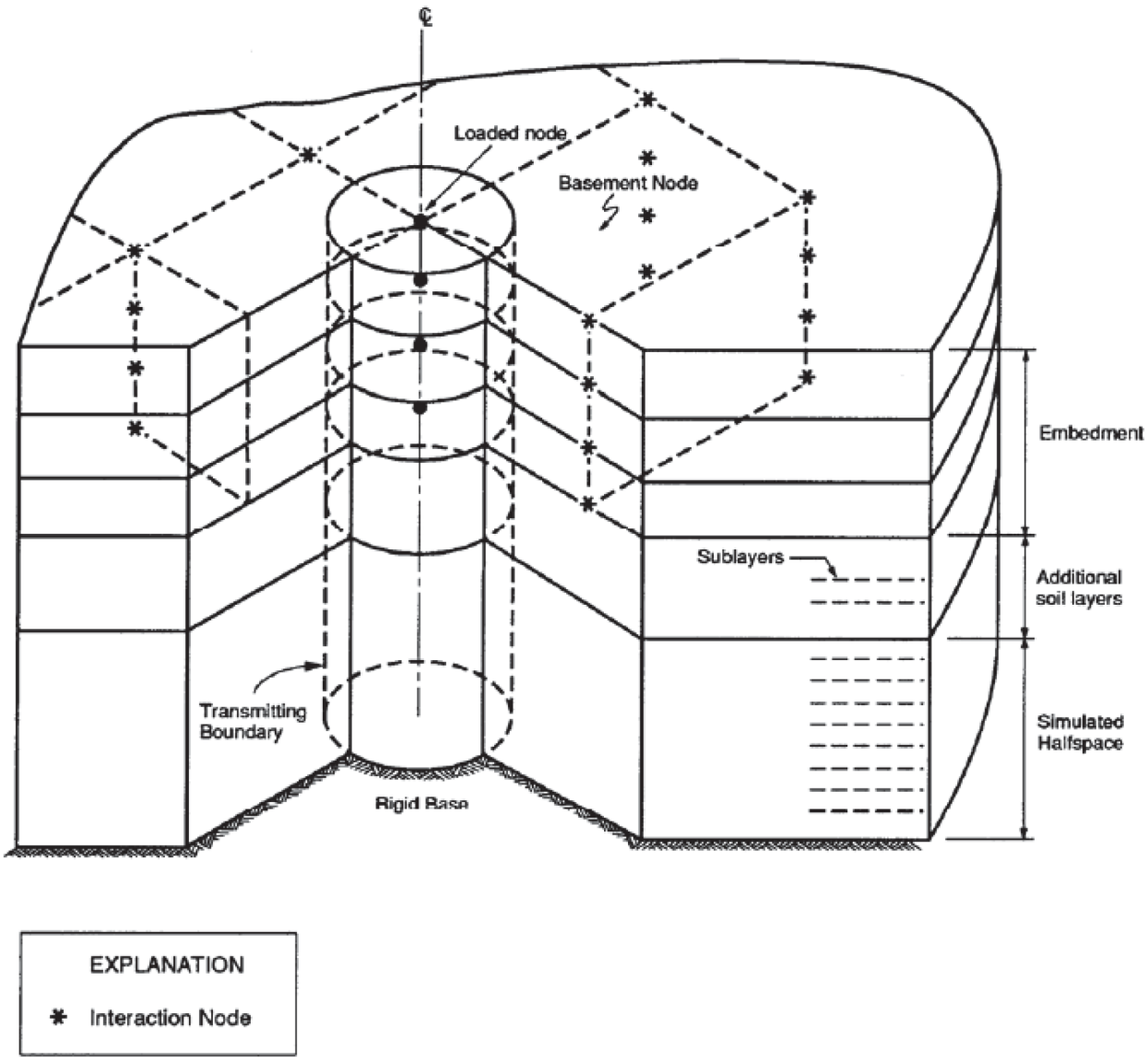

Figure 5-1 SASSI axisymmetric model for impedance analysis (Reference 9.1.11)

© Copyright 2019 by NuScale Power, LLC

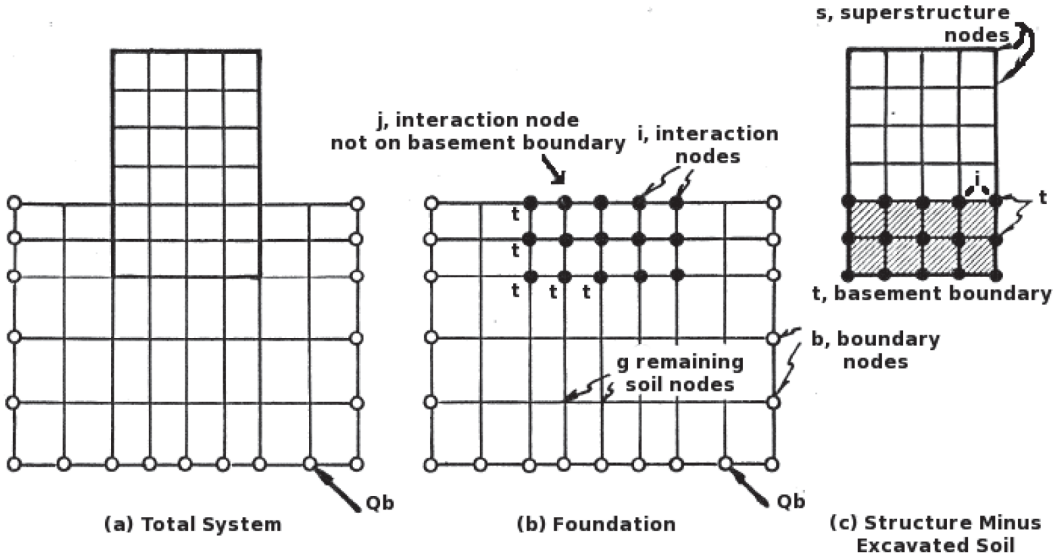

Figure 5-2 SASSI flexible volume substructuring (Reference 9.1.11)

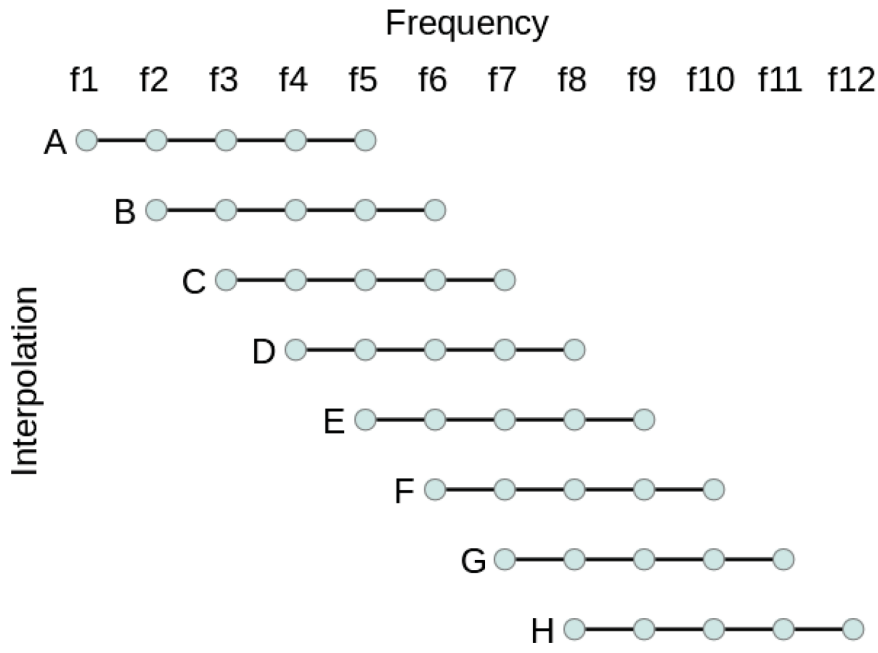

Figure 5-3 Schematic of transfer function interpolation

© Copyright 2019 by NuScale Power, LLC

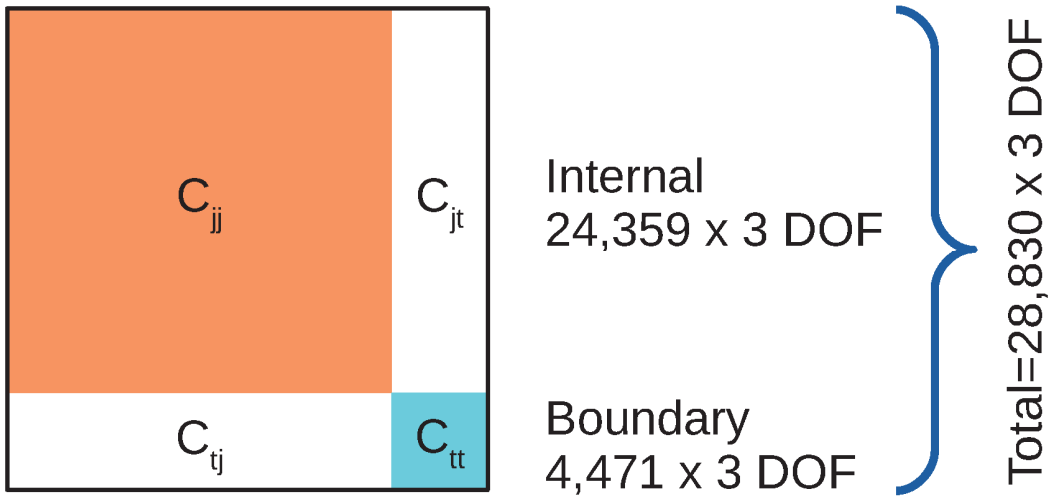

Figure 5-4 Example partition for impedance matrix reduction

© Copyright 2019 by NuScale Power, LLC

6.0 Demonstation Problems

Four different problems are presented to demonstrate the use of the soil library and to demonstrate the equivalency of the ANSYS frequency domain solution using the Soil Library to the SASSI solution.

Problem 1 is a surface founded containment building included in the SASSI user manual, Problem 2 is a partially embedded box-shaped building with SSI, Problem 3 is a partially embedded box-shaped building with soil-structure-fluid interaction, and Problem 4 is a representative Small Modular Reactor Building (RXB) including twelve reactor modules (RXM), reactor pool, backfill and soil-structure-fluid interaction.

6.1 Example 1: Surface Reactor Problem from SASSI User's Manual

Example 1 is the calculation of soil impedance and seismic response for a surface PWR. This problem is an example in the SASSI User's Manual, (Reference 9.1.15) The PWR containment and reactor internals are represented by lumped mass stick models supported on a rigid foundation resting on the surface of an elastic half space.

The building is shown schematically in Figure 6-1. The sticks are supported on rigid beams attached to a rigid disk of 8-node brick elements, supported on the soil surface as shown in Figure 6-2. Material properties for the structural elements and soil are given in Reference 9.1.15. This problem has a total of 158 nodes with 69 interaction nodes.

6.1.1 Soil Impedance

An Example 1 Soil Library is developed for the 13 frequency numbers considered in Reference 9.1.15: N_f =10, 30, 50, 60, 80, 100, 120, 140, 160, 180, 210, 230 and 260. The ground motion has a time step of 0.005 seconds with 2048 data points, for a frequency step of Δf =1/10.24 Hz. Thus, the analysis frequency range extends to 25.39 Hz.

Example 1 does not have interaction nodes that are not part of the basement boundary and the reduction in Equation 5-34 is omitted for this problem.

The soil impedance at the 69 boundary nodes is stored in 13 files with file namesf_xxxxK_s22kRed.mtx, where xxxx is the frequency number, N_f, with leading zeros (0010, 0030. . . 0260) as discussed in Section 7.1. The files are in the Matrix Market file format (Reference 9.1.5). The degrees of freedom are contained in a file titled "node.dat."

© Copyright 2019 by NuScale Power, LLC

The impedance of a rigid massless foundation is calculated by applying unit loads to the rigid foundation, omitting foundation mass and the building sticks, and calculating deformations (Reference 9.1.15). The impedance is the unit load divided by the corresponding displacement δ_{ii}. The impedance is split into real and imaginary parts:

$$Kr = \Re(K), \qquad Ki = \frac{\Im(K)}{\omega} \qquad \text{Equation 6-1}$$

and shown in Figure 6-3 through Figure 6-6 with the label “SASSI.” Note that this is the same impedance plotted in the SASSI User’s Manual (Reference 9.1.15).

The Soil Library impedance is converted to a lumped parameter impedance using the transformation discussed in Section 5.2.2. The resulting impedances are included in the figures and identified as “S.L.” There are slight differences between these lumped parameter impedances and the impedance values labeled SASSI because the “SASSI” impedances neglect translational-rocking coupling.

Benchmark solutions from Luco and Veletsos and Verbric (VV) are also presented in the figures. These solutions have an impedance of $Z = k1 + i\omega k2$ where:

$$k1_{XX} = f1_{XX}\frac{8GR}{2-\nu}, \qquad k2_{XX} = f2_{XX}k1_{XX}\frac{R}{Vs}$$
$$k1_{RR} = f1_{RR}\frac{8GR^3}{3(1-\nu)}, \qquad k2_{RR} = f2_{RR}k1_{RR}\frac{R}{Vs} \qquad \text{Equation 6-2}$$

where G is the shear modulus, Vs is the shear wave velocity, v is Poisson’s ratio, R is the radius, and $f1$ and $f2$ are coefficients given in Figure B29 of Reference 9.1.23

While the benchmark solutions generally agree with each other, there are differences, less than 10%, due to different analytical solution methods. Note that the Luco solutions are a refinement of the solutions developed by Veletsos and Verbric (VV) and are presumed to be more accurate than the VV solution. These differences are an indicator of the anticipated accuracy in soil impedance solutions. The agreement between the “SASSI,” “S.L,” “Luco,” and “VV” solutions is good. This indicates that the lumped parameter soil stiffness developed from the Soil Library is consistent with the impedance previously developed using unit loads.

6.1.2 Seismic Response

The seismic response of the PWR stick model is calculated using SASSI and ANSYS frequency domain solutions. The SASSI solution uses the HOUSE element stiffness. The

© Copyright 2019 by NuScale Power, LLC

ANSYS solution uses the Soil Library and ANSYS beam and brick elements. Results for the SASSI and ANSYS solutions are compared below.

The lateral transfer functions for a surface control motion are shown in Figure 6-7 for the top of the containment and Figure 6-8 for the top of reactor internals. The comparison between SASSI and ANSYS transfer function plots is good.

The seismic response of the reactor is calculated for the 1940 NS El Centro ground motion applied in the lateral direction. The peak acceleration responses[7] are extracted from acceleration time histories and summarized in Table 6-2. The maximum difference in peak acceleration is approximately {{ }}$^{2(a),(c)}$ and the average difference in peak acceleration is less than {{ }}$^{2(a),(c)}$. Thus, the comparison between the SASSI and ANSYS peak accelerations is good.

In-Structure Response Spectra (ISRS) are calculated for 2% damping and are shown in Figure 6-9 for the top of the containment and Figure 6-10 for the top of reactor internals. The comparison between SASSI and ANSYS ISRS is good. Note that the ISRS at the top of the reactor internals is also plotted in Figure 4.6-15 of Reference 9.1.15 and the difference between the SASSI and ANSYS ISRS in Figure 6-10 is smaller than the difference between SASSI and FASS[8] in Reference 9.1.15.

Both SASSI and ANSYS can be used to recover stress time histories of selected elements. The overturning moments at the base of the containment are compared in Figure 6-11 and at the base of the reactor internals in Figure 6-12. Note that the SASSI forces are recovered from a SASSI HOUSE module beam element while the ANSYS forces are recovered from an ANSYS beam element. While there are local differences in portions of the time history, the overall comparison is good. The key parameter for design is the peak overturning moment, as summarized in Table 6-3. The difference in peak overturning moment is less than {{ }}$^{2(a),(c)}$.

[7] Reference 9.1.15 publishes these peak accelerations to two significant digits. A larger number of digits is presented in Table 6-2 to allow the comparison of two different numerical solutions.

[8] FASS is Bechtel Computer Program CE033 “Fourier Analysis of Soil-Structure Systems”

© Copyright 2019 by NuScale Power, LLC

6.1.3 Dynamic Modal Characteristics from Fixed Base Analysis

Modal analysis of the fixed base structure is performed with nodes at the soil surface fixed, i.e., nodes at elevation -10 feet on Figure 6-1 are fixed. Frequencies and modal masses from the modal analysis of the fixed-base structure are shown in Table 6-1.

Table 6-1 Frequencies, modal mass, and cumulative mass for Example 1

Mode Number	Frequency (Hz)	Modal Masses (kip * sec^2 / ft)					
		X-Direction		Y-Direction		Z-Direction	
		Modal Mass	Cumulative Modal Mass	Modal Mass	Cumulative Modal Mass	Modal Mass	Cumulative Modal Mass
1	5.26	904.9	904.9	0.0	0.0	0.0	0.0
2	5.26	0.0	905.0	904.9	905.0	0.0	0.0
3	11.96	181.5	1086.5	0.3	905.2	0.0	0.0
4	11.96	0.3	1086.7	181.5	1086.7	0.0	0.0
5	15.64	0.0	1086.7	0.0	1086.7	1006.8	1006.8
6	16.24	52.1	1138.9	141.3	1228.0	0.0	1006.8
7	16.24	141.3	1280.2	52.1	1280.2	0.0	1006.8
8	17.49	416.4	1696.6	1.1	1281.3	0.0	1006.8
9	17.49	1.1	1697.7	416.4	1697.7	0.0	1006.8
10	29.18	47.6	1745.3	0.2	1697.9	0.0	1006.8
11	29.18	0.2	1745.5	47.6	1745.5	0.0	1006.8
12	39.35	0.0	1745.5	0.0	1745.5	643.0	1649.8
13	41.69	19.6	1765.1	1.2	1746.7	0.0	1649.8
14	41.69	1.2	1766.3	19.6	1766.3	0.0	1649.8
15	44.03	0.0	1766.3	0.0	1766.3	102.8	1752.6
16	46.52	29.3	1795.6	136.0	1902.3	0.0	1752.6
17	46.52	136.0	1931.6	29.3	1931.6	0.0	1752.6
18	53.58	1.7	1933.3	6.2	1937.8	0.0	1752.6
19	53.58	6.2	1939.5	1.7	1939.5	0.0	1752.6
20	61.88	1.3	1940.8	1.6	1941.0	0.0	1752.6
21	61.88	1.6	1942.3	1.3	1942.3	0.0	1752.6
22	64.28	0.0	1942.3	0.0	1942.3	43.3	1795.9

© Copyright 2019 by NuScale Power, LLC

Mode Number	Frequency (Hz)	Modal Masses (kip * sec^2 / ft)					
		X-Direction		Y-Direction		Z-Direction	
		Modal Mass	Cumulative Modal Mass	Modal Mass	Cumulative Modal Mass	Modal Mass	Cumulative Modal Mass
23	69.02	0.0	1942.3	0.0	1942.3	39.4	1835.4
24	69.59	0.0	1942.4	1.8	1944.1	0.0	1835.4
25	69.59	1.8	1944.2	0.0	1944.2	0.0	1835.4
26	76.87	3.2	1947.4	0.1	1944.3	0.0	1835.4
27	76.87	0.1	1947.5	3.2	1947.5	0.0	1835.4
28	77.76	0.7	1948.1	0.0	1947.5	0.0	1835.4
29	77.76	0.0	1948.2	0.7	1948.2	0.0	1835.4
30	83.49	0.1	1948.3	0.0	1948.2	0.0	1835.4
31	83.49	0.0	1948.3	0.1	1948.3	0.0	1835.4
32	87.36	5.5	1953.8	8.3	1956.6	0.0	1835.4
33	87.36	8.3	1962.2	5.5	1962.2	0.0	1835.4
34	91.07	0.0	1962.2	0.0	1962.2	0.0	1835.4
35	91.07	0.0	1962.2	0.0	1962.2	0.0	1835.4
36	96.40	0.0	1962.2	0.0	1962.2	18.9	1854.2

6.1.4 Example 1 Summary

Example 1 demonstrated the use of the Soil Library to develop the impedance and load vector for a surface foundation. The Soil Library impedances were converted to lumped parameter impedances and compare well with published benchmark solutions.

The seismic response of the PWR stick model is calculated using both SASSI and ANSYS. The ANSYS solution uses the Soil Library, ANSYS structural elements, the frequency domain solver, incorporates transfer function interpolation (Section 5.1.7), uses complex response analysis (Section 5.1.2), generates ISRS, and extracts force time histories. There is good comparison between the SASSI and ANSYS results. This problem demonstrates that the ANSYS frequency domain solution using the Soil Library is functionally equivalent to the SASSI frequency domain solution.

© Copyright 2019 by NuScale Power, LLC

Table 6-2 Comparison of SASSI and ANSYS peak accelerations (g)

{{

}}[2(a),(c)]

Table 6-3 Comparison of SASSI and ANSYS peak overturning moments (ft-kip)

{{

}}[2(a),(c)]

© Copyright 2019 by NuScale Power, LLC

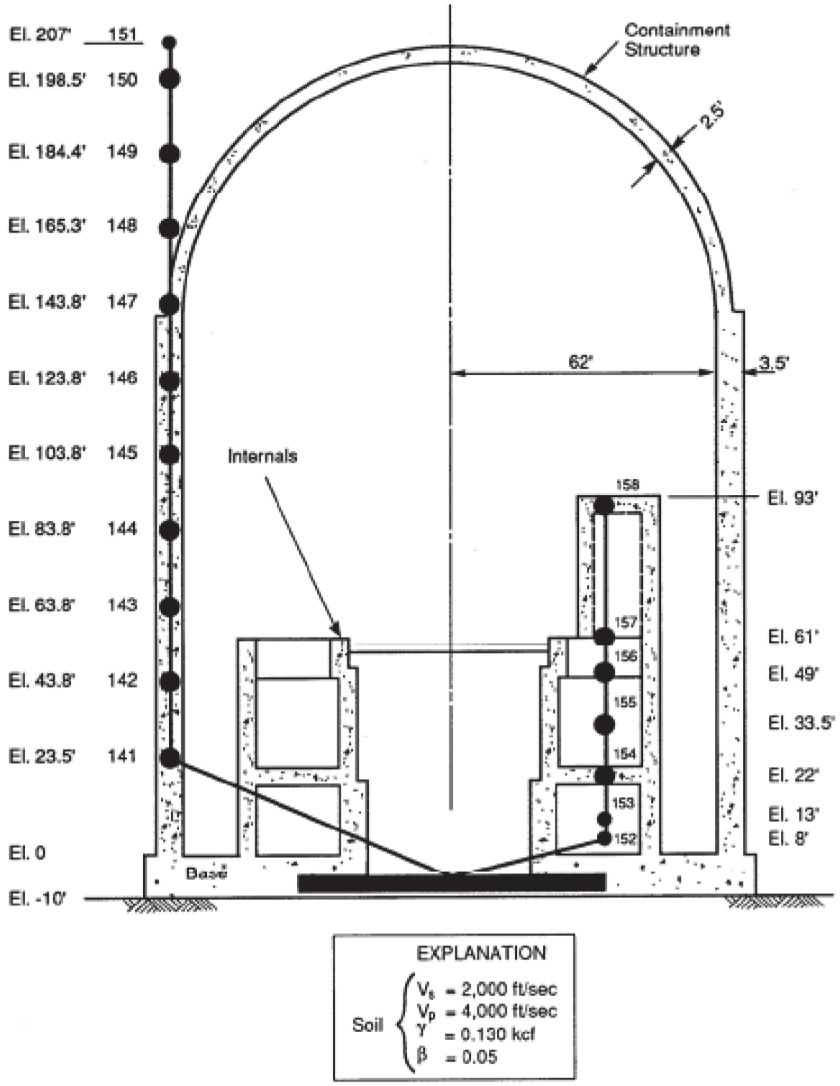

Figure 6-1 Stick model of PWR containment and internals (Reference 9.1.15)

© Copyright 2019 by NuScale Power, LLC

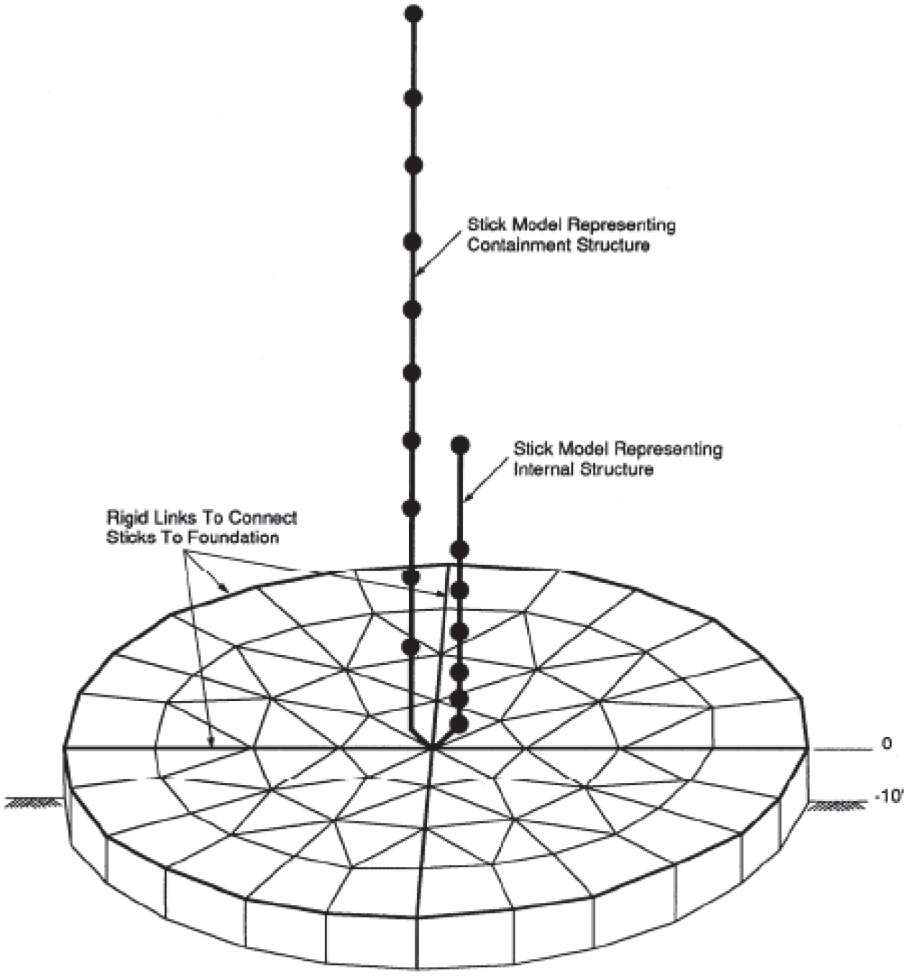

Figure 6-2 Example 1 model (Reference 9.1.15)

© Copyright 2019 by NuScale Power, LLC

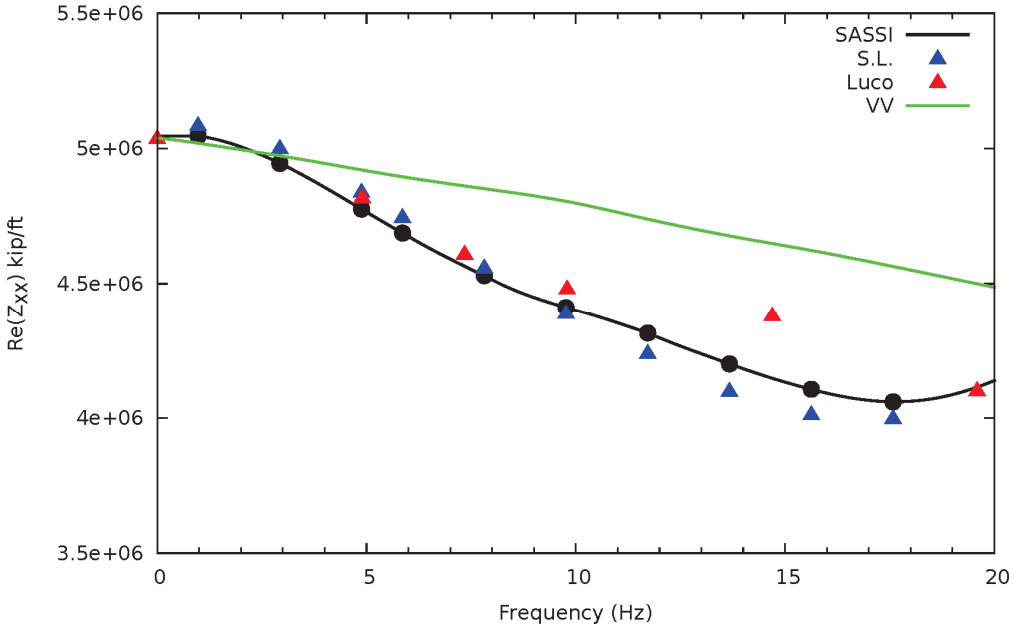

Figure 6-3 Comparison of real translational impedance, example 1

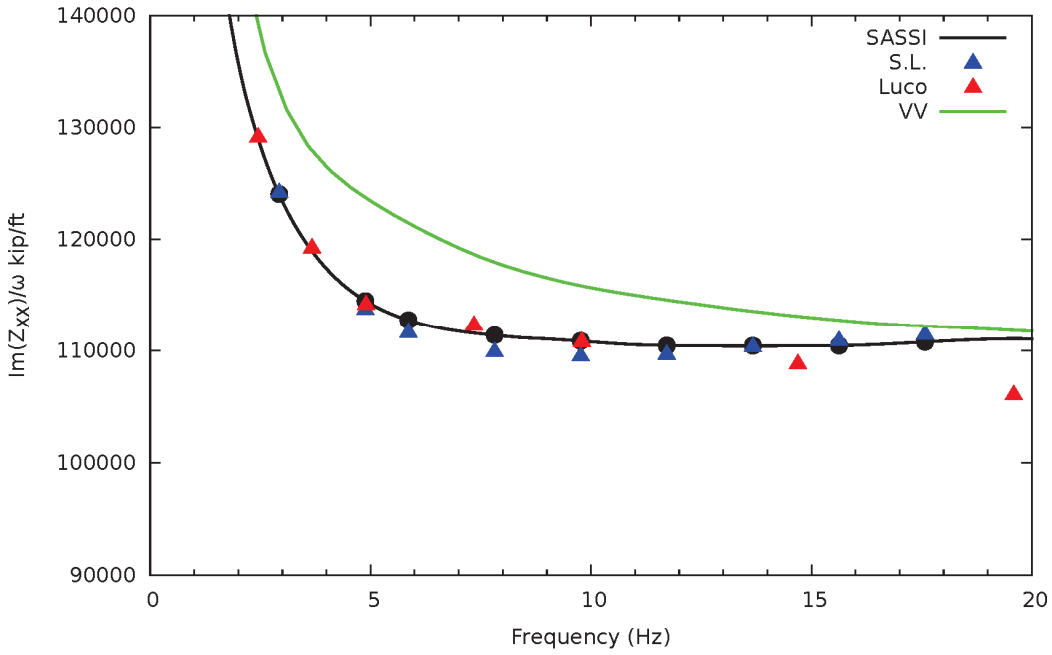

Figure 6-4 Comparison of imaginary translational impedance, example 1

© Copyright 2019 by NuScale Power, LLC

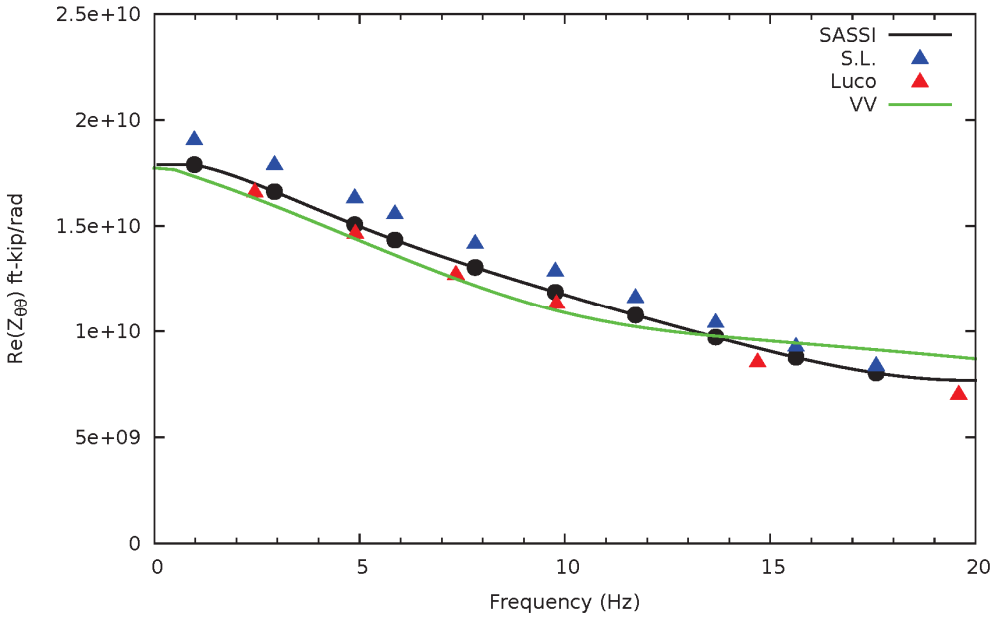

Figure 6-5 Comparison of real rotational impedance, example 1

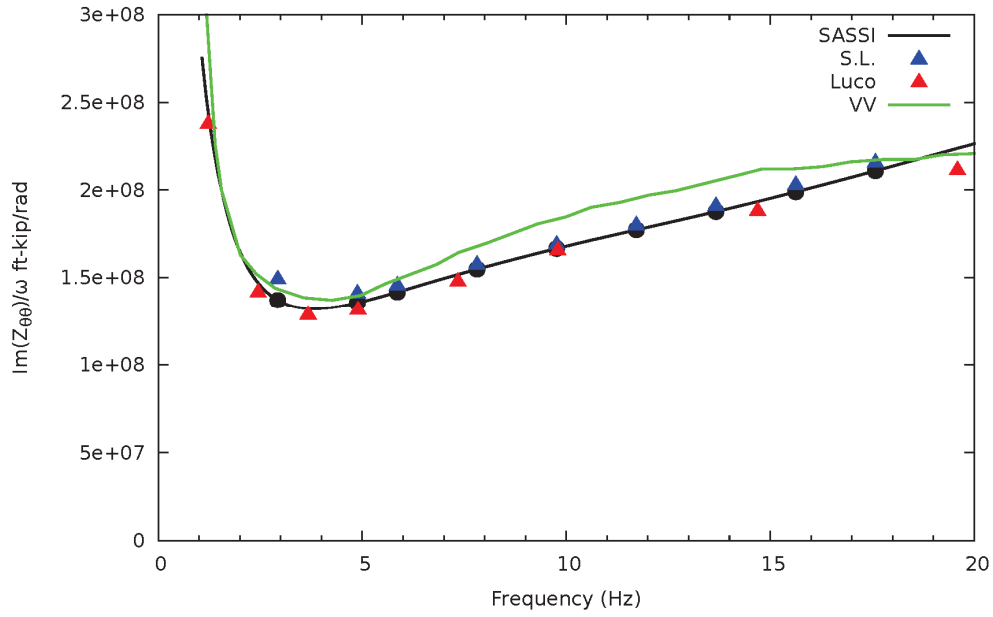

Figure 6-6 Comparison of imaginary rotational impedance, example 1

© Copyright 2019 by NuScale Power, LLC

{{

}}2(a),(c)

Figure 6-7 Comparison of transfer functions, top of containment, example 1

{{

}}2(a),(c)

Figure 6-8 Comparison of transfer functions, top of internals, example 1

© Copyright 2019 by NuScale Power, LLC

{{

}}2(a),(c)

Figure 6-9 Comparison of 2% damped ISRS, top of containment, example 1

{{

}}2(a),(c)

Figure 6-10 Comparison of 2% damped ISRS, top of internals, example 1

© Copyright 2019 by NuScale Power, LLC

{{

}}2(a),(c)

Figure 6-11 Comparison of overturning moment, base of containment, example 1

{{

}}2(a),(c)

Figure 6-12 Comparison of overturning moment, base of internals, example 1

© Copyright 2019 by NuScale Power, LLC

6.2 Example 2: Embedded Building with Soil-Structure Interaction

This example calculates the seismic response of a reinforced concrete building, partially embedded in a stiff soil site. Transfer functions are used to quantify the buildings seismic response. This example problem demonstrates that the SASSI and ANSYS frequency domain solutions are functionally equivalent.

Reduced excavated soil impedances for this problem were developed and stored in the Soil Library. Both the final SASSI and ANSYS solutions use the Soil Library. ANSYS is used to develop the properties of the building structure. These properties are used in the final comparison.

As an intermediate step, a SASSI HOUSE building stiffness is evaluated and the differences in response due to element formulations are noted. A traditional SASSI solution, without the Soil Library, was performed to demonstrate that the Soil Library solution and traditional SASSI solutions are equivalent.

6.2.1 Building Model

This example problem consists of a 94.83 ft long, 47.45 ft wide, 25 ft high building embedded 18.75 ft in a stiff soil site, for a total building height of 43.75 ft. The inside of the building model is empty.

The building model without soil is shown in Figure 6-13, and consists of 592 shell elements. East is the positive X direction and North is the positive Y direction.

The building element size is 6.25 ft vertically and roughly 5.9 ft horizontally. The lower three rows of elements are embedded in the soil. The upper four rows of elements project above the ground surface.

The building consists of a 2 ft thick reinforced concrete shell with the following properties:

Elastic Modulus	759500 ksf
Poisson’s Ratio	0.17
Unit Weight	0.15 kcf Typical 0.668 kcf Roof Slab
Damping	4%

© Copyright 2019 by NuScale Power, LLC

The roof mass was selected to obtain a fixed base natural frequency of about 8 Hz in the North-South direction and 15 Hz in the East-West direction. Vertically, the natural frequency of the roof slab is approximately 4.4 Hz. As discussed below, the building model is analyzed once using SASSI HOUSE module 4-node shell elements, and again with the ANSYS Shell 181 elements.

Loading consists of separate seismic loads applied (1) at the top of the free field surface and (2) at the top of free field layer four which is the same elevation as the base of the foundation. Response is calculated for seismic loads in three orthogonal directions. Response is limited to transfer functions.

An input time history with a time step of 0.005 seconds and 8192 time steps is used. This yields a time history duration of T=40.96 seconds and a frequency step of $\Delta f = 1/T$ = 0.02241 Hz. The Nyquist frequency for this time history is $f_{Nyquist} = 1/(2\Delta t)$ = 100 Hz. The frequency of each Fourier component is $N_f \Delta f$, where N_f is the frequency number. Thus, the frequency for $N_f = 1$ is $f = \Delta f$ = 0.02241 Hz and N_f =4096 is f=100 Hz.

Note that the size of the building model elements is typical of the element size used in the analysis of nuclear facilities. The ability of this mesh to represent natural modes of vibration up to 100 Hz, particularly in out-of-plane wall flexure, was not evaluated for the building geometry. Appendix C contains a study which suggests that, at best, the building roof mesh is only capable of representing out-of-plane flexural modes less than 28 Hz.

6.2.2 Excavated Soil Model

The excavated soil model matches the mesh used for the building model as shown in Figure 6-14 with elements that are approximately 5.93 ft wide by 6.25 ft high. This problem has 612 interaction nodes, of which 297 interaction nodes are common with the basement walls and floor slab.

The excavated soil model has 384 brick elements. The excavated soil is modeled using the SASSI HOUSE Module 8-node brick elements. The SASSI brick elements use a mixed lumped and consistent mass formulation. As discussed in Section 5.1.4, the mixed formulation has better convergence characteristics than a lumped or consistent mass formulation alone.

6.2.3 Soil Site

The layered halfspace site consists of a stiff soil (rock) with a shear wave velocity between 4800 and 5000 fps as shown in Figure 6-15. The halfspace, with a shear wave velocity of 5000 fps, is located at a depth of 300 ft.

© Copyright 2019 by NuScale Power, LLC

The soil column natural frequency for a shear wave, over the depth of the excavation, is:

$$fn = \frac{Vs}{4H} = \frac{4990}{4(3 \times 6.25)} = 66Hz \qquad \text{Equation 6-3}$$

which is within the 100 Hz frequency range considered for this problem.

Poisson's ratio is 0.38 near the surface and reduces to 0.3 at the halfspace. Thus, the P-wave velocity ranges from 11,350 fps near the surface to 8900 fps at depth. The P-wave natural frequency, calculated over the depth of the excavation, is:

$$fn = \frac{Vp}{4H} = \frac{11,350}{4(3 \times 6.25)} = 151Hz \qquad \text{Equation 6-4}$$

which is outside the 100 Hz frequency range considered for this problem.

Material damping for this stiff soil ranges from 0.4% at the surface to 1.4% at depth. The unit weight varies from 120 to 135 psf.

6.2.4 Soil Library

The soil impedance and load vector were generated for Example 2 using the flowchart in Figure 4-4.

Excavated Soil Impedance

Excavated soil impedance is developed using SASSI for 257 frequency numbers, N_f = 1, 16, 32, 48, 64, . . . 4096, which have a typical frequency spacing of ≈ 0.39 Hz for frequencies up to 100 Hz. Of the 257 frequency solutions developed, only a select number of frequencies, 129, were used in this example problem.

The excavated soil model has 612 interaction nodes. Of the 612 interaction nodes, 315 nodes are internal to the excavation. The impedance at these internal nodes is condensed out, as discussed in Section 5.2.1, on a frequency-by-frequency basis, resulting in 297 boundary nodes. The storage size for a symmetric impedance matrix, where each complex number is represented by two 64 bit numbers, is provided below. For Example 2, the

© Copyright 2019 by NuScale Power, LLC

condensation in Equation 5-34 reduces the memory and file size required to store the impedance matrix, by a factor of approximately four.

Case	Nodes	DOF	Memory[9]
Full	612	1,836	25.7 MB
Reduced	297	891	6.1 MB

The reduced excavated soil impedance at these 297 boundary nodes is stored in 257 files with file namesf_xxxxM_s22kRed.mtx, where xxxx is the frequency number, N_f with leading zeros (0001, 0016, . . . 4096) as discussed in Section 7.1. The files are in the Matrix Market file format. The degrees of freedom are contained in a file titled “node.dat.”

The reduced impedance matrix consists of 297 x 3 = 891 degrees of freedom. The response of degree of freedom (i) to an applied displacement at degree of freedom (j) is a local interaction. The out-of-plane bending of a basement wall is affected by local interaction. The response of a rigid massless building is a global effect. The global effect of the 891 DOF reduced impedance matrix can be quantified by constraining the impedance DOF to a single node (Node 536 at center basemat) with six degrees of freedom, as discussed in Section 5.2.2.

The global, or lumped parameter soil impedances are shown in Figure 6-16 through Figure 6-18 and the phase angles are shown in Figure 6-19. The phase angle indicates that the stiffness for low frequencies is dominated by the real term, and for high frequencies is dominated by the imaginary term. Note that the cross coupling stiffness term, $K_{Y\Theta x}$, is negative and the negative term ($\varphi + \pi$) is plotted. The low frequency impedance values are summarized in Table 6-4.

The center of rotation is the cross coupling term, divided by the translation term, i.e., $K_{X\Theta y}/K_{XX}$ and $K_{Y\Theta x}/K_{YY}$ as shown in Figure 6-20.

The lateral deformation impedance terms, K_{XX}, K_{YY}, $K_{X\Theta y,}$ and $K_{Y\Theta x}$, have a small oscillatory amplitude, as seen in Figure 6-16 and Figure 6-17. In the site model, the halfspace is located at a depth of 300 feet with a shear wave velocity of 5000 fps. SASSI simulates the halfspace with 10 additional layers and a transmitting boundary. The depth to the SASSI simulated halfspace is increased from 300 feet to 400 feet by inserting an additional 20 layers of soil with halfspace material properties. A comparison of the two impedances for the K_{XX} impedance is contained in Figure 6-21, and a comparison of the remainder of the terms is contained in Appendix D. Note that the 300 foot and 400 foot

[9] Ideal memory, without overhead. Minimum size for a binary data file

© Copyright 2019 by NuScale Power, LLC

translational impedance oscillations are frequency shifted which indicates that the oscillations are due to shear wave reflections off of the transmitting boundary. Thus, these minor impedance oscillations are an artifact of the analysis method, not actual soil behavior.

Table 6-4 Example 2, low frequency lumped parameter impedance

{{

}}2(a),(c)

Seismic Load Vector

Seismic load vectors corresponding to unit X, Y, and Z input motions at the free field surface, Layer 1, and at the base of the excavation or the top of Layer 4, are developed using SASSI for the same frequencies as the soil impedance. The seismic input is described at two different elevations to understand how the choice of input layer affects the transfer functions.

Similar to the soil impedance, the seismic load vector also has terms at each of the 612 interaction nodes. The seismic load vector is condensed, on a frequency by frequency basis, to the 297 boundary nodes.

The load vector at these 297 boundary nodes is provided in 257 files with file names f_xxxxM_f2Red.mtx, where xxxx is the frequency number as described in the impedance discussion. Each load vector has 891 rows, with each row corresponding to a degree of freedom. Each column in the load vector corresponds to the following load:

Column 1: Unit free-field seismic input in the X direction at the top Layer 1.
Column 2: Unit free-field seismic input in the Y direction at the top Layer 1.
Column 3: Unit free-field seismic input in the Z direction at the top Layer 1.
Column 4: Unit free-field seismic input in the X direction at the top Layer 4.
Column 5: Unit free-field seismic input in the Y direction at the top Layer 4.
Column 6: Unit free-field seismic input in the Z direction at the top Layer 4.

© Copyright 2019 by NuScale Power, LLC

The seismic input is an in-layer motion. Outcrop motions need to be converted to in-layer motions to use these load vectors.

6.2.5 Seismic Response

Several sets of results are presented. The first set of results focuses on seismic response calculated with and without the Soil Library and demonstrates that seismic results with the Soil Library are equivalent to a traditional SASSI solution. The second set of results demonstrates that the ANSYS frequency domain solution, with the Soil Library, is functionally equivalent to a SASSI frequency domain solution. The first set of comparisons are based on the SASSI HOUSE shell element. The second set of comparisons are based on the ANSYS Shell 181 element. As an intermediate step, the SASSI results based on the SASSI HOUSE shell element and the ANSYS Shell 181 element are also compared.

The seismic response is reported at the nodes identified in Figure 6-22. Nodes 857 and 536 are at the center of the roof and basemat, respectively. Node 796 is at the top South-West Corner and is used to quantify rocking. Nodes 368 and 387 are at grade elevation, in the center of the West and South walls, respectively. Nodes 320, 416 and 464 are used to measure fluid pressure acting on the West wall in Example 3. Similarly, nodes 339, 435 and 532 are used to measure fluid pressure acting on the South wall in Example 3.

Seismic Response with Soil Library

A traditional SASSI analysis of the Example 2 structure was performed using the SASSI HOUSE Module to generate the stiffness, and follows the flow chart in Figure 4-8. Transfer functions for the center of the roof are labeled SASSI and shown in Figure 6-23 and Figure 6-24 for input at layer 1 and layer 4, respectively.

A second set of transfer functions in the figures are calculated in two steps using the Soil Library, developed along with SASSI and a SASSI HOUSE building model, as shown in the flow chart in Figure 4-7. The second set of transfer functions is labeled “Soil Library & HOUSE.”

As seen in Figure 6-23 and Figure 6-24, the transfer functions for these two cases are nearly equal. Note that the “Soil Library & HOUSE” response is calculated at 257 equally spaced frequencies, while the “SASSI” response is calculated at 129 equally spaced frequencies.

Peak transfer function responses are observed at the predominant building frequencies of {{ }}[2(a),(c)] in the X, Y and Z directions, respectively. Note that

© Copyright 2019 by NuScale Power, LLC

the stiff soil site increases the building frequency in the Y direction. The response with the control motion at the base of the building, Layer 4, also has a peak corresponding to the 18.75 foot soil column lateral response at 66 Hz, as seen in Figure 6-24a and Figure 6-24b Material damping in the upper portion of the soil column is less than 1%, as seen in Figure 6-15. Thus, the peaks for these transfer functions have an amplitude greater than 50. Vertically the soil column frequency is 151 Hz and this soil column response is outside of the frequency range considered.

Comparison of Element Behavior

The SASSI HOUSE Module 4-node shell element is a thin shell with lumped mass while the ANSYS Shell 181 element is a moderately thick shell with consistent mass. The response with these two different element formulations are compared in this section. It is anticipated that the ANSYS Shell 181 yields more accurate results than the simpler shell element implemented in SASSI.

The response with the SASSI element was presented in the previous section and is labeled “Soil Library & HOUSE” on the plots. The ANSYS solution is a two step solution using the Soil Library and the ANSYS building model, as shown in the flow chart in Figure 4-6, and labeled “Soil Library & ANSYS.” Transfer functions for the center of the roof are shown in Figure 6-25 and Figure 6-26.

The X and Y translation transfer functions compare to about {{ }}$^{2(a),(c)}$ as seen in Figure 6-25a and Figure 6-25b. Translation of the roof node is governed by in-plane behavior and the two elements are approximately equivalent for in-plane behavior up to about {{ }}$^{2(a),(c)}$.

When the control motion is input at the base of the structure, the {{ }}$^{2(a),(c)}$ soil column frequency dominates the response and partially obscures differences in the response. Note that the {{ }}$^{2(a),(c)}$ soil column frequency is not dependent on the element formulation, but the amplitude of response at {{ }}$^{2(a),(c)}$ is rather a function of element formulation, as seen in Figure 6-26a and Figure 6-26b.

Vertical response of the roof is governed by out-of-plane bending and the out-of-plane behavior of the two elements diverges above approximately {{ }}$^{2(a),(c)}$ as seen in Figure 6-25c.

The mesh convergence studies necessary to demonstrate that either the SASSI HOUSE or the ANSYS Shell 181 elements transmit motion up to 100 Hz have not been performed for the Example 2 structure. However, the results with these meshes were compared to demonstrate that the Soil Library and associated analysis techniques are acceptable.

© Copyright 2019 by NuScale Power, LLC

Comparison of ANSYS and SASSI Response

Transfer functions are compared for the following analyses:

- SASSI with the Soil Library and ANSYS element stiffness/mass as described in Figure 4-6, referred to as SASSI in the following discussion and
- ANSYS frequency domain solution with the Soil Library and ANSYS element stiffness/mass as described in Figure 4-5, referred to as ANSYS in the following discussion.

Summary plots of the seismic roof response consisting of transfer functions due to X, Y and Z seismic input are shown in Figure 6-27 and Figure 6-28.

The response calculated using SASSI and the ANSYS frequency domain in Figure 6-27 and Figure 6-28 are equivalent. Note that both solutions use the Soil Library and the ANSYS shell 181 element stiffness.

The excavation and structure are symmetric with respect to the X=0 and Y=0 planes. Thus, the cross coupling seismic response between lateral directions is approximately zero. There is cross coupling between the lateral and vertical directions as the foundation rocks.

Detailed results are provided in Appendix E. Additional results are reported for the following locations:

- SW Roof corner to observe lateral-vertical coupling,
- Center of South wall at grade elevation,
- Center of West wall at grade elevation, and
- Center of the basemat.

Similar to center roof, the response calculated using SASSI and the ANSYS frequency domain solutions are equivalent.

6.2.6 Dynamic Modal Characteristics from Fixed Base Analysis

Modal analysis of the fixed base structure is performed by fixing nodes at bottom of the excavation (i.e., nodes 18.75 foot below grade are fixed). Nodes above the bottom of the excavation (on the sides of the excavation) are not fixed. Frequencies and modal masses from the modal analysis of the fixed-base structure are shown in Table 6-5.

© Copyright 2019 by NuScale Power, LLC

Table 6-5 Frequencies, modal mass, and cumulative mass for Example 2

Mode Number	Frequency (Hz)	Modal Masses (kip * sec^2 / ft)					
		X-Direction		Y-Direction		Z-Direction	
		Modal Mass	Cumulative Modal Mass	Modal Mass	Cumulative Modal Mass	Modal Mass	Cumulative Modal Mass
1	4.36	0.0	0.0	0.0	0.0	110.1	110.1
2	6.35	0.1	0.1	0.0	0.0	0.0	110.1
3	7.96	0.0	0.1	253.8	253.8	0.0	110.1
4	9.58	0.0	0.1	0.0	253.8	17.6	127.7
5	11.16	0.0	0.1	0.0	253.8	0.0	127.7
6	13.07	0.0	0.1	0.0	253.8	1.0	128.7
7	13.63	71.3	71.4	0.0	253.8	0.0	128.7
8	13.65	0.0	71.4	0.0	253.8	0.0	128.7
9	14.91	167.8	239.2	0.0	253.8	0.0	128.7
10	15.90	0.0	239.2	1.5	255.4	0.0	128.7
11	16.04	18.9	258.0	0.0	255.4	0.0	128.7
12	16.62	0.0	258.0	0.0	255.4	0.0	128.8
13	17.18	0.0	258.0	0.0	255.4	0.0	128.8
14	17.85	0.0	258.0	0.1	255.5	0.0	128.8
15	18.74	2.1	260.2	0.0	255.5	0.0	128.8
16	20.24	0.0	260.2	0.0	255.5	0.0	128.8
17	21.27	0.0	260.2	0.0	255.5	8.4	137.1
18	22.61	0.0	260.2	4.5	260.0	0.0	137.1
19	22.74	0.0	260.2	0.0	260.0	0.0	137.1
20	23.23	0.0	260.2	0.0	260.0	0.2	137.3
21	27.79	0.0	260.2	0.0	260.0	24.7	162.0
22	28.84	0.0	260.2	0.0	260.0	0.0	162.0
23	29.21	0.9	261.1	0.0	260.0	0.0	162.0
24	29.94	0.2	261.2	0.0	260.0	0.0	162.0
25	30.07	0.0	261.2	0.0	260.0	0.0	162.0
26	32.37	0.0	261.3	0.0	260.0	0.0	162.0

© Copyright 2019 by NuScale Power, LLC

Mode Number	Frequency (Hz)	Modal Masses (kip * sec^2 / ft)					
		X-Direction		Y-Direction		Z-Direction	
		Modal Mass	Cumulative Modal Mass	Modal Mass	Cumulative Modal Mass	Modal Mass	Cumulative Modal Mass
27	32.96	0.0	261.3	9.9	269.9	0.0	162.0
28	33.22	0.0	261.3	0.0	269.9	4.7	166.7
29	34.72	0.0	261.3	2.9	272.8	0.0	166.7
30	34.75	0.0	261.3	0.0	272.8	0.5	167.2
31	36.20	0.0	261.3	0.0	272.8	0.0	167.2
32	37.55	0.0	261.3	0.0	272.8	0.0	167.2
33	37.89	0.1	261.4	0.0	272.8	0.0	167.2
34	38.86	0.0	261.4	2.7	275.5	0.0	167.2
35	38.88	0.0	261.4	0.0	275.5	5.5	172.7
36	39.90	0.0	261.4	0.0	275.5	8.9	181.7
37	40.25	0.0	261.4	0.0	275.5	0.0	181.7
38	41.86	2.1	263.5	0.0	275.5	0.0	181.7
39	42.38	0.0	263.5	0.0	275.5	0.0	181.7
40	42.58	0.0	263.5	0.0	275.5	3.5	185.1
41	43.22	0.9	264.4	0.0	275.5	0.0	185.1
42	44.99	0.0	264.4	0.0	275.5	4.2	189.3
43	46.11	0.0	264.4	0.0	275.5	0.5	189.8
44	46.15	0.0	264.4	1.5	277.0	0.0	189.8
45	47.09	0.0	264.4	1.3	278.3	0.0	189.8
46	47.78	0.0	264.4	0.2	278.5	0.0	189.8
47	48.03	0.0	264.4	0.0	278.5	1.5	191.3
48	49.45	0.0	264.4	0.0	278.5	0.0	191.3
49	50.19	0.2	264.6	0.0	278.5	0.0	191.3
50	50.39	0.0	264.6	0.0	278.5	0.0	191.3
51	52.48	0.0	264.6	0.0	278.5	0.0	191.3
52	53.32	0.0	264.6	0.0	278.5	0.0	191.3
53	54.94	0.0	264.6	0.1	278.6	0.0	191.3

© Copyright 2019 by NuScale Power, LLC

Mode Number	Frequency (Hz)	Modal Masses (kip * sec^2 / ft)					
		X-Direction		Y-Direction		Z-Direction	
		Modal Mass	Cumulative Modal Mass	Modal Mass	Cumulative Modal Mass	Modal Mass	Cumulative Modal Mass
54	55.63	0.0	264.6	0.0	278.6	0.0	191.3
55	55.85	0.3	264.9	0.0	278.6	0.0	191.3
56	57.40	0.0	264.9	0.0	278.6	0.0	191.3
57	57.77	0.0	264.9	0.0	278.7	0.0	191.3
58	58.46	0.0	264.9	0.0	278.7	33.7	225.0
59	58.90	0.1	265.0	0.0	278.7	0.0	225.0
60	59.02	4.8	269.8	0.0	278.7	0.0	225.0
61	59.54	0.0	269.8	1.0	279.6	0.0	225.0
62	61.25	0.0	269.8	0.0	279.6	0.8	225.8
63	61.96	0.0	269.8	0.0	279.6	0.0	225.8
64	62.05	0.0	269.8	0.0	279.6	37.6	263.4
65	63.36	0.0	269.8	0.0	279.6	0.0	263.4
66	64.04	7.1	276.9	0.0	279.6	0.0	263.4
67	64.59	0.0	276.9	0.0	279.6	0.3	263.7
68	65.03	0.0	276.9	0.2	279.9	0.0	263.7
69	65.31	0.0	276.9	0.0	279.9	0.0	263.7
70	65.85	0.0	276.9	0.0	279.9	1.8	265.5
71	66.61	1.3	278.3	0.0	279.9	0.0	265.5
72	67.73	0.0	278.3	0.0	279.9	0.8	266.2
73	68.27	0.0	278.3	2.9	282.7	0.0	266.2
74	70.52	0.0	278.3	0.0	282.7	0.7	266.9
75	71.62	0.0	278.3	0.0	282.7	0.0	266.9
76	71.81	0.0	278.3	0.0	282.7	0.0	266.9
77	72.00	0.0	278.3	0.8	283.5	0.0	266.9
78	72.93	0.8	279.1	0.0	283.5	0.0	266.9
79	73.43	0.0	279.1	2.4	285.9	0.0	266.9
80	74.46	0.1	279.2	0.0	285.9	0.0	266.9

© Copyright 2019 by NuScale Power, LLC

Mode Number	Frequency (Hz)	Modal Masses (kip * sec^2 / ft)					
		X-Direction		Y-Direction		Z-Direction	
		Modal Mass	Cumulative Modal Mass	Modal Mass	Cumulative Modal Mass	Modal Mass	Cumulative Modal Mass
81	76.66	0.0	279.2	0.3	286.2	0.0	266.9
82	77.41	0.0	279.2	0.0	286.2	0.0	266.9
83	77.81	0.0	279.2	0.0	286.2	2.1	268.9
84	79.27	0.0	279.2	0.0	286.2	1.7	270.6
85	79.84	0.0	279.2	0.0	286.2	0.0	270.6
86	80.09	0.8	280.0	0.0	286.2	0.0	270.6
87	81.18	1.1	281.0	0.0	286.2	0.0	270.6
88	81.20	0.0	281.0	0.2	286.4	0.0	270.6
89	83.63	0.1	281.1	0.0	286.4	0.0	270.6
90	83.84	0.0	281.1	0.9	287.3	0.0	270.6
91	84.40	0.0	281.1	0.0	287.3	0.0	270.6
92	85.55	0.0	281.1	0.0	287.3	0.0	270.6
93	85.66	0.0	281.1	0.0	287.3	0.0	270.7
94	86.24	0.0	281.1	0.0	287.3	0.1	270.7
95	87.62	0.0	281.1	0.0	287.3	0.0	270.7
96	88.37	0.0	281.1	0.0	287.3	0.7	271.4
97	88.86	0.0	281.1	0.0	287.3	0.5	271.9
98	88.98	0.7	281.8	0.0	287.3	0.0	271.9
99	89.55	1.2	283.0	0.0	287.3	0.0	271.9
100	90.62	0.0	283.0	0.2	287.5	0.0	271.9
101	91.16	0.0	283.0	0.0	287.5	0.1	272.0
102	91.41	0.0	283.0	0.0	287.5	0.0	272.0
103	91.47	0.0	283.0	0.8	288.3	0.0	272.0
104	91.61	0.7	283.7	0.0	288.3	0.0	272.0
105	94.07	0.0	283.7	0.0	288.3	0.0	272.0
106	94.09	0.0	283.7	0.0	288.3	0.0	272.0
107	94.27	0.0	283.7	0.0	288.3	1.2	273.2

© Copyright 2019 by NuScale Power, LLC

Mode Number	Frequency (Hz)	Modal Masses (kip * sec^2 / ft)					
		X-Direction		Y-Direction		Z-Direction	
		Modal Mass	Cumulative Modal Mass	Modal Mass	Cumulative Modal Mass	Modal Mass	Cumulative Modal Mass
108	94.43	0.0	283.7	0.0	288.3	0.0	273.2
109	95.00	0.0	283.7	0.0	288.3	0.0	273.2
110	96.29	0.0	283.7	0.5	288.8	0.0	273.2
111	98.33	0.0	283.7	0.0	288.8	0.0	273.2
112	99.43	0.0	283.7	0.0	288.8	0.1	273.3

6.2.7 Example 2 Summary

Example 2 demonstrates the use of the Soil Library to develop the impedance and load vector for a partially embedded building. A comparison of building responses with and without the Soil Library demonstrates that the use of the Soil Library, including pre-calculated impedances and load vectors, with the reduction discussed in Section 5.2.1 is functionally equivalent to a traditional SASSI analysis.

The seismic response of the Example 2 building is calculated using both SASSI and ANSYS. The ANSYS solution uses the Soil Library, ANSYS structural elements, the frequency domain solver, and incorporates transfer function interpolation (Section 5.1.7). There is good comparison between the SASSI and ANSYS results. This problem demonstrates that the ANSYS frequency domain solution is functionally equivalent to the SASSI frequency domain solution.

ANSYS Shell 181 is a moderately thick shell stiffness formulation with a consistent mass matrix. The response of this element was compared to the response based on the SASSI thin shell with a lumped mass matrix. Differences in response due to the different element formulations are noted. This comparison illustrates the advantages of accessing modern finite elements in a soil-structure interaction analysis.

© Copyright 2019 by NuScale Power, LLC

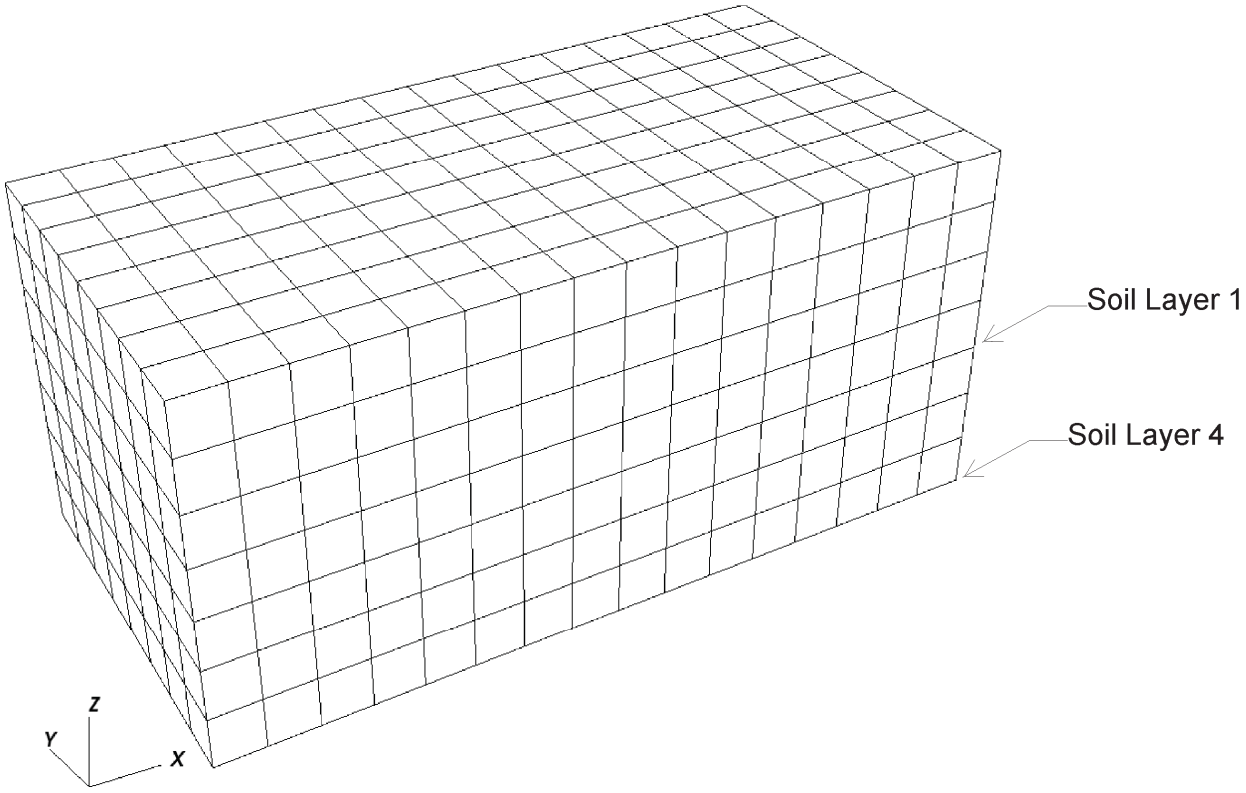

Figure 6-13 Example 2, building model, +Y is north and +X is east

© Copyright 2019 by NuScale Power, LLC

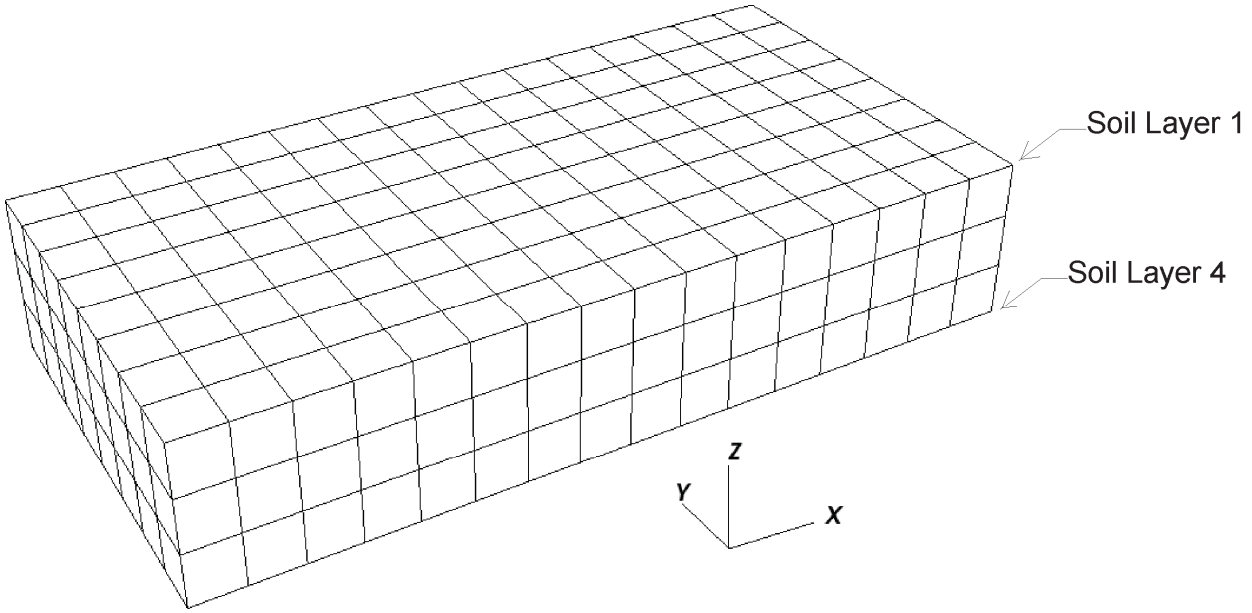

Figure 6-14 Example 2, excavated soil model, +Y is north and +X is east

© Copyright 2019 by NuScale Power, LLC

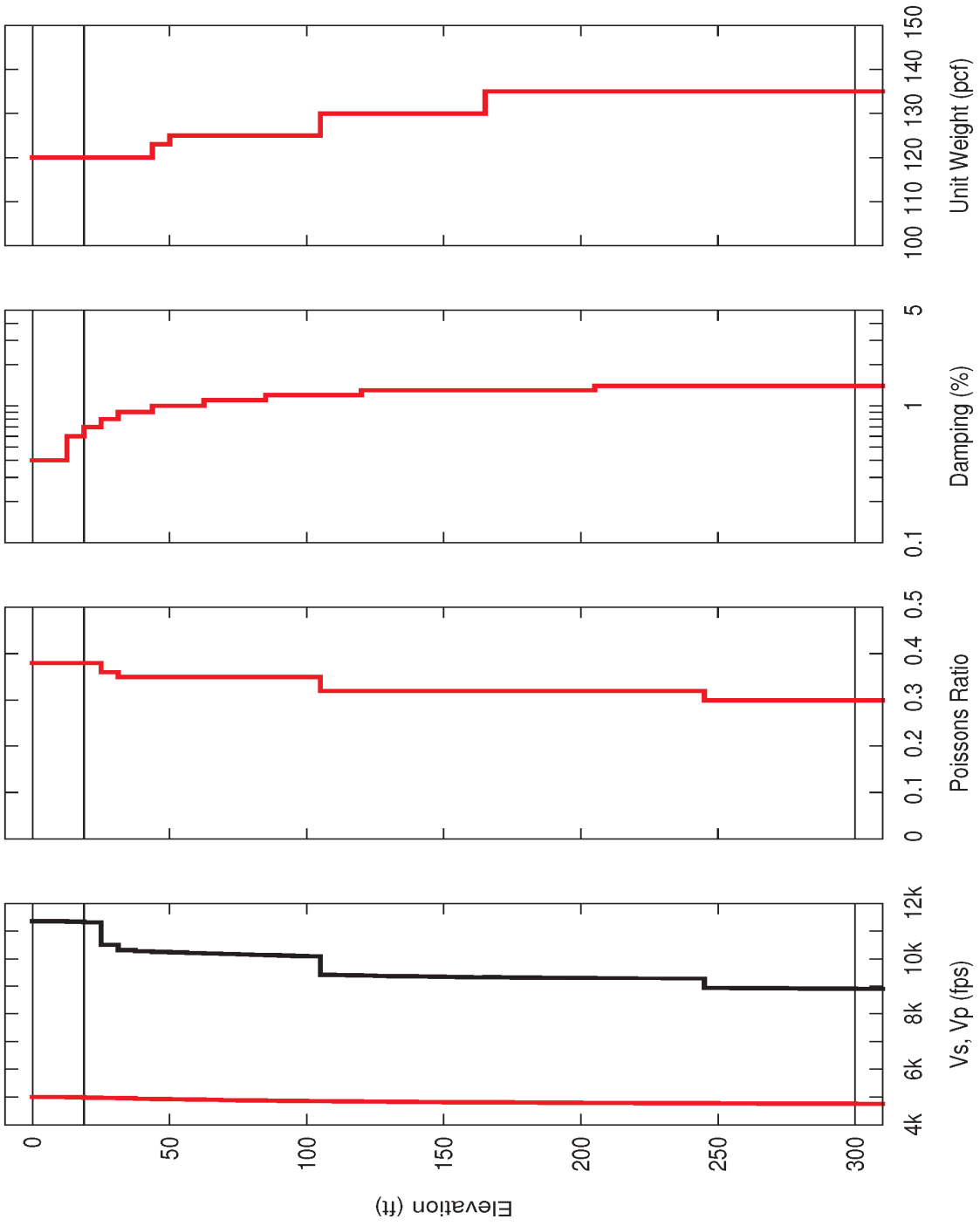

Figure 6-15 Example problem 2 soil site

© Copyright 2019 by NuScale Power, LLC

{{

}}2(a),(c)

Figure 6-16 Translation soil impedance, example 2

{{

}}2(a),(c)

Figure 6-17 Translation-rocking soil impedance, example 2

© Copyright 2019 by NuScale Power, LLC

{{

}}2(a),(c)

Figure 6-18 Rocking, torsion soil impedance, example 2

{{

}}2(a),(c)

Figure 6-19 Soil impedance phase angle, example 2

© Copyright 2019 by NuScale Power, LLC

{{

}}2(a),(c)

Figure 6-20 Soil impedance center of rotation, example 2

© Copyright 2019 by NuScale Power, LLC

{{

}}2(a),(c)

Figure 6-21 Comparison of *Kxx* lumped parameter soil impedance

© Copyright 2019 by NuScale Power, LLC

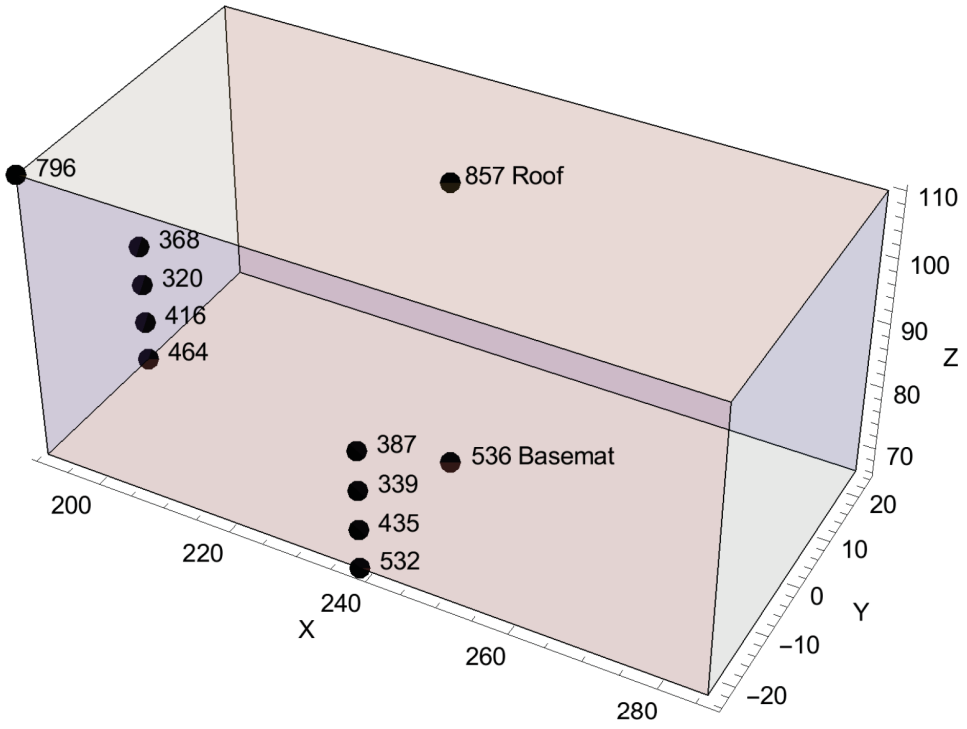

+X is East
+Y is North
+Z is Up

Nodes		Depth Below
West Wall	South Wall	Grade (ft)
368	387	0
320	339	6.25
416	436	12.5
464	532	18.75

Figure 6-22 Node locations with reported seismic response

© Copyright 2019 by NuScale Power, LLC

{{

}}2(a),(c)

Figure 6-23 Comparison of SASSI and soil library solutions, center roof response, layer 1 input

© Copyright 2019 by NuScale Power, LLC

{{

}}2(a),(c)

Figure 6-24 Comparison of SASSI and soil library solutions, center roof response, layer 4 input

© Copyright 2019 by NuScale Power, LLC

{{

}}2(a),(c)

Figure 6-25 Comparison of SASSI and ANSYS plate element formulations, center roof response, layer 1 input

© Copyright 2019 by NuScale Power, LLC

{{

}}2(a),(c)

Figure 6-26 Comparison of SASSI and ANYSYS plate element formulations, center roof response, layer 4 input

© Copyright 2019 by NuScale Power, LLC

{{

}}2(a),(c)

Figure 6-27 Comparison of SASSI and ANSYS solution, center roof response, layer 1 input

© Copyright 2019 by NuScale Power, LLC

{{

}}2(a),(c)

Figure 6-28 Comparison of SASSI and ANSYS solution, center roof response, layer 4 input

© Copyright 2019 by NuScale Power, LLC

6.3 Example 3: Embedded Building with Soil-Structure-Fluid Interaction

This example calculates the seismic response of a reinforced concrete building with an internal pool, and considers the interaction between soil, structure, and fluid substructures. This example demonstrates that the SASSI and ANSYS frequency domain solutions are functionally equivalent for Soil-Structure-Fluid Interaction (SSFI) problems.

The Soil Library impedance and building models from Example 2 are reused in this problem. The pool is modeled using ANSYS acoustic (Fluid 30) elements that are capable of representing pressure transients during a seismic event. Sloshing of the pool was not considered in this formulation, and is beyond the scope of this Topical Report. Sloshing occurs at very low frequencies - less than those in the harmonic analysis. Sloshing should be considered during a comprehensive structural analysis. These elements introduce pressure degrees of freedom to the mathematical model. The acoustic elements also introduce unsymmetric stiffness and mass coupling terms. Thus, an unsymmetric solver was used for Example 3.

Similar to Example 2, transfer functions are used to quantify the seismic response of the building and fluid. The Example 2 and Example 3 results are also compared to understand the effects of fluid interaction on this soil-structure system.

6.3.1 Analytical Model

This example problem consists of a 94.83 ft long by 47.45 ft wide by 25 ft high building embedded 18.75 ft in a stiff soil site, for a total building height of 43.75 feet. An 18.75 ft deep pool is located inside the building. Thus, the top of the pool and exterior grade are at the same elevation.

The Example 2 building model, shown in Figure 6-13, was used in this analysis. The Example 2 Soil Library consisting of soil impedance and seismic load vectors were also used in this analysis. Acoustic fluid properties used in the analysis are:

Fluid unit weight, γ	0.062 kcf
Fluid P-wave velocity	5003 fps
Shear viscosity	1.423×10^{-8} kip sec/ft^2
Bulk viscosity	$0.6 \times 1.423 \times 10^{-8}$ kip sec/ft^2

The fluid mesh has the same geometry as the excavated soil mesh in Figure 6-14.

© Copyright 2019 by NuScale Power, LLC

6.3.2 Fluid Structure Interaction

The equation of motion for the fluid structure interaction portion of the analysis, in the frequency domain, is:

$$\left(-\omega^2\begin{bmatrix}[M_S] & 0\\ \bar{\rho}_0[R]^T & [M_F]\end{bmatrix}+i\omega\begin{bmatrix}[C_S] & 0\\ 0 & [C_F]\end{bmatrix}+\begin{bmatrix}[K_S] & [R]\\ 0 & [K_F]\end{bmatrix}\right)\begin{Bmatrix}\{X\}\\ \{P\}\end{Bmatrix}=\begin{Bmatrix}F_S\\ F_F\end{Bmatrix} \quad \text{Equation 6-5}$$

Where,
X is the structural displacements,

P is the acoustic pressure with the units (ksf sec^2/ft),

F_S and F_F are applied structural and fluid loads, respectively,

$[M_S]$, $[C_S]$, and $[K_S]$ are the mass, viscous damping and stiffness of the ANSYS Shell elements. Note that the structural viscous damping[10] in this problem is zero,

$[M_F]$, $[C_F]$, and $[K_F]$ are the acoustic fluid mass, acoustic fluid damping and acoustic fluid stiffness matrices of the ANSYS Fluid 30 element,

$\bar{\rho}_0$ is the acoustic fluid mass density constant, and

[*R***]** is the acoustic fluid boundary matrix which relates acoustic pressure, P, to structural forces acting on the element at the water-solid interface, *{F }* = [*R*]*{P}*. Both [*R*] and $\bar{\rho}_0$ are generated by the ANSYS Fluid 30 element.

The term within parentheses on the left side of Equation 6-5 is the dynamic stiffness of the structure. Partition the degrees-of-freedom (DOFs) into structural DOFs and soil interaction DOFs which may be shared with the structural DOFs, i.e.:

$$\begin{Bmatrix}\{X\}\\ \{P\}\end{Bmatrix}=\begin{Bmatrix}X_s\\ X_i\\ P\end{Bmatrix} \quad \text{Equation 6-6}$$

[10] The fluid elements, $[C_F]$, have viscous damping while the structural elements do not have viscous damping. Structural damping is represented by a complex stiffness.

© Copyright 2019 by NuScale Power, LLC

For the fluid and structure without soil-structure interaction, Equation 6-5 can be written as:

$$[S]\begin{Bmatrix} X_s \\ X_i \\ P \end{Bmatrix} = \begin{bmatrix} S_{ss} & S_{si} & S_{sp} \\ S_{is} & S_{ii} & S_{ip} \\ S_{ps} & S_{pi} & S_{pp} \end{bmatrix}\begin{Bmatrix} X_s \\ X_i \\ P \end{Bmatrix} = \begin{Bmatrix} F_s \\ F_i \\ F_F \end{Bmatrix} \quad \text{Equation 6-7}$$

The structural dynamic stiffness matrices S_{ss}, S_{si}, S_{is} and S_{is} are of the same form as previously defined for the structure by Equation 5-5.

The dynamic stiffness matrices representing fluid and FSI are:

$$S_{sp} = [R] \quad \text{Equation 6-8}$$

$$S_{ps} = -\omega^2 \bar{\rho}_0 [R]^T \quad \text{Equation 6-9}$$

$$S_{pp} = -\omega^2 [M_F] + i\omega [C_F] + [K_F] \quad \text{Equation 6-10}$$

Generally the FSI surfaces are not directly coupled to the soil degrees of freedom, and therefore S_{ip} = 0 and S_{pi} = 0. The equation of motion for the structure alone is:

$$[S]\begin{Bmatrix} X_s \\ X_i \\ P \end{Bmatrix} = \begin{bmatrix} S_{ss} & S_{si} & S_{sp} \\ S_{is} & S_{ii} & 0 \\ S_{ps} & 0 & S_{pp} \end{bmatrix}\begin{Bmatrix} X_s \\ X_i \\ P \end{Bmatrix} = \begin{Bmatrix} F_s \\ F_i \\ F_F \end{Bmatrix} \quad \text{Equation 6-11}$$

For seismic loading, the external forces F_s and F_F are both zero. The force F_i and equations of motion of the total soil-fluid-structure system are determined following the same steps as described in Section 5.1.6 for the soil-structure system without fluid. The final equation for the structural motion is the same as Equation 5-21 but with the addition

© Copyright 2019 by NuScale Power, LLC

of fluid forces. Fluid pressures are coupled to the structural motion but not directly coupled to soil. The final equation of motion is:

$$\begin{bmatrix} S_{ss} & S_{st} & S_{sp} \\ S_{ts} & S_{tt} + Z - S'_{ii} & 0 \\ S_{ps} & 0 & S_{pp} \end{bmatrix} \begin{Bmatrix} X_s \\ X_i \\ P \end{Bmatrix} = \begin{Bmatrix} 0 \\ F_{EQ} \\ 0 \end{Bmatrix}$$ Equation 6-12

F_{EQ} is given by Equation 5-22 and is unchanged by the fluid. Likewise, the excavated impedance matrix Z - S'_{ii} is unchanged by the fluid. The fluid-structure coupling S_{sp} and S_{ps} are produced from the fluid-structure boundary matrix, [*R*], in Equation 6-5, Due to the terms S_{sp} and S_{ps}, the equations of motion for the soil-structure-fluid system are not symmetric.

Recall that the acoustic pressure is due to an *x* =1 foot cyclic displacement of the control layer at the specified frequency, or:

$$h(\omega)e^{i\omega t} = TF(\omega) \cdot x(\omega)e^{i\omega t}$$ Equation 6-13

where *h*(*ω*) is a frequency response function or transfer function. Taking the second derivative of displacement yields an acceleration of $\ddot{x}(\omega)e^{i\omega t} = -\omega^2 x(\omega)e^{i\omega t}$.

Substituting, the pressure as a function of applied acceleration becomes:

$$h(\omega)e^{i\omega t} = \frac{1}{-\omega^2} TF(\omega) \cdot \ddot{x}(\omega)e^{i\omega t}$$ Equation 6-14

For an acceleration expressed in ft/sec^2.

Since we are interested in acoustic pressure given an acceleration, the acoustic pressure transfer functions are reported as:

$$h(\omega)_{Pressure} = \frac{1}{-\omega^2} TF(\omega)$$ Equation 6-15

© Copyright 2019 by NuScale Power, LLC

which has the units ksf sec^2/ft. The acoustic pressure transfer function for a 1g acceleration on the control layer is:

$$h(\omega)_{Pressure} = \frac{32.2}{-\omega^2} TF(\omega) \qquad \text{Equation 6-16}$$

and the transfer function has the units ksf.

6.3.3 Seismic Response

Several sets of results are presented. The first set of results demonstrates that the ANSYS frequency domain solution, with the Soil Library, and fluid structure interaction is functionally equivalent to a SASSI frequency domain solution.

The surface time histories shown in Figure 6-29, with spectra in Figure 6-30, are used as input to this analysis to evaluate the structural response. These time histories are extracted from the PEER NGA Strong Motion Database and are scaled to 1g. Structural responses, represented by In-Structure Response Spectra (ISRS), are compared along with acoustic pressure time history responses.

The second set of results focuses on the effects of fluid interaction and consists of a fixed base comparison of the building models with and without fluid elements. The third set of results compares the soil-structure interaction in Example 2 with the soil-structure-fluid interaction in Example 3.

Figure 6-22 identities the nodes where the structural and fluid response to seismic loads are reported.

Comparison of ANSYS and SASSI Response

Transfer functions are calculated using

- SASSI with the Soil Library and ANSYS element stiffness as described in Figure 4-6, referred to as the SASSI solution in the following discussion, and

- ANSYS frequency domain solution with the Soil Library and ANSYS element stiffness as described in Figure 4-5, referred to as the ANSYS solution in the following discussion.

These transfer functions are compared in this section.

© Copyright 2019 by NuScale Power, LLC

Structural Response: The structural response, represented by transfer functions of the center roof node are compared in Figure 6-31 for input at Layer 1 and Figure 6-32 for input at Layer 4. As seen in the figures, the responses calculated using SASSI and ANSYS are equivalent.

Transfer functions at nodes on the southwest roof corner, center of the basemat, and center of the West and South walls, are also compared in Appendix F. As seen in Appendix F, the response calculated using SASSI and ANSYS at these additional nodes are equivalent.

The h1, h2 and v time histories are input at Layer 1 and used to generate time-history response at each node. The time history response is then used to generate 5% damped in-structure response spectra[11]. A representative response spectra for the center of the roof slab is presented in Figure 6-33. As seen in the figure, the response calculated using SASSI and ANSYS are equivalent for the horizontal directions. Additional pressure time history comparisons are contained in Appendix F.

Fluid Response: The fluid response at the base of the West and South walls, and at the center of the basemat for ground motions in the X, Y, and Z directions at Layer 1, is provided in Figure 6-34. The SASSI and ANSYS fluid pressure transfer functions are equivalent. Similarly, the fluid pressure transfer functions are compared for the Layer 4 input in Figure 6-35. Again, the SASSI and ANSYS fluid pressure transfer functions for this case are equivalent.

Transfer functions for nodes with different depths at the center of the West and South walls are compared in Appendix F. As seen in Appendix F, the response calculated using SASSI and ANSYS at these additional nodes are also equivalent.

Note that the transfer functions in Figure 6-34, Figure 6-35, and Apendix F are based on acceleration input per Equation 6-15.

The transfer function pressures near the zero frequency represent a near static condition and are summarized in Table 6-6. For the vertical ground motion, the fluid is contained by the four walls and basemat and the resulting pressure is approximately equivalent to the node depth from the free surface. Thus, the pressure at the base of the pool, in engineering units, is:

$$P_{Eng} = \gamma \cdot h = 1.1625\ ksf = 8.1\ psi \qquad \text{Equation 6-17}$$

[11] Linear interpolation of the in-structure acceleration time history is performed to obtain a minimum of 20 points per period.

© Copyright 2019 by NuScale Power, LLC

where γ is the unit weight of water, γ =0.062 kcf. Dividing by gravity yields the acoustic pressure:

$$P = \frac{P_{Eng}}{g} = \frac{\gamma}{g} h = 0.0361 \ (ksf sec^2/ft) \qquad \text{Equation 6-18}$$

where g is 32.2 ft/sec^2.

Table 6-6 Example 3 low frequency acoustic pressure

Location	Depth	Acoustic Pressure (ksf sec^2/ft)		
		X Input	Y Input	Z Input
{{				
				}}$^{2(a),(c)}$

Note that these pressures are independent of the ground motion input layer because there is no dynamic amplification at low frequency.

P is equal to the pressure at the bottom of the pool, in Table 6-6, with low frequency (nearly static) vertical acceleration. Scaling the pressure at the {{ }}$^{2(a),(c)}$ yields {{ }}$^{2(a),(c)}$ ksf sec^2/ft, which compares well with the pressures calculated by both ANSYS and SASSI.

For lateral base movement, the fluid is unrestrained and the only elements with pressure are on the surface perpendicular to the axis of motion.

Figure 6-36 compares the acoustic pressure time history at three depths on the west wall for an X direction h1 ground motion with input at Layer 1. The acoustic pressures calculated by SASSI and ANSYS compare well. Additional pressure time history comparisons are contained in Appendix F.

Fixed Base Response Comparisons With and Without Fluid

The fixed base response of the Example 2 building model with and without fluid are compared to understand how the fluid changes the buildings response. The basemat nodes, including the nodes at the base of the wall, are restrained in the fixed base analysis and unit cyclic base motions are imposed in the X, Y and Z direction. The fixed base response is computed using SDE-SASSI.

© Copyright 2019 by NuScale Power, LLC

Typical transfer functions are shown in Figure 6-37. The effect of the fluid is to increase the amplitude of response for the overall building by roughly {{ }}[2(a),(c)] as seen by the center roof response in Figure 6-37a. The shift in overall building frequency from the added fluid mass is negligible.

The effect of the fluid on the first out-of-plane wall mode is to increase the amplitude by roughly {{ }}[2(a),(c)] and reduce the natural frequency slightly as seen in Figure 6-37b. Additional locations and input directions are examined in Appendix G. The fluid effects on some of the building's higher modes are more dramatic than the impact on the first mode.

SSI Response With and Without Fluid

The SSI responses of the Example 2 building model with and without fluid are compared to understand how the fluid changes the SSI response. Typical transfer functions are shown in Figure 6-38 and Figure 6-39 for input at soil layers 1 and 4. The overall building response due to X input, shown in Figure 6-38a, indicates that the fluid has a minor effect on the building's SSI response. When the input is moved to layer 4, the soil column frequency dominates the response and the effect of fluid on SSI is smaller, as shown in Figure 6-39b

The effect of fluid on the out-of-plane response of the wall, shown in Figure 6-38b, indicates that the fluid has a negligible effect on the low frequency behavior and that the fluid has a minor effect on the high frequency response. Comparing Figure 6-38b with the fixed base response, Figure 6-37b, the soil attached to the wall has suppressed motion below {{ }}[2(a),(c)] and has resulted in a significant reduction in the overall wall response. This suggests the nearly 5000 fps soil is rigid compared to the building for out-of-plane wall response.

6.3.4 Dynamic Modal Characteristics from Fixed Base Analysis

Modal analysis of the fixed base structure is performed by fixing nodes at bottom of the excavation (i.e. nodes 18.75 foot below grade are fixed). Nodes above the bottom of the excavation (on the sides of the excavation) are not fixed. Frequencies and modal masses from the modal analysis of the fixed-base structure are shown in Table 6-7.

© Copyright 2019 by NuScale Power, LLC

Table 6-7 Frequencies, modal mass, and cumulative mass for Example 3

Mode Number	Frequency (Hz)	Modal Masses (kip * sec^2 / ft)					
		X-Direction		Y-Direction		Z-Direction	
		Modal Mass	Cumulative Modal Mass	Modal Mass	Cumulative Modal Mass	Modal Mass	Cumulative Modal Mass
1	4.36	0.0	0.0	0.0	0.0	109.6	109.6
2	6.35	0.1	0.1	0.0	0.0	0.0	109.6
3	7.89	0.0	0.1	275.8	275.8	0.0	109.6
4	9.57	0.0	0.1	0.0	275.8	17.7	127.3
5	10.63	0.0	0.1	0.2	276.0	0.0	127.3
6	11.58	0.0	0.1	0.0	276.0	1.4	128.7
7	13.07	0.0	0.1	0.0	276.0	0.0	128.7
8	13.15	83.1	83.3	0.0	276.0	0.0	128.7
9	14.59	0.3	83.6	0.0	276.0	0.0	128.7
10	14.68	0.0	83.6	4.8	280.9	0.0	128.7
11	14.89	174.9	258.5	0.0	280.9	0.0	128.7
12	14.93	0.0	258.5	0.0	280.9	0.1	128.8
13	16.24	0.0	258.5	0.0	280.9	0.0	128.8
14	16.71	14.7	273.2	0.0	280.9	0.0	128.8
15	17.67	0.0	273.2	0.9	281.8	0.0	128.8
16	19.65	0.0	273.2	0.0	281.8	0.0	128.8
17	20.40	0.0	273.2	0.0	281.8	0.3	129.0
18	20.47	0.0	273.2	6.4	288.2	0.0	129.0
19	20.99	0.0	273.2	0.0	288.2	8.3	137.4
20	22.71	0.0	273.2	0.0	288.2	0.0	137.4
21	26.09	0.0	273.2	0.0	288.2	13.2	150.6
22	27.45	0.0	273.2	0.0	288.2	0.0	150.6
23	28.27	3.1	276.3	0.0	288.2	0.0	150.6
24	28.67	0.5	276.9	0.0	288.2	0.0	150.6
25	28.75	0.0	276.9	0.3	288.5	0.0	150.6
26	28.99	0.0	276.9	0.0	288.5	0.0	150.6
27	30.17	0.0	276.9	2.1	290.6	0.0	150.6
28	31.13	0.0	276.9	16.8	307.4	0.0	150.6

© Copyright 2019 by NuScale Power, LLC

Mode Number	Frequency (Hz)	Modal Masses (kip * sec^2 / ft)					
		X-Direction		Y-Direction		Z-Direction	
		Modal Mass	Cumulative Modal Mass	Modal Mass	Cumulative Modal Mass	Modal Mass	Cumulative Modal Mass
29	31.54	0.0	276.9	0.0	307.4	0.0	150.6
30	32.00	0.0	276.9	0.0	307.4	0.4	150.9
31	32.44	0.0	276.9	0.0	307.4	5.2	156.1
32	33.25	0.0	276.9	0.0	307.4	17.6	173.7
33	33.44	0.0	276.9	2.6	310.0	0.0	173.7
34	34.46	0.0	276.9	0.0	310.0	0.0	173.7
35	35.11	3.4	280.3	0.0	310.0	0.0	173.7
36	36.08	1.0	281.3	0.0	310.0	0.0	173.7
37	36.82	0.0	281.3	0.0	310.0	0.0	173.7
38	36.98	0.0	281.3	0.0	310.0	0.2	173.8
39	37.24	0.3	281.6	0.0	310.0	0.0	173.8
40	39.04	0.0	281.6	4.4	314.4	0.0	173.8
41	39.68	0.0	281.6	0.0	314.4	7.1	181.0
42	40.42	0.0	281.6	0.0	314.4	0.0	181.0
43	41.05	0.0	281.6	0.0	314.4	0.2	181.2
44	41.60	0.0	281.6	0.0	314.4	5.2	186.4
45	42.14	0.0	281.6	0.1	314.6	0.0	186.4
46	43.32	0.0	281.6	0.0	314.6	1.2	187.6
47	45.82	0.0	281.6	0.0	314.6	0.0	187.6
48	46.53	0.0	281.6	0.0	314.6	0.0	187.6
49	47.73	0.2	281.8	0.0	314.6	0.0	187.6
50	48.59	0.0	281.8	0.1	314.7	0.0	187.6
51	49.06	0.0	281.8	0.0	314.7	0.0	187.6
52	50.06	0.0	281.8	0.1	314.8	0.0	187.6
53	50.26	0.4	282.2	0.0	314.8	0.0	187.6
54	50.51	0.0	282.2	0.0	314.8	0.0	187.6
55	52.23	0.0	282.2	0.0	314.8	0.0	187.6
56	53.68	0.0	282.2	0.0	314.8	0.0	187.6
57	54.46	2.3	284.5	0.0	314.8	0.0	187.6
58	55.85	0.0	284.5	0.0	314.8	1.2	188.8

© Copyright 2019 by NuScale Power, LLC

Mode Number	Frequency (Hz)	Modal Masses (kip * sec^2 / ft)					
		X-Direction		Y-Direction		Z-Direction	
		Modal Mass	Cumulative Modal Mass	Modal Mass	Cumulative Modal Mass	Modal Mass	Cumulative Modal Mass
59	56.61	0.0	284.5	0.4	315.2	0.0	188.8
60	57.59	0.0	284.5	0.5	315.7	0.0	188.8
61	57.79	0.0	284.5	0.0	315.7	0.0	188.8
62	58.51	0.0	284.5	0.1	315.7	0.0	188.8
63	58.63	0.0	284.5	0.0	315.7	37.6	226.4
64	58.67	8.1	292.6	0.0	315.7	0.0	226.4
65	59.21	0.0	292.6	0.0	315.7	0.0	226.4
66	59.81	0.0	292.6	0.0	315.7	4.9	231.3
67	60.18	0.0	292.6	0.0	315.7	5.2	236.5
68	60.28	0.0	292.6	0.0	315.7	0.0	236.5
69	62.09	0.0	292.6	0.0	315.7	22.5	259.0
70	62.19	0.0	292.6	0.0	315.7	0.0	259.0
71	63.26	0.7	293.3	0.0	315.7	0.0	259.0
72	64.67	0.0	293.3	0.0	315.7	5.6	264.6
73	65.96	3.3	296.5	0.0	315.7	0.0	264.6
74	66.02	0.0	296.5	4.5	320.3	0.0	264.6
75	67.49	0.0	296.5	0.0	320.3	0.2	264.8
76	67.96	0.0	296.5	0.0	320.3	0.0	264.8
77	68.67	0.0	296.5	3.8	324.1	0.0	264.8
78	68.93	0.0	296.5	0.0	324.1	0.2	265.0
79	70.12	0.1	296.6	0.0	324.1	0.0	265.0
80	70.66	0.0	296.6	0.0	324.1	0.0	265.0
81	73.06	0.0	296.6	0.0	324.1	0.0	265.0
82	73.12	0.0	296.6	0.0	324.1	0.0	265.0
83	73.45	0.0	296.6	0.0	324.1	0.8	265.8
84	73.90	0.0	296.6	0.0	324.1	0.0	265.8
85	74.35	0.0	296.6	0.1	324.2	0.0	265.8
86	75.25	0.0	296.6	0.0	324.2	0.6	266.3
87	75.31	1.8	298.4	0.0	324.2	0.0	266.3
88	75.68	0.0	298.4	0.0	324.2	0.0	266.3

© Copyright 2019 by NuScale Power, LLC

Mode Number	Frequency (Hz)	Modal Masses (kip * sec^2 / ft)					
		X-Direction		Y-Direction		Z-Direction	
		Modal Mass	Cumulative Modal Mass	Modal Mass	Cumulative Modal Mass	Modal Mass	Cumulative Modal Mass
89	75.96	0.0	298.4	0.0	324.2	0.6	267.0
90	76.70	0.0	298.4	0.1	324.3	0.0	267.0
91	77.08	0.4	298.8	0.0	324.3	0.0	267.0
92	78.59	0.0	298.8	0.0	324.3	0.0	267.0
93	79.13	0.6	299.4	0.0	324.3	0.0	267.0
94	79.85	0.0	299.4	0.0	324.3	0.0	267.0
95	80.91	0.0	299.4	0.0	324.3	1.2	268.1
96	81.18	0.0	299.4	0.0	324.3	0.0	268.1
97	81.71	0.8	300.1	0.0	324.3	0.0	268.1
98	82.29	0.0	300.1	0.0	324.3	0.0	268.1
99	82.65	0.0	300.1	0.4	324.7	0.0	268.1
100	83.35	0.0	300.1	0.2	324.9	0.0	268.1
101	84.21	0.0	300.1	0.0	324.9	0.0	268.1
102	85.03	0.4	300.5	0.0	324.9	0.0	268.1
103	85.54	0.0	300.5	0.0	324.9	1.1	269.3
104	87.49	0.0	300.5	0.1	325.1	0.0	269.3
105	87.65	0.0	300.5	0.0	325.1	0.0	269.3
106	88.54	0.0	300.5	0.1	325.2	0.0	269.3
107	88.60	0.0	300.5	0.0	325.2	0.0	269.3
108	89.61	0.0	300.5	0.0	325.2	0.0	269.3
109	89.90	0.0	300.5	0.0	325.2	0.1	269.3
110	90.55	0.3	300.8	0.0	325.2	0.0	269.3
111	92.07	0.0	300.8	0.0	325.2	1.8	271.1
112	92.72	0.0	300.8	0.0	325.2	0.0	271.1
113	93.10	0.0	300.8	0.1	325.2	0.0	271.1
114	94.23	0.1	301.0	0.0	325.2	0.0	271.1
115	94.49	0.0	301.0	0.0	325.2	0.0	271.1
116	94.99	0.0	301.0	0.0	325.2	0.1	271.2
117	96.30	0.0	301.0	0.0	325.2	0.0	271.2
118	96.69	0.0	301.0	0.0	325.2	0.0	271.2

© Copyright 2019 by NuScale Power, LLC

Mode Number	Frequency (Hz)	Modal Masses (kip * sec^2 / ft)					
		X-Direction		Y-Direction		Z-Direction	
		Modal Mass	Cumulative Modal Mass	Modal Mass	Cumulative Modal Mass	Modal Mass	Cumulative Modal Mass
119	97.32	0.0	301.0	0.0	325.2	0.0	271.2
120	97.93	0.0	301.0	0.0	325.2	0.0	271.2
121	98.51	1.4	302.3	0.0	325.2	0.0	271.2

6.3.5 Example 3 Summary

Example 3 extends the SSI response considered in Example 2 to include soil- structure-fluid interaction. Acoustic fluid interaction is incorporated by adding ANSYS Fluid 30 elements to the structural model and adding pressure degrees of freedom as solution variables. Note that the acoustic coupling stiffness and mass matrices are unsymmetric and an unsymmetric solver is used in Example 3 by both SASSI and ANSYS.

Since the building footprint and soil properties for Example 3 are the same as Example 2, the Soil Library developed for Example 2 is reused for Example 3. The Soil Library includes load vectors for a Layer 1 control motion, which is the free-field surface, and Layer 4 control motion, which is at the base of the structure.

A surface seismic ground motion is assumed and used with the Layer 1 load vectors to compute seismic response time histories. In-structure response spectra are compared for selected structural components and acoustic pressure time histories are compared at different depths in the pool.

The seismic response of the Example 3 building is calculated using both SASSI and ANSYS. The ANSYS solution uses the Soil Library, ANSYS structural elements, the frequency domain solver and incorporates transfer function interpolation (Section 5.1.7). The SASSI solution uses the Soil Library and the ANSYS generated mass, damping and stiffness matrices. There is excellent comparison between the SASSI and ANSYS results and this problem demonstrates that the ANSYS frequency domain solution is functionally equivalent to the SASSI frequency domain solution.

Since Examples 2 and 3 are the same structure with and without fluid, the fixed base and SSI responses of these two structures are compared. For the fixed base response, the addition of fluid increased the amplitude of primary building response transfer function by approximately {{ }}$^{2(a),(c)}$. For local modes, such as out-of-plane wall response, the addition of fluid to the fixed base response resulted in a {{ }}$^{2(a),(c)}$ increase in transfer function amplitude and a slight shift in natural frequency. Additionally, the fluid has an impact on some of the higher frequency out-of-plane wall modes.

© Copyright 2019 by NuScale Power, LLC

The soil site considered in Examples 2 and 3 is stiff, with a shear wave velocity of approximately 5000 fps. This stiff soil site resists the out-of-plane fluid loads acting on the building walls and the SSI response of the out-of-plane modes is significantly smaller than the fixed base response. The fixed base case and the 5000 fps soil case bound the out-of-plane wall behavior for the intermediate soils.

© Copyright 2019 by NuScale Power, LLC

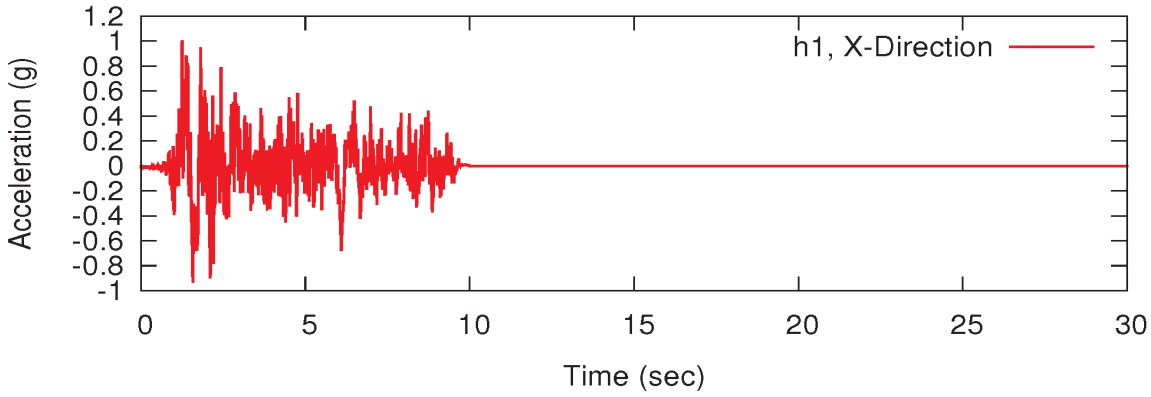

h1) RSN496_NAHANNI_S2330.AT2 PEER NGA Strong Motion Database

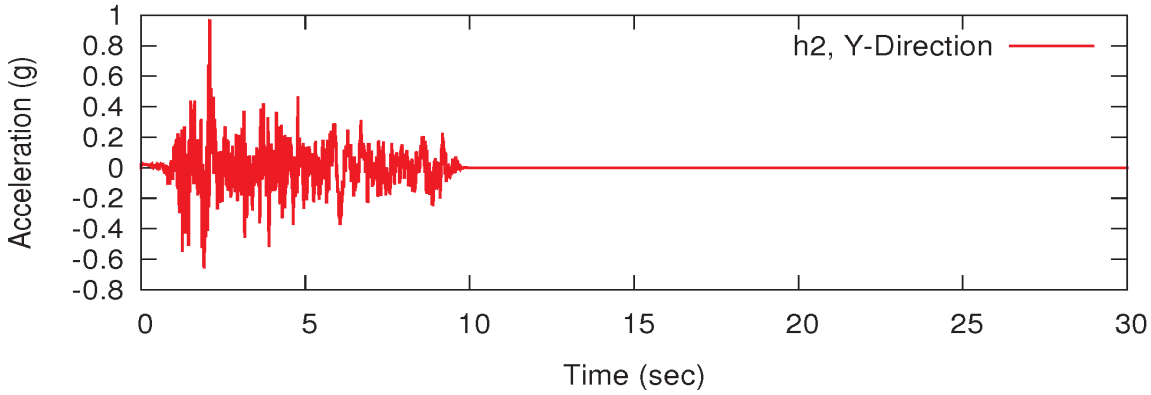

h2) RSN496_NAHANNI_S2240.AT2 PEER NGA Strong Motion Database

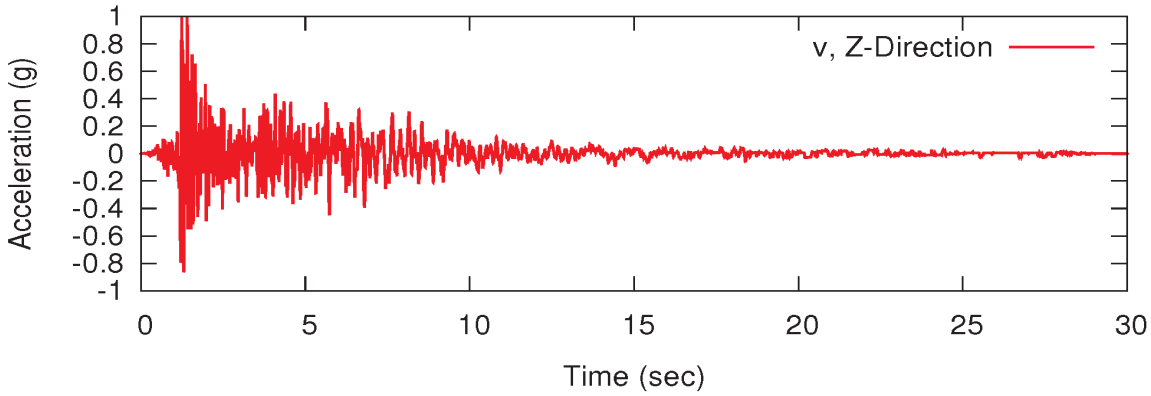

v) RSN455_MORGAN_G01-UP.AT2 PEER NGA Strong Motion Database

Figure 6-29 Example 3, surface input time histories

© Copyright 2019 by NuScale Power, LLC

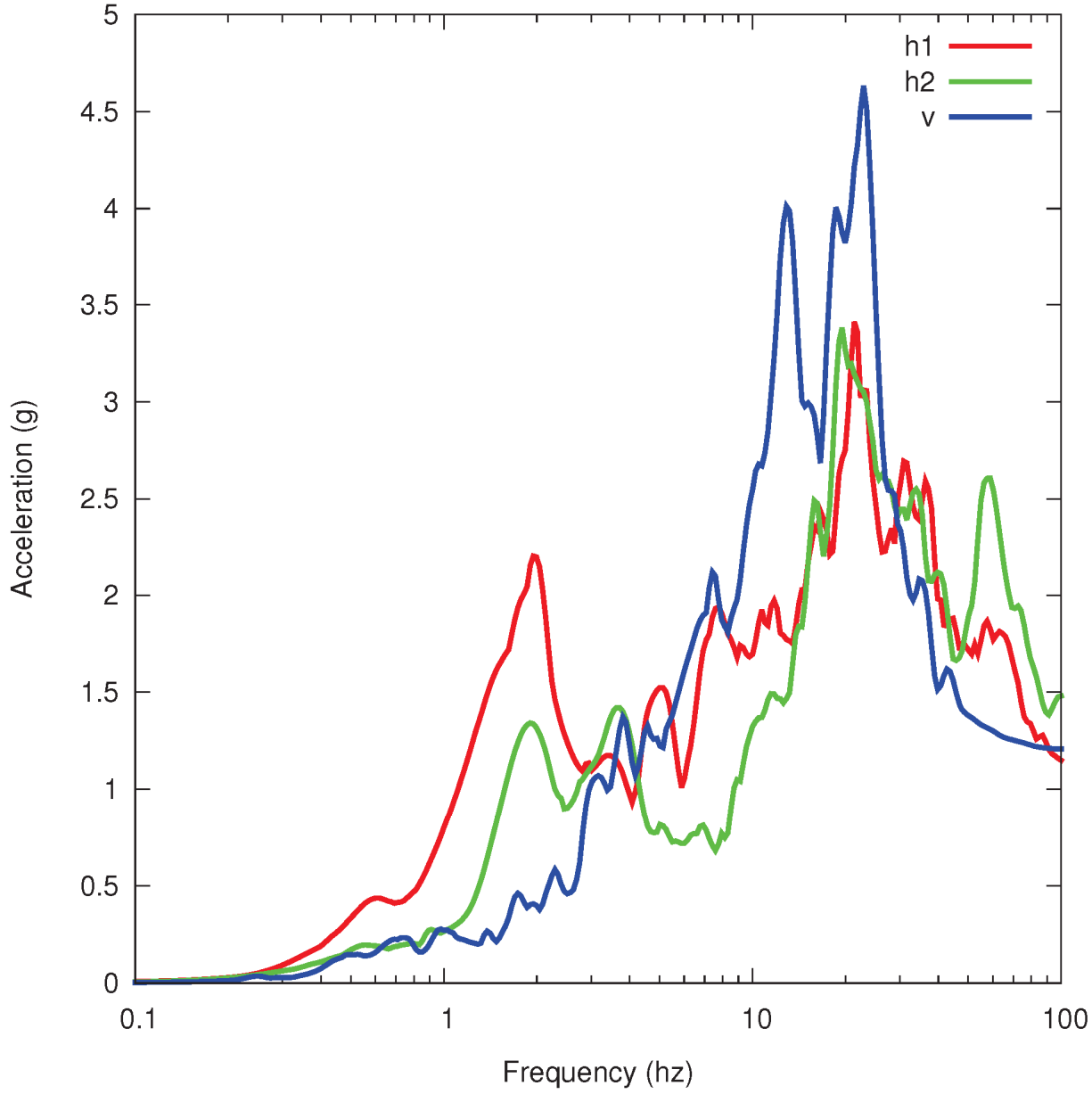

Figure 6-30 5% damped response spectra for example 3 surface input time histories

© Copyright 2019 by NuScale Power, LLC

{{

}}2(a),(c)

Figure 6-31 Comparison of SASSI and ANSYS solutions, center roof structural response, layer 1 input

© Copyright 2019 by NuScale Power, LLC

{{

}}2(a),(c)

Figure 6-32 Comparison of SASSI and ANSYS solutions, center roof structural response, layer 4 input

© Copyright 2019 by NuScale Power, LLC

{{

}}2(a),(c)

Figure 6-33 Comparison of SASSI and ANSYS 5% damped ISRS, center roof structural response

© Copyright 2019 by NuScale Power, LLC

{{

}}2(a),(c)

Figure 6-34 Comparison of SASSI and ANSYS solutions, fluid pressure, layer 1 input

© Copyright 2019 by NuScale Power, LLC

{{

}}2(a),(c)

Figure 6-35 Comparison of SASSI and ANSYS solutions, fluid pressure, layer 4 input

© Copyright 2019 by NuScale Power, LLC

{{

}}2(a),(c)

Figure 6-36 Comparison of SASSI and ANSYS acoustic fluid pressure (ksf sec^2/ft) time histories

© Copyright 2019 by NuScale Power, LLC

{{

}}2(a),(c)

Figure 6-37 Comparison of fixed base response for example problems 2 and 3

© Copyright 2019 by NuScale Power, LLC

{{

}}2(a),(c)

Figure 6-38 Comparison of SSI response for example problems 2 and 3

© Copyright 2019 by NuScale Power, LLC

{{

}}2(a),(c)

Figure 6-39 Comparison of SSI response for example problems 2 and 3

© Copyright 2019 by NuScale Power, LLC

6.4 Representative Reactor Building with Soil-Structure-Fluid Interaction

This example problem compares the dynamic response of a representative small modular Reactor Building (RXB), including twelve reactor power modules RXM, fluid-structure-RXM interaction, and soil structure interaction computed using ANSYS to the dynamic response using SASSI. The RXB is a concrete structure approximately 350 feet long in the x direction, 150 feet wide in the y direction, and 165 feet tall, with 85 feet of embedment. Inside the building is a large pool of water and the submerged RXMs. The walls of the structure are five feet thick, and there is a ten foot thick basemat and four foot thick roof. Outside the pool area there are multiple floor elevations, and each floor is three foot thick.

The purpose of this example problem is to demonstrate the implementation of the *Soil Library Methodology* using a complex structural model and to demonstrate that the ANSYS and SASSI solutions are consistent.

The reduced excavated soil impedance library was written using SDE SASSI (Reference 9.1.6) with inputs taken from the soil model for Soil Type 7 (Reference 9.1.13) and geometry of the RXB excavation.

The RXB ANSYS model is shown in Figure 6-40 and includes twelve RXMs, the reactor pool (shown in purple in Figure 6-40b), backfill soil and the Soil Library developed for soil type 7.

This example problem will demonstrate the soil library concept by comparing transfer functions and ISRS calculated using the ANSYS model plus soil library methodology versus results computed using SASSI. The comparison will be performed at selected locations documented herein.

© Copyright 2019 by NuScale Power, LLC

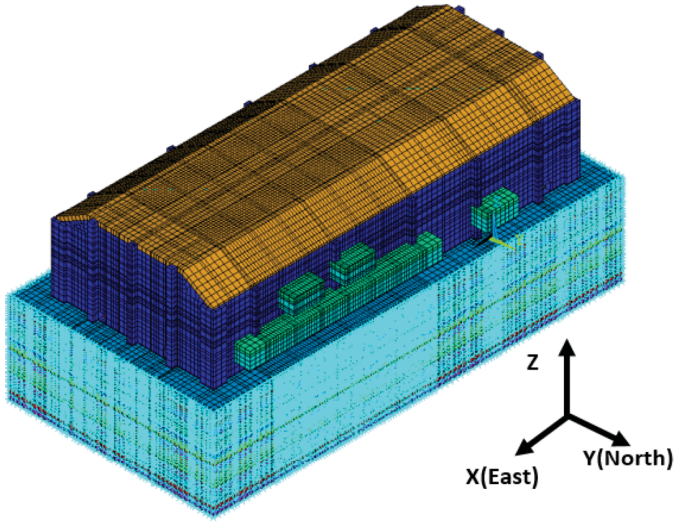

Figure 6-40a Isometric view

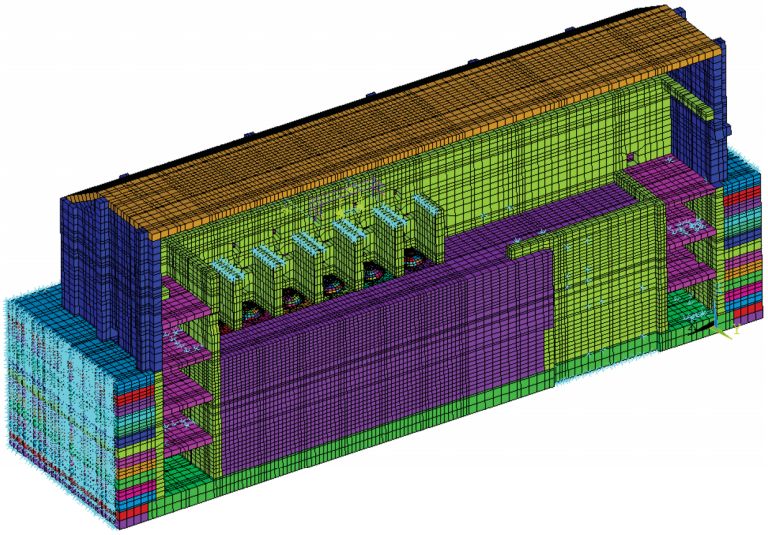

Figure 6-40b Longitudinal section

© Copyright 2019 by NuScale Power, LLC

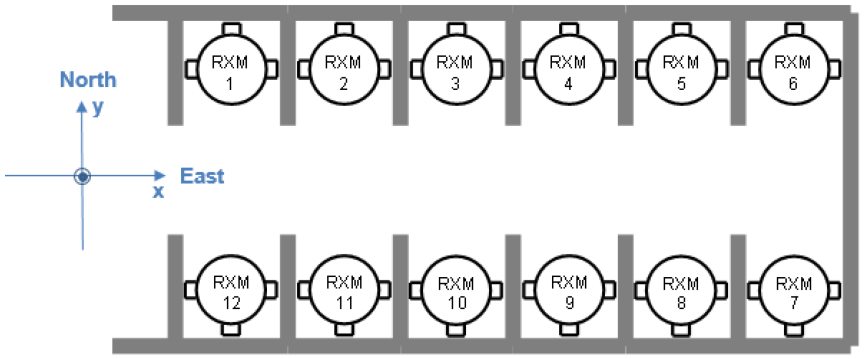

Figure 6-40c Reactor pool with 12 RXM

6.4.1 Input, Assumptions and Software

6.4.1.1 Input

The RXB building stiffness, mass and damping matrices, along with nodal coordinates and a DOF correspondence table are obtained from the RXB ANSYS model. These structural matrices are used to create the RXB SASSI model. The RXB model coordinate system has positive X to the East, positive Y to the North and positive Z is up.

The constant g, the acceleration due to gravity used in the ANSYS analysis is 386.2 inches/second^2, while portions of this calculation use a g value of 386.4 inches/second^2. The use of these different values of g results in a response difference of less than 0.1%, which is imperceptible.

The 100 analysis frequency numbers in Table 6-8 were used, covering the range from 0.1953 Hz to 100 Hz. Transfer function results are explicitly calculated at these frequencies and intermediate values of transfer functions are obtained via interpolation. For the RXB, the frequency, f, is

$$f = \frac{n}{81.92}(Hz) \qquad \text{Equation 6-19}$$

where n is the frequency number in Table 6-8 and the constant 81.92 is the duration of the response in seconds.

The input motion is defined at the free field ground surface. The input time histories for this analysis are the CSDRS-compatible Capitola time histories shown below (Reference 9.1.27):

- CAPEW2.THI
- CAPNS2.THI

© Copyright 2019 by NuScale Power, LLC

- CAPVT2.THI

These time histories have a time step of 0.005 seconds and peak ground accelerations of 0.5g horizontally and 0.4g vertically. Each time history has roughly 40 seconds of ground motion. With zero packing, each time history has a total of N=16,384 terms for a total duration of 81.92 seconds. Five percent damped response spectra for these time histories are shown in Figure 6-41.

6.4.1.2 Assumptions

This example problem is based on the following assumptions.

- The structural behavior is linear elastic.
- The strain compatible soil properties correspond to Type 7 Soil.
- The power module is connected to the RXB basemat at all coincident nodes.
- Only seismic loads are considered.

Table 6-8 Analysis Frequency Numbers

Frequency No.	(Hz)	Frequency No.	(Hz)	Frequency No.	(Hz)	Frequency No.	(Hz)	Frequency No.	(Hz)
16	0.1953	336	4.1016	656	8.0078	1200	14.6484	2416	29.4922
32	0.3906	352	4.2969	672	8.2031	1232	15.0391	2496	30.4688
48	0.5859	368	4.4922	688	8.3984	1280	15.6250	2656	32.4219
64	0.7813	384	4.6875	704	8.5938	1312	16.0156	2912	35.5469
80	0.9766	400	4.8828	720	8.7891	1360	16.6016	3104	37.8906
96	1.1719	416	5.0781	736	8.9844	1392	16.9922	3328	40.6250
112	1.3672	432	5.2734	752	9.1797	1440	17.5781	3488	42.5781
128	1.5625	448	5.4688	768	9.3750	1472	17.9688	3712	45.3125
144	1.7578	464	5.6641	784	9.5703	1520	18.5547	3904	47.6563
160	1.9531	480	5.8594	800	9.7656	1568	19.1406	4128	50.3906
176	2.1484	496	6.0547	816	9.9609	1600	19.5313	4544	55.4688
192	2.3438	512	6.2500	832	10.1563	1680	20.5078	4928	60.1563
208	2.5391	528	6.4453	864	10.5469	1760	21.4844	5376	65.6250
224	2.7344	544	6.6406	912	11.1328	1856	22.6563	5760	70.3125
240	2.9297	560	6.8359	944	11.5234	1936	23.6328	6144	75.0000
256	3.1250	576	7.0313	992	12.1094	2016	24.6094	6592	80.4688
272	3.3203	592	7.2266	1024	12.5000	2096	25.5859	6976	85.1563
288	3.5156	608	7.4219	1072	13.0859	2176	26.5625	7424	90.6250
304	3.7109	624	7.6172	1104	13.4766	2256	27.5391	7808	95.3125
320	3.9063	640	7.8125	1152	14.0625	2336	28.5156	8192	100.0000

© Copyright 2019 by NuScale Power, LLC

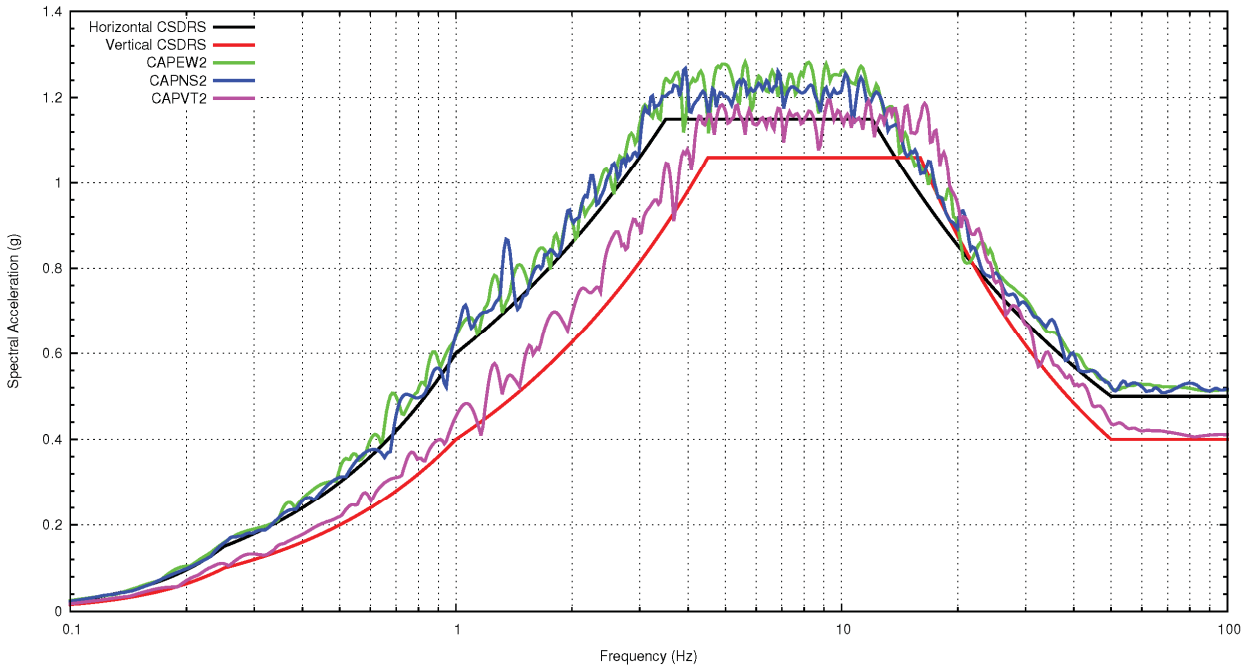

Figure 6-41 Input Motion Response Spectra, 5% Damping

6.4.2 Solution Methodology

The RXB model mass and complex stiffness matrices are combined with the Soil Type 7 impedance matrices. The combined dynamic stiffness is solved for the Soil Type 7 load vectors for each of the 100 computed frequencies identified in Table 6-8. The resulting displacements represent the response to a X, Y or Z unit cyclic displacement of the surface control layer, which are also called transfer functions. The response at intermediate frequencies is determined via interpolation which is described in Section 5.1.7. The response in the frequency domain is determined by multiplying the FFT of the input motion by the transfer function. The time domain response is obtained via an inverse FFT.

6.4.3 Comparison of Dynamic Results

The dynamic response is discussed in this section and dynamic results developed using ANSYS and SASSI are compared.

6.4.3.1 Acceleration Response

The acceleration response is compared at each of the 32 nodes summarized in Table 6-9.

Acceleration transfer functions for the 32 nodes are compared in Appendix I. Overall, the comparison between the ANSYS and SASSI transfer functions is excellent, as shown by the response of the top of RXM-1 in Figure 6-42. In these figures, computed transfer

© Copyright 2019 by NuScale Power, LLC

functions are denoted with a plot symbol while interpolated transfer functions are denoted with a line.

There are some observable differences in interpolated transfer function spikes. Two examples are the Z response to Z input near 7 Hz for node 331292 as shown in Figure I-51, and the Z response to Y input for node 392378 as shown in Figure I-68. None of these interpolated spikes contain sufficient volume to significantly affect results.

Acceleration time histories for the 32 nodes are compared in Appendix J. Overall, the comparison between the ANSYS and SASSI time histories is excellent, as shown by the response[12] of the top of RXM-1 in Figure 6-43.

Four percent damped, in-structure response spectra for the 32 nodes are compared in Appendix K. Overall, the comparison between the ANSYS and SASSI in-structure response spectra is excellent, as shown by the response of the top of RXM-1 in Figure 6-44.

The time histories for the Y response of Node 331222 to X input, shown in Figure J-46 differ due to the difference in magnitude of an interpolated spike in Figure I-46. Note that this is in a cross coupling term, X input - Y response, with a peak acceleration on the order of 0.1g. The response of the direct term, Y input - Y response, has a peak acceleration on the order of 0.8g as shown in Figure J-47. Thus, the differences noted in Figure J-46 will be diminished when the combined response is examined. Examining the response spectra in Figure K-46 and Figure K-47 at 6Hz yields roughly 0.5g and 2.5g response to X and Y input, respectively. The SRSS combination of these two responses is roughly 2.55, which indicates that this response is dominated by the Y input, and the differences due to the spikes are inconsequential.

Table 6-9 Nodes for Acceleration Comparisons

Node	X	Y	Z	Description
120933	-30	903	120	Northwest Corner on Top of Basemat
120978	1902	903	120	Mid-Span of North Exterior Wall on Top of Basemat
121053	4122	903	120	Northeast Corner on Top of Basemat
4914	2019.5	305.5	132	RXM 1 Floor Node under Module
46054	3494.5	305.5	132	RXM 6 Floor Node under Module
185505	30	843	432	Northwest Corner at El. 50’
182529	182	-30	432	Mid-Span of West Slab along Grid Line RX-C at El. 50’
184359	1842	483	432	Edge of Slab at Grid Line RX-4 at El. 50’
185174	2343.9	687	432	Mid-Span of North Slab between Grid Lines RX-4

[12] Note that the full resolution version of this electronic PDF file (95+ Mb) has zoom capabilities that allow a closer examination of these figures.

© Copyright 2019 by NuScale Power, LLC

Node	X	Y	Z	Description
				and RX-5 at El. 50’
185623	4062	843	432	Northeast Corner at El. 50’
255527	30	843	732	Northwest Corner at El. 75’
255195	2314.5	687	732	Mid-Span of North Slab between Grid Lines RX-4 and RX-5 at El. 75’
254481	3702	483	732	Edge of East Slab along Grid Line RX-6 at El. 75’
332235	30	843	1032	Northwest Corner of Exterior Wall at El. 100’
331936	2314.5	687	1032	Mid-Span of North Slab between Grid Lines RX-4 and RX-5 at El. 100’
331222	1842	483	1032	Edge of North Slab along Grid Line RX-4 at El. 100’
331292	3702	483	1032	Edge of East Slab along Grid Line RX-6 at El. 100’
352669	30	843	1344	Northwest Corner of Exterior Wall at El. 125’
351629	1902	483	1344	Northwest Corner of Bio Shield
352370	2314.5	687	1344	Mid-Span of North Slab at between Grid Lines RX-4 and RX-5 at El. 125’
351696	3702	483	1344	Northeast Corner of Bio Shield
392329	-30	-30	2004	Top of Roof at Grid Line RX-1
392378	2019.5	-30	2004	Roof Slab between Grid Lines RX-4 and RX-5
394770	4122	555.75	2004	Northeast Corner of Roof Slab
8216	1917.6	305.5	673.6	RXM-1 West Lug
8215	2019.5	407.38	673.6	RXM-1 North Lug
8214	2121.4	305.5	673.6	RXM-1 East Lug
1900	2019.5	305.5	1040.5	RXM-1 Top
49356	3392.6	305.5	673.6	RXM-6 West Lug
49355	3494.5	407.38	673.6	RXM-6 North Lug
49354	3596.4	305.5	673.6	RXM-6 East Lug
43040	3494.5	305.5	1040.5	RXM-6 Top

© Copyright 2019 by NuScale Power, LLC

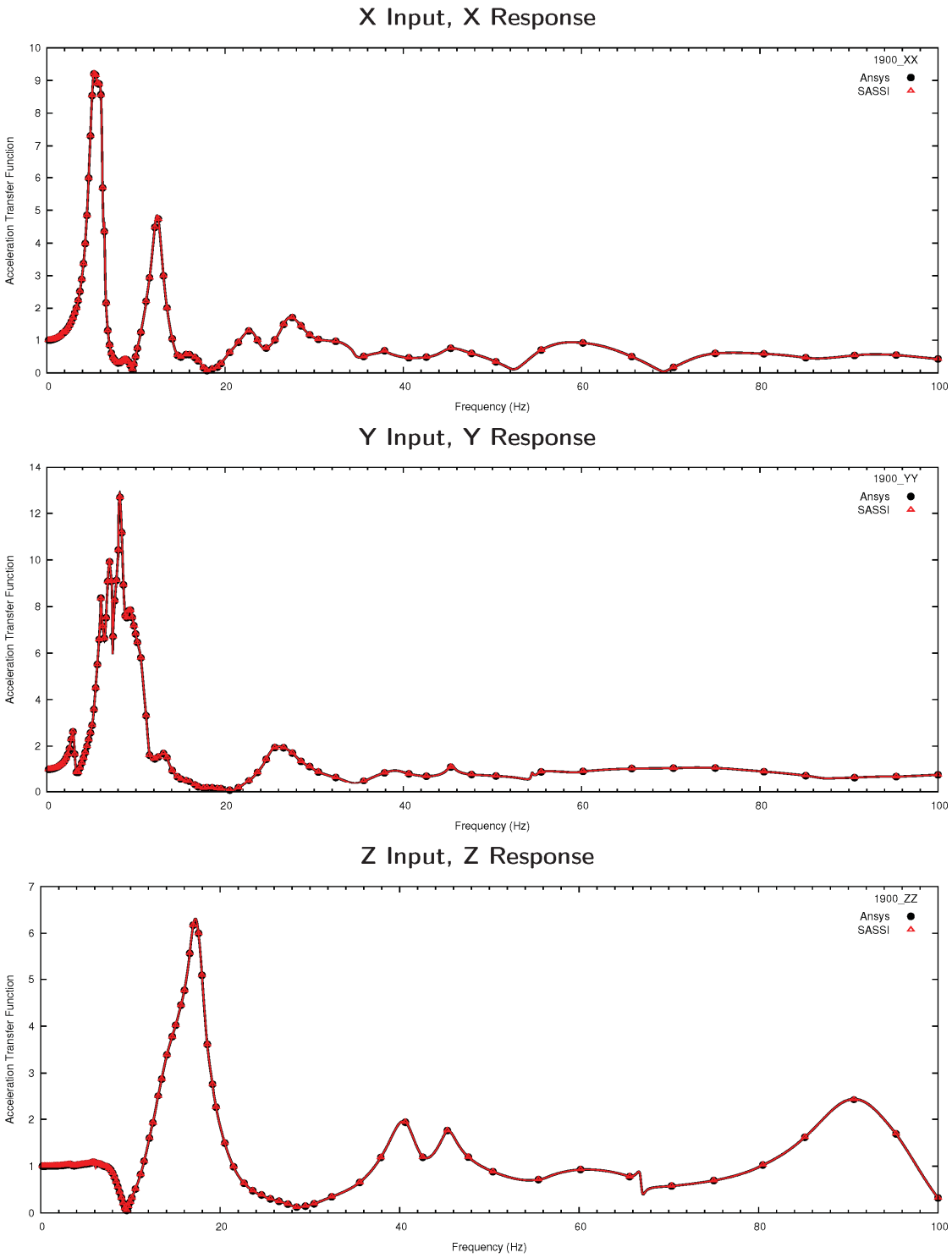

Figure 6-42 Transfer Functions for Node 1900, Top of RXM-1

© Copyright 2019 by NuScale Power, LLC

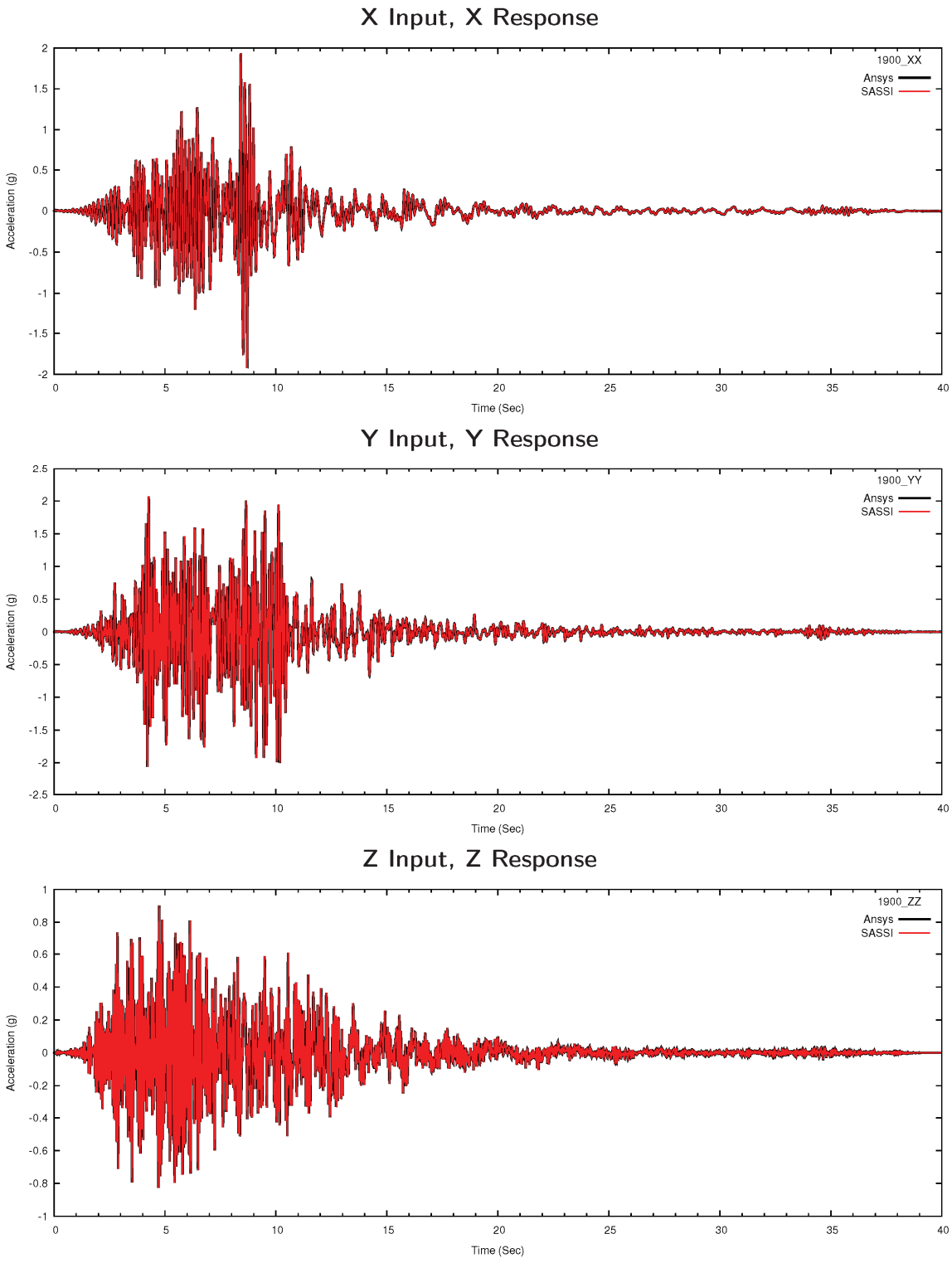

Figure 6-43 Acceleration Time Histories for Node 1900, Top of RXM-1

© Copyright 2019 by NuScale Power, LLC

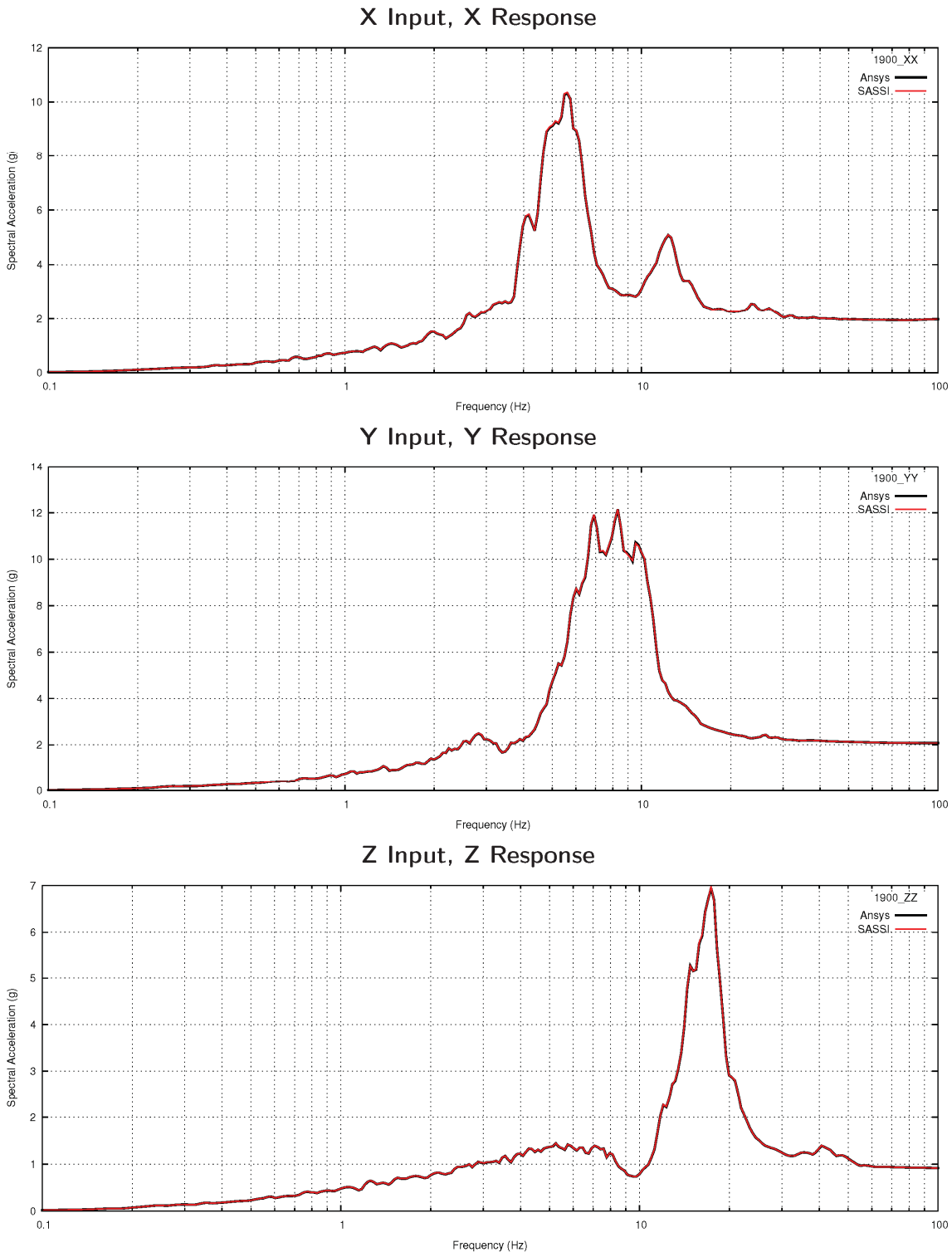

Figure 6-44 In-Structure Response Spectra for Node 1900, Top of RXM-1

© Copyright 2019 by NuScale Power, LLC

6.4.4 Fluid Pressures

Fluid pressure is measured at three locations on either side of the southern wing wall on Gridline RX4.3 at the nodes in Table 6-10. The location of the pressure nodes acting on the wall are shown in Figure 6-45.

Table 6-10 Nodes for Fluid Pressure Comparisons

	Wall Facing	
Elevation	West	East
732 inches	97727	89399
396 inches	96376	87960
132 inches	95777	87499

Comparison of ANSYS and SASSI Results: Transfer functions for the six pressure nodes are compared in Appendix L. There are no visible differences between the computed ANSYS and SASSI transfer function amplitudes, as seen in Figure 6-46 for Node 87499 at the basemat.

There are minor differences in the amplitude of some interpolated transfer function spikes, for example the pressure response at Node 96376 due to Y direction input near 6 Hz in Figure L-4. Overall, there is an excellent comparison between the ANSYS and SASSI transfer functions.

Pressure time histories for the six pressure nodes are compared in Appendix M. Overall, the ANSYS and SASSI time histories compare well, as seen in Figure 6-47 for Node 87499.

© Copyright 2019 by NuScale Power, LLC

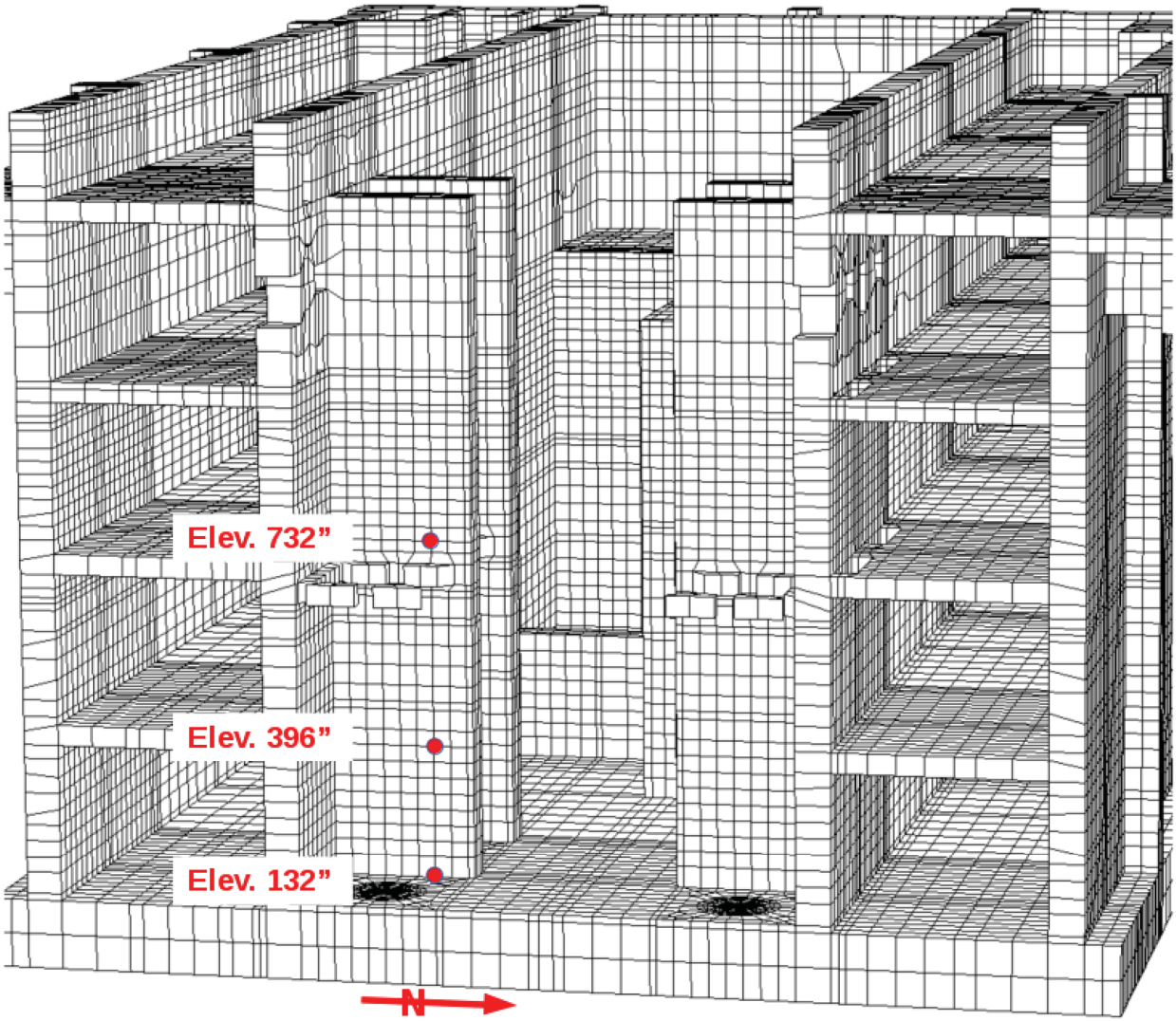

Figure 6-45 Location of Fluid Pressure Nodes on Near Side of Wall, Additional Nodes are on the Far Side

© Copyright 2019 by NuScale Power, LLC

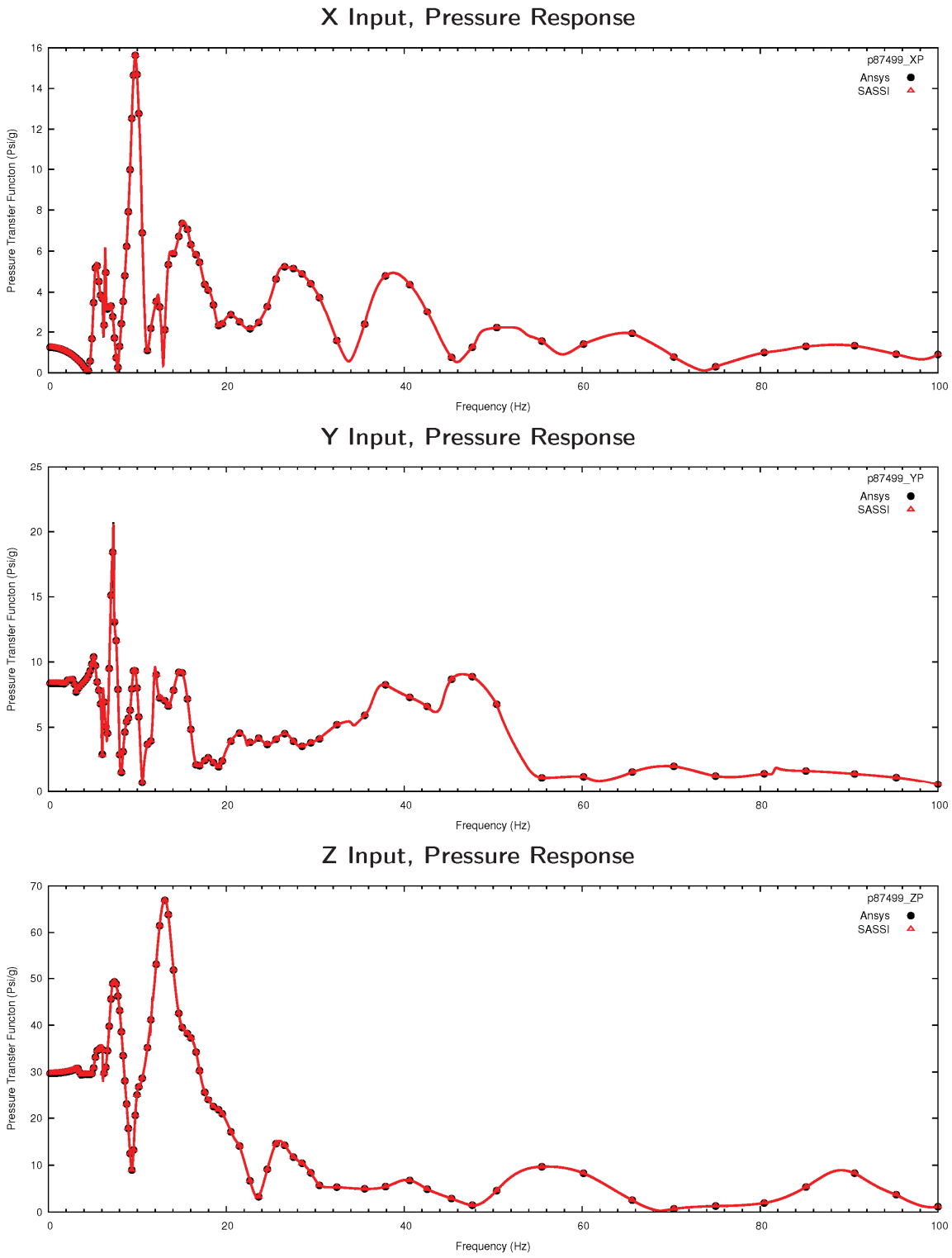

Figure 6-46 Pressure Transfer Functions for Node 87499

© Copyright 2019 by NuScale Power, LLC

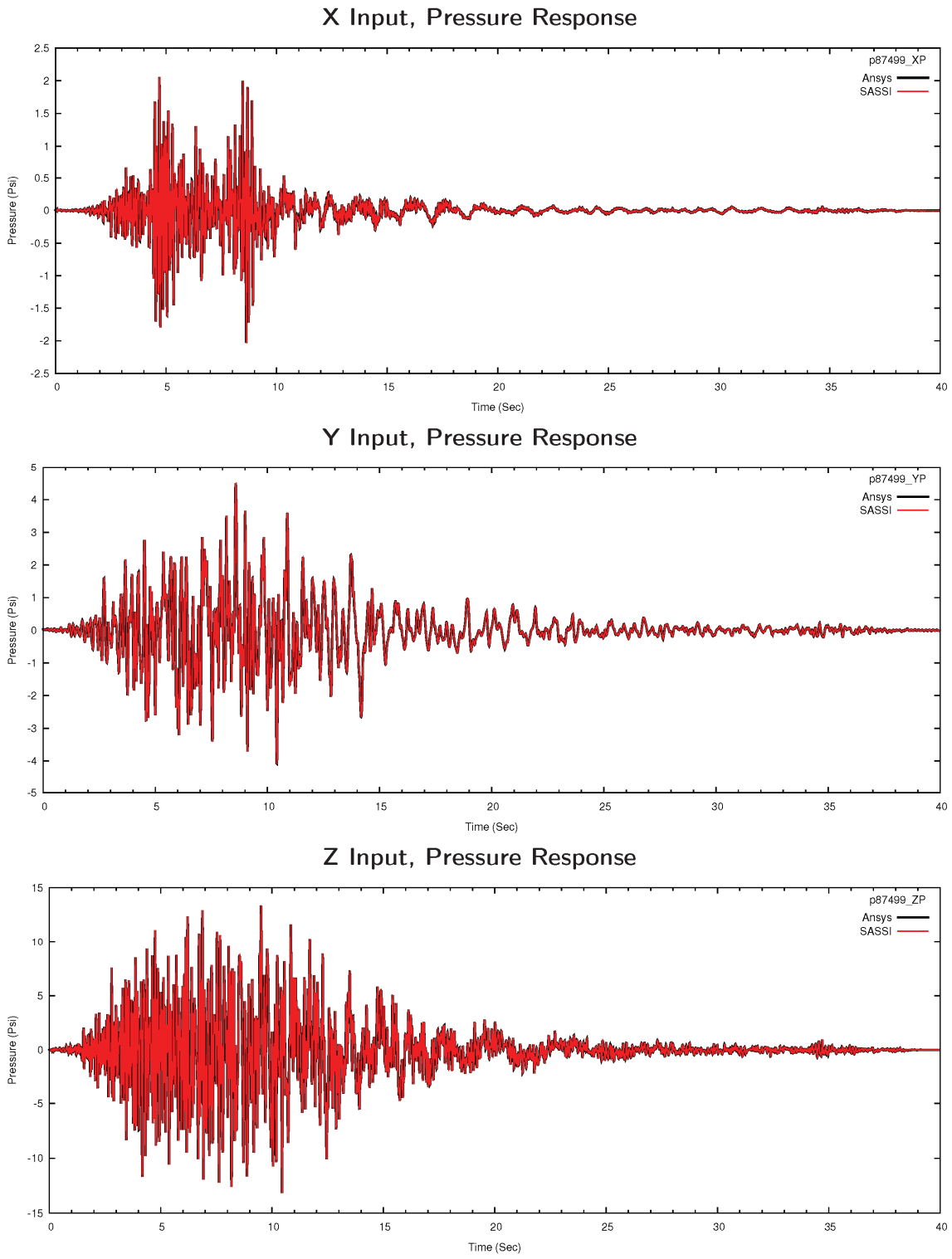

Figure 6-47 Pressure Time Histories for Node 87499

© Copyright 2019 by NuScale Power, LLC

6.4.5 Relative Displacements

The relative displacements between the 32 nodes in Table 6-9 and the top center basemat are compared in this section. Unfortunately, a node is not located at the center of the basemat, and an average of the two nodes on either side of the center are used instead. The coordinates of the nodes representing the top center of the basemat are:

	Cooridnates (inch)		
Node	X	Y	Z
124515	2048.90	-12.00	132.00
124635	2048.90	12.00	132.00
Average	2048.90	0.00	132.00

A transfer function that converts free-field input acceleration to relative displacement, at the calculated frequencies are obtained by

$$TF_{\text{Relative, Node i, DOF j}} = \frac{TF_{\text{Node i, DOF j}} - \frac{1}{2}\left(TF_{124515,\ \text{DOF j}} + TF_{124635,\ \text{DOF j}}\right)}{-\omega^2} g \qquad \text{Equation 6-20}$$

where $TF_{\text{Node i, DOF j}}$ is the transfer function[13] for Node i and degree of freedom j. The term g is the acceleration due to gravity, inch/sec^2. Note that the units of the relative displacement transfer function are inch/g. SASSI transfer function interpolation is used to obtain transfer function values at intermediate frequencies.

Comparison of ANSYS and SASSI Results: Relative displacement transfer functions for the ANSYS and SASSI response are compared in Appendix N. Overall, the comparison between these two transfer functions is excellent, as shown in Figure 6-48 for the relative displacement of the top of RXM-1.

As observed in the acceleration transfer functions, some of the displacement transfer functions also have narrow spikes as observed in Z input, Z response behavior in Figure 6-48.

Relative displacement time histories for the ANSYS and SASSI response are compared in Appendix O. Overall, the comparison between these time histories is also excellent, as shown in Figure 6-49 for the relative displacement of the top of RXM-1.

[13] Transfer free-field ground displacement to absolute structural displacement, or transfer free-field ground acceleration to absolute structural acceleration.

© Copyright 2019 by NuScale Power, LLC

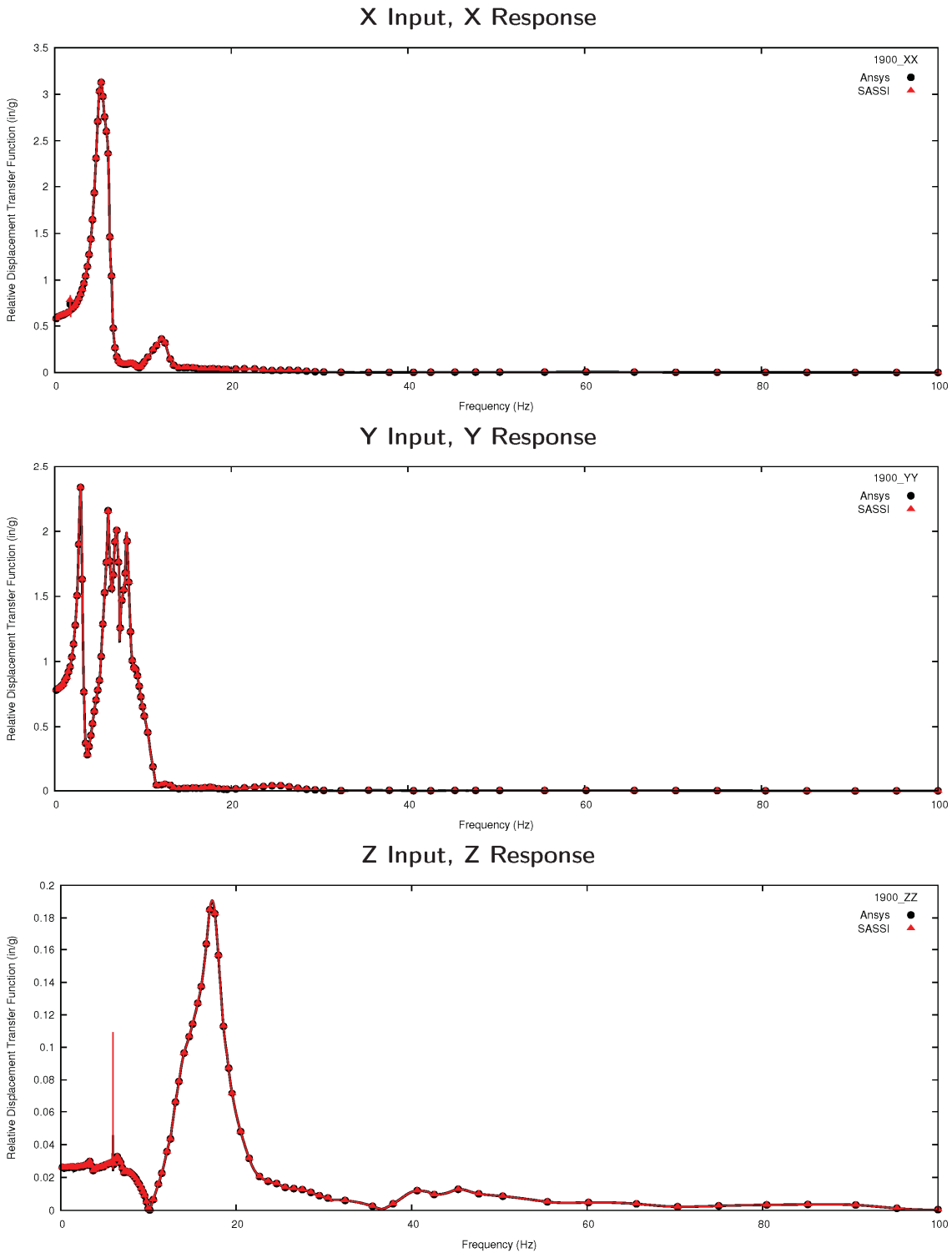

Figure 6-48 Relative Displacement Transfer Functions for Node 1900, Top of RXM-1

© Copyright 2019 by NuScale Power, LLC

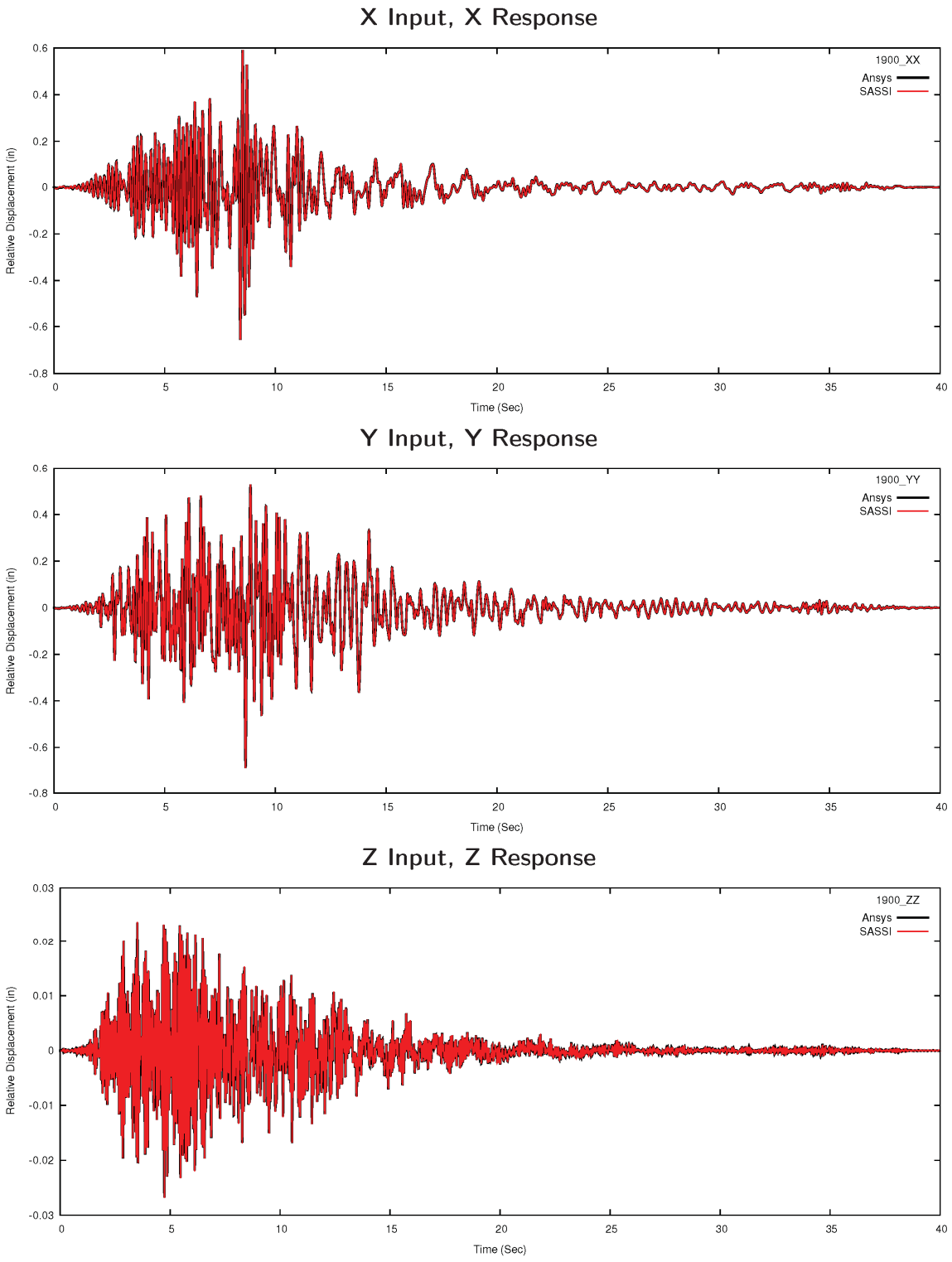

Figure 6-49 Relative Displacement Time Histories for Node 1900, Top of RXM-1

© Copyright 2019 by NuScale Power, LLC

6.4.6 RXM Support Reactions

Support reactions for RXM 1 and RXM 6 are presented in this section. The reactions consist of support lug forces, which act in the North-South direction for lugs on the East and West wing walls. The support lug forces for the North lug act in the East-West direction. RXM base reactions are also developed and consist of three components of force and moment.

The RXM lug forces are represented by a spring, with stiffness K_{spring}, between the two nodes in Table 6-11. The following transfer function converts free-field input acceleration to spring reaction force, at the calculated frequencies

$$TF_{\text{Force, DOF k}} = K_{spring} \frac{TF_{\text{Node i, DOF k}} - TF_{\text{Node j, DOF k}}}{-\omega^2} g \qquad \text{Equation 6-21}$$

where $TF_{\text{Node i, DOF k}}$ is the transfer function[14] for Node i and degree of freedom k. The term g is the acceleration due to gravity, inch/sec^2. Note that the units of the force transfer function are kips/g. SASSI transfer function interpolation is used to obtain transfer function values at intermediate frequencies.

Transfer functions for the RXM base reactions are developed from

$$TF_{[\text{Fx, Fy, Fz, Mx, My, Mz}]} = [c] \times [k] \left(\frac{g}{-\omega^2}\right) TF_{DOF} \qquad \text{Equation 6-22}$$

where [*k*] is the element stiffness matrix which was developed by ANSYS, [*c*] is a constraint matrix consisting of rigid links between the 48 ring support nodes at Elev 141 and a central node about which the overturning moments are summed, and TF_{DOF} represent the transfer functions for each DOF in the stiffness matrix [*k*]. The resulting transfer function units are kips/g for force and in-kips/g for moments.

Comparison of ANSYS and SASSI Results: The RXM Lug force transfer functions for the ANSYS and SASSI results are compared in Appendix P. Overall, the comparison is excellent as shown by the example for the RXM-1 west lug force in Figure 6-50.

[14] Transfer free-field ground displacement to absolute structural displacement, or transfer free-field ground acceleration to absolute structural acceleration.

© Copyright 2019 by NuScale Power, LLC

Table 6-11 RXM Lug Nodes

	ID	Node i	Node j	K_{spring} (lbs/inch)
1	RXM1 West Lug	8216	508457	$1.00x10^{12}$
2	RXM1 North Lug	8215	508458	$1.00x10^{12}$
3	RXM1 East Lug	8214	508459	$1.00x10^{12}$
4	RXM6 West Lug	49356	508472	$1.00x10^{12}$
5	RXM6 North Lug	49355	508473	$1.00x10^{12}$
6	RXM6 East Lug	49354	508474	$1.00x10^{12}$

Force time histories for the ANSYS and SASSI results are compared in Appendix Q. Overall, the comparison is good as shown by the example for the RXM-1 west lug force in Figure 6-51.

RXM support force transfer functions for the ANSYS and SASSI results are compared in Appendix R. Overall, the comparison is good as shown by the example for the RXM-1 F_y base reactions shown in Figure 6-52.

Force time histories for the ANSYS and SASSI results are compared in Appendix S. Overall, the comparison is excellent as shown by the example for the RXM-1 west lug force in Figure 6-53.

The RXM-6, F_x base time history due to Y input, shown in middle plot of Figure S-7, has different calculated responses. The transfer function for this response, shown in Figure R-7, are dominated by an interpolated spike near 6 Hz, which is causing the difference in response. Note that this is the response in a cross coupling term. The peak SASSI responses in Figure S-7 are 456k, 83k and 175k for input in the X, Y and Z directions respectively. Comparing the SRSS response from the 3 inputs indicates the SRSS response changes less than 1% if the Y input is halved. Thus, the transfer function spikes in Figure R-7 have a negligible impact on the total response.

© Copyright 2019 by NuScale Power, LLC

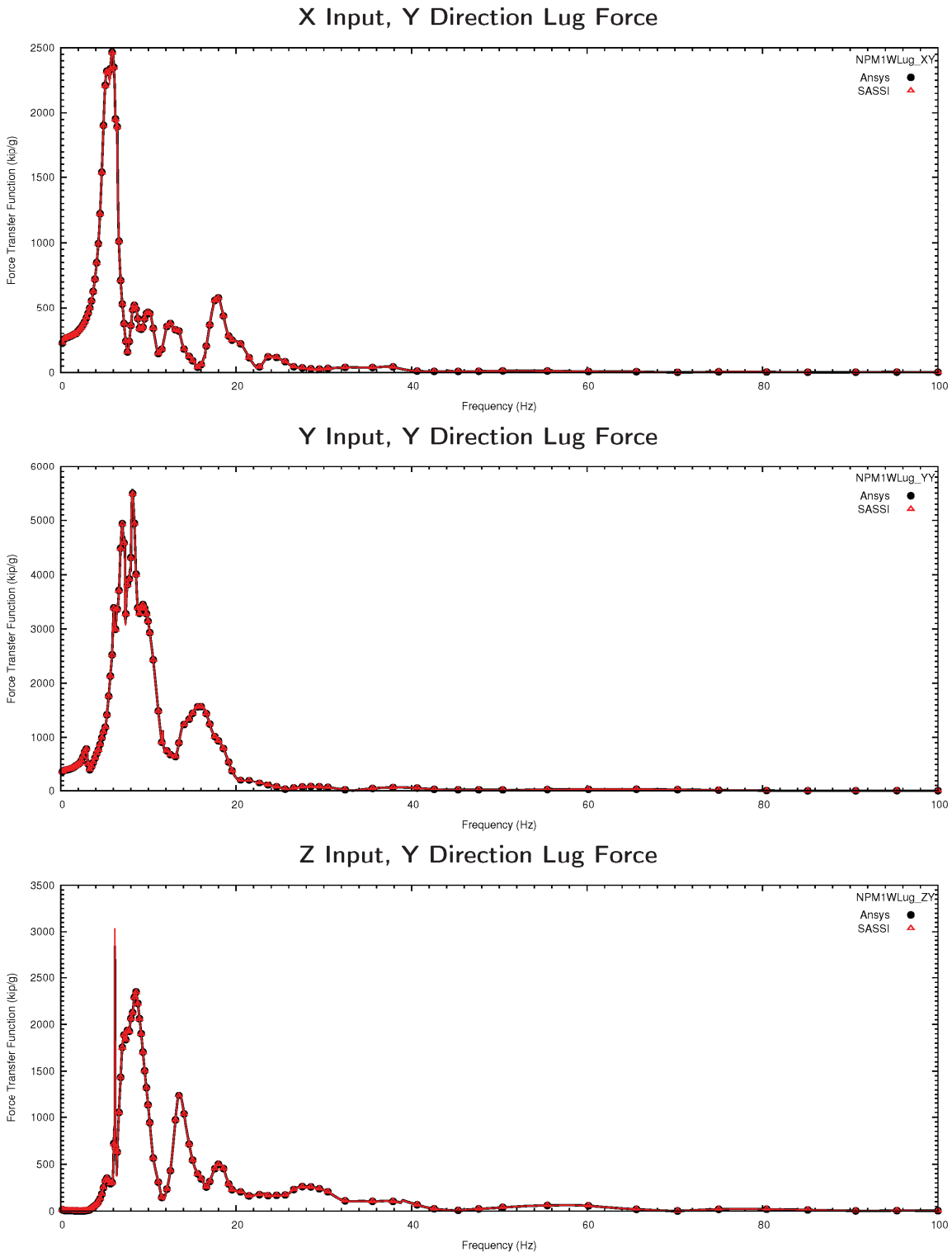

Figure 6-50 Force Transfer Functions for RXM-1, West Lug

© Copyright 2019 by NuScale Power, LLC

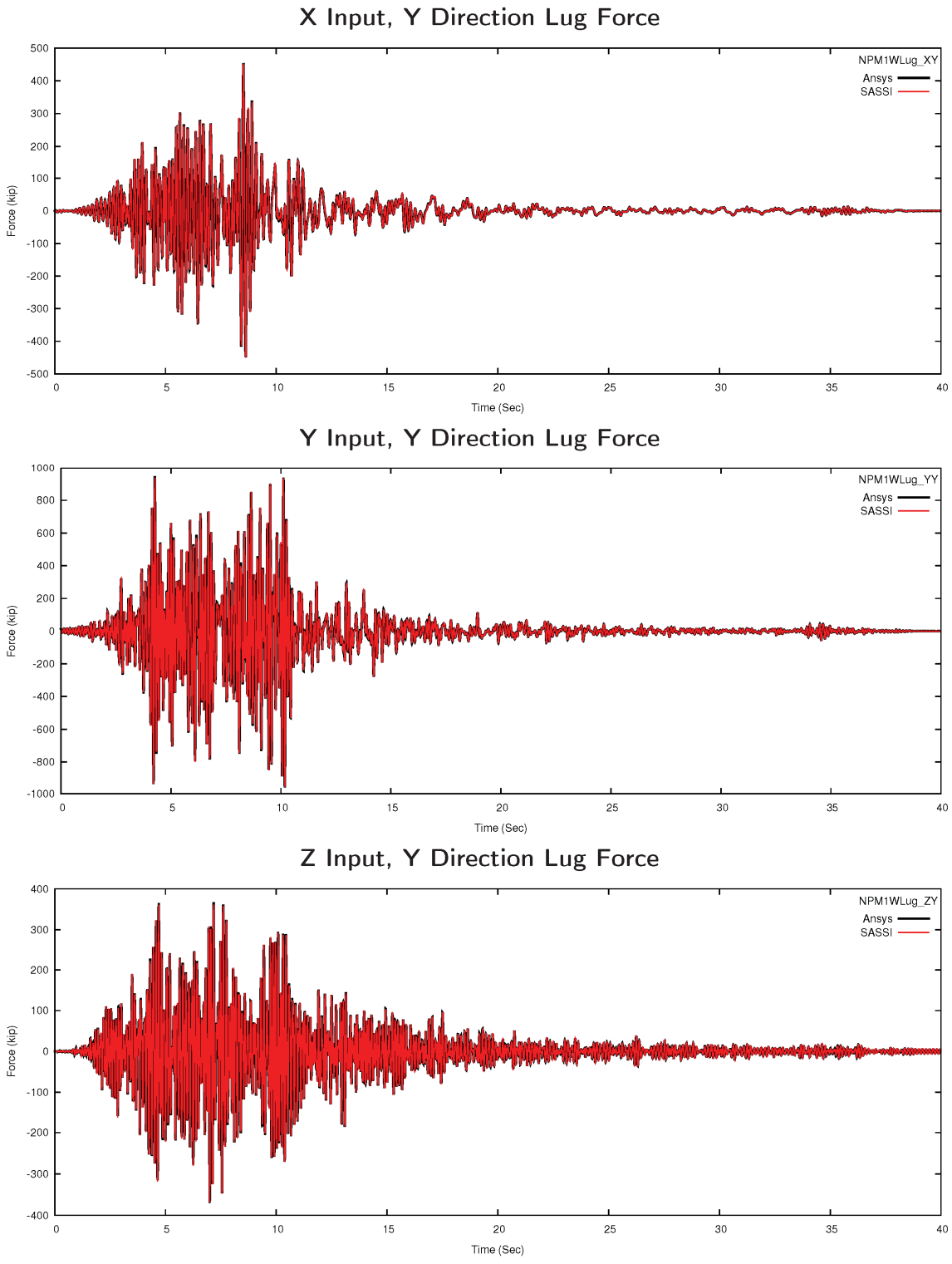

Figure 6-51 Force Time Histories for RXM-1, West Lug

© Copyright 2019 by NuScale Power, LLC

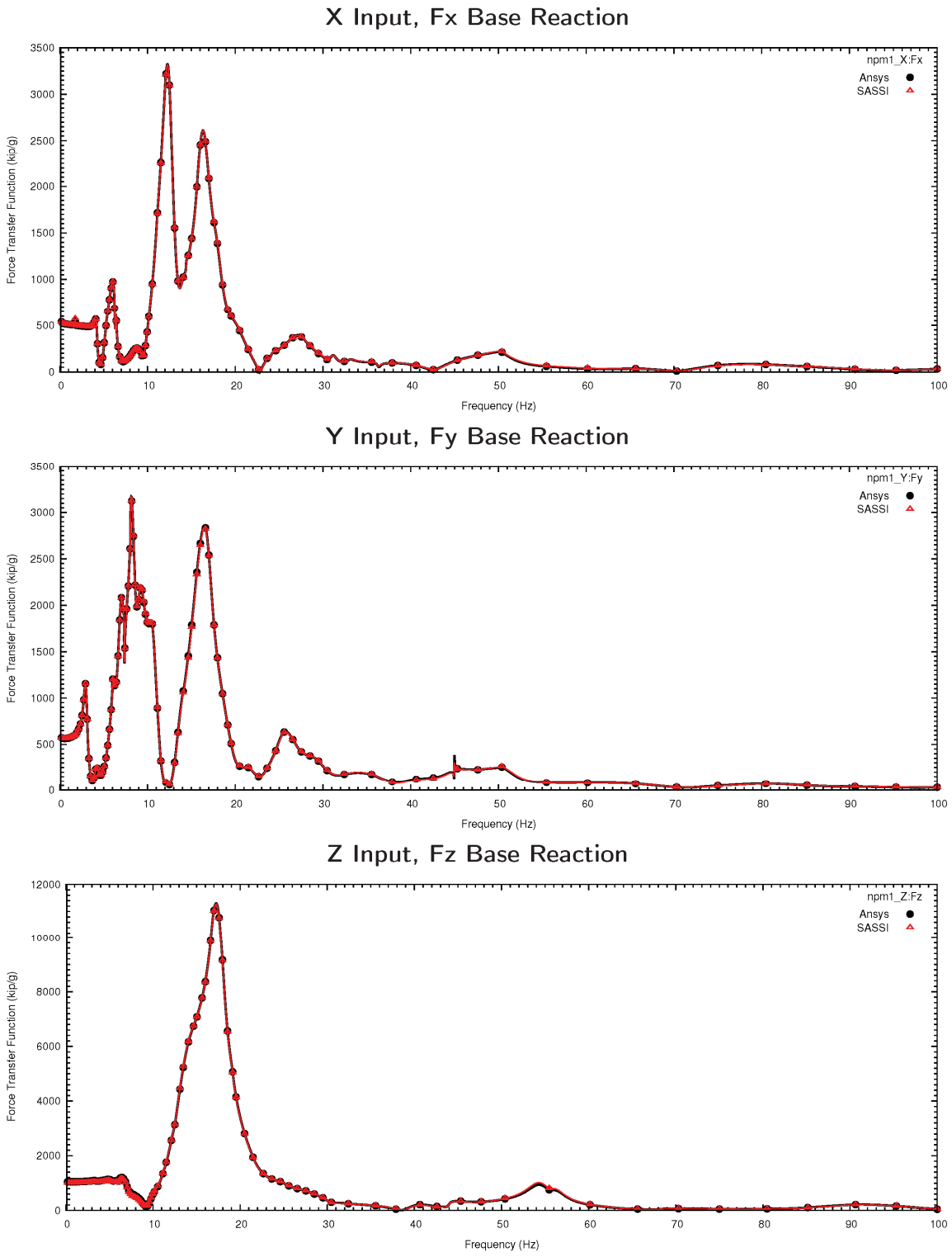

Figure 6-52 Base Reaction Transfer Functions for RXM-1

© Copyright 2019 by NuScale Power, LLC

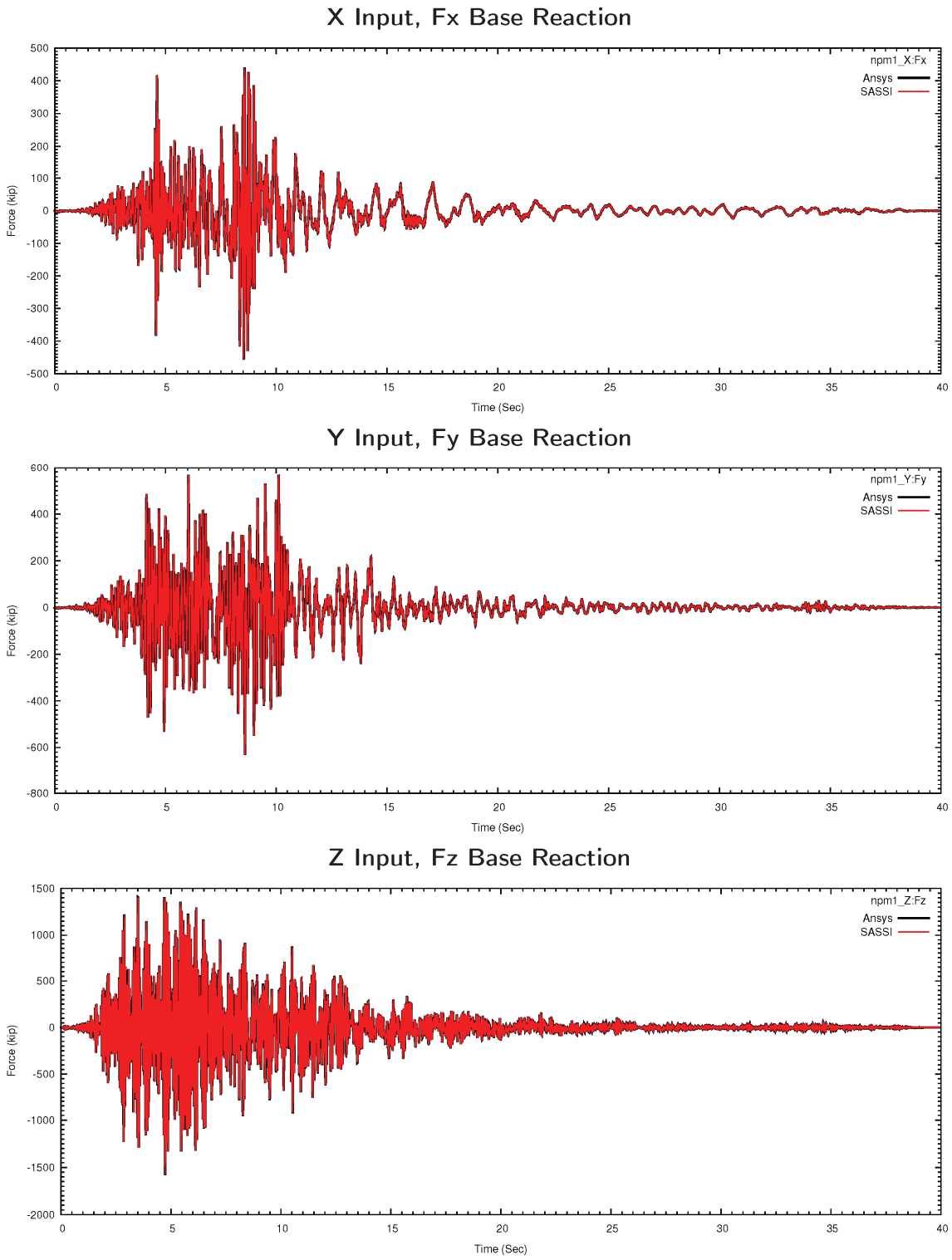

Figure 6-53 Base Reaction Time Histories for RXM-1

© Copyright 2019 by NuScale Power, LLC

6.4.7 Example 4 Summary

This example problem demonstrates the implementation of the *Soil Library Methodology* using a full RXB model which includes 12 reactor power modules (RXM), fluid-structure-equipment interaction, and soil-structure interaction. The ANSYS solution uses the Soil Library for soil type 7, ANSYS structural elements, the frequency domain solver and incorporates SASSI transfer function interpolation (Section 5.1.7). The SASSI solution uses the ANSYS generated mass, damping and stiffness matrices.

The ANSYS and SASSI results comparison is excellent for:

- acceleration transfer functions,
- acceleration time histories,
- in-structure response spectra,
- fluid pressure transfer functions,
- fluid pressure time histories,
- relative displacement transfer functions,
- relative displacement time histories,
- RXM lug force transfer functions,
- RXM lug force time histories,
- RXM base support force transfer functions,
- RXM base support force time histories

Response time histories were obtained using the CSDRS-compatible CAPITOLA input motion. Differences in responses were observed in a limited number of quantities, due to transfer function spikes which are an artifact of the transfer function interpolation algorithm implemented in SASSI and subsequently adopted for use in ANSYS. These spikes are frequently encountered in frequency domain SSI analyses, and are a known issue in SASSI.

The comparison between the SASSI and ANSYS results demonstrates that the ANSYS frequency domain solution is functionally equivalent to the SASSI frequency domain solution.

© Copyright 2019 by NuScale Power, LLC

7.0 Soil Library Implementation

The Soil Library solution procedure is shown schematically in Figure 4-4 and consists of the following steps for calculated impedances and load vectors.

Site Response: Determine the free-field response of the site model, including the free-field response, to vertically propagating P-waves and S-waves, that are saved on Tape1. This is performed in the SASSI SITE Module. Eigenvalues and eigenvectors describing the site response are saved on Tape2 for use in the POINT Module solution.

Point Response: Determine the response of the 3D axisymmetric model for impedance analysis, shown in Figure 5-1, and store results on Tape3 for transmission to the SDE-SASSI Anal16 Module. This data is used by Anal16 to assemble the free-field flexibility matrix. This point response is calculated in the SASSI POINT3 Module.

Excavated Soil Model: Develop the mass and stiffness of the excavated soil model using the SASSI HOUSE Module. Utilize the mixed lumped/consistent mass formulation in HOUSE to support the $\lambda/5$ mesh size criteria.

Layered Halfspace Impedance: Assemble and invert the layered halfspace flexibility matrix as discussed in Section 5.1.5. This is performed in the SDE-SASSI Anal16 Module. The flexibility inversion utilizes more computational resources than any other part of the SSI analysis.

Layered Halfspace Load Vector: Develop the seismic load vector as described in Section 5.1.6. This is performed in the SDE-SASSI Anal16 Module.

Excavated Impedance: Subtract the excavated soil stiffness from the layered halfspace impedance as shown by the term ($[Z] - [S'_{ii}]$) in Equation 5-31. This is performed in the SDE-SASSI Anal16 Module.

Reduced Excavated Impedance and Load Vector: Condense out the interaction DOF which are not on the basement boundary, as discussed in Section 5.2.1. This is performed in the SDE-SASSI Anal16 Module.

The resulting computed reduced excavated soil impedance and load vectors can be used to solve soil-structure interaction problems.

7.1 Soil Library Organization

The Soil Library can represent different soil sites and different excavation geometries. The data for a specific soil site and excavation geometry are organized into directories as shown schematically in Figure 4-3.

For a given soil site and excavation geometry, the Soil Library is represented by a collection of files for

© Copyright 2019 by NuScale Power, LLC

- computed impedances at various frequencies
- computed seismic load vectors at various frequencies

Each file name consists of the following parts, A_B_C.mtx where

Part A is “f” for computed values or “i[descriptor]” for interpolated frequencies where “descriptor” describes the interpolation. Note that impedance interpolation is not used.

Part B describes the frequency number and contains a zero-packed integer followed by an alpha descriptor for the number of terms in the Fourier transform. The alpha descriptors are:

i	alpha	$N_{fft} = 2^i$
11	K[15]	2,048
12	L	4,096
13	M	8,192
14	N	16,384
15	O	32,768

For example, 0016M is a frequency number 16 in a series with N_{fft} = 8,192.

Part C is s22kRed for a reduced impedance and f2Red for a reduced load vector.

Type .mtx signifies that the data is in the Matrix Market file format (Reference 9.1.5)

For example, f_4096M_s22kRed.mtx is the calculated reduced impedance for frequency number 4096 with N_{fft} =8,192.

The rows and columns in the reduced impedance matrix and the rows in the reduced load vector correspond to interaction degrees of freedom. Interaction degrees of freedom are related to the node number, nodal coordinates, and soil layer via a file labeled “node.dat.”

The columns in the load vector pertain to different load cases, such as

1. vertically propagating shear waves in the X direction with input at Layer 1
2. vertically propagating shear waves in the Y direction with input at Layer 1

[15] K is the 11th letter of the alphabet.

© Copyright 2019 by NuScale Power, LLC

3. vertically propagating P-waves in the Z direction with input at Layer 1
4. vertically propagating shear waves in the X direction with input at Layer k
5. vertically propagating shear waves in the Y direction with input at Layer k
6. vertically propagating P-waves in the Z direction with input at Layer k

Alternately, the load vectors could correspond to isolated unit loads on each layer which would allow the assembly of different wave fields acting on the structure. The specific seismic load vectors are documented in the Soil Library.

7.2 Reduced Impedance and Load Vectors

Reduced impedance and load vectors are obtained by condensing out the interaction DOFs which are not on the basement boundary as discussed in Section 5.2.1.

In Example 2, a traditional SASSI analysis is performed and compared to a Soil Library solution, including reduced impedance and load vectors. The results for these two solutions are equivalent as shown in Figure 6-23 and Figure 6-24.

© Copyright 2019 by NuScale Power, LLC

8.0 Summary and Conclusions

This report develops and demonstrates an improved frequency domain analysis methodology for the coupled soil-structure-fluid interaction analysis for complicated structures.

The solution uses SASSI to develop a library containing frequency dependent soil impedance matrices and load vectors. Next, a commercial finite element program, ANSYS, is used to perform frequency domain seismic analysis of the combined soil, building, fluid, and equipment substructures. Post processing of the seismic loads, including combination of seismic and non-seismic loads, is performed with ANSYS.

The soil impedance and seismic load vectors are pre-calculated, using SASSI, at several analysis frequencies and stored, as substructures, in a Soil Library.

This report also contains four example problems which compare the response calculated using the proposed methodology (i.e., the Soil Library with ANSYS) with the response calculated using SASSI. Response parameters compared include transfer functions, in-structure response spectra, overturning moment time histories, acoustic pressure time histories, relative displacements, and support reactions. The comparison of results demonstrates that the solution based on the Soil Library and ANSYS is functionally equivalent to a SASSI solution.

The proposed methodology extends the capability to analyze complex structural dynamic behavior beyond the capability provided by the SASSI computer code. For example, the ANSYS acoustic element permits a more accurate representation of fluid-structure interaction phenomena than that obtained using the library of structural element types provided by SASSI.

Using the element library and sub-structuring capabilities of the ANSYS computer code, more detailed and realistic models are practical, resulting in increased accuracy. Due to limits on SASSI model size, building and subsystems are currently analyzed in a two-step process. In the first step a model of the system is developed using simplified models of the building and subsystems. This is followed by a detailed analysis of the building and subsystems using input boundary conditions from the first analysis. This two-step process can be a source of error. With the proposed methodology, it is practical to use detailed models of the building and subsystems in a single step. Therefore, the need for a two-step analysis process and simplified models with assumed boundary conditions is eliminated, resulting in better accuracy and quality of results.

© Copyright 2019 by NuScale Power, LLC

9.0 References

9.1 Referenced Documents

9.1.1 Anderson, E., Bai, Z., Bischof, C., Blackford, S., Demmel, J., Dongarra,J., Du Croz, J., Greenbaum, A., Hammarling, S., McKenney, A., and Sorensen, D. *LAPACK Users' Guide (Third ed.),* Society for Industrial and Applied Mathematics, 1999.

9.1.2 ASCE 4-2016, *Seismic Analysis of Safety-Related Nuclear Structures and Commentary,* American Society of Civil Engineers.

9.1.3 ASCE 43-05, *Seismic Design Criteria for Structures, Systems, and Components in Nuclear Facilities,* American Society of Civil Engineers, 2005.

9.1.4 Blevins, R.D., *Formulas for Natural Frequency and Mode Shape,* Krieger Publishing, 1995.

9.1.5 Boisvert, R.F., Pozo, R. and Remington, K.A., *The Matrix Market Exchange Formats: Initial Design,* NISTIR 5935, National Institute of Standards and Technology, 1996.

9.1.6 CJC-SDE-V-002, *Acceptance Testing Report on Linux Cluster*, SDE-SASSI v2.1.1 Carl J. Costantino and Associates.

9.1.7 CJC-NUS-M-001, Rev 2, *QA Plan and Evaluation of Purchase OrderCWA-17-001.CJC (Project 1700624),* Carl J. Costantino and Associates, 7/3/2017.

9.1.8 Kausel, E., *Forced Vibrations of Circular Foundations on Layered Media,* Research Report 74-11, Massachusetts Institute of Technology, 1974.

9.1.9 Kramer, S.L,. *Geotechnical Earthquake Engineering,* Prentice Hall, 1996.

9.1.10 Lysmer, J., *Analytical Procedures in Soil Dynamics,* Report No.UCB/EERC-78/29, University of California, Berkeley, 1978.

9.1.11 Lysmer, J. Tabatabaie-Raissi, M., Tajirian, F., Vahdani, S. and Ostadan, F., *SASSI, A System for Analysis of Soil-Structure Interaction,* Report No. UCB/GT/81-02, University of California, Berkeley, 1981.

9.1.12 *Mathematica v11,* Wolfram Research Inc., Champaign, Il. 2016.

9.1.13 Development of Soil Impedance Library for Type 7 Soil, EC-F010-6438, Revision 2.

© Copyright 2019 by NuScale Power, LLC

9.1.14 Nigam, N.C. and Jennings, P.C. *Digital Calculation of Response Spectra from Strong-Motion Earthquake Records,* Earthquake Engineering Research Laboratory, California Institute of Technology, 1968.

9.1.15 Ostadan, F., *SASSI 2000, A System for Analysis of Soil-Structure Interaction, Version 3, User's Manual* University of California, Berkeley, 2007.

9.1.16 Ostadan, F., *SASSI, A System for Analysis of Soil-Structure Interaction, Version 3, Theoretical Manual,* University of California, Berkeley, 2007.

9.1.17 Press, W.H., Teukolsky, S.A., Vetterling, W.T. and Flannery, B.P., *Numerical Recipes in Fortran, The Art of Scientific Computing,* Second Edition, Cambridge University Press, 1992.

9.1.18 Schnabel, P.B., Lysmer, J. and Seed, H.B., *SHAKE A Computer Program for Earthquake Response Analysis of Horizontally Layered Sites,* EERC 72-12, University of California, Berkeley, 1972.

9.1.19 Sieffert, J.G. and Cevaer, F., *Handbook of Impedance Functions,* Ouest Editions, 1991.

9.1.20 Tajirian, Fredrick, F., *Impedance Matricies and Interpolation Techniques for 3-D Interaction Analysis of the Flexible Volume Method,* Dissertation, University of California, Berkeley, 1981.

9.1.21 Thomson, W.T., *Theory of Vibration with Applications,* Second Edition, Prentice-Hall, 1981.

9.1.22 *Verification and Validation of SASSI, SASSI-VV-CAL-Task 3 Rev.0, Task 3 - Verification of Post-Processing Computations of SASSI, Revision 0, March 28, 2014,* U.S. Department of Energy, https://energy.gov/em/system-analysis-soil-structure-interaction-sassiverification-validation-vv-problem-set

9.1.23 *Verification and Validation of SASSI, SASSI-VV-CAL-Task 6 Rev. 2, Task 6-Impedance and Compliance of Surface Foundations, Revision 2, March 28, 2014,* U.S. Department of Energy, https://energy.gov/em/systemanalysis-soil-structure-interaction-sassi-verification-validation-vvproblem-set

9.1.24 *Verification and Validation of SASSI, SASSI-VV-CAL-Task 8 Rev. 2,Task 8 - Impedance and Scattering Response of Embedded Foundations, Revision 2, June 12, 2014,* U.S. Department of Energy, https://energy.gov/em/system-analysis-soil-structure-interaction-sassiverification-validation-vv-problem-set

9.1.25 Weaver, W. and Johnson, P.R. *Structural Dynamics by Finite Elements,* Prentice-Hall, 1987.

9.1.26 ANSYS, Inc., ANSYS Release 18.1, April, 2017.

© Copyright 2019 by NuScale Power, LLC

9.1.27 Development of Time Histories Compatible with NuScale CSDRS using Earthquake Seeds, EC-F010-1889, Revision 5.

© Copyright 2019 by NuScale Power, LLC

Appendix A. Response of a Single Degree of Freedom System with Base Motion

The response of a single degree of freedom (SDOF) system with base motion is calculated in this appendix to demonstrate how base motion is incorporated and to demonstrate the differences in response for structural and viscous damping.

Consider the simple mass-spring-dashpot system shown in Figure A-1. The dynamic stiffness, *S*, at frequency ω is:

$$S = \begin{bmatrix} k + i\omega c - \omega^2 m & -k - i\omega c \\ -k - i\omega c & k + i\omega c - \omega^2 m \end{bmatrix} \quad \text{Equation A-1}$$

where the first row represents forces acting on DOF 1 and the second row represents forces acting on DOF 2. Let the applied force be equal to zero, F=0, and impose a displacement on DOF 2, $X = \{x1, x2\}$. Thus, the equation of motion becomes

$$SX = \begin{bmatrix} (k + i\omega c - \omega^2 m)x1 & (-k - i\omega c)x2 \\ (-k - i\omega c)x1 & (k + i\omega c - \omega^2 m)x2 \end{bmatrix} = 0 \quad \text{Equation A-2}$$

Extracting the force of the free field DOF, i.e., the first row, and solving for the displacement *x*1, given the displacement *x*2, yields:

$$x1 = \frac{(k + i\omega c)x2}{k + i\omega c - \omega^2 m} \quad \text{Equation A-3}$$

The response of *x*1 is expressed as a transfer function, TF, times *x*2, or:

$$TF = \frac{x1}{x2} = \frac{k + i\omega c}{k + i\omega c - \omega^2 m} \quad \text{Equation A-4}$$

The transfer function is also referred to as the frequency response function and is often denoted $h(\omega)$.

Assume three 1 Hz systems with (1) 10% viscous damping, (2) 10% structural damping, and (3) 10% structural damping using the simplified damping formulation. The parameters for the viscous damping case become:

© Copyright 2019 by NuScale Power, LLC

$$\begin{aligned} \omega &= (2\pi)1 \\ \xi &= 0.10 \\ m &= 1 \\ k &= \omega^2 m \\ c &= 2 \times \xi \sqrt{km} \\ TF_{Viscous} &= \frac{k + i\omega c}{k + i\omega c - \omega^2 m} = \frac{5 + if}{5 + if - 5f^2} \end{aligned}$$

Equation A-5

The unique parameters for the structural damping case are:

$$\begin{aligned} k^* &= k(1 - 2\xi^2 + 2i\xi\sqrt{1 - \xi^2}) \\ c &= 0 \\ TF_{Structural} &= \frac{k}{k - \omega^2 m} = \frac{49 + 3i\sqrt{11}}{49 + 3i\sqrt{11} - 50f^2} \end{aligned}$$

Equation A-6

and the unique parameters for the simplified structural damping case are:

$$\begin{aligned} k^* &= k(1 + 2i\xi) \\ c &= 0 \\ TF_{Simple} &= \frac{k}{k - \omega^2 m} = \frac{5 + i}{5 + i - 5f^2} \end{aligned}$$

Equation A-7

Plots of the amplitude and phase angle of the viscous and structural damping transfer functions are shown in Figure A-2, Figure A-3, and Figure A-4. The difference in transfer function amplitude in Figure A-2 is on the order of a line thickness. There are slight differences in phase angle. The differences between viscous and structural damping decrease with damping ratio.

The expanded scale of the peak, Figure A-3, indicates that the structural and viscous damping cases reduce the natural frequency at resonance, while the simplified viscous damping case does not reduce the natural frequency. The simplified damping case has an effective stiffness of $k\sqrt{(1 + \xi^2)}$. The structural damping case has a slightly reduced peak amplitude at resonance.

The real part of the sum of damping and spring force for the viscous system is:

$$F_{Viscous} = \Re\left((i\omega c + k)e^{i\omega t}\right)$$

Equation A-8

© Copyright 2019 by NuScale Power, LLC

and the real part of the complex spring force for the structural damping system is:

$$F_{Structural} = \Re\left(k^*_{Structural} e^{i\omega t}\right)$$
$$F_{Simple} = \Re\left(k^*_{Simple} e^{i\omega t}\right)$$

Equation A-9

where $\Re$ ( ) represents the real part of the complex value.

Forces $F_{Structural}$, F_{Simple} and $F_{Viscous}$ are plotted in Figure A-5 along with the displacement for a 1 Hz cyclic displacement, using the properties developed above. The overall behavior of $F_{Structural}$, F_{Simple} and $F_{Viscous}$ are similar. The forces near 1 second are shown in Figure A-6. The (1) peak viscous force and simplified structural damping force is slightly larger than the peak structural force, and (2) the peak structural, simplified structural and viscous forces occur before the peak displacement.

Forces $F_{Structural}$, F_{Simple} and $F_{Viscous}$ are plotted versus a 1 Hz cyclic displacement in Figure A-7. The area inside the hysteresis loop represents the dissipated energy in one cycle. At 1 Hz, the three cases have essentially the same energy dissipation.

The same forces are cycled at 0.5 Hz and 2 Hz and the resulting hysteresis loops are shown in Figure A-8 and Figure A-9. Note that the energy dissipated by the structural damping and simplified structural damping formulation remains constant[17] while the energy dissipated by the viscous damping formulation is dependent on the frequency.

[17] Structural damping is also referred to as frequency independent damping.

© Copyright 2019 by NuScale Power, LLC

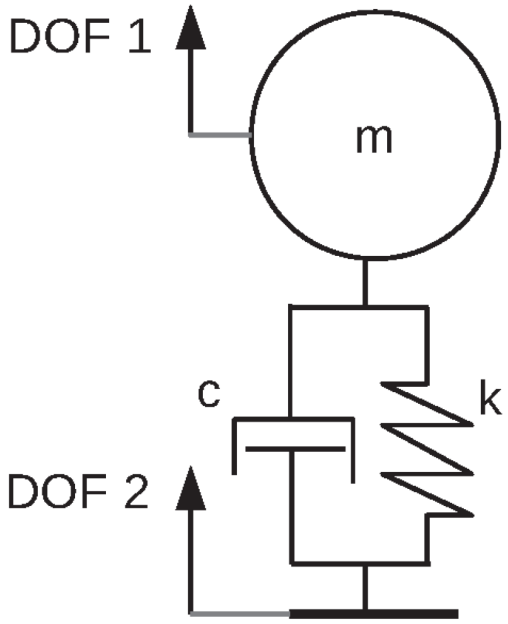

Figure A-1 Simple mass-spring-dashpot system

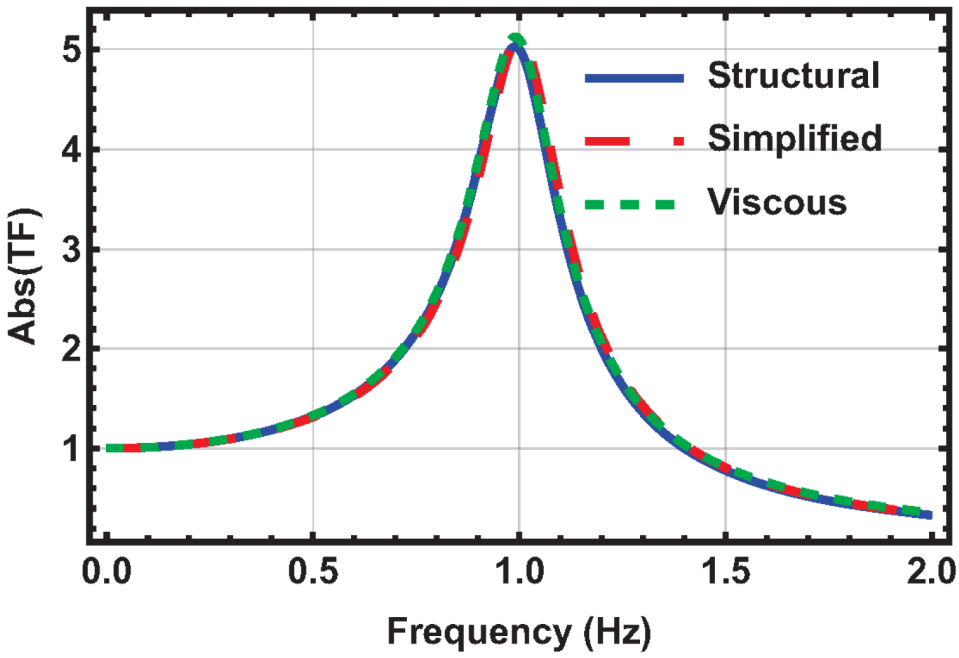

Figure A-2 Transfer function amplitude for 1 Hz SDOF systems with 10% structural, simplified structural, or viscous damping

© Copyright 2019 by NuScale Power, LLC

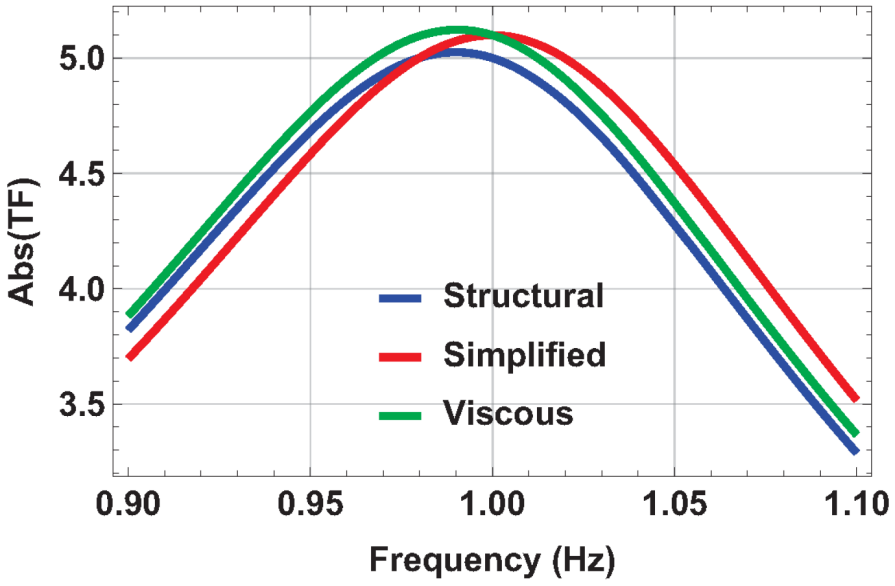

Figure A-3 Transfer function amplitude for 1 Hz SDOF systems with 10% structural, simplified structural, or viscous damping, expanded scale

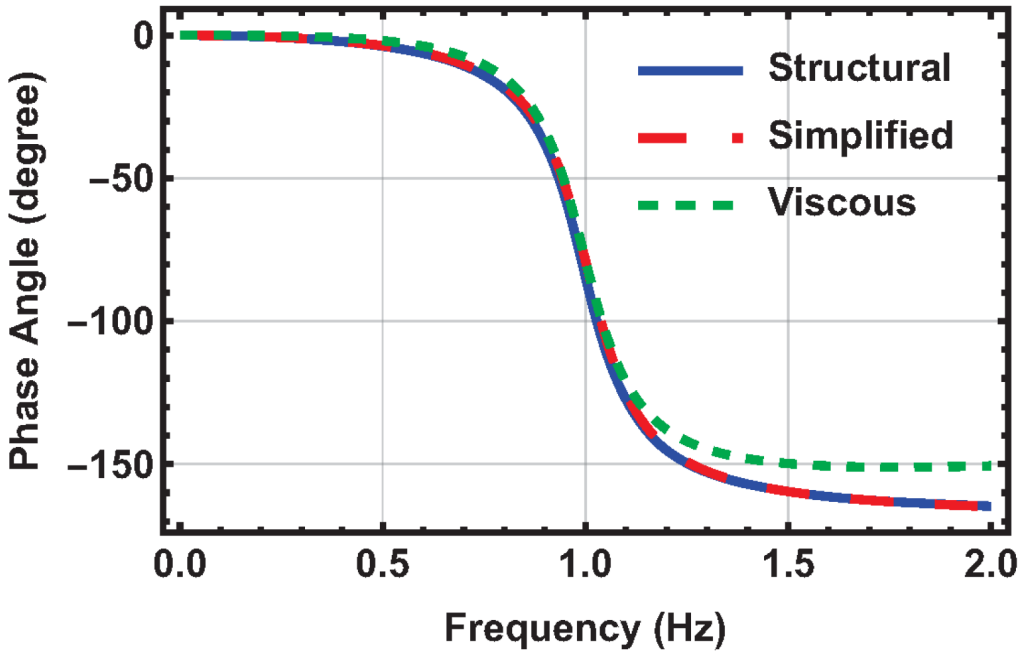

Figure A-4 Transfer function phase angle for 1 Hz SDOF systems with 10% structural, simplified structural, or viscous damping

© Copyright 2019 by NuScale Power, LLC

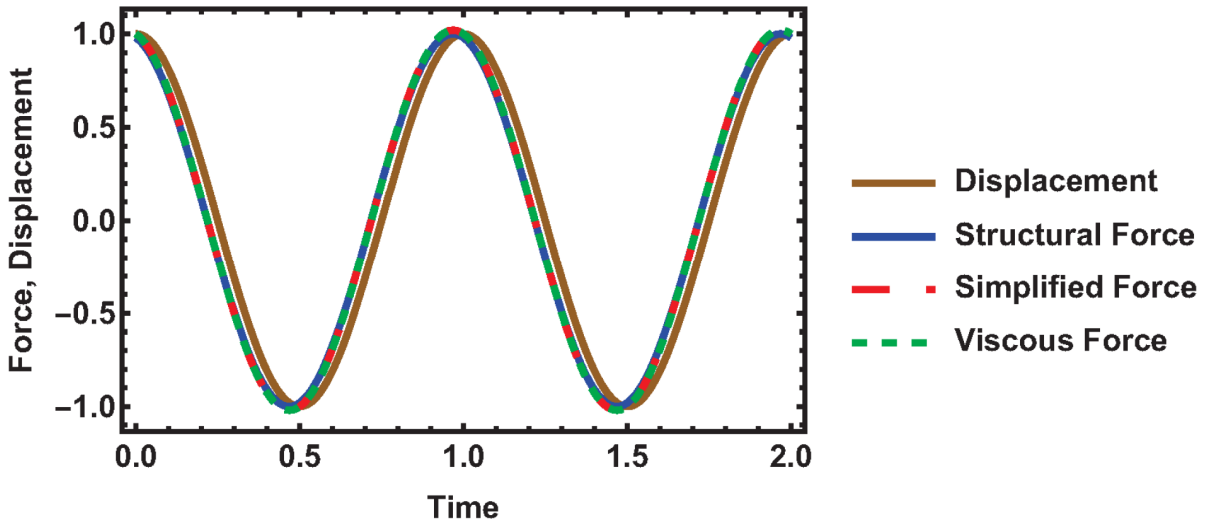

Figure A-5 Combined spring and dashpot forces for SDOF systems with 10% structural, simplified structural, or viscous damping, cycled at 1 Hz

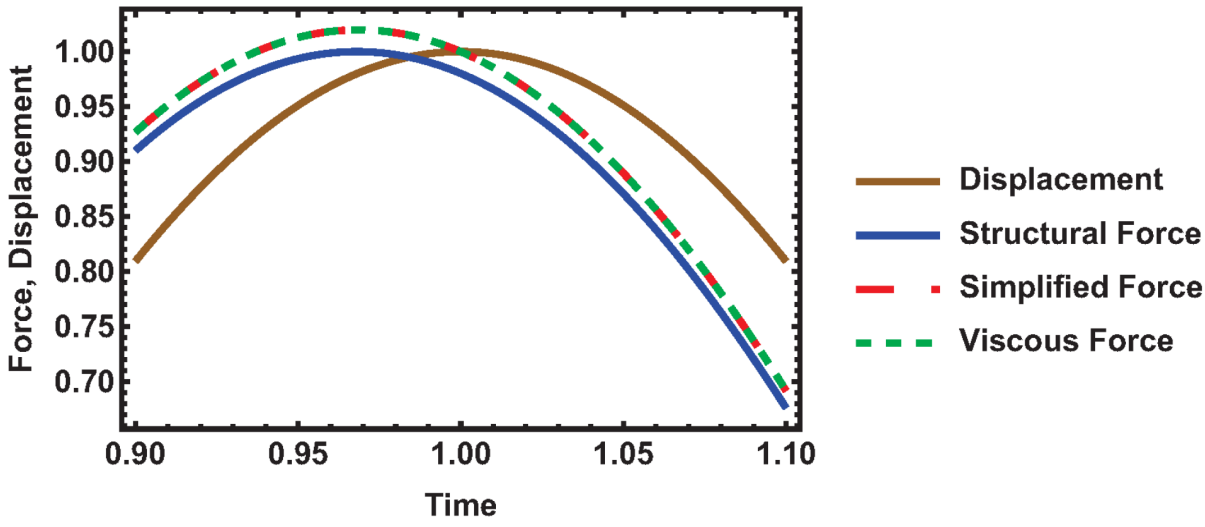

Figure A-6 Combined spring and dashpot forces for SDOF systems with 10% structural, simplified structural, or viscous damping, cycled at 1 Hz, expanded scale

© Copyright 2019 by NuScale Power, LLC

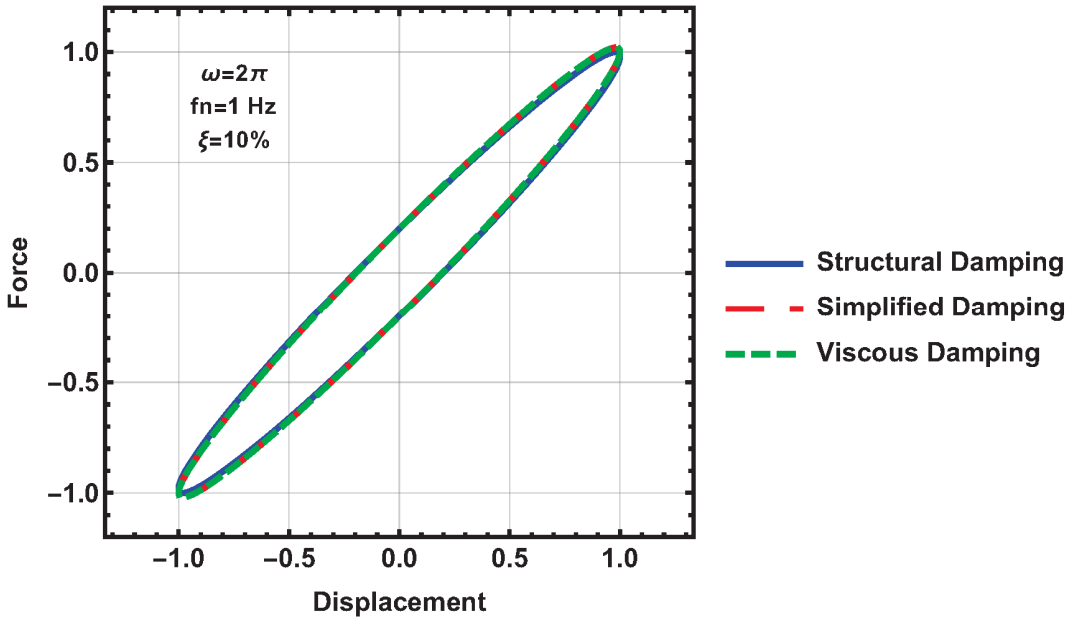

Figure A-7 Combined spring and dashpot forces for SDOF systems with 10% structural, simplified structural, or viscous damping, cycled at 1 Hz

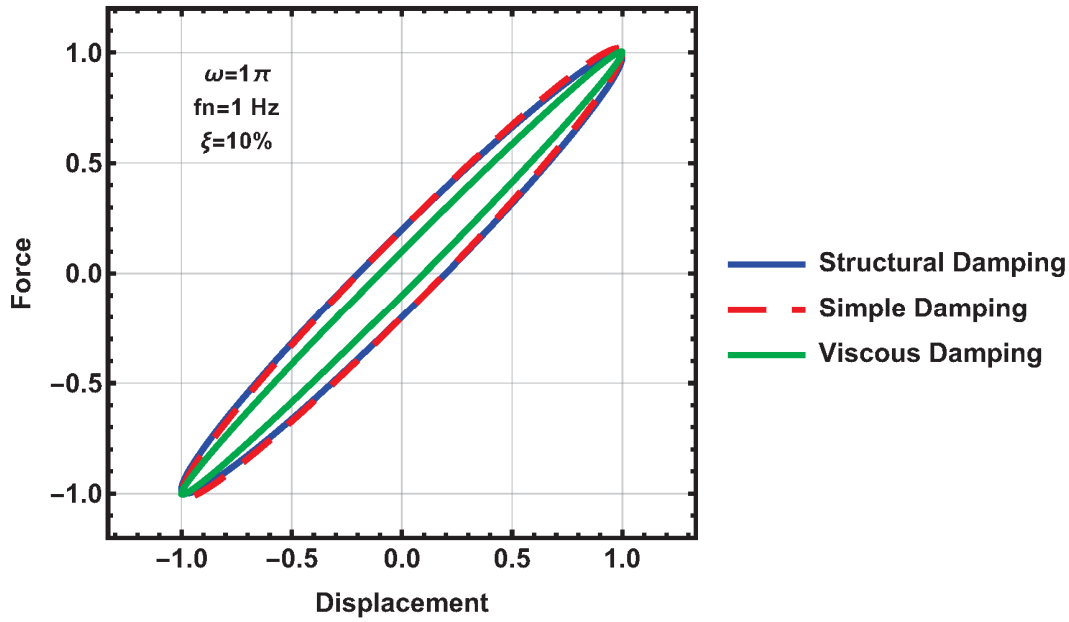

Figure A-8 Combined spring and dashpot forces for SDOF systems with 10% structural, simplified structural, or viscous damping, cycled at 0.5 Hz

© Copyright 2019 by NuScale Power, LLC

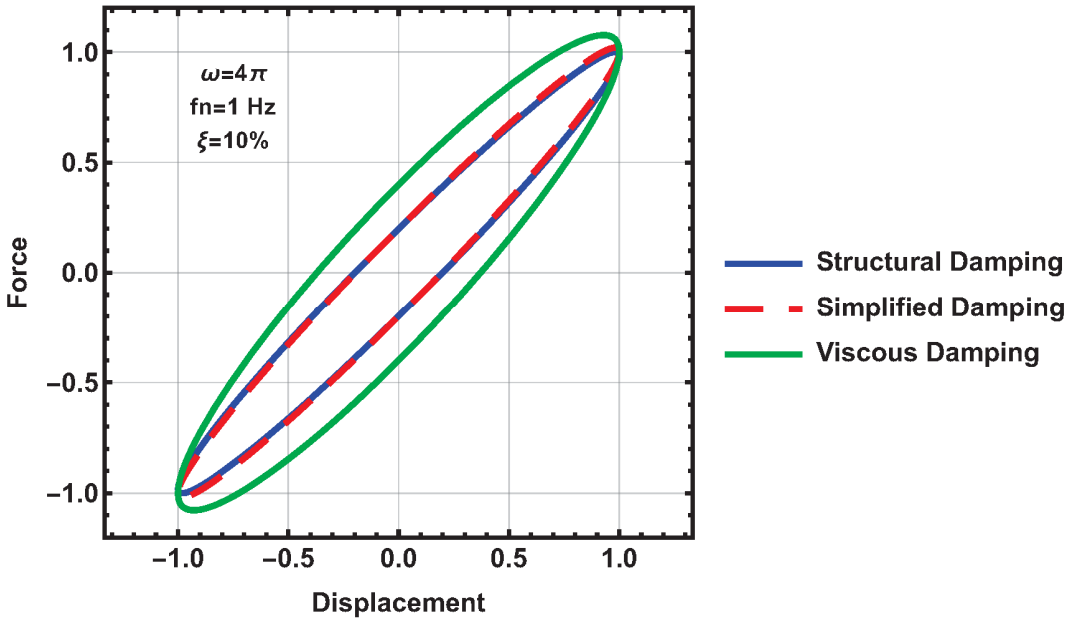

Figure A-9 Combined spring and dashpot forces for SDOF systems with 10% structural, simplified structural, or viscous damping, cycled at 2 Hz

© Copyright 2019 by NuScale Power, LLC

Appendix B. Effect of Mass Formulations on Response

The free field response of a soil column is approximated using a shear beam and the shear beam is represented by a series of masses and springs. Lumped, consistent and mixed lumped-consistent mass matrices are considered. The same stiffness with complex damping is used for each of the shear beam solutions. The resulting transfer functions are compared to the 1D wave equation solution implemented in SHAKE (Reference 9.1.18). The response using the mixed lumped-consistent mass formulation has less error than a response based on either the lumped mass or consistent mass formulations.

A 100 foot tall soil column is considered with a shear wave velocity, V_s, of 800 fps and a unit weight of 0.12 k/ft^3 or a density of ρ = 0.12⁄32.2 kip-sec/ft^4, and 2% damping. The soil column has a fundamental frequency of:

$$fn = \frac{Vs}{4H} = 2\ Hz \qquad \text{Equation B-1}$$

with higher modes at 3, 5, 7, . . . times 2 Hz or 6, 10, 14. . . Hz. The wavelength, λ, at each frequency is V s/f . The model consists of 20, 5 foot long beam segments. The frequency, wavelength, and number of elements per wavelength are summarized in the Table B-1.

Table B-1 Soil column modes

Mode	Frequency (Hz)	λ (ft)	Elements/λ
1	2	400.	80.0
2	6	133.	26.7
3	10	80.0	16.0
4	14	57.1	11.4
5	18	44.4	8.9
6	22	36.4	7.3
7	26	30.7	6.1
8	30	26.6	5.3
9	34	23.5	4.7
10	38	21.0	4.2

Lysmer (Reference 9.1.10) provides convergence criteria that targets less than 10% error on wave amplitude:

© Copyright 2019 by NuScale Power, LLC

$$f_{cutoff} = \frac{Vs}{8L} = 20\ Hz \quad \text{for lumped mass}$$
$$f_{cutoff} = \frac{Vs}{8L} = 20\ Hz \quad \text{for consistent mass}$$
$$f_{cutoff} = \frac{Vs}{5L} = 32\ Hz \quad \text{for mixed mass}$$

Equation B-2

Alternately, Lysmer's criteria can be stated as $\lambda/8$ for lumped or consistent mass and $\lambda/5$ for mixed mass. Comparing Lysmer's criteria to elements per wavelength in Table B-1, the lumped and consistent mass formulations represent the first 5 modes and the mixed mass formulation represents the first 8 modes.

Each beam element used to represent the soil column is a shear spring with a stiffness of:

$$k = \frac{G \times A}{L} = \frac{\rho V_s^2 \times A}{L} = \frac{\frac{0.12}{32.2} 800^2 \times 1}{5} = 477 kip/ft$$

Equation B-3

The spring stiffness matrix is:

$$K = k^* \begin{bmatrix} 1 & -1 \\ -1 & 1 \end{bmatrix}$$

Equation B-4

where $k^* = k\ (1 - 2\xi^2 + 2i\xi\sqrt{(1 - \xi^2)})$, and $\xi = 0.02$.

The mass matrix corresponding to a spring element is:

$$M = \frac{m}{6} \begin{bmatrix} 2+\mu & 1-\mu \\ 1-\mu & 2+\mu \end{bmatrix}$$

Equation B-5

where m is the total mass of the element:

$$m = \rho \times AL = 0.12/32.2 \times 5 = 0.01863\ kip\ sec^2/ft$$

Equation B-6

© Copyright 2019 by NuScale Power, LLC

and μ = 1 for a lumped mass formulation, μ = 0 for a consistent mass formulation, and μ = 0.5 for a mixed lumped-consistent mass formulation. SASSI uses the mixed lumped-consistent mass formulation for excavated soil elements. NASTRAN also uses a mixed lumped-consistent mass formulation for some elements.

The base of the soil column is excited with a unit sinusoidal base motion and the resulting transfer functions for the free field surface are shown in Figure B-1.

A benchmark solution is also included in Figure B-1. The benchmark is the closed form transfer function (Reference 9.1.9) for the surface response given input at the bottom of a uniform damped layer, or:

$$TF = \frac{2}{e^{-i\,z} + e^{i\,z}} = \sec(i\,z), \quad z = \frac{2\pi f\,H}{V_s(1+\xi\,i)} \qquad \text{Equation B-7}$$

where V_s =800, H =100, ξ =0.02, i = $\sqrt{-1}$, sec is the secant, sec = 1/ cos and f is the frequency in Hz.

Starting with the 4th mode, at 14 Hz with 11.4 elements per wavelength, the lumped mass formulation underestimates the modes natural frequency while the consistent mass formulation overestimates the modes natural frequency. The mixed lumped-consistent mass formulation does a better job of representing the frequency of the first 8 modes, 30 Hz.

At the 8th mode, 30 Hz with 5.3 elements per wavelength, the responses of the three models are compared to the benchmark, Equation B-7. The amplitude at 30 Hz is TF=2.046.

Case	Frequency 30 Hz	Mode 8 Amp. 2.046	30 Hz Amp. 2.046
Lumped Mass	0.94	0.86	0.42
Lumped-Consistent Mass	0.995	0.88	0.86
Consistent Mass	1.06	0.89	0.39

Comparing the amplitude at 30 Hz, the lumped and consistent mass formulations have a large error and the mixed mass formulation has a smaller 10% error. Comparing the amplitude of the 8th mode, the lumped and consistent mass formulations have approximately 10% error in amplitude with approximately 6% error (1.7 Hz) in frequency.

Limiting the available analysis tools to either lumped or consistent mass, the response at the 5th mode, 18 Hz with 8.9 elements per wavelength has a frequency of 0.97 and 1.04

© Copyright 2019 by NuScale Power, LLC

times the 18 Hz wave equation frequency. Thus, the frequency error with the lumped mass model at 8.9 elements/wavelength is larger than the error with the lumped-consistent mass model at 5.3 elements/wavelength.

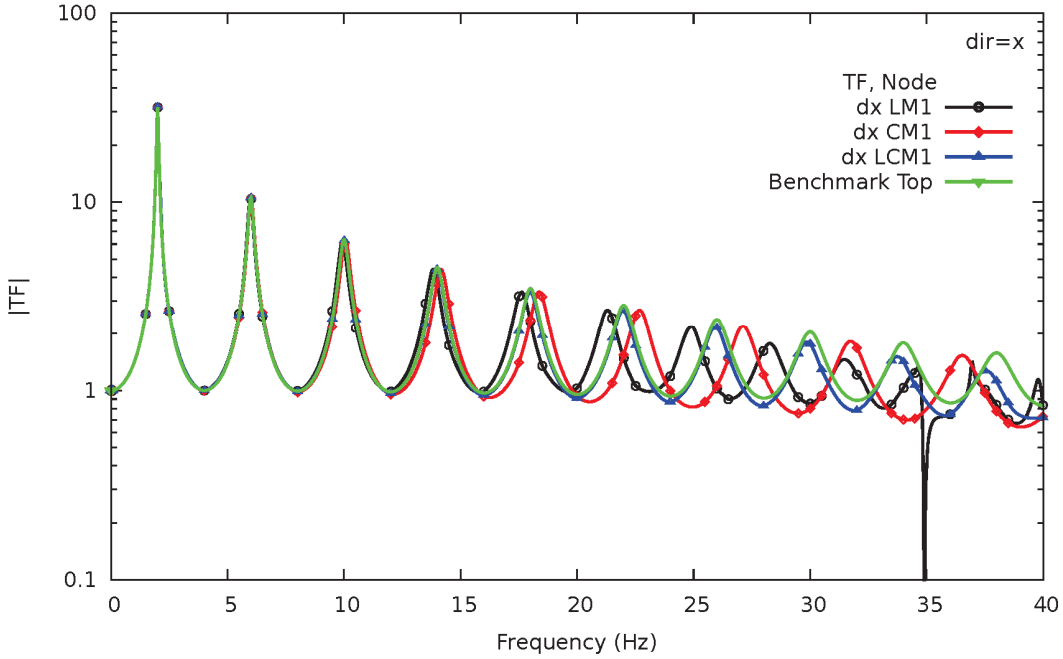

Figure B-1 Lumped mass (LM), consistent mass (CM), and lumped-consistent mass (LCM) transfer function comparison with wave equation benchmark, Vs/5L = 32 Hz

© Copyright 2019 by NuScale Power, LLC

Appendix C. Structural Meshing for High Frequency Response

The roof slab in Example 2 is approximated as a simply supported flat plate and the natural frequency and mode shape are calculated using Blevins (Reference 9.1.4). The modes with natural frequencies less than 100 Hz are examined and the number of elements required to obtain response at these frequencies is estimated.

Blevins provides the following expressions for the natural frequency of a rectangular plate simply supported on all four sides:

$$fn_{i,j} = \frac{\lambda_{i,j}^2}{2\pi a^2}\sqrt{\frac{Eh^3}{12\rho(1-\nu^2)}} \qquad \text{Equation C-1}$$

where $\lambda_{i,j}$ is a mode shape factor:

$$\lambda_{i,j}^2 = \pi^2\left[i^2 + j^2\left(\frac{a}{b}\right)^2\right] \qquad \text{Equation C-2}$$

i is the number of modes in the *a* direction, *j* is the number of modes in the *b* direction, *a* and *b* are the plate dimensions, *a* =94.83 ft, *b* =47.45 ft, *h* is the plate thickness, *h* = 2 ft, *E* is the elastic modulus, *E* =759500 ksf, *γ* is the plate density, *γ* =0.668/32.2 kip-sec^2/ft^4 and *v* is Poisson's ratio, *v* =0.17. Blevins also provides the mode shape for a simply supported rectangular plate as:

$$z(x,y) = \sin\frac{i\pi x}{a}\sin\frac{j\pi y}{b} \qquad \text{Equation C-3}$$

The natural frequencies for different modes are summarized in Table C-1. The following modes have natural frequencies less than 100 Hz.

Mode i	Mode j	Frequency (Hz)	Mode Shape
10	1	91.07	Figure C-1
9	2	70.04	Figure C-2
8	3	87.52	Figure C-3
7	4	98.87	Figure C-4
3	5	95.32	Figure C-5

© Copyright 2019 by NuScale Power, LLC

Table C-1 Natural frequency (Hz)

Mode	Mode j					
i	1	2	3	4	5	6
1	4.37	14.87	32.35	56.84	88.32	126.79
2	7.	17.49	34.98	59.46	90.94	129.42
3	11.38	21.87	39.36	63.84	95.32	133.8
4	17.51	28.	45.49	69.97	101.45	139.93
5	25.39	35.88	53.37	77.85	109.33	147.81
6	35.02	45.52	63.	87.49	118.97	157.44
7	46.41	56.9	74.39	98.87	130.35	168.82
8	59.54	70.04	87.52	112.01	143.49	181.96
9	74.43	84.92	102.41	126.89	158.37	196.85
10	91.07	101.56	119.05	143.53	175.01	213.48
11	109.46	119.95	137.44	161.92	193.4	231.87
12	129.6	140.09	157.58	182.06	213.54	252.02

As seen in Equation C-3 and Figure C-1 through Figure C-5, each mode is a half sine wave.

- With 5 elements approximating a full sine wave, the first mode is a half sine wave approximated using three elements. However, the peak amplitude is under-represented with 3 elements approximating the shape of a half sine wave.

- With 8 elements approximating a full sine wave, there is a center node in the half sine wave to represent the peak amplitude.

Based on these two assumptions, the number of elements required to approximate each mode is:

Mode	Number of Elements 5 Elem/2π	Number of Elements 8 Elem/2π
1	3	4
2	5	8
3	8	12
4	10	16
5	13	20
6	15	24
7	18	28
8	20	32
9	23	36
10	25	40

© Copyright 2019 by NuScale Power, LLC

The roof mesh in Example 2 has 16 elements in the *a* direction and is able to represent the I = 4 mode. In the *b* direction, the mesh has 8 elements and is able to represent the j = 2 mode. From Table C-1, the maximum frequency for i, j = 4,1 and i, j = 4,2 is 28 Hz and the corresponding mode shape is shown in Figure C-6. Thus, the mesh in Example 2 is capable of representing the frequency and amplitude at 28 Hz.

If 5 elements per full sine wave are considered, then we are able to detect a mode at a higher frequency, but there are inadequate elements to represent the amplitude of that mode.

Note that this assessment is based on an assumption that 8 elements are capable of representing the deformation of a full sine wave. Additional concerns are the quality of the element stiffness and mass formulation which can also affect results. For example, if an element is not able to represent the second mode for a one-way simple span case with 8 elements across the span, then the required number of elements discussed above is inadequate.

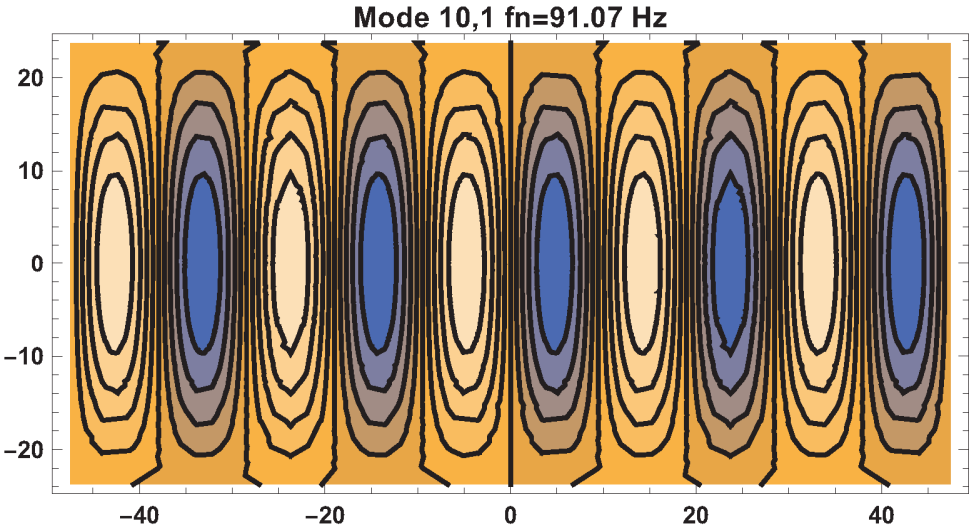

Figure C-1 Rectangular plate model 10, 1

© Copyright 2019 by NuScale Power, LLC

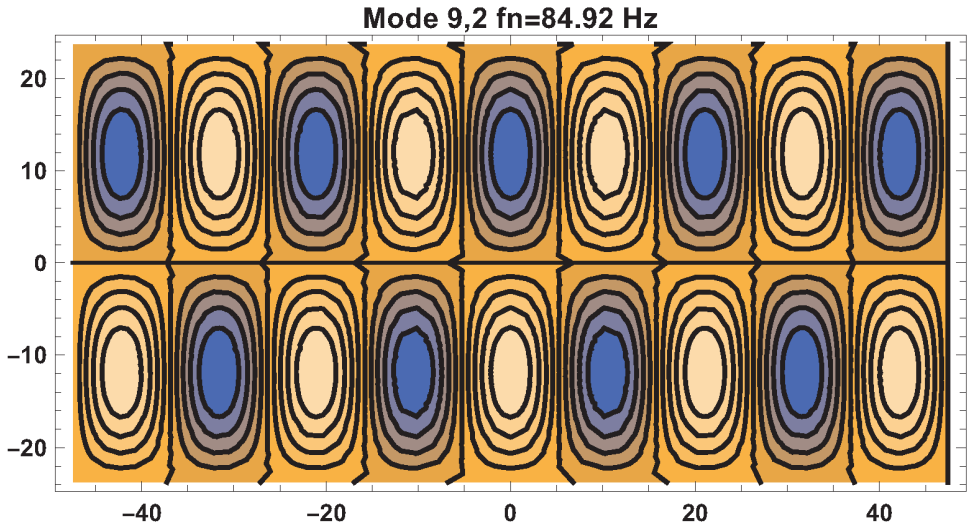

Figure C-2 Rectangular plate model 9, 2

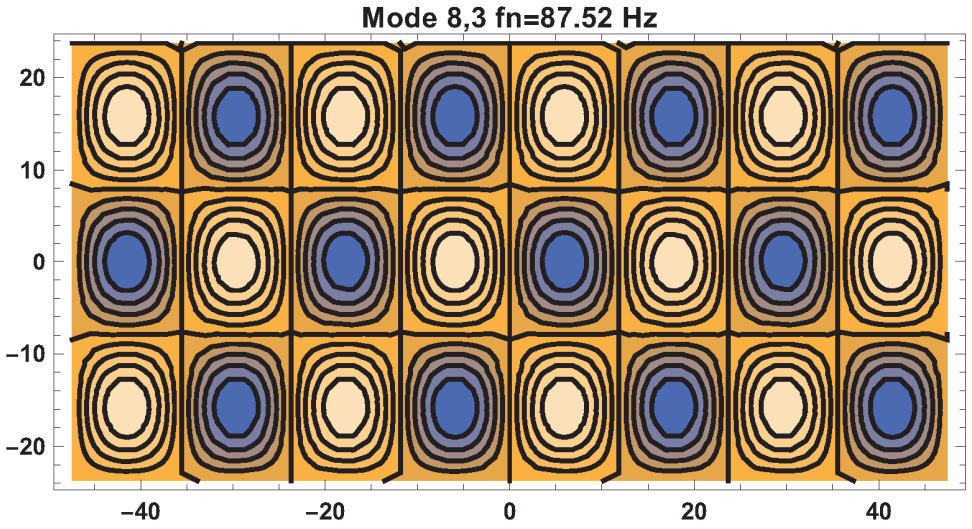

Figure C-3 Rectangular plate model 8, 3

© Copyright 2019 by NuScale Power, LLC

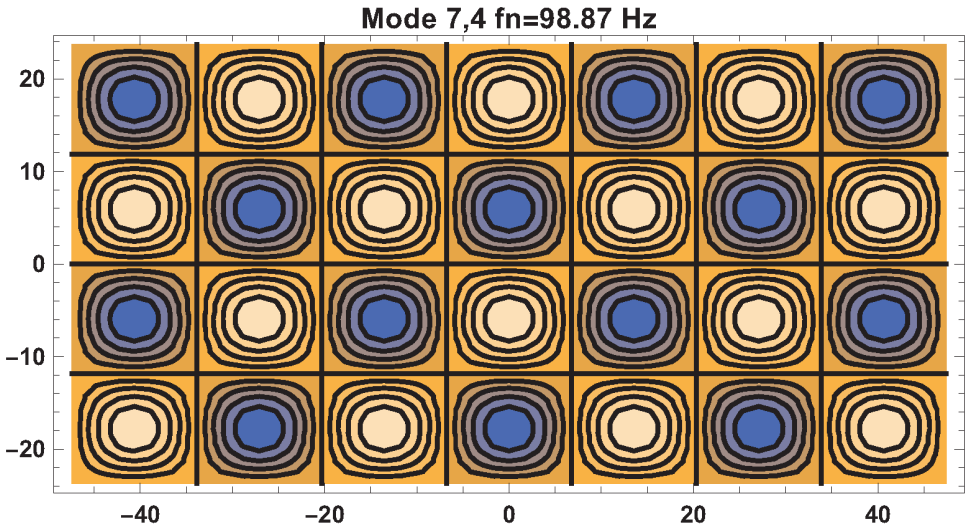

Figure C-4 Rectangular plate model 7, 4

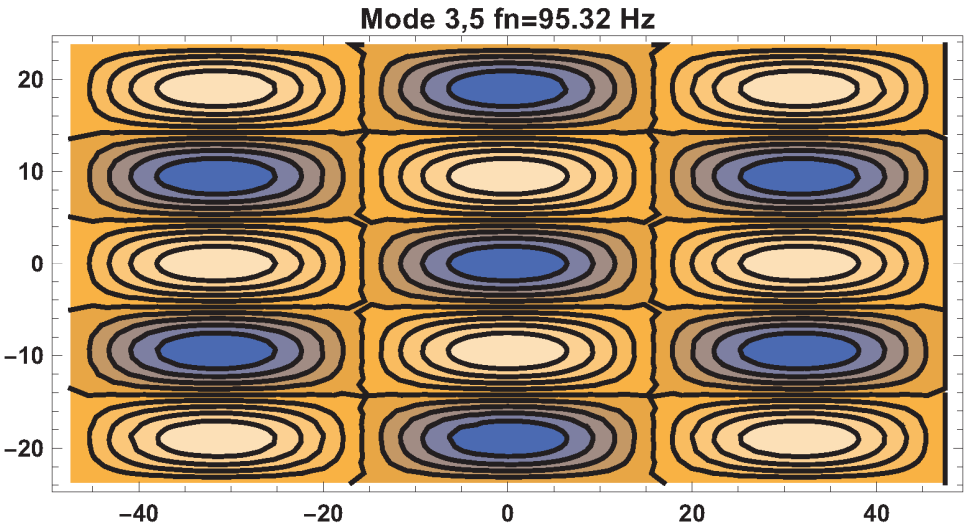

Figure C-5 Rectangular plate model 3, 5

© Copyright 2019 by NuScale Power, LLC

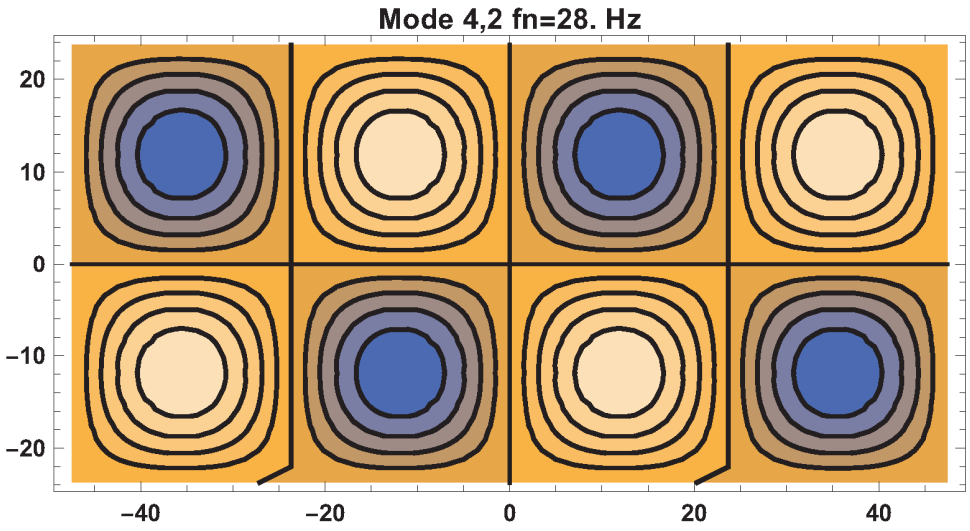

Figure C-6 Rectangular plate model 4, 2

© Copyright 2019 by NuScale Power, LLC

Appendix D. Influence of Halfspace Depth

Oscillations of the translational lumped parameter soil impedance[18] for Example 2 are observed in Figure 6-16 and Figure 6-17. These impedances are based on the soil profile shown in Figure 6-15 which considers the halfspace at a depth of 300 feet with a shear wave velocity of 5000 fps. SASSI simulates the halfspace with 10 additional layers and a transmittingboundary.

The depth to the SASSI simulated halfspace is increased from 300 feet to 400 feet by inserting an additional twenty 5-foot thick soil layers with halfspace material properties. A comparison of the two impedances is contained in the following figures:

	X	Y	Z	θ_X	θ_Y	θ_Z
X	Figure D-1	_	_	_	Figure D-2	_
Y	-	Figure D-3	-	Figure D-1	-	-
Z	_	_	Figure D-5	_	_	_
θ_X	-	Figure D-4	-	Figure D-6	-	-
θ_Y	Figure D-2	_	_	_	Figure D-7	_
θ_Z	_	_	_	_	_	Figure D-8

where the impedances are normalized by the low frequency impedance in Table 6-4.

Note that the 300 foot and 400 foot translation impedance oscillations are frequency shifted, as seen in Figure D-1 through Figure D-4. The frequency shift indicates that the oscillations are due to shear wave reflections off of the transmitting boundary. Thus, these minor impedance oscillations are an artifact of the analysis method, not actual soil behavior.

Note that the P-wave impedance term, K_{ZZ}, rocking impedance terms, $K_{\theta x \theta x}$, $K_{\theta y \theta y}$, and the torsion term, $K_{\theta z \theta z}$ have the same impedance for both halfspace depths. This implies that the reflections are associated with the radial degree of freedom in Figure 5-9.

Note that a typical SASSI analysis does not study the variation in rigid-massless soil impedance at every 0.4 Hz, and these minor impedance oscillations may not be detected.

[18] The lumped parameter soil impedance is derived from the excavated soil impedance using the approach described in Section 5.2.2

© Copyright 2019 by NuScale Power, LLC

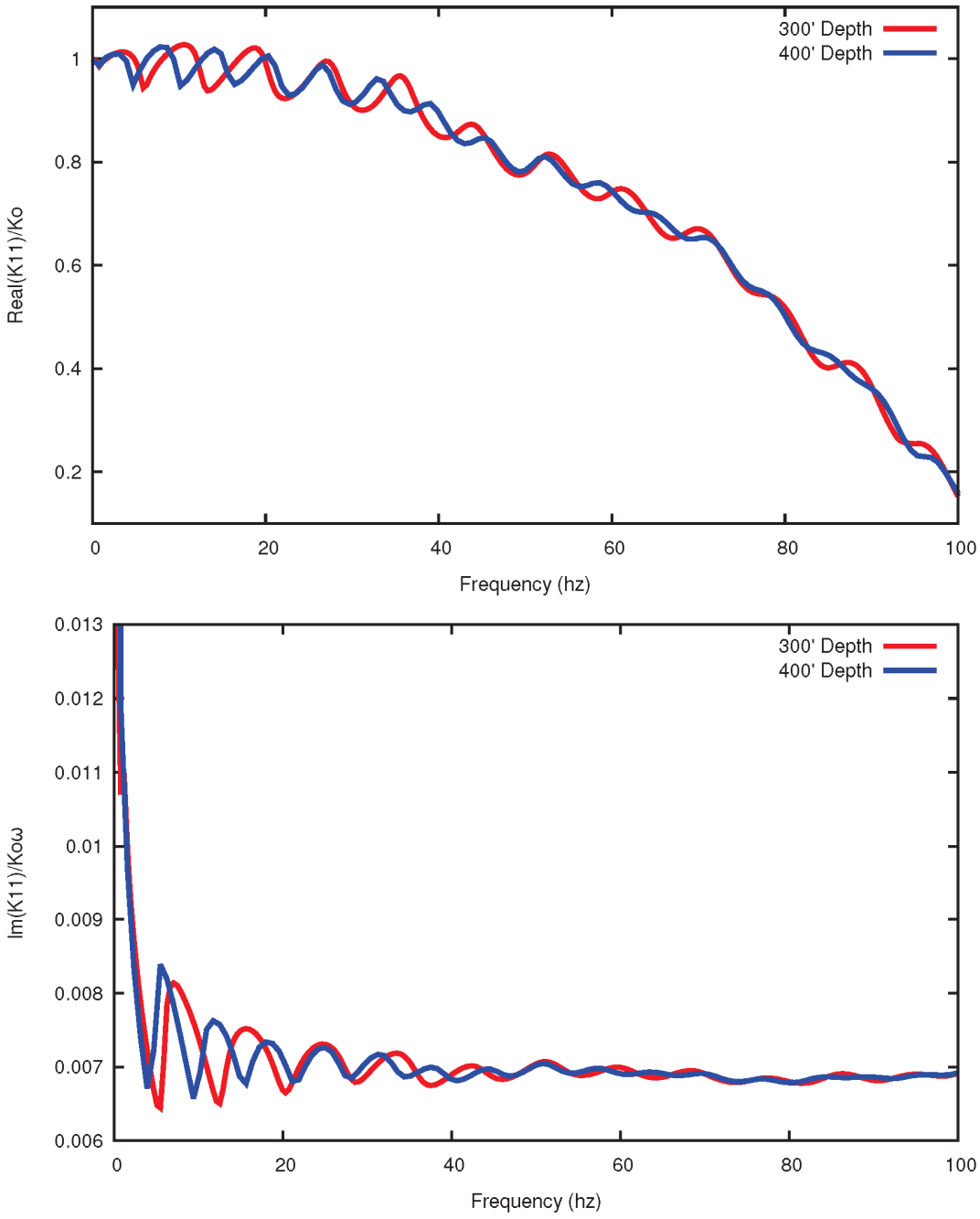

Figure D-1 Comparison of *Kxx* lumped parameter soil impedance

© Copyright 2019 by NuScale Power, LLC

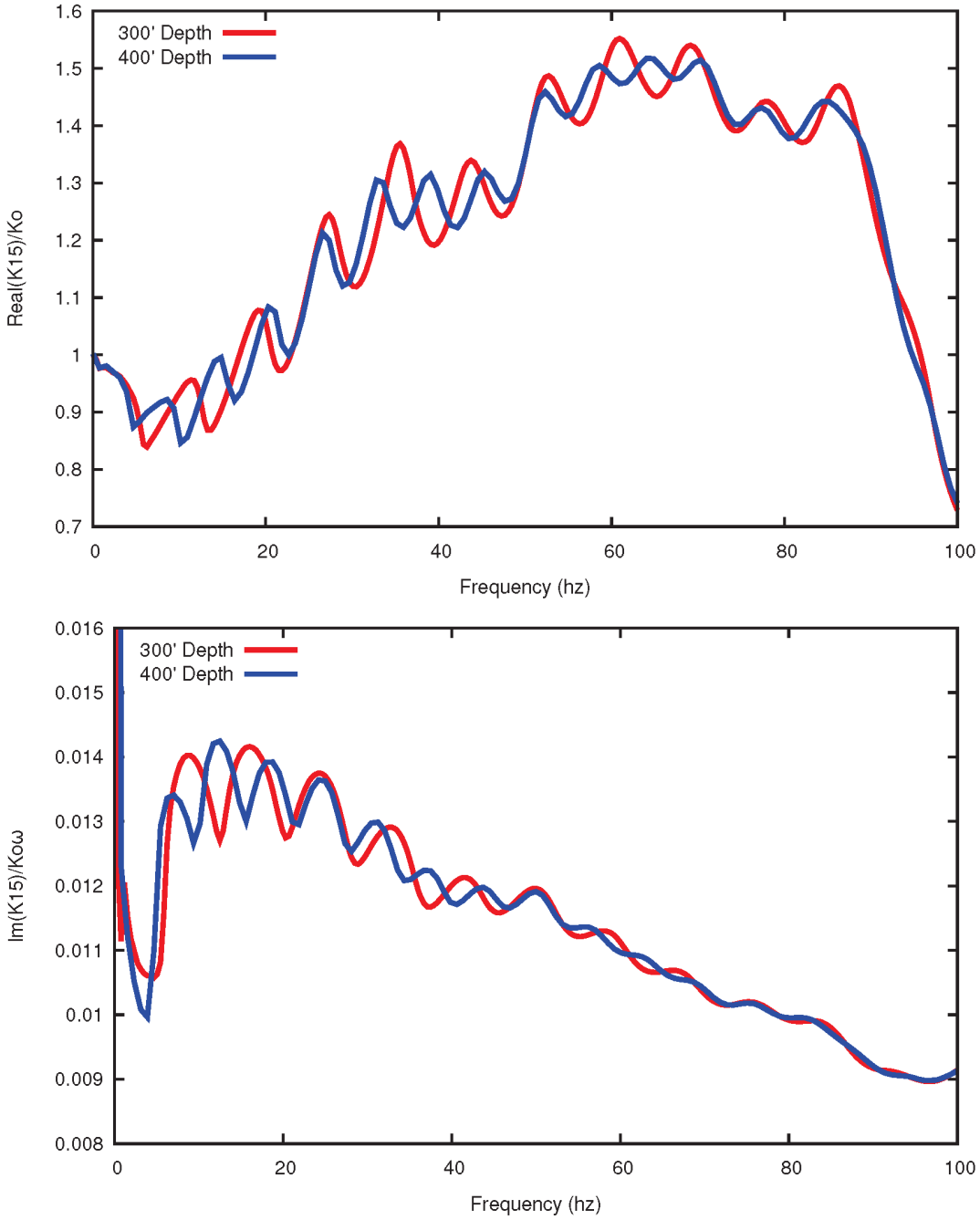

Figure D-2 Comparison of $K_{X\theta Y}$ lumped parameter soil impedance

© Copyright 2019 by NuScale Power, LLC

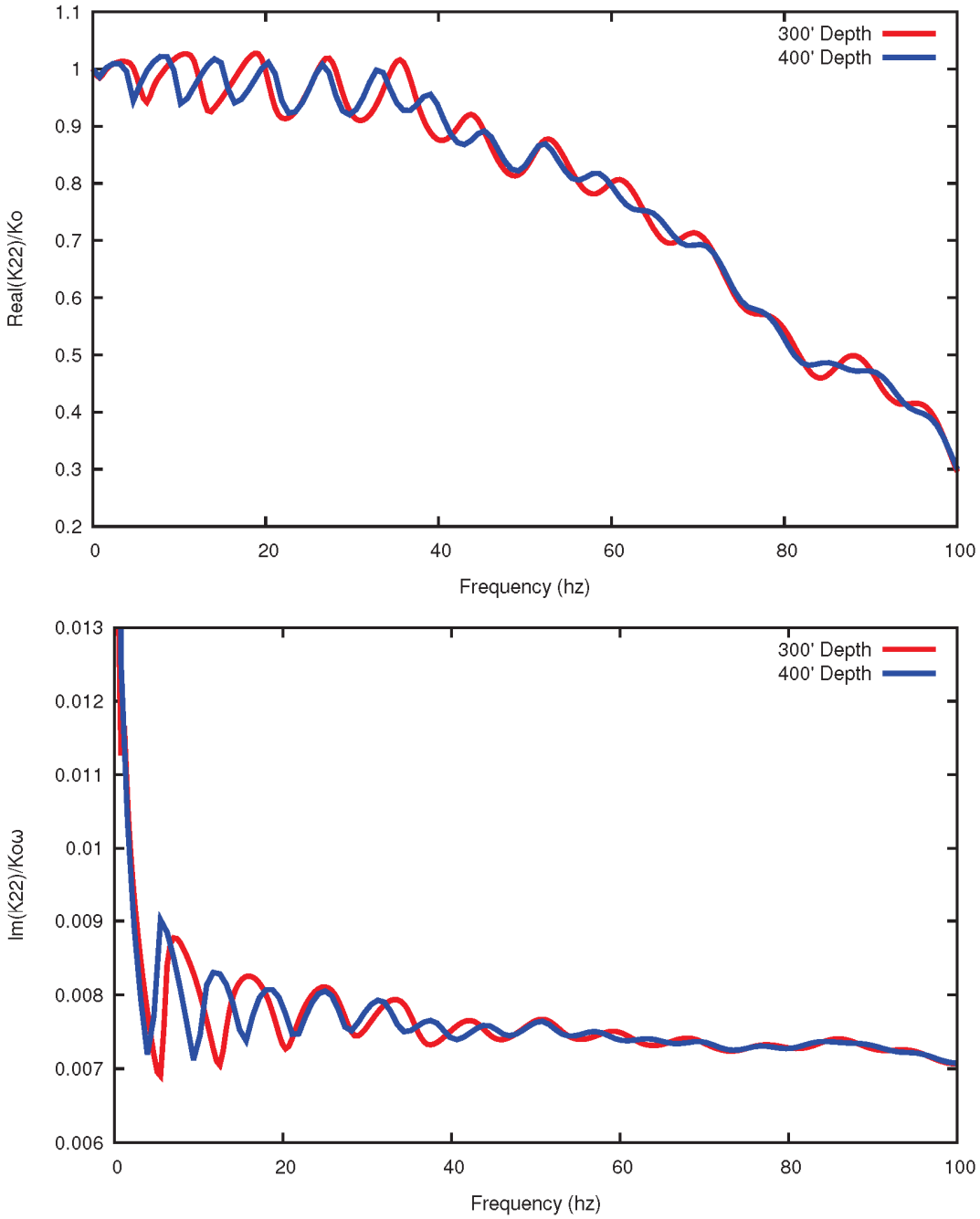

Figure D-3 Comparison of K_{YY} lumped parameter soil impedance

© Copyright 2019 by NuScale Power, LLC

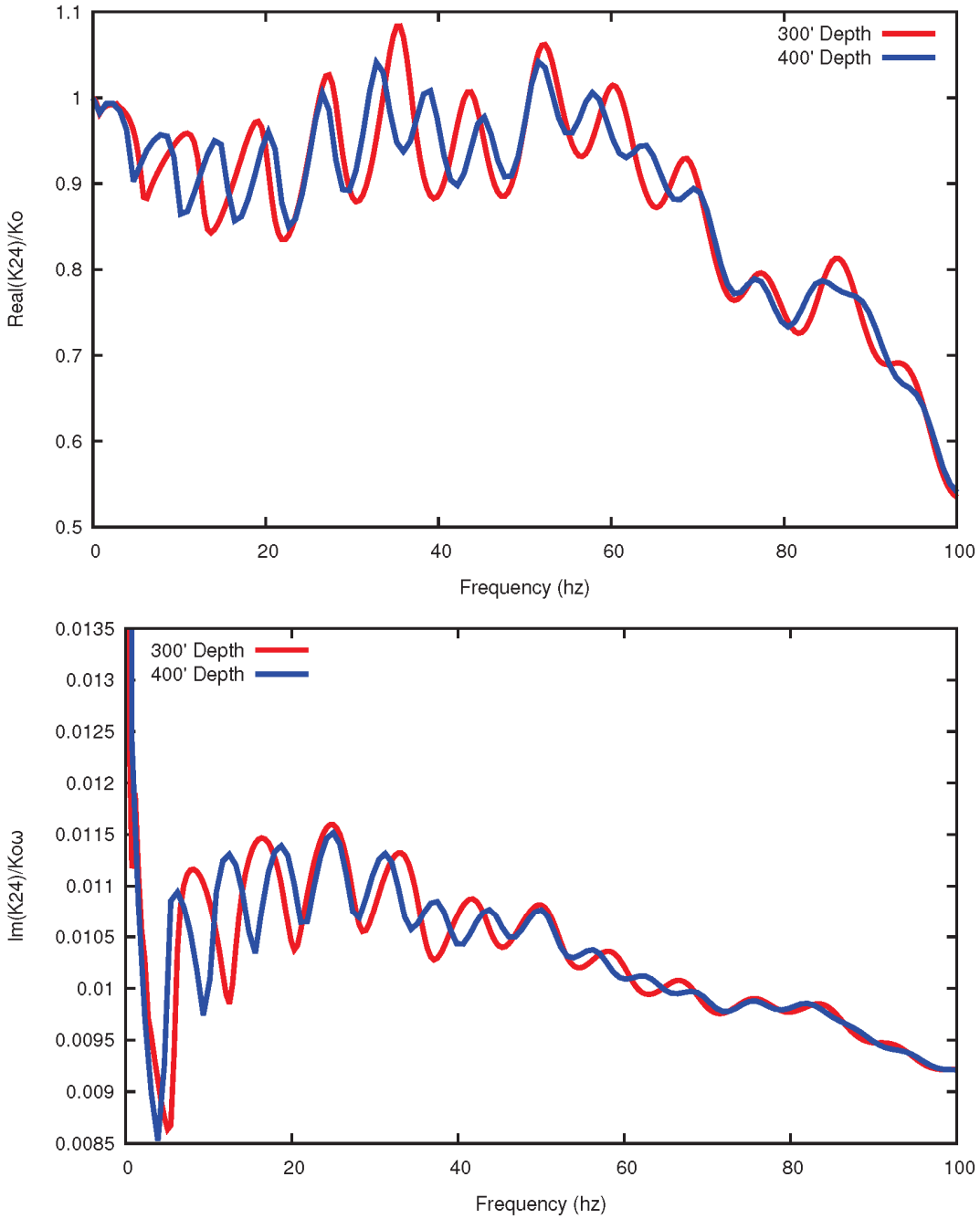

Figure D-4 Comparison of $K_{Y\theta X}$ lumped parameter soil impedance

© Copyright 2019 by NuScale Power, LLC

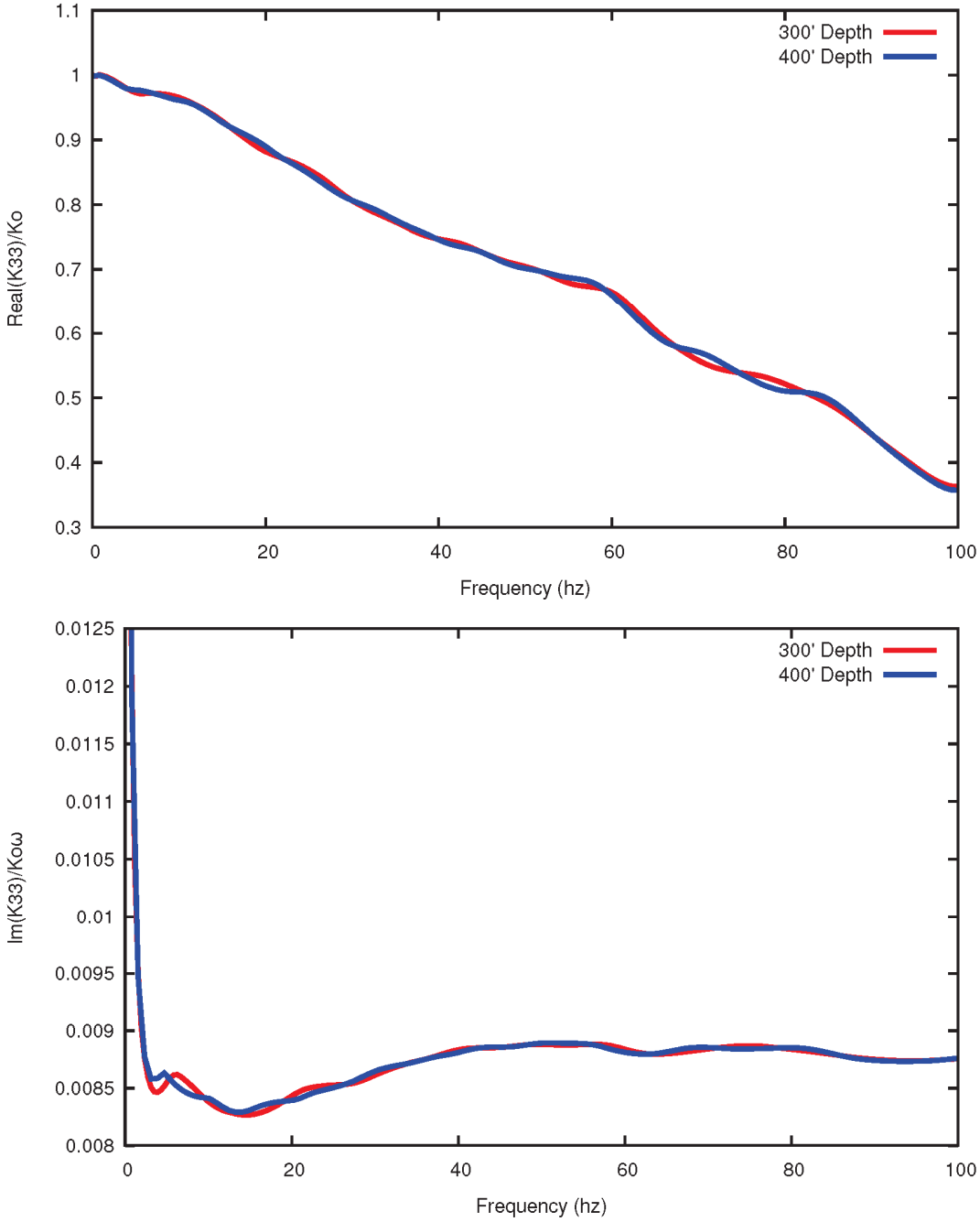

Figure D-5 Comparison of K_{ZZ} lumped parameter soil impedance

© Copyright 2019 by NuScale Power, LLC

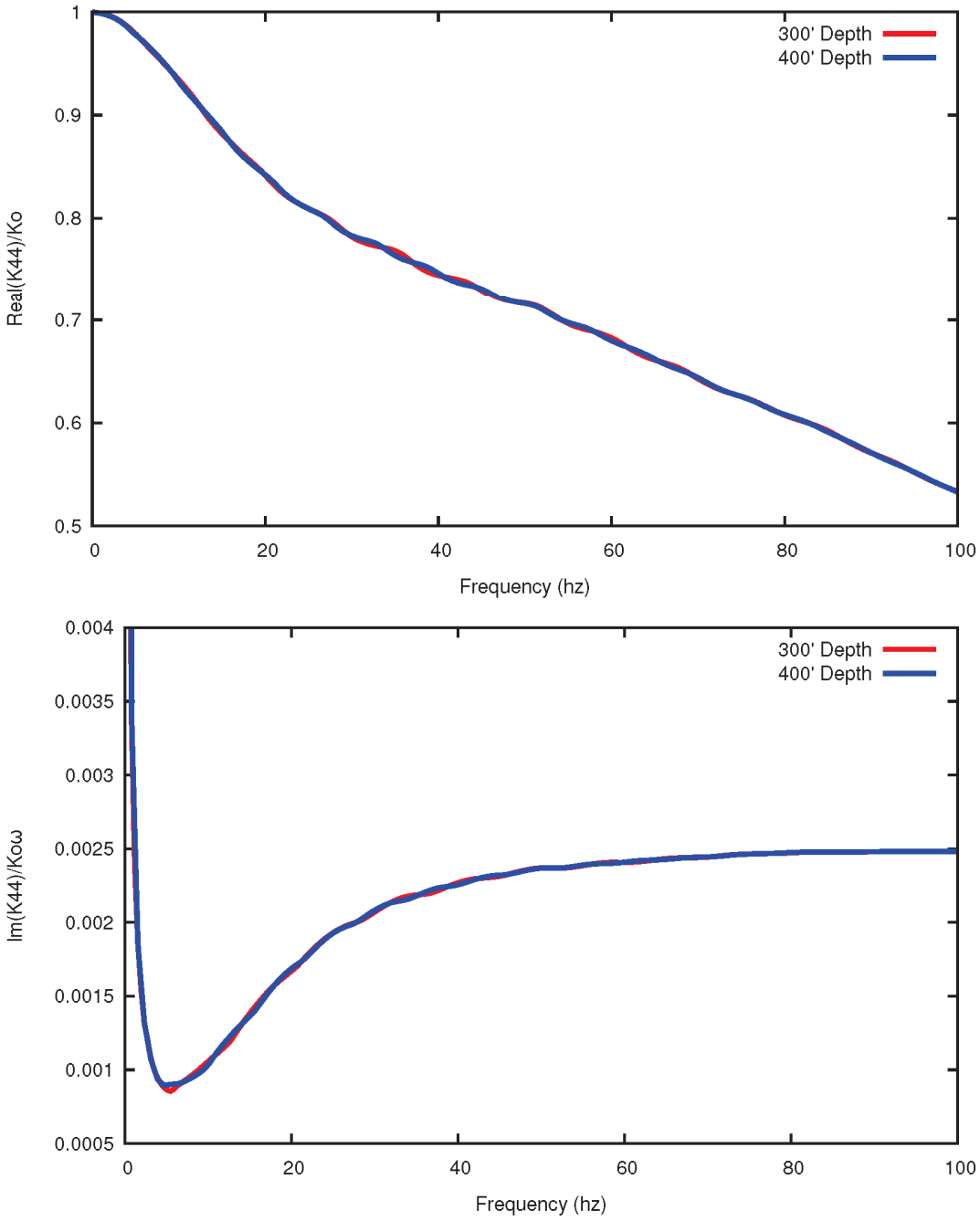

Figure D-6 Comparison of $K_{\theta X \theta X}$ lumped parameter soil impedance

© Copyright 2019 by NuScale Power, LLC

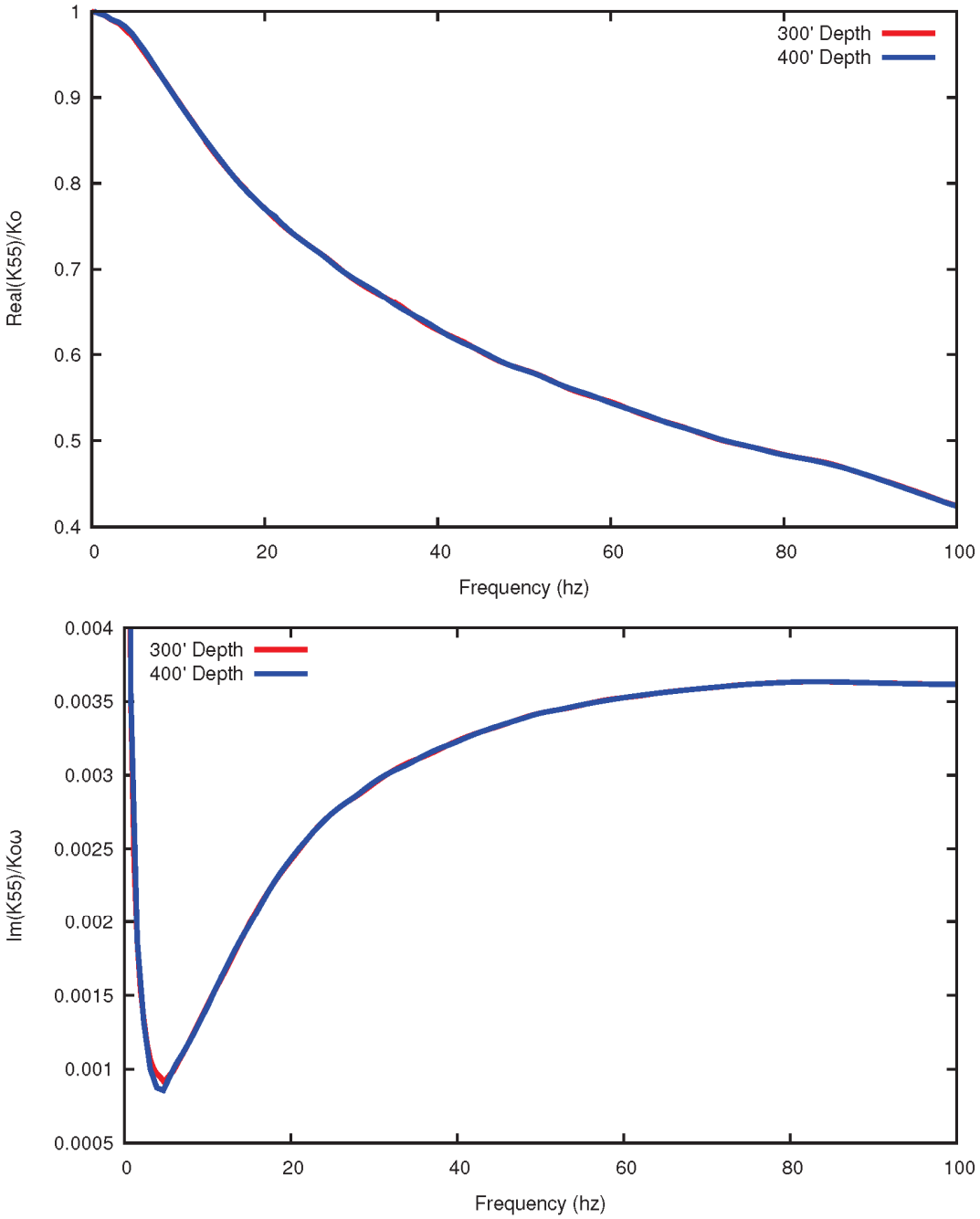

Figure D-7 Comparison of $K_{\theta y \theta y}$ lumped parameter soil impedance

© Copyright 2019 by NuScale Power, LLC

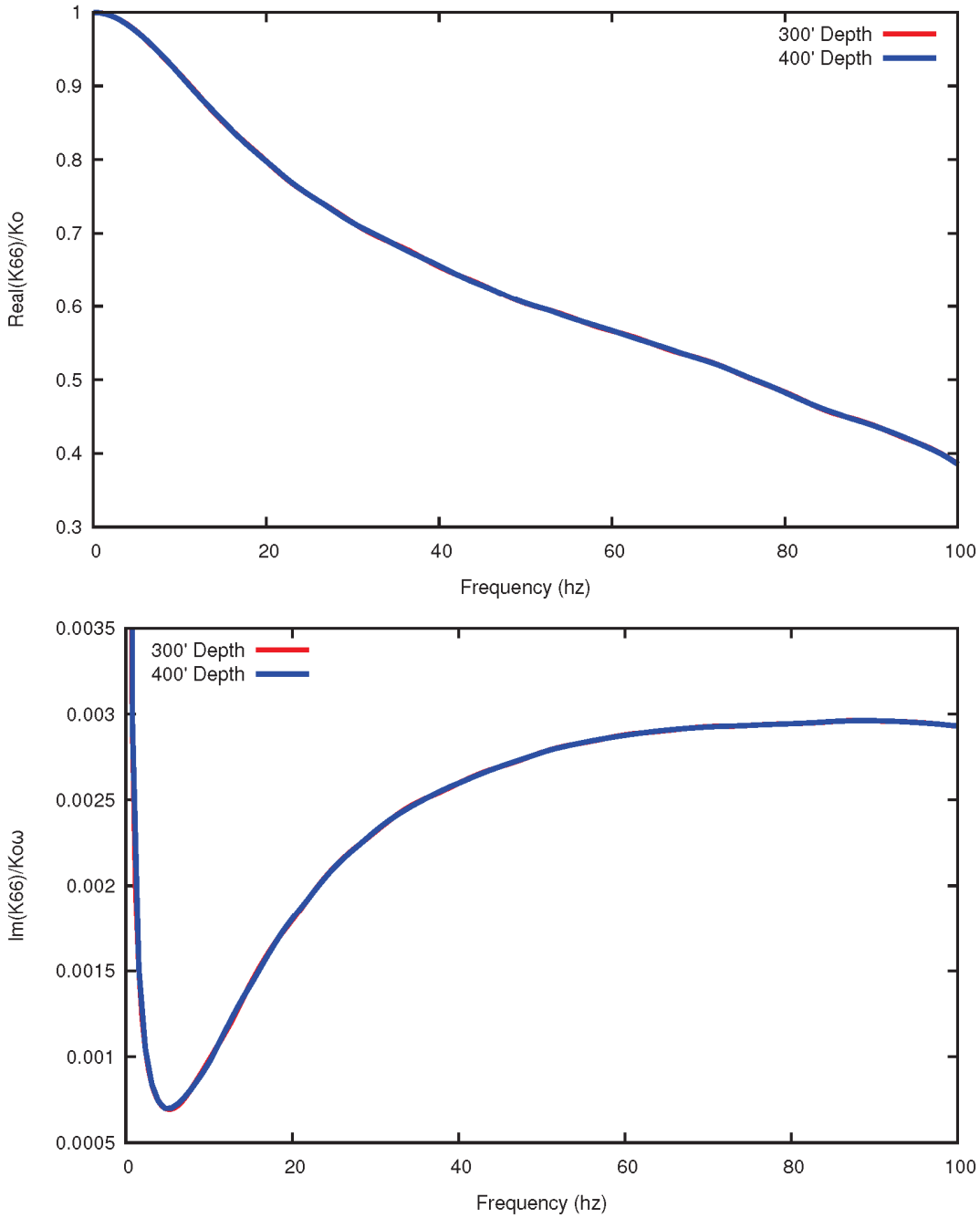

Figure D-8 Comparison of $K_{\theta Z \theta Z}$ lumped parameter soil impedance

© Copyright 2019 by NuScale Power, LLC

Appendix E. Example 2, SASSI vs ANSYS Results

The seismic response of Example 2 is discussed in Section 6.2.5 and the detailed results are summarized in this appendix.

The seismic response consisting of transfer functions due to X, Y and Z seismic input are presented below. The excavation and structure are symmetric with respect to the X = 0 and Y = 0 planes. Thus, the cross-coupling seismic response between lateral directions are approximately zero. There is cross-coupling between the lateral and vertical directions as the foundation rocks.

Example 2 Structural Response

Location	Input	Response	Control Motion Layer 1	Control Motion Layer 4
Center Roof	X	X	Figure E-1	Figure E-16
Roof SW Corner	X	X	Figure E-2	Figure E-17
Roof SW Corner	X	Z	Figure E-3	Figure E-18
Center Basemat	X	X	Figure E-4	Figure E-19
West Wall	X	X	Figure E-5	Figure E-20
West Wall	X	Z	Figure E-6	Figure E-21
Center Roof	Y	Y	Figure E-7	Figure E-22
Roof SW Corner	Y	Y	Figure E-8	Figure E-23
Roof SW Corner	Y	Z	Figure E-9	Figure E-24
Center Basemat	Y	Y	Figure E-10	Figure E-25
South Wall	Y	Y	Figure E-11	Figure E-26
South Wall	Y	Z	Figure E-12	Figure E-27
Center Roof	Z	Z	Figure E-13	Figure E-28
Roof SW Corner	Z	Z	Figure E-14	Figure E-29
Center Basemat	Z	Z	Figure E-15	Figure E-30

© Copyright 2019 by NuScale Power, LLC

{{

}}2(a),(c)

Figure E-1 Center roof, *X* response to layer 1 *X* seismic input, example 2

{{

}}2(a),(c)

Figure E-2 SW corner roof, *X* response to layer 1 *X* seismic input, example 2

© Copyright 2019 by NuScale Power, LLC

{{

}}2(a),(c)

Figure E-3 SW corner roof, *Z* response to layer 1 *X* seismic input, example 2

{{

}}2(a),(c)

Figure E-4 Center basemat, *X* response to layer 1 *X* seismic input, example 2

© Copyright 2019 by NuScale Power, LLC

{{

}}2(a),(c)

Figure E-5 West wall, *X* response to layer 1 *X* seismic input, example 2

{{

}}2(a),(c)

Figure E-6 West wall, *Z* response to layer 1 *X* seismic input, example 2

© Copyright 2019 by NuScale Power, LLC

{{

}}2(a),(c)

Figure E-7 Center roof, *Y* response to layer 1 *Y* seismic input, example 2

{{

}}2(a),(c)

Figure E-8 SW corner roof, *Y* response to layer 1 *Y* seismic input, example 2

© Copyright 2019 by NuScale Power, LLC

{{

}}2(a),(c)

Figure E-9 SW corner roof, *Z* response to layer 1 *Y* seismic input, example 2

{{

}}2(a),(c)

Figure E-10 Center basemat, *Y* response to layer 1 *Y* seismic input, example 2

© Copyright 2019 by NuScale Power, LLC

{{

}}2(a),(c)

Figure E-11 South wall, *Y* response to layer 1 *Y* seismic input, example 2

{{

}}2(a),(c)

Figure E-12 South wall, *Z* response to layer 1 *Y* seismic input, example 2

© Copyright 2019 by NuScale Power, LLC

{{

}}2(a),(c)

Figure E-13 Center roof, *Z* response to layer 1 *Z* seismic input, example 2

{{

}}2(a),(c)

Figure E-14 SW corner roof, *Z* response to layer 1 *Z* seismic input, example 2

© Copyright 2019 by NuScale Power, LLC

{{

}}2(a),(c)

Figure E-15 Center basemat, *Z* response to layer 1 *Z* seismic input, example 2

{{

}}2(a),(c)

Figure E-16 Center roof, *X* response to layer 4 *X* seismic input, example 2

© Copyright 2019 by NuScale Power, LLC

{{

}}2(a),(c)

Figure E-17 SW corner roof, *X* response to layer 4 *X* seismic input, example 2

{{

}}2(a),(c)

Figure E-18 SW corner roof, *Z* response to layer 4 *X* seismic input, example 2

© Copyright 2019 by NuScale Power, LLC

{{

}}2(a),(c)

Figure E-19 Center basemat, *X* response to layer 4 *X* seismic input, example 2

{{

}}2(a),(c)

Figure E-20 West wall, *X* response to layer 4 *X* seismic input, example 2

© Copyright 2019 by NuScale Power, LLC

{{

}}2(a),(c)

Figure E-21 West wall, *Z* response to layer 4 *X* seismic input, example 2

{{

}}2(a),(c)

Figure E-22 Center roof, *Y* response to layer 4 *Y* seismic input, example 2

© Copyright 2019 by NuScale Power, LLC

{{

}}2(a),(c)

Figure E-23 SW corner roof, *Y* response to layer 4 *Y* seismic input, example 2

{{

}}2(a),(c)

Figure E-24 SW corner roof, *Z* response to layer 4 *Y* seismic input, example 2

© Copyright 2019 by NuScale Power, LLC

{{

}}2(a),(c)

Figure E-25 Center basemat, *Y* response to layer 4 *Y* seismic input, example 2

{{

}}2(a),(c)

Figure E-26 South wall, *Y* response to layer 4 *Y* seismic input, example 2

© Copyright 2019 by NuScale Power, LLC

{{

}}2(a),(c)

Figure E-27 South wall, *Z* response to layer 4 *Y* seismic input, example 2

{{

}}2(a),(c)

Figure E-28 Center roof, *Z* response to layer 4 *Z* seismic input, example 2

© Copyright 2019 by NuScale Power, LLC

{{

}}2(a),(c)

Figure E-29 SW corner roof, *Z* response to layer 4 *Z* seismic input, example 2

{{

}}2(a),(c)

Figure E-30 Center basemat, *Z* response to layer 4 *Z* seismic input, example 2

© Copyright 2019 by NuScale Power, LLC

Appendix F. Example 3, SASSI vs ANSYS Results

The seismic response of Example 3 is discussed in Section 6.3.3 and the detailed results are summarized in this appendix.

The seismic response consisting of transfer functions due to *X*, *Y* and *Z* seismic input are presented below. The excavation and structure are symmetric with respect to the *X* = 0 and *Y* = 0 planes. Thus, the cross-coupling seismic response between lateral directions is approximately zero. There is cross-coupling between the lateral and vertical directions as the foundation rocks.

Acoustic pressure results are reported on the *Y* = 0 plane for the West Wall and a line of nodes on the western end of the building. Results are also reported on the *X* = 0 plane for the South Wall and a line of nodes on the southern end of the building.

Example 3 Structural Response

Location	Input	Response	Control Motion Layer 1	Control Motion Layer 4
Center Roof	X	X	Figure F-1	Figure F-16
Roof SW Corner	X	X	Figure F-2	Figure F-17
Roof SW Corner	X	Z	Figure F-3	Figure F-18
Center Basemat	X	X	Figure F-4	Figure F-19
West Wall	X	X	Figure F-5	Figure F-20
West Wall	X	Z	Figure F-6	Figure F-21
Center Roof	Y	Y	Figure F-7	Figure F-22
Roof SW Corner	Y	Y	Figure F-8	Figure F-23
Roof SW Corner	Y	Z	Figure F-9	Figure F-24
Center Basemat	Y	Y	Figure F-10	Figure F-25
South Wall	Y	Y	Figure F-11	Figure F-26
South Wall	Y	Z	Figure F-12	Figure F-27
Center Roof	Z	Z	Figure F-13	Figure F-28
Roof SW Corner	Z	Z	Figure F-14	Figure F-29
Center Basemat	Z	Z	Figure F-15	Figure F-30

© Copyright 2019 by NuScale Power, LLC

Example 3 In-Structure Response Spectra

Location	
Center Roof	Figure F-31
Roof SW Corner	Figure F-32
West Wall	Figure F-33
South Wall	Figure F-34
Center Basemat	Figure F-35

Example 3 Fluid Pressure Response

Location	Input	Depth (ft)	Layer 1	Layer 4
West Wall	X	6.25	Figure F-36	Figure F-49
West Wall	X	12.50	Figure F-37	Figure F-50
West Wall	X	18.75	Figure F-38	Figure F-51
South Wall	Y	6.25	Figure F-39	Figure F-52
South Wall	Y	12.50	Figure F-40	Figure F-53
South Wall	Y	18.75	Figure F-41	Figure F-54
West Wall	Z	6.25	Figure F-42	Figure F-55
West Wall	Z	12.50	Figure F-43	Figure F-56
West Wall	Z	18.75	Figure F-44	Figure F-57
South Wall	Z	6.25	Figure F-45	Figure F-58
South Wall	Z	12.50	Figure F-46	Figure F-59
South Wall	Z	18.75	Figure F-47	Figure F-60
Center Basemat	Z	18.75	Figure F-48	Figure F-61

Example 3 Fluid Pressure Time Histories

Location	Input	Time History
West Wall	X	Figure F-62
South Wall	Y	Figure F-63
West Wall	Z	Figure F-64
South Wall	Z	Figure F-65
Center Basemat	Z	Figure F-66

© Copyright 2019 by NuScale Power, LLC

{{

}}2(a),(c)

Figure F-1 Center roof, *X* response to layer 1 *X* seismic input, example 3

{{

}}2(a),(c)

Figure F-2 SW corner roof, *X* response to layer 1 *X* seismic input, example 3

© Copyright 2019 by NuScale Power, LLC

{{

}}2(a),(c)

Figure F-3 SW corner roof, *Z* response to layer 1 *X* seismic input, example 3

{{

}}2(a),(c)

Figure F-4 Center basemat, *X* response to layer 1 *X* seismic input, example 3

© Copyright 2019 by NuScale Power, LLC

{{

}}2(a),(c)

Figure F-5 West wall, *X* response to layer 1 *X* seismic input, example 3

{{

}}2(a),(c)

Figure F-6 West wall, *Z* response to layer 1 *X* seismic input, example 3

© Copyright 2019 by NuScale Power, LLC

{{

}}2(a),(c)

Figure F-7 Center roof, *Y* response to layer 1 *Y* seismic input, example 3

{{

}}2(a),(c)

Figure F-8 SW corner roof, *Y* response to layer 1 *Y* seismic input, example 3

© Copyright 2019 by NuScale Power, LLC

{{

}}2(a),(c)

Figure F-9 SW corner roof, *Z* response to layer 1 *Y* seismic input, example 3

{{

}}2(a),(c)

Figure F-10 Center basemat, *Y* response to layer 1 *Y* seismic input, example 3

© Copyright 2019 by NuScale Power, LLC

{{

}}2(a),(c)

Figure F-11 South wall, *Y* response to layer 1 *Y* seismic input, example 3

{{

}}2(a),(c)

Figure F-12 South wall, *Z* response to layer 1 *Y* seismic input, example 3

© Copyright 2019 by NuScale Power, LLC

{{

}}2(a),(c)

Figure F-13 Center roof, *Z* response to layer 1 *Z* seismic input, example 3

{{

}}2(a),(c)

Figure F-14 SW corner roof, *Z* response to layer 1 *Z* seismic input, example 3

© Copyright 2019 by NuScale Power, LLC

{{

}}2(a),(c)

Figure F-15 Center basemat, *Z* response to layer 1 *Z* seismic input, example 3

{{

}}2(a),(c)

Figure F-16 Center roof, *X* response to layer 4 *X* seismic input, example 3

© Copyright 2019 by NuScale Power, LLC

{{

}}2(a),(c)

Figure F-17 SW corner roof, *X* response to layer 4 *X* seismic input, example 3

{{

}}2(a),(c)

Figure F-18 SW corner roof, *Z* response to layer 4 *X* seismic input, example 3

© Copyright 2019 by NuScale Power, LLC

{{

}}2(a),(c)

Figure F-19 Center basemat, *X* response to layer 4 *X* seismic input, example 3

{{

}}2(a),(c)

Figure F-20 West wall, *X* response to layer 4 *X* seismic input, example 3

© Copyright 2019 by NuScale Power, LLC

{{

}}2(a),(c)

Figure F-21 West wall, *Z* response to layer 4 *X* seismic input, example 3

{{

}}2(a),(c)

Figure F-22 Center roof, *Y* response to layer 4 *Y* seismic input, example 3

© Copyright 2019 by NuScale Power, LLC

{{

}}2(a),(c)

Figure F-23 SW corner roof, *Y* response to layer 4 *Y* seismic input, example 3

{{

}}2(a),(c)

Figure F-24 SW corner roof, *Z* response to layer 4 *Y* seismic input, example 3

© Copyright 2019 by NuScale Power, LLC

{{

}}2(a),(c)

Figure F-25 Center basemat, *Y* response to layer 4 *Y* seismic input, example 3

{{

}}2(a),(c)

Figure F-26 South wall, *Y* response to layer 4 *Y* seismic input, example 3

© Copyright 2019 by NuScale Power, LLC

{{

}}2(a),(c)

Figure F-27 South wall, *Z* response to layer 4 *Y* seismic input, example 3

{{

}}2(a),(c)

Figure F-28 Center roof, *Z* response to layer 4 *Z* seismic input, example 3

© Copyright 2019 by NuScale Power, LLC

{{

}}2(a),(c)

Figure F-29 SW corner roof, *Z* response to layer 4 *Z* seismic input, example 3

{{

}}2(a),(c)

Figure F-30 Center basemat, *Z* response to layer 4 *Z* seismic input, example 3

© Copyright 2019 by NuScale Power, LLC

{{

}}2(a),(c)

Figure F-31 Comparison of SASSI and ANSYS 5% damped ISRS, center roof structural response

© Copyright 2019 by NuScale Power, LLC

{{

}}2(a),(c)

Figure F-32 Comparison of SASSI and ANSYS 5% damped ISRS, roof SW corner

© Copyright 2019 by NuScale Power, LLC

{{

}}2(a),(c)

Figure F-33 Comparison of SASSI and ANSYS 5% damped ISRS, center of west wall at grade elevation

© Copyright 2019 by NuScale Power, LLC

{{

}}2(a),(c)

Figure F-34 Comparison of SASSI and ANSYS 5% damped ISRS, center of south wall at grade elevation

© Copyright 2019 by NuScale Power, LLC

{{

}}2(a),(c)

Figure F-35 Comparison of SASSI and ANSYS 5% damped ISRS, center of basemat

© Copyright 2019 by NuScale Power, LLC

{{

}}2(a),(c)

Figure F-36 West wall, 6.25 ft deep, pressure response to layer 1 *X* seismic input, example 3

{{

}}2(a),(c)

Figure F-37 West wall, 12.5 ft deep, pressure response to layer 1 *X* seismic input, example 3

© Copyright 2019 by NuScale Power, LLC

{{

}}2(a),(c)

Figure F-38 West wall, 18.75 ft deep, pressure response to layer 1 *X* seismic input, example 3

{{

}}2(a),(c)

Figure F-39 South wall, 6.25 ft deep, pressure response to layer 1 *Y* seismic input, example 3

© Copyright 2019 by NuScale Power, LLC

{{

}}2(a),(c)

Figure F-40 South wall, 12.5 ft deep, pressure response to layer 1 *Y* seismic input, example 3

{{

}}2(a),(c)

Figure F-41 South wall, 18.75 ft deep, pressure response to layer 1 *Y* seismic input, example 3

© Copyright 2019 by NuScale Power, LLC

{{

}}2(a),(c)

Figure F-42 West wall, 6.25 ft deep, pressure response to layer 1 Z seismic input, example 3

{{

}}2(a),(c)

Figure F-43 West wall, 12.5 ft deep, pressure response to layer 1 *Z* seismic input, example 3

© Copyright 2019 by NuScale Power, LLC

{{

}}2(a),(c)

Figure F-44 West wall, 18.75 ft deep, pressure response to layer 1 *Z* seismic input, example 3

{{

}}2(a),(c)

Figure F-45 South wall, 6.25 ft deep, pressure response to layer 1 *Z* seismic input, example 3

© Copyright 2019 by NuScale Power, LLC

{{

}}2(a),(c)

Figure F-46 South wall, 12.5 ft deep, pressure response to layer 1 *Z* seismic input, example 3

{{

}}2(a),(c)

Figure F-47 South wall, 18.75 ft Deep, pressure response to layer 1 *Z* seismic input, example 3

© Copyright 2019 by NuScale Power, LLC

{{

}}2(a),(c)

Figure F-48 Center basemat, 18.75 ft deep, pressure response to layer 1 *Z* seismic input, example 3

{{

}}2(a),(c)

Figure F-49 West wall, 6.25 ft deep, pressure response to layer 4 *X* seismic input, example 3

© Copyright 2019 by NuScale Power, LLC

{{

}}2(a),(c)

Figure F-50 West wall, 12.5 ft deep, pressure response to layer 4 *X* seismic input, example 3

{{

}}2(a),(c)

Figure F-51 West wall, 18.75 ft deep, pressure response to layer 4 *X* seismic input, example 3

© Copyright 2019 by NuScale Power, LLC

{{

}}2(a),(c)

Figure F-52 South wall, 6.25 ft deep, pressure response to layer 4 *Y* seismic input, example 3

{{

}}2(a),(c)

Figure F-53 South wall, 12.5 ft deep, pressure response to layer 4 *Y* seismic input, example 3

© Copyright 2019 by NuScale Power, LLC

{{

}}2(a),(c)

Figure F-54 South wall, 18.75 ft deep, pressure response to layer 4 *Y* seismic input, example 3

{{

}}2(a),(c)

Figure F-55 West wall, 6.25 ft deep, pressure response to layer 4 *Z* seismic input, example 3

© Copyright 2019 by NuScale Power, LLC

{{

}}2(a),(c)

Figure F-56 West wall, 12.5 ft deep, pressure response to layer 4 *Z* seismic input, example 3

{{

}}2(a),(c)

Figure F-57 West wall, 18.75 ft deep, pressure response to layer 4 *Z* seismic input, example 3

© Copyright 2019 by NuScale Power, LLC

{{

}}2(a),(c)

Figure F-58 South wall, 6.25 ft deep, pressure response to layer 4 *Z* seismic input, example 3

{{

}}2(a),(c)

Figure F-59 South wall, 12.5 ft deep, pressure response to layer 4 *Z* seismic input, example 3

© Copyright 2019 by NuScale Power, LLC

{{

}}2(a),(c)

Figure F-60 South wall, 18.75 ft deep, pressure response to layer 4 *Z* seismic input, example 3

{{

}}2(a),(c)

Figure F-61 Center basemat, 18.75 ft deep, pressure response to layer 4 *Z* seismic input, example 3

© Copyright 2019 by NuScale Power, LLC

{{

}}2(a),(c)

Figure F-62 Comparison of SASSI and ANSYS acoustic fluid pressure (ksf sec^2/ft) time histories, center of west wall

© Copyright 2019 by NuScale Power, LLC

{{

}}2(a),(c)

Figure F-63 Comparison of SASSI and ANSYS acoustic fluid pressure (ksf sec^2/ft) time histories, center of south wall

© Copyright 2019 by NuScale Power, LLC

{{

}}2(a),(c)

Figure F-64 Comparison of SASSI and ANSYS acoustic fluid pressure (ksf sec^2/ft) time histories, center of west wall

© Copyright 2019 by NuScale Power, LLC

{{

}}2(a),(c)

Figure F-65 Comparison of SASSI and ANSYS acoustic fluid pressure (ksf sec^2/ft) time histories, center of south wall

© Copyright 2019 by NuScale Power, LLC

{{

}}2(a),(c)

Figure F-66 Comparison of SASSI and ANSYS acoustic fluid pressure (ksf sec^2/ft) time histories, center of basemat

© Copyright 2019 by NuScale Power, LLC

Appendix G. Fixed Base Response for Examples 2 and 3

The fixed-base building response is considered in this section for the building model in Example 2 and the building-fluid model in Example 3. The basemat response of both buildings is restrained and the soil impedance is omitted. These analyses are used to isolate the building and building/fluid response.

The fixed base response for Examples 2 and 3 is discussed in Section 6.3.3. The building response is shown in the following figures.

Location	Input	Response	Figure
Center Roof	X	X	Figure G-1
Roof SW Corner	X	X	Figure G-2
Roof SW Corner	X	Z	Figure G-3
West Wall	X	X	Figure G-4
West Wall	X	Z	Figure G-5
Center Roof	Y	Y	Figure G-6
Roof SW Corner	Y	Y	Figure G-7
Roof SW Corner	Y	Z	Figure G-8
South Wall	Y	Y	Figure G-9
South Wall	Y	Z	Figure G-10
Center Roof	Z	Z	Figure G-11
Roof SW Corner	Z	Z	Figure G-12

© Copyright 2019 by NuScale Power, LLC

{{

}}2(a),(c)

Figure G-1 Center roof, *X* response to *X* seismic input, example 3

{{

}}2(a),(c)

Figure G-2 SW corner roof, *X* response to *X* seismic input, example 3

© Copyright 2019 by NuScale Power, LLC

{{

}}2(a),(c)

Figure G-3 SW corner roof, *Z* response to *X* seismic input, example 3

{{

}}2(a),(c)

Figure G-4 West wall, *X* response to *X* seismic input, example 3

© Copyright 2019 by NuScale Power, LLC

{{

}}2(a),(c)

Figure G-5 West wall, *Z* response to *X* seismic input, example 3

{{

}}2(a),(c)

Figure G-6 Center roof, *Y* response to *Y* seismic input, example 3

© Copyright 2019 by NuScale Power, LLC

{{

}}2(a),(c)

Figure G-7 SW corner roof, *Y* response to *Y* seismic input, example 3

{{

}}2(a),(c)

Figure G-8 SW corner roof, *Z* response to *Y* seismic input, example 3

© Copyright 2019 by NuScale Power, LLC

{{

}}2(a),(c)

Figure G-9 South wall, *Y* response to *Y* seismic input, example 3

{{

}}2(a),(c)

Figure G-10 South wall, *Z* response to *Y* seismic input, example 3

© Copyright 2019 by NuScale Power, LLC

{{

}}2(a),(c)

Figure G-11 Center roof, *Z* response to *Z* seismic input, example 3

{{

}}2(a),(c)

Figure G-12 SW corner roof, *Z* response to *Z* seismic input, example 3

© Copyright 2019 by NuScale Power, LLC

Appendix H. SSI Response for Examples 2 and 3

The seismic response is considered in this section for the building model in Example 2 and the building-fluid model in Example 3. Example 2 considers soil-structure interaction while Example 3 considers soil-structure-fluid interaction. The transfer functions for these two problems are compared to understand the effect of the fluid on structural response.

The SSI response for Examples 2 and 3 is discussed in Section 6.3.3. The building response is shown in the following figures.

Example 2 vs Example 3 Structural Response

Location	Input	Response	Control Motion Layer 1	Control Motion Layer 4
Center Roof	X	X	Figure H-1	Figure H-16
Roof SW Corner	X	X	Figure H-2	Figure H-17
Roof SW Corner	X	Z	Figure H-3	Figure H-18
Center Basemat	X	X	Figure H-4	Figure H-19
West Wall	X	X	Figure H-5	Figure H-20
West Wall	X	Z	Figure H-6	Figure H-21
Center Roof	Y	Y	Figure H-7	Figure H-22
Roof SW Corner	Y	Y	Figure H-8	Figure H-23
Roof SW Corner	Y	Z	Figure H-9	Figure H-24
Center Basemat	Y	Y	Figure H-10	Figure H-25
South Wall	Y	Y	Figure H-11	Figure H-26
South Wall	Y	Z	Figure H-12	Figure H-27
Center Roof	Z	Z	Figure H-13	Figure H-28
Roof SW Corner	Z	Z	Figure H-14	Figure H-29
Center Basemat	Z	Z	Figure H-15	Figure H-30

© Copyright 2019 by NuScale Power, LLC

{{

}}2(a),(c)

Figure H-1 Center roof, *X* response to layer 1 *X* seismic input, example 3

{{

}}2(a),(c)

Figure H-2 SW corner roof, *X* response to layer 1 *X* seismic input, example 3

© Copyright 2019 by NuScale Power, LLC

{{

}}2(a),(c)

Figure H-3 SW corner roof, *Z* response to layer 1 *X* seismic input, example 3

{{

}}2(a),(c)

Figure H-4 Center basemat, *X* response to layer 1 *X* seismic input, example 3

© Copyright 2019 by NuScale Power, LLC

{{

}}2(a),(c)

Figure H-5 West wall, *X* response to layer 1 *X* seismic input, example 3

{{

}}2(a),(c)

Figure H-6 West wall, *Z* response to layer 1 *X* seismic input, example 3

© Copyright 2019 by NuScale Power, LLC

{{

}}2(a),(c)

Figure H-7 Center roof, *Y* response to layer 1 *Y* seismic input, example 3

{{

}}2(a),(c)

Figure H-8 SW corner roof, *Y* response to layer 1 *Y* seismic input, example 3

© Copyright 2019 by NuScale Power, LLC

{{

}}2(a),(c)

Figure H-9 SW corner roof, *Z* response to layer 1 *Y* seismic input, example 3

{{

}}2(a),(c)

Figure H-10 Center basemat, *Y* response to layer 1 *Y* seismic input, example 3

© Copyright 2019 by NuScale Power, LLC

{{

}}2(a),(c)

Figure H-11 South wall, *Y* response to layer 1 *Y* seismic input, example 3

{{

}}2(a),(c)

Figure H-12 South wall, *Z* response to layer 1 *Y* seismic input, example 3

© Copyright 2019 by NuScale Power, LLC

{{

}}2(a),(c)

Figure H-13 Center roof, *Z* response to layer 1 *Z* seismic input, example 3

{{

}}2(a),(c)

Figure H-14 SW corner roof, *Z* response to layer 1 *Z* seismic input, example 3

© Copyright 2019 by NuScale Power, LLC

{{

}}2(a),(c)

Figure H-15 Center basemat, *Z* response to layer 1 *Z* seismic input, example 3

{{

}}2(a),(c)

Figure H-16 Center roof, *X* response to layer 4 *X* seismic input, example 3

© Copyright 2019 by NuScale Power, LLC

{{

}}2(a),(c)

Figure H-17 SW corner roof, *X* response to layer 4 *X* seismic input, example 3

{{

}}2(a),(c)

Figure H-18 SW corner roof, *Z* response to layer 4 *X* seismic input, example 3

© Copyright 2019 by NuScale Power, LLC

{{

}}2(a),(c)

Figure H-19 Center basemat, *X* response to layer 4 *X* seismic input, example 3

{{

}}2(a),(c)

Figure H-20 West wall, *X* response to layer 4 *X* seismic input, example 3

© Copyright 2019 by NuScale Power, LLC

{{

}}2(a),(c)

Figure H-21 West wall, *Z* response to layer 4 *X* seismic input, example 3

{{

}}2(a),(c)

Figure H-22 Center roof, *Y* response to layer 4 *Y* seismic input, example 3

© Copyright 2019 by NuScale Power, LLC

{{

}}2(a),(c)

Figure H-23 SW corner roof, *Y* response to layer 4 *Y* seismic input, example 3

{{

}}2(a),(c)

Figure H-24 SW corner roof, *Z* response to layer 4 *Y* seismic input, example 3

© Copyright 2019 by NuScale Power, LLC

{{

}}2(a),(c)

Figure H-25 Center basemat, *Y* response to layer 4 *Y* seismic input, example 3

{{

}}2(a),(c)

Figure H-26 South wall, *Y* response to layer 4 *Y* seismic input, example 3

© Copyright 2019 by NuScale Power, LLC

{{

}}2(a),(c)

Figure H-27 South wall, *Z* response to layer 4 *Y* seismic input, example 3

{{

}}2(a),(c)

Figure H-28 Center roof, *Z* response to layer 4 *Z* seismic input, example 3

© Copyright 2019 by NuScale Power, LLC

{{

}}2(a),(c)

Figure H-29 SW corner roof, *Z* response to layer 4 *Z* seismic input, example 3

{{

}}2(a),(c)

Figure H-30 Center basemat, *Z* response to layer 4 *Z* seismic input, example 3

© Copyright 2019 by NuScale Power, LLC

Appendix I. Example 4, Acceleration Transfer Functions

The following plots have a title on the plot legend that consists of the node number followed by two letters. The first letter corresponds to the direction of ground motion or input. The second letter corresponds to the response direction or output.

Results on a given page correspond to a common input direction, i.e. X, Y or Z. The top plot corresponds to output in the X direction, the center plot corresponds to output in the Y direction, and the bottom plot corresponds to output in the Z direction.

X is East, Y is North and Z is up.

© Copyright 2019 by NuScale Power, LLC

{{

}}2(a),(c)

Figure I-1 Transfer Function, X Input, Node 120933, Northwest Corner on Top of Basemat

© Copyright 2019 by NuScale Power, LLC

{{

}}2(a),(c)

Figure I-2 Transfer Function, Y Input, Node 120933, Northwest Corner on Top of Basemat

© Copyright 2019 by NuScale Power, LLC

{{

}}2(a),(c)

Figure I-3 Transfer Function, Z Input, Node 120933, Northwest Corner on Top of Basemat

© Copyright 2019 by NuScale Power, LLC

{{

}}2(a),(c)

Figure I-4 Transfer Function, X Input, Node 120978, Mid-Span of North Exterior Wall on Top of Basemat

© Copyright 2019 by NuScale Power, LLC

{{

}}2(a),(c)

Figure I-5 Transfer Function, Y Input, Node 120978, Mid-Span of North Exterior Wall on Top of Basemat

© Copyright 2019 by NuScale Power, LLC

{{

}}2(a),(c)

Figure I-6 Transfer Function, Z Input, Node 120978, Mid-Span of North Exterior Wall on Top of Basemat

© Copyright 2019 by NuScale Power, LLC

{{

}}2(a),(c)

Figure I-7 Transfer Function, X Input, Node 121053, Northeast Corner on Top of Basemat

© Copyright 2019 by NuScale Power, LLC

{{

}}2(a),(c)

Figure I-8 Transfer Function, Y Input, Node 121053, Northeast Corner on Top of Basemat

© Copyright 2019 by NuScale Power, LLC

{{

}}2(a),(c)

Figure I-9 Transfer Function, Z Input, Node 121053, Northeast Corner on Top of Basemat

© Copyright 2019 by NuScale Power, LLC

{{

}}2(a),(c)

Figure I-10 Transfer Function, X Input, Node 4914, RXM 1 Floor Node under Module

© Copyright 2019 by NuScale Power, LLC

{{

}}2(a),(c)

Figure I-11 Transfer Function, Y Input, Node 4914, RXM 1 Floor Node under Module

© Copyright 2019 by NuScale Power, LLC

{{

}}2(a),(c)

Figure I-12 Transfer Function, Z Input, Node 4914, RXM 1 Floor Node under Module

© Copyright 2019 by NuScale Power, LLC

{{

}}2(a),(c)

Figure I-13 Transfer Function, X Input, Node 46054, RXM 6 Floor Node under Module

© Copyright 2019 by NuScale Power, LLC

{{

}}2(a),(c)

Figure I-14 Transfer Function, Y Input, Node 46054, RXM 6 Floor Node under Module

© Copyright 2019 by NuScale Power, LLC

{{

}}2(a),(c)

Figure I-15 Transfer Function, Z Input, Node 46054, RXM 6 Floor Node under Module

© Copyright 2019 by NuScale Power, LLC

{{

}}2(a),(c)

Figure I-16 Transfer Function, X Input, Node 185505, Northwest Corner at El. 50’

© Copyright 2019 by NuScale Power, LLC

{{

}}2(a),(c)

Figure I-17 Transfer Function, Y Input, Node 185505, Northwest Corner at El. 50’

© Copyright 2019 by NuScale Power, LLC

{{

}}2(a),(c)

Figure I-18 Transfer Function, Z Input, Node 185505, Northwest Corner at El. 50’

© Copyright 2019 by NuScale Power, LLC

{{

}}2(a),(c)

Figure I-19 Transfer Function, X Input, Node 182529, Mid-Span of West Slab along Grid Line RX-C at El. 50’

© Copyright 2019 by NuScale Power, LLC

{{

}}2(a),(c)

Figure I-20 Transfer Function, Y Input, Node 182529, Mid-Span of West Slab along Grid Line RX-C at El. 50’

© Copyright 2019 by NuScale Power, LLC

{{

}}2(a),(c)

Figure I-21 Transfer Function, Z Input, Node 182529, Mid-Span of West Slab along Grid Line RX-C at El. 50’

© Copyright 2019 by NuScale Power, LLC

{{

}}2(a),(c)

Figure I-22 Transfer Function, X Input, Node 184359, Edge of Slab at Grid Line RX-4 at El. 50’

© Copyright 2019 by NuScale Power, LLC

{{

}}2(a),(c)

Figure I-23 Transfer Function, Y Input, Node 184359, Edge of Slab at Grid Line RX-4 at El. 50’

© Copyright 2019 by NuScale Power, LLC

{{

}}2(a),(c)

Figure I-24 Transfer Function, Z Input, Node 184359, Edge of Slab at Grid Line RX-4 at El. 50’

© Copyright 2019 by NuScale Power, LLC

{{

}}2(a),(c)

Figure I-25 Transfer Function, X Input, Node 185174, Mid-Span of North Slab between Grid Lines RX-4 and RX-5 at El. 50’

© Copyright 2019 by NuScale Power, LLC

{{

}}2(a),(c)

Figure I-26 Transfer Function, Y Input, Node 185174, Mid-Span of North Slab between Grid Lines RX-4 and RX-5 at El. 50’

© Copyright 2019 by NuScale Power, LLC

{{

}}2(a),(c)

Figure I-27 Transfer Function, Z Input, Node 185174, Mid-Span of North Slab between Grid Lines RX-4 and RX-5 at El. 50’

© Copyright 2019 by NuScale Power, LLC

{{

}}2(a),(c)

Figure I-28 Transfer Function, X Input, Node 185623, Northeast Corner at El. 50’

© Copyright 2019 by NuScale Power, LLC

{{

}}2(a),(c)

Figure I-29 Transfer Function, Y Input, Node 185623, Northeast Corner at El. 50’

© Copyright 2019 by NuScale Power, LLC

{{

}}2(a),(c)

Figure I-30 Transfer Function, Z Input, Node 185623, Northeast Corner at El. 50’

© Copyright 2019 by NuScale Power, LLC

{{

}}2(a),(c)

Figure I-31 Transfer Function, X Input, Node 255527, Northwest Corner at El. 75’

© Copyright 2019 by NuScale Power, LLC

{{

}}2(a),(c)

Figure I-32 Transfer Function, Y Input, Node 255527, Northwest Corner at El. 75’

© Copyright 2019 by NuScale Power, LLC

{{

}}2(a),(c)

Figure I-33 Transfer Function, Z Input, Node 255527, Northwest Corner at El. 75’

© Copyright 2019 by NuScale Power, LLC

{{

}}2(a),(c)

Figure I-34 Transfer Function, X Input, Node 255195, Mid-Span of North Slab between Grid Lines RX-4 and RX-5 at El. 75’

© Copyright 2019 by NuScale Power, LLC

{{

}}2(a),(c)

Figure I-35 Transfer Function, Y Input, Node 255195, Mid-Span of North Slab between Grid Lines RX-4 and RX-5 at El. 75’

© Copyright 2019 by NuScale Power, LLC

{{

}}2(a),(c)

Figure I-36 Transfer Function, Z Input, Node 255195, Mid-Span of North Slab between Grid Lines RX-4 and RX-5 at El. 75’

© Copyright 2019 by NuScale Power, LLC

{{

}}2(a),(c)

Figure I-37 Transfer Function, X Input, Node 254481, Edge of East Slab along Grid Line RX-6 at El. 75’

© Copyright 2019 by NuScale Power, LLC

{{

}}2(a),(c)

Figure I-38 Transfer Function, Y Input, Node 254481, Edge of East Slab along Grid Line RX-6 at El. 75’

© Copyright 2019 by NuScale Power, LLC

{{

}}2(a),(c)

Figure I-39 Transfer Function, Z Input, Node 254481, Edge of East Slab along Grid Line RX-6 at El. 75’

© Copyright 2019 by NuScale Power, LLC

{{

}}2(a),(c)

Figure I-40 Transfer Function, X Input, Node 332235, Northwest Corner of Exterior Wall at El 100’

© Copyright 2019 by NuScale Power, LLC

{{

}}2(a),(c)

Figure I-41 Transfer Function, Y Input, Node 332235, Northwest Corner of Exterior Wall at El 100’

© Copyright 2019 by NuScale Power, LLC

{{

}}2(a),(c)

Figure I-42 Transfer Function, Z Input, Node 332235, Northwest Corner of Exterior Wall at El 100’

© Copyright 2019 by NuScale Power, LLC

{{

}}2(a),(c)

Figure I-43 Transfer Function, X Input, Node 331936, Mid-Span of North Slab between Grid Lines RX-4 and RX-5 at El 100’

© Copyright 2019 by NuScale Power, LLC

{{

}}2(a),(c)

Figure I-44 Transfer Function, Y Input, Node 331936, Mid-Span of North Slab between Grid Lines RX-4 and RX-5 at El 100’

© Copyright 2019 by NuScale Power, LLC

{{

}}2(a),(c)

Figure I-45 Transfer Function, Z Input, Node 331936, Mid-Span of North Slab between Grid Lines RX-4 and RX-5 at El 100’

© Copyright 2019 by NuScale Power, LLC

{{

}}2(a),(c)

Figure I-46 Transfer Function, X Input, Node 331222, Edge of North Slab along Grid Line RX-4 at El 100’

© Copyright 2019 by NuScale Power, LLC

{{

}}2(a),(c)

Figure I-47 Transfer Function, Y Input, Node 331222, Edge of North Slab along Grid Line RX-4 at El 100’

© Copyright 2019 by NuScale Power, LLC

{{

}}2(a),(c)

Figure I-48 Transfer Function, Z Input, Node 331222, Edge of North Slab along Grid Line RX-4 at El 100’

© Copyright 2019 by NuScale Power, LLC

{{

}}2(a),(c)

Figure I-49 Transfer Function, X Input, Node 331292, Edge of East Slab along Grid Line RX-6 at El 100’

© Copyright 2019 by NuScale Power, LLC

{{

}}2(a),(c)

Figure I-50 Transfer Function, Y Input, Node 331292, Edge of East Slab along Grid Line RX-6 at El 100’

© Copyright 2019 by NuScale Power, LLC

{{

}}2(a),(c)

Figure I-51 Transfer Function, Z Input, Node 331292, Edge of East Slab along Grid Line RX-6 at El 100’

© Copyright 2019 by NuScale Power, LLC

{{

}}2(a),(c)

Figure I-52 Transfer Function, X Input, Node 352669, Northwest Corner of Exterior Wall at El 125’

© Copyright 2019 by NuScale Power, LLC

{{

}}2(a),(c)

Figure I-53 Transfer Function, Y Input, Node 352669, Northwest Corner of Exterior Wall at El 125’

© Copyright 2019 by NuScale Power, LLC

{{

}}2(a),(c)

Figure I-54 Transfer Function, Z Input, Node 352669, Northwest Corner of Exterior Wall at El 125’

© Copyright 2019 by NuScale Power, LLC

{{

}}2(a),(c)

Figure I-55 Transfer Function, X Input, Node 351629, Northwest Corner of Bio Shield

© Copyright 2019 by NuScale Power, LLC

{{

}}2(a),(c)

Figure I-56 Transfer Function, Y Input, Node 351629, Northwest Corner of Bio Shield

© Copyright 2019 by NuScale Power, LLC

{{

}}2(a),(c)

Figure I-57 Transfer Function, Z Input, Node 351629, Northwest Corner of Bio Shield

© Copyright 2019 by NuScale Power, LLC

{{

}}2(a),(c)

Figure I-58 Transfer Function, X Input, Node 352370, Mid-Span of North Slab at between Grid Lines RX-4 and RX-5 at El 125’

© Copyright 2019 by NuScale Power, LLC

{{

}}2(a),(c)

Figure I-59 Transfer Function, Y Input, Node 352370, Mid-Span of North Slab at between Grid Lines RX-4 and RX-5 at El 125’

© Copyright 2019 by NuScale Power, LLC

{{

}}2(a),(c)

Figure I-60 Transfer Function, Z Input, Node 352370, Mid-Span of North Slab at between Grid Lines RX-4 and RX-5 at El 125’

© Copyright 2019 by NuScale Power, LLC

{{

}}2(a),(c)

Figure I-61 Transfer Function, X Input, Node 351696, Northeast Corner of Bio Shield

© Copyright 2019 by NuScale Power, LLC

{{

}}2(a),(c)

Figure I-62 Transfer Function, Y Input, Node 351696, Northeast Corner of Bio Shield

© Copyright 2019 by NuScale Power, LLC

{{

}}2(a),(c)

Figure I-63 Transfer Function, Z Input, Node 351696, Northeast Corner of Bio Shield

© Copyright 2019 by NuScale Power, LLC

{{

}}2(a),(c)

Figure I-64 Transfer Function, X Input, Node 392329, Top of Roof at Grid Line RX-1

© Copyright 2019 by NuScale Power, LLC

{{

}}2(a),(c)

Figure I-65 Transfer Function, Y Input, Node 392329, Top of Roof at Grid Line RX-1

© Copyright 2019 by NuScale Power, LLC

{{

}}2(a),(c)

Figure I-66 Transfer Function, Z Input, Node 392329, Top of Roof at Grid Line RX-1

© Copyright 2019 by NuScale Power, LLC

{{

}}2(a),(c)

Figure I-67 Transfer Function, X Input, Node 392378, Roof Slab between Grid Lines RX-4 and RX-5

© Copyright 2019 by NuScale Power, LLC

{{

}}2(a),(c)

Figure I-68 Transfer Function, Y Input, Node 392378, Roof Slab between Grid Lines RX-4 and RX-5

© Copyright 2019 by NuScale Power, LLC

{{

}}2(a),(c)

Figure I-69 Transfer Function, Z Input, Node 392378, Roof Slab between Grid Lines RX-4 and RX-5

© Copyright 2019 by NuScale Power, LLC

{{

}}2(a),(c)

Figure I-70 Transfer Function, X Input, Node 394770, Northeast Corner of Roof Slab

© Copyright 2019 by NuScale Power, LLC

{{

}}2(a),(c)

Figure I-71 Transfer Function, Y Input, Node 394770, Northeast Corner of Roof Slab

© Copyright 2019 by NuScale Power, LLC

{{

}}2(a),(c)

Figure I-72 Transfer Function, Z Input, Node 394770, Northeast Corner of Roof Slab

© Copyright 2019 by NuScale Power, LLC

{{

}}2(a),(c)

Figure I-73 Transfer Function, X Input, Node 8216, RXM-1 West Lug

© Copyright 2019 by NuScale Power, LLC

{{

}}2(a),(c)

Figure I-74 Transfer Function, Y Input, Node 8216, RXM-1 West Lug

© Copyright 2019 by NuScale Power, LLC

{{

}}2(a),(c)

Figure I-75 Transfer Function, Z Input, Node 8216, RXM-1 West Lug

© Copyright 2019 by NuScale Power, LLC

{{

}}2(a),(c)

Figure I-76 Transfer Function, X Input, Node 8215, RXM-1 North Lug

© Copyright 2019 by NuScale Power, LLC

{{

}}2(a),(c)

Figure I-77 Transfer Function, Y Input, Node 8215, RXM-1 North Lug

© Copyright 2019 by NuScale Power, LLC

{{

}}2(a),(c)

Figure I-78 Transfer Function, Z Input, Node 8215, RXM-1 North Lug

© Copyright 2019 by NuScale Power, LLC

{{

}}2(a),(c)

Figure I-79 Transfer Function, X Input, Node 8214, RXM-1 East Lug

© Copyright 2019 by NuScale Power, LLC

{{

}}2(a),(c)

Figure I-80 Transfer Function, Y Input, Node 8214, RXM-1 East Lug

© Copyright 2019 by NuScale Power, LLC

{{

}}2(a),(c)

Figure I-81 Transfer Function, Z Input, Node 8214, RXM-1 East Lug

© Copyright 2019 by NuScale Power, LLC

{{

}}2(a),(c)

Figure I-82 Transfer Function, X Input, Node 1900, RXM-1 Top

© Copyright 2019 by NuScale Power, LLC

{{

}}2(a),(c)

Figure I-83 Transfer Function, Y Input, Node 1900, RXM-1 Top

© Copyright 2019 by NuScale Power, LLC

{{

}}2(a),(c)

Figure I-84 Transfer Function, Z Input, Node 1900, RXM-1 Top

© Copyright 2019 by NuScale Power, LLC

{{

}}2(a),(c)

Figure I-85 Transfer Function, X Input, Node 49356, RXM-6 West Lug

© Copyright 2019 by NuScale Power, LLC

{{

}}2(a),(c)

Figure I-86 Transfer Function, Y Input, Node 49356, RXM-6 West Lug

© Copyright 2019 by NuScale Power, LLC

{{

}}2(a),(c)

Figure I-87 Transfer Function, Z Input, Node 49356, RXM-6 West Lug

© Copyright 2019 by NuScale Power, LLC

{{

}}2(a),(c)

Figure I-88 Transfer Function, X Input, Node 49355, RXM-6 North Lug

© Copyright 2019 by NuScale Power, LLC

{{

}}2(a),(c)

Figure I-89 Transfer Function, Y Input, Node 49355, RXM-6 North Lug

© Copyright 2019 by NuScale Power, LLC

{{

}}2(a),(c)

Figure I-90 Transfer Function, Z Input, Node 49355, RXM-6 North Lug

© Copyright 2019 by NuScale Power, LLC

{{

}}2(a),(c)

Figure I-91 Transfer Function, X Input, Node 49354, RXM-6 East Lug

© Copyright 2019 by NuScale Power, LLC

{{

}}2(a),(c)

Figure I-92 Transfer Function, Y Input, Node 49354, RXM-6 East Lug

© Copyright 2019 by NuScale Power, LLC

{{

}}2(a),(c)

Figure I-93 Transfer Function, Z Input, Node 49354, RXM-6 East Lug

© Copyright 2019 by NuScale Power, LLC

{{

}}2(a),(c)

Figure I-94 Transfer Function, X Input, Node 43040, RXM-6 Top

© Copyright 2019 by NuScale Power, LLC

{{

}}2(a),(c)

Figure I-95 Transfer Function, Y Input, Node 43040, RXM-6 Top

© Copyright 2019 by NuScale Power, LLC

{{

}}2(a),(c)

Figure I-96 Transfer Function, Z Input, Node 43040, RXM-6 Top

© Copyright 2019 by NuScale Power, LLC

Appendix J. Example 4, Acceleration Time Histories

The following plots have a title on the plot legend that consists of the node number followed by two letters. The first letter corresponds to the direction of ground motion or input. The second letter corresponds to the response direction or output.

Results on a given page correspond to a common input direction, i.e. X, Y or Z. The top plot corresponds to output in the X direction, the center plot corresponds to output in the Y direction, and the bottom plot corresponds to output in the Z direction.

X is East, Y is North and Z is up.

© Copyright 2019 by NuScale Power, LLC

{{

}}2(a),(c)

Figure J-1 Acceleration Time History, X Input, Node 120933, Northwest Corner on Top of Basemat

© Copyright 2019 by NuScale Power, LLC

{{

}}2(a),(c)

Figure J-2 Acceleration Time History, Y Input, Node 120933, Northwest Corner on Top of Basemat

© Copyright 2019 by NuScale Power, LLC

{{

}}2(a),(c)

Figure J-3 Acceleration Time History, Z Input, Node 120933, Northwest Corner on Top of Basemat

© Copyright 2019 by NuScale Power, LLC

{{

}}2(a),(c)

Figure J-4 Acceleration Time History, X Input, Node 120978, Mid-Span of North Exterior Wall on Top of Basemat

© Copyright 2019 by NuScale Power, LLC

{{

}}2(a),(c)

Figure J-5 Acceleration Time History, Y Input, Node 120978, Mid-Span of North Exterior Wall on Top of Basemat

© Copyright 2019 by NuScale Power, LLC

{{

}}2(a),(c)

Figure J-6 Acceleration Time History, Z Input, Node 120978, Mid-Span of North Exterior Wall on Top of Basemat

© Copyright 2019 by NuScale Power, LLC

{{

}}2(a),(c)

Figure J-7 Acceleration Time History, X Input, Node 121053, Northeast Corner on Top of Basemat

© Copyright 2019 by NuScale Power, LLC

{{

}}2(a),(c)

Figure J-8 Acceleration Time History, Y Input, Node 121053, Northeast Corner on Top of Basemat

© Copyright 2019 by NuScale Power, LLC

{{

}}2(a),(c)

Figure J-9 Acceleration Time History, Z Input, Node 121053, Northeast Corner on Top of Basemat

© Copyright 2019 by NuScale Power, LLC

{{

}}2(a),(c)

Figure J-10 Acceleration Time History, X Input, Node 4914, RXM 1 Floor Node under Module

© Copyright 2019 by NuScale Power, LLC

{{

}}2(a),(c)

Figure J-11 Acceleration Time History, Y Input, Node 4914, RXM 1 Floor Node under Module

© Copyright 2019 by NuScale Power, LLC

{{

}}2(a),(c)

Figure J-12 Acceleration Time History, Z Input, Node 4914, RXM 1 Floor Node under Module

© Copyright 2019 by NuScale Power, LLC

{{

}}2(a),(c)

Figure J-13 Acceleration Time History, X Input, Node 46054, RXM 6 Floor Node under Module

© Copyright 2019 by NuScale Power, LLC

{{

}}2(a),(c)

Figure J-14 Acceleration Time History, Y Input, Node 46054, RXM 6 Floor Node under Module

© Copyright 2019 by NuScale Power, LLC

{{

}}2(a),(c)

Figure J-15 Acceleration Time History, Z Input, Node 46054, RXM 6 Floor Node under Module

© Copyright 2019 by NuScale Power, LLC

{{

}}2(a),(c)

Figure J-16 Acceleration Time History, X Input, Node 185505, Northwest Corner at El. 50’

© Copyright 2019 by NuScale Power, LLC

{{

}}2(a),(c)

Figure J-17 Acceleration Time History, Y Input, Node 185505, Northwest Corner at El. 50’

© Copyright 2019 by NuScale Power, LLC

{{

}}2(a),(c)

Figure J-18 Acceleration Time History, Z Input, Node 185505, Northwest Corner at El. 50’

© Copyright 2019 by NuScale Power, LLC

{{

}}2(a),(c)

Figure J-19 Acceleration Time History, X Input, Node 182529, Mid-Span of West Slab along Grid Line RX-C at El. 50’

© Copyright 2019 by NuScale Power, LLC

{{

}}2(a),(c)

Figure J-20 Acceleration Time History, Y Input, Node 182529, Mid-Span of West Slab along Grid Line RX-C at El. 50’

© Copyright 2019 by NuScale Power, LLC

{{

}}2(a),(c)

Figure J-21 Acceleration Time History, Z Input, Node 182529, Mid-Span of West Slab along Grid Line RX-C at El. 50’

© Copyright 2019 by NuScale Power, LLC

{{

}}2(a),(c)

Figure J-22 Acceleration Time History, X Input, Node 184359, Edge of Slab at Grid Line RX-4 at El. 50’

© Copyright 2019 by NuScale Power, LLC

{{

}}2(a),(c)

Figure J-23 Acceleration Time History, Y Input, Node 184359, Edge of Slab at Grid Line RX-4 at El. 50’

© Copyright 2019 by NuScale Power, LLC

{{

}}2(a),(c)

Figure J-24 Acceleration Time History, Z Input, Node 184359, Edge of Slab at Grid Line RX-4 at El. 50’

© Copyright 2019 by NuScale Power, LLC

{{

}}2(a),(c)

Figure J-25 Acceleration Time History, X Input, Node 185174, Mid-Span of North Slab between Grid Lines RX-4 and RX-5 at El. 50’

© Copyright 2019 by NuScale Power, LLC

{{

}}2(a),(c)

Figure J-26 Acceleration Time History, Y Input, Node 185174, Mid-Span of North Slab between Grid Lines RX-4 and RX-5 at El. 50’

© Copyright 2019 by NuScale Power, LLC

{{

}}2(a),(c)

Figure J-27 Acceleration Time History, Z Input, Node 185174, Mid-Span of North Slab between Grid Lines RX-4 and RX-5 at El. 50’

© Copyright 2019 by NuScale Power, LLC

{{

}}2(a),(c)

Figure J-28 Acceleration Time History, X Input, Node 185623, Northeast Corner at El. 50’

© Copyright 2019 by NuScale Power, LLC

{{

}}2(a),(c)

Figure J-29 Acceleration Time History, Y Input, Node 185623, Northeast Corner at El. 50’

© Copyright 2019 by NuScale Power, LLC

{{

}}2(a),(c)

Figure J-30 Acceleration Time History, Z Input, Node 185623, Northeast Corner at El. 50’

© Copyright 2019 by NuScale Power, LLC

{{

}}2(a),(c)

Figure J-31 Acceleration Time History, X Input, Node 255527, Northwest Corner at El. 75’

© Copyright 2019 by NuScale Power, LLC

{{

}}2(a),(c)

Figure J-32 Acceleration Time History, Y Input, Node 255527, Northwest Corner at El. 75’

© Copyright 2019 by NuScale Power, LLC

{{

}}2(a),(c)

Figure J-33 Acceleration Time History, Z Input, Node 255527, Northwest Corner at El. 75’

© Copyright 2019 by NuScale Power, LLC

{{

}}2(a),(c)

Figure J-34 Acceleration Time History, X Input, Node 255195, Mid-Span of North Slab between Grid Lines RX-4 and RX-5 at El. 75’

© Copyright 2019 by NuScale Power, LLC

{{

}}2(a),(c)

Figure J-35 Acceleration Time History, Y Input, Node 255195, Mid-Span of North Slab between Grid Lines RX-4 and RX-5 at El. 75’

© Copyright 2019 by NuScale Power, LLC

{{

}}2(a),(c)

Figure J-36 Acceleration Time History, Z Input, Node 255195, Mid-Span of North Slab between Grid Lines RX-4 and RX-5 at El. 75’

© Copyright 2019 by NuScale Power, LLC

{{

}}2(a),(c)

Figure J-37 Acceleration Time History, X Input, Node 254481, Edge of East Slab along Grid Line RX-6 at El. 75’

© Copyright 2019 by NuScale Power, LLC

{{

}}2(a),(c)

Figure J-38 Acceleration Time History, Y Input, Node 254481, Edge of East Slab along Grid Line RX-6 at El. 75’

© Copyright 2019 by NuScale Power, LLC

{{

}}2(a),(c)

Figure J-39 Acceleration Time History, Z Input, Node 254481, Edge of East Slab along Grid Line RX-6 at El. 75’

© Copyright 2019 by NuScale Power, LLC

{{

}}2(a),(c)

Figure J-40 Acceleration Time History, X Input, Node 332235, Northwest Corner of Exterior Wall at El 100’

© Copyright 2019 by NuScale Power, LLC

{{

}}2(a),(c)

Figure J-41 Acceleration Time History, Y Input, Node 332235, Northwest Corner of Exterior Wall at El 100’

© Copyright 2019 by NuScale Power, LLC

{{

}}2(a),(c)

Figure J-42 Acceleration Time History, Z Input, Node 332235, Northwest Corner of Exterior Wall at El 100’

© Copyright 2019 by NuScale Power, LLC

{{

}}2(a),(c)

Figure J-43 Acceleration Time History, X Input, Node 331936, Mid-Span of North Slab between Grid Lines RX-4 and RX-5 at El 100’

© Copyright 2019 by NuScale Power, LLC

{{

}}2(a),(c)

Figure J-44 Acceleration Time History, Y Input, Node 331936, Mid-Span of North Slab between Grid Lines RX-4 and RX-5 at El 100’

© Copyright 2019 by NuScale Power, LLC

{{

}}2(a),(c)

Figure J-45 Acceleration Time History, Z Input, Node 331936, Mid-Span of North Slab between Grid Lines RX-4 and RX-5 at El 100’

© Copyright 2019 by NuScale Power, LLC

{{

}}2(a),(c)

Figure J-46 Acceleration Time History, X Input, Node 331222, Edge of North Slab along Grid Line RX-4 at El 100’

© Copyright 2019 by NuScale Power, LLC

{{

}}2(a),(c)

Figure J-47 Acceleration Time History, Y Input, Node 331222, Edge of North Slab along Grid Line RX-4 at El 100’

© Copyright 2019 by NuScale Power, LLC

{{

}}2(a),(c)

Figure J-48 Acceleration Time History, Z Input, Node 331222, Edge of North Slab along Grid Line RX-4 at El 100’

© Copyright 2019 by NuScale Power, LLC

{{

}}2(a),(c)

Figure J-49 Acceleration Time History, X Input, Node 331292, Edge of East Slab along Grid Line RX-6 at El 100’

© Copyright 2019 by NuScale Power, LLC

{{

}}2(a),(c)

Figure J-50 Acceleration Time History, Y Input, Node 331292, Edge of East Slab along Grid Line RX-6 at El 100’

© Copyright 2019 by NuScale Power, LLC

{{

}}2(a),(c)

Figure J-51 Acceleration Time History, Z Input, Node 331292, Edge of East Slab along Grid Line RX-6 at El 100’

© Copyright 2019 by NuScale Power, LLC

{{

}}2(a),(c)

Figure J-52 Acceleration Time History, X Input, Node 352669, Northwest Corner of Exterior Wall at El 125’

© Copyright 2019 by NuScale Power, LLC

{{

}}2(a),(c)

Figure J-53 Acceleration Time History, Y Input, Node 352669, Northwest Corner of Exterior Wall at El 125’

© Copyright 2019 by NuScale Power, LLC

{{

}}2(a),(c)

Figure J-54 Acceleration Time History, Z Input, Node 352669, Northwest Corner of Exterior Wall at El 125’

© Copyright 2019 by NuScale Power, LLC

{{

}}2(a),(c)

Figure J-55 Acceleration Time History, X Input, Node 351629, Northwest Corner of Bio Shield

© Copyright 2019 by NuScale Power, LLC

{{

}}2(a),(c)

Figure J-56 Acceleration Time History, Y Input, Node 351629, Northwest Corner of Bio Shield

© Copyright 2019 by NuScale Power, LLC

{{

}}2(a),(c)

Figure J-57 Acceleration Time History, Z Input, Node 351629, Northwest Corner of Bio Shield

© Copyright 2019 by NuScale Power, LLC

{{

}}2(a),(c)

Figure J-58 Acceleration Time History, X Input, Node 352370, Mid-Span of North Slab at between Grid Lines RX-4 and RX-5 at El 125’

© Copyright 2019 by NuScale Power, LLC

{{

}}2(a),(c)

Figure J-59 Acceleration Time History, Y Input, Node 352370, Mid-Span of North Slab at between Grid Lines RX-4 and RX-5 at El 125’

© Copyright 2019 by NuScale Power, LLC

{{

}}2(a),(c)

Figure J-60 Acceleration Time History, Z Input, Node 352370, Mid-Span of North Slab at between Grid Lines RX-4 and RX-5 at El 125’

© Copyright 2019 by NuScale Power, LLC

{{

}}2(a),(c)

Figure J-61 Acceleration Time History, X Input, Node 351696, Northeast Corner of Bio Shield

© Copyright 2019 by NuScale Power, LLC

{{

}}2(a),(c)

Figure J-62 Acceleration Time History, Y Input, Node 351696, Northeast Corner of Bio Shield

© Copyright 2019 by NuScale Power, LLC

{{

}}2(a),(c)

Figure J-63 Acceleration Time History, Z Input, Node 351696, Northeast Corner of Bio Shield

© Copyright 2019 by NuScale Power, LLC

{{

}}2(a),(c)

Figure J-64 Acceleration Time History, X Input, Node 392329, Top of Roof at Grid Line RX-1

© Copyright 2019 by NuScale Power, LLC

{{

}}2(a),(c)

Figure J-65 Acceleration Time History, Y Input, Node 392329, Top of Roof at Grid Line RX-1

© Copyright 2019 by NuScale Power, LLC

{{

}}2(a),(c)

Figure J-66 Acceleration Time History, Z Input, Node 392329, Top of Roof at Grid Line RX-1

© Copyright 2019 by NuScale Power, LLC

{{

}}2(a),(c)

Figure J-67 Acceleration Time History, X Input, Node 392378, Roof Slab between Grid Lines RX-4 and RX-5

© Copyright 2019 by NuScale Power, LLC

{{

}}2(a),(c)

Figure J-68 Acceleration Time History, Y Input, Node 392378, Roof Slab between Grid Lines RX-4 and RX-5

© Copyright 2019 by NuScale Power, LLC

{{

}}2(a),(c)

Figure J-69 Acceleration Time History, Z Input, Node 392378, Roof Slab between Grid Lines RX-4 and RX-5

© Copyright 2019 by NuScale Power, LLC

{{

}}2(a),(c)

Figure J-70 Acceleration Time History, X Input, Node 394770, Northeast Corner of Roof Slab

© Copyright 2019 by NuScale Power, LLC

{{

}}2(a),(c)

Figure J-71 Acceleration Time History, Y Input, Node 394770, Northeast Corner of Roof Slab

© Copyright 2019 by NuScale Power, LLC

{{

}}2(a),(c)

Figure J-72 Acceleration Time History, Z Input, Node 394770, Northeast Corner of Roof Slab

© Copyright 2019 by NuScale Power, LLC

{{

}}2(a),(c)

Figure J-73 Acceleration Time History, X Input, Node 8216, RXM-1 West Lug

© Copyright 2019 by NuScale Power, LLC

{{

}}2(a),(c)

Figure J-74 Acceleration Time History, Y Input, Node 8216, RXM-1 West Lug

© Copyright 2019 by NuScale Power, LLC

{{

}}2(a),(c)

Figure J-75 Acceleration Time History, Z Input, Node 8216, RXM-1 West Lug

© Copyright 2019 by NuScale Power, LLC

{{

}}2(a),(c)

Figure J-76 Acceleration Time History, X Input, Node 8215, RXM-1 North Lug

© Copyright 2019 by NuScale Power, LLC

{{

}}2(a),(c)

Figure J-77 Acceleration Time History, Y Input, Node 8215, RXM-1 North Lug

© Copyright 2019 by NuScale Power, LLC

{{

}}2(a),(c)

Figure J-78 Acceleration Time History, Z Input, Node 8215, RXM-1 North Lug

© Copyright 2019 by NuScale Power, LLC

{{

}}2(a),(c)

Figure J-79 Acceleration Time History, X Input, Node 8214, RXM-1 East Lug

© Copyright 2019 by NuScale Power, LLC

{{

}}2(a),(c)

Figure J-80 Acceleration Time History, Y Input, Node 8214, RXM-1 East Lug

© Copyright 2019 by NuScale Power, LLC

{{

}}2(a),(c)

Figure J-81 Acceleration Time History, Z Input, Node 8214, RXM-1 East Lug

© Copyright 2019 by NuScale Power, LLC

{{

}}2(a),(c)

Figure J-82 Acceleration Time History, X Input, Node 1900, RXM-1 Top

© Copyright 2019 by NuScale Power, LLC

{{

}}2(a),(c)

Figure J-83 Acceleration Time History, Y Input, Node 1900, RXM-1 Top

© Copyright 2019 by NuScale Power, LLC

{{

}}2(a),(c)

Figure J-84 Acceleration Time History, Z Input, Node 1900, RXM-1 Top

© Copyright 2019 by NuScale Power, LLC

{{

}}2(a),(c)

Figure J-85 Acceleration Time History, X Input, Node 49356, RXM-6 West Lug

© Copyright 2019 by NuScale Power, LLC

{{

}}2(a),(c)

Figure J-86 Acceleration Time History, Y Input, Node 49356, RXM-6 West Lug

© Copyright 2019 by NuScale Power, LLC

{{

}}2(a),(c)

Figure J-87 Acceleration Time History, Z Input, Node 49356, RXM-6 West Lug

© Copyright 2019 by NuScale Power, LLC

{{

}}2(a),(c)

Figure J-88 Acceleration Time History, X Input, Node 49355, RXM-6 North Lug

© Copyright 2019 by NuScale Power, LLC

{{

}}2(a),(c)

Figure J-89 Acceleration Time History, Y Input, Node 49355, RXM-6 North Lug

© Copyright 2019 by NuScale Power, LLC

{{

}}2(a),(c)

Figure J-90 Acceleration Time History, Z Input, Node 49355, RXM-6 North Lug

© Copyright 2019 by NuScale Power, LLC

{{

}}2(a),(c)

Figure J-91 Acceleration Time History, X Input, Node 49354, RXM-6 East Lug

© Copyright 2019 by NuScale Power, LLC

{{

}}2(a),(c)

Figure J-92 Acceleration Time History, Y Input, Node 49354, RXM-6 East Lug

© Copyright 2019 by NuScale Power, LLC

{{

}}2(a),(c)

Figure J-93 Acceleration Time History, Z Input, Node 49354, RXM-6 East Lug

© Copyright 2019 by NuScale Power, LLC

{{

}}2(a),(c)

Figure J-94 Acceleration Time History, X Input, Node 43040, RXM-6 Top

© Copyright 2019 by NuScale Power, LLC

{{

}}2(a),(c)

Figure J-95 Acceleration Time History, Y Input, Node 43040, RXM-6 Top

© Copyright 2019 by NuScale Power, LLC

{{

}}2(a),(c)

Figure J-96 Acceleration Time History, Z Input, Node 43040, RXM-6 Top

© Copyright 2019 by NuScale Power, LLC

Appendix K. Example 4, In-Structure Response Spectra

All in-structure response spectra in this appendix are based on 4% damping.

The following plots have a title on the plot legend that consists of the node number followed by two letters. The first letter corresponds to the direction of ground motion or input. The second letter corresponds to the response direction or output.

Results on a given page correspond to a common input direction, i.e. X, Y or Z. The top plot corresponds to output in the X direction, the center plot corresponds to output in the Y direction, and the bottom plot corresponds to output in the Z direction.

X is East, Y is North and Z is up.

© Copyright 2019 by NuScale Power, LLC

{{

}}2(a),(c)

Figure K-1 In-Structure Response Spectra, X Input, Node 120933, Northwest Corner on Top of Basemat

© Copyright 2019 by NuScale Power, LLC

{{

}}2(a),(c)

Figure K-2 In-Structure Response Spectra, Y Input, Node 120933, Northwest Corner on Top of Basemat

© Copyright 2019 by NuScale Power, LLC

{{

}}2(a),(c)

Figure K-3 In-Structure Response Spectra, Z Input, Node 120933, Northwest Corner on Top of Basemat

© Copyright 2019 by NuScale Power, LLC

{{

}}2(a),(c)

Figure K-4 In-Structure Response Spectra, X Input, Node 120978, Mid-Span of North Exterior Wall on Top of Basemat

© Copyright 2019 by NuScale Power, LLC

{{

}}2(a),(c)

Figure K-5 In-Structure Response Spectra, Y Input, Node 120978, Mid-Span of North Exterior Wall on Top of Basemat

© Copyright 2019 by NuScale Power, LLC

{{

}}2(a),(c)

Figure K-6 In-Structure Response Spectra, Z Input, Node 120978, Mid-Span of North Exterior Wall on Top of Basemat

© Copyright 2019 by NuScale Power, LLC

{{

}}2(a),(c)

Figure K-7 In-Structure Response Spectra, X Input, Node 121053, Northeast Corner on Top of Basemat

© Copyright 2019 by NuScale Power, LLC

{{

}}2(a),(c)

Figure K-8 In-Structure Response Spectra, Y Input, Node 121053, Northeast Corner on Top of Basemat

© Copyright 2019 by NuScale Power, LLC

{{

}}2(a),(c)

Figure K-9 In-Structure Response Spectra, Z Input, Node 121053, Northeast Corner on Top of Basemat

© Copyright 2019 by NuScale Power, LLC

{{

}}2(a),(c)

Figure K-10 In-Structure Response Spectra, X Input, Node 4914, RXM 1 Floor Node under Module

© Copyright 2019 by NuScale Power, LLC

{{

}}2(a),(c)

Figure K-11 In-Structure Response Spectra, Y Input, Node 4914, RXM 1 Floor Node under Module

© Copyright 2019 by NuScale Power, LLC

{{

}}2(a),(c)

Figure K-12 In-Structure Response Spectra, Z Input, Node 4914, RXM 1 Floor Node under Module

© Copyright 2019 by NuScale Power, LLC

{{

}}2(a),(c)

Figure K-13 In-Structure Response Spectra, X Input, Node 46054, RXM 6 Floor Node under Module

© Copyright 2019 by NuScale Power, LLC

{{

}}2(a),(c)

Figure K-14 In-Structure Response Spectra, Y Input, Node 46054, RXM 6 Floor Node under Module

© Copyright 2019 by NuScale Power, LLC

{{

}}2(a),(c)

Figure K-15 In-Structure Response Spectra, Z Input, Node 46054, RXM 6 Floor Node under Module

© Copyright 2019 by NuScale Power, LLC

{{

}}2(a),(c)

Figure K-16 In-Structure Response Spectra, X Input, Node 185505, Northwest Corner at El. 50’

© Copyright 2019 by NuScale Power, LLC

{{

}}2(a),(c)

Figure K-17 In-Structure Response Spectra, Y Input, Node 185505, Northwest Corner at El. 50’

© Copyright 2019 by NuScale Power, LLC

{{

}}2(a),(c)

Figure K-18 In-Structure Response Spectra, Z Input, Node 185505, Northwest Corner at El. 50’

© Copyright 2019 by NuScale Power, LLC

{{

}}2(a),(c)

Figure K-19 In-Structure Response Spectra, X Input, Node 182529, Mid-Span of West Slab along Grid Line RX-C at El. 50’

© Copyright 2019 by NuScale Power, LLC

{{

}}2(a),(c)

Figure K-20 In-Structure Response Spectra, Y Input, Node 182529, Mid-Span of West Slab along Grid Line RX-C at El. 50’

© Copyright 2019 by NuScale Power, LLC

{{

}}2(a),(c)

Figure K-21 In-Structure Response Spectra, Z Input, Node 182529, Mid-Span of West Slab along Grid Line RX-C at El. 50’

© Copyright 2019 by NuScale Power, LLC

{{

}}2(a),(c)

Figure K-22 In-Structure Response Spectra, X Input, Node 184359, Edge of Slab at Grid Line RX-4 at El. 50’

© Copyright 2019 by NuScale Power, LLC

{{

}}2(a),(c)

Figure K-23 In-Structure Response Spectra, Y Input, Node 184359, Edge of Slab at Grid Line RX-4 at El. 50’

© Copyright 2019 by NuScale Power, LLC

{{

}}2(a),(c)

Figure K-24 In-Structure Response Spectra, Z Input, Node 184359, Edge of Slab at Grid Line RX-4 at El. 50’

© Copyright 2019 by NuScale Power, LLC

{{

}}2(a),(c)

Figure K-25 In-Structure Response Spectra, X Input, Node 185174, Mid-Span of North Slab between Grid Lines RX-4 and RX-5 at El. 50’

© Copyright 2019 by NuScale Power, LLC

{{

}}2(a),(c)

Figure K-26 In-Structure Response Spectra, Y Input, Node 185174, Mid-Span of North Slab between Grid Lines RX-4 and RX-5 at El. 50’

© Copyright 2019 by NuScale Power, LLC

{{

}}2(a),(c)

Figure K-27 In-Structure Response Spectra, Z Input, Node 185174, Mid-Span of North Slab between Grid Lines RX-4 and RX-5 at El. 50’

© Copyright 2019 by NuScale Power, LLC

{{

}}2(a),(c)

Figure K-28 In-Structure Response Spectra, X Input, Node 185623, Northeast Corner at El. 50’

© Copyright 2019 by NuScale Power, LLC

{{

}}2(a),(c)

Figure K-29 In-Structure Response Spectra, Y Input, Node 185623, Northeast Corner at El. 50’

© Copyright 2019 by NuScale Power, LLC

{{

}}2(a),(c)

Figure K-30 In-Structure Response Spectra, Z Input, Node 185623, Northeast Corner at El. 50’

© Copyright 2019 by NuScale Power, LLC

{{

}}2(a),(c)

Figure K-31 In-Structure Response Spectra, X Input, Node 255527, Northwest Corner at El. 75’

© Copyright 2019 by NuScale Power, LLC

{{

}}2(a),(c)

Figure K-32 In-Structure Response Spectra, Y Input, Node 255527, Northwest Corner at El. 75’

© Copyright 2019 by NuScale Power, LLC

{{

}}2(a),(c)

Figure K-33 In-Structure Response Spectra, Z Input, Node 255527, Northwest Corner at El. 75’

© Copyright 2019 by NuScale Power, LLC

{{

}}2(a),(c)

Figure K-34 In-Structure Response Spectra, X Input, Node 255195, Mid-Span of North Slab between Grid Lines RX-4 and RX-5 at El. 75’

© Copyright 2019 by NuScale Power, LLC

{{

}}2(a),(c)

Figure K-35 In-Structure Response Spectra, Y Input, Node 255195, Mid-Span of North Slab between Grid Lines RX-4 and RX-5 at El. 75’

© Copyright 2019 by NuScale Power, LLC

{{

}}2(a),(c)

Figure K-36 In-Structure Response Spectra, Z Input, Node 255195, Mid-Span of North Slab between Grid Lines RX-4 and RX-5 at El. 75’

© Copyright 2019 by NuScale Power, LLC

{{

}}2(a),(c)

Figure K-37 In-Structure Response Spectra, X Input, Node 254481, Edge of East Slab along Grid Line RX-6 at El. 75’

© Copyright 2019 by NuScale Power, LLC

{{

}}2(a),(c)

Figure K-38 In-Structure Response Spectra, Y Input, Node 254481, Edge of East Slab along Grid Line RX-6 at El. 75’

© Copyright 2019 by NuScale Power, LLC

{{

}}2(a),(c)

Figure K-39 In-Structure Response Spectra, Z Input, Node 254481, Edge of East Slab along Grid Line RX-6 at El. 75’

© Copyright 2019 by NuScale Power, LLC

{{

}}2(a),(c)

Figure K-40 In-Structure Response Spectra, X Input, Node 332235, Northwest Corner of Exterior Wall at El 100’

© Copyright 2019 by NuScale Power, LLC

{{

}}2(a),(c)

Figure K-41 In-Structure Response Spectra, Y Input, Node 332235, Northwest Corner of Exterior Wall at El 100’

© Copyright 2019 by NuScale Power, LLC

{{

}}2(a),(c)

Figure K-42 In-Structure Response Spectra, Z Input, Node 332235, Northwest Corner of Exterior Wall at El 100’

© Copyright 2019 by NuScale Power, LLC

{{

}}2(a),(c)

Figure K-43 In-Structure Response Spectra, X Input, Node 331936, Mid-Span of North Slab between Grid Lines RX-4 and RX-5 at El 100’

© Copyright 2019 by NuScale Power, LLC

{{

}}2(a),(c)

Figure K-44 In-Structure Response Spectra, Y Input, Node 331936, Mid-Span of North Slab between Grid Lines RX-4 and RX-5 at El 100’

© Copyright 2019 by NuScale Power, LLC

{{

}}2(a),(c)

Figure K-45 In-Structure Response Spectra, Z Input, Node 331936, Mid-Span of North Slab between Grid Lines RX-4 and RX-5 at El 100’

© Copyright 2019 by NuScale Power, LLC

{{

}}2(a),(c)

Figure K-46 In-Structure Response Spectra, X Input, Node 331222, Edge of North Slab along Grid Line RX-4 at El 100’

© Copyright 2019 by NuScale Power, LLC

{{

}}2(a),(c)

Figure K-47 In-Structure Response Spectra, Y Input, Node 331222, Edge of North Slab along Grid Line RX-4 at El 100’

© Copyright 2019 by NuScale Power, LLC

{{

}}2(a),(c)

Figure K-48 In-Structure Response Spectra, Z Input, Node 331222, Edge of North Slab along Grid Line RX-4 at El 100’

© Copyright 2019 by NuScale Power, LLC

{{

}}2(a),(c)

Figure K-49 In-Structure Response Spectra, X Input, Node 331292, Edge of East Slab along Grid Line RX-6 at El 100’

© Copyright 2019 by NuScale Power, LLC

{{

}}2(a),(c)

Figure K-50 In-Structure Response Spectra, Y Input, Node 331292, Edge of East Slab along Grid Line RX-6 at El 100’

© Copyright 2019 by NuScale Power, LLC

{{

}}2(a),(c)

Figure K-51 In-Structure Response Spectra, Z Input, Node 331292, Edge of East Slab along Grid Line RX-6 at El 100’

© Copyright 2019 by NuScale Power, LLC

{{

}}2(a),(c)

Figure K-52 In-Structure Response Spectra, X Input, Node 352669, Northwest Corner of Exterior Wall at El 125’

© Copyright 2019 by NuScale Power, LLC

{{

}}2(a),(c)

Figure K-53 In-Structure Response Spectra, Y Input, Node 352669, Northwest Corner of Exterior Wall at El 125’

© Copyright 2019 by NuScale Power, LLC

{{

}}2(a),(c)

Figure K-54 In-Structure Response Spectra, Z Input, Node 352669, Northwest Corner of Exterior Wall at El 125’

© Copyright 2019 by NuScale Power, LLC

{{

}}2(a),(c)

Figure K-55 In-Structure Response Spectra, X Input, Node 351629, Northwest Corner of Bio Shield

© Copyright 2019 by NuScale Power, LLC

{{

}}2(a),(c)

Figure K-56 In-Structure Response Spectra, Y Input, Node 351629, Northwest Corner of Bio Shield

© Copyright 2019 by NuScale Power, LLC

{{

}}2(a),(c)

Figure K-57 In-Structure Response Spectra, Z Input, Node 351629, Northwest Corner of Bio Shield

© Copyright 2019 by NuScale Power, LLC

{{

}}2(a),(c)

Figure K-58 In-Structure Response Spectra, X Input, Node 352370, Mid-Span of North Slab at between Grid Lines RX-4 and RX-5 at El 125’

© Copyright 2019 by NuScale Power, LLC

{{

}}2(a),(c)

Figure K-59 In-Structure Response Spectra, Y Input, Node 352370, Mid-Span of North Slab at between Grid Lines RX-4 and RX-5 at El 125’

© Copyright 2019 by NuScale Power, LLC

{{

}}2(a),(c)

Figure K-60 In-Structure Response Spectra, Z Input, Node 352370, Mid-Span of North Slab at between Grid Lines RX-4 and RX-5 at El 125’

© Copyright 2019 by NuScale Power, LLC

{{

}}2(a),(c)

Figure K-61 In-Structure Response Spectra, X Input, Node 351696, Northeast Corner of Bio Shield

© Copyright 2019 by NuScale Power, LLC

{{

}}2(a),(c)

Figure K-62 In-Structure Response Spectra, Y Input, Node 351696, Northeast Corner of Bio Shield

© Copyright 2019 by NuScale Power, LLC

{{

}}2(a),(c)

Figure K-63 In-Structure Response Spectra, Z Input, Node 351696, Northeast Corner of Bio Shield

© Copyright 2019 by NuScale Power, LLC

{{

}}2(a),(c)

Figure K-64 In-Structure Response Spectra, X Input, Node 392329, Top of Roof at Grid Line RX-1

© Copyright 2019 by NuScale Power, LLC

{{

}}2(a),(c)

Figure K-65 In-Structure Response Spectra, Y Input, Node 392329, Top of Roof at Grid Line RX-1

© Copyright 2019 by NuScale Power, LLC

{{

}}2(a),(c)

Figure K-66 In-Structure Response Spectra, Z Input, Node 392329, Top of Roof at Grid Line RX-1

© Copyright 2019 by NuScale Power, LLC

{{

}}2(a),(c)

Figure K-67 In-Structure Response Spectra, X Input, Node 392378, Roof Slab between Grid Lines RX-4 and RX-5

© Copyright 2019 by NuScale Power, LLC

{{

}}2(a),(c)

Figure K-68 In-Structure Response Spectra, Y Input, Node 392378, Roof Slab between Grid Lines RX-4 and RX-5

© Copyright 2019 by NuScale Power, LLC

{{

}}2(a),(c)

Figure K-69 In-Structure Response Spectra, Z Input, Node 392378, Roof Slab between Grid Lines RX-4 and RX-5

© Copyright 2019 by NuScale Power, LLC

{{

}}2(a),(c)

Figure K-70 In-Structure Response Spectra, X Input, Node 394770, Northeast Corner of Roof Slab

© Copyright 2019 by NuScale Power, LLC

{{

}}2(a),(c)

Figure K-71 In-Structure Response Spectra, Y Input, Node 394770, Northeast Corner of Roof Slab

© Copyright 2019 by NuScale Power, LLC

{{

}}2(a),(c)

Figure K-72 In-Structure Response Spectra, Z Input, Node 394770, Northeast Corner of Roof Slab

© Copyright 2019 by NuScale Power, LLC

{{

}}2(a),(c)

Figure K-73 In-Structure Response Spectra, X Input, Node 8216, RXM-1 West Lug

© Copyright 2019 by NuScale Power, LLC

{{

}}2(a),(c)

Figure K-74 In-Structure Response Spectra, Y Input, Node 8216, RXM-1 West Lug

© Copyright 2019 by NuScale Power, LLC

{{

}}2(a),(c)

Figure K-75 In-Structure Response Spectra, Z Input, Node 8216, RXM-1 West Lug

© Copyright 2019 by NuScale Power, LLC

{{

}}2(a),(c)

Figure K-76 In-Structure Response Spectra, X Input, Node 8215, RXM-1 North Lug

© Copyright 2019 by NuScale Power, LLC

{{

}}2(a),(c)

Figure K-77 In-Structure Response Spectra, Y Input, Node 8215, RXM-1 North Lug

© Copyright 2019 by NuScale Power, LLC

{{

}}2(a),(c)

Figure K-78 In-Structure Response Spectra, Z Input, Node 8215, RXM-1 North Lug

© Copyright 2019 by NuScale Power, LLC

{{

}}2(a),(c)

Figure K-79 In-Structure Response Spectra, X Input, Node 8214, RXM-1 East Lug

© Copyright 2019 by NuScale Power, LLC

{{

}}2(a),(c)

Figure K-80 In-Structure Response Spectra, Y Input, Node 8214, RXM-1 East Lug

© Copyright 2019 by NuScale Power, LLC

{{

}}2(a),(c)

Figure K-81 In-Structure Response Spectra, Z Input, Node 8214, RXM-1 East Lug

© Copyright 2019 by NuScale Power, LLC

{{

}}2(a),(c)

Figure K-82 In-Structure Response Spectra, X Input, Node 1900, RXM-1 Top

© Copyright 2019 by NuScale Power, LLC

{{

}}2(a),(c)

Figure K-83 In-Structure Response Spectra, Y Input, Node 1900, RXM-1 Top

© Copyright 2019 by NuScale Power, LLC

{{

}}2(a),(c)

Figure K-84 In-Structure Response Spectra, Z Input, Node 1900, RXM-1 Top

© Copyright 2019 by NuScale Power, LLC

{{

}}2(a),(c)

Figure K-85 In-Structure Response Spectra, X Input, Node 49356, RXM-6 West Lug

© Copyright 2019 by NuScale Power, LLC

{{

}}2(a),(c)

Figure K-86 In-Structure Response Spectra, Y Input, Node 49356, RXM-6 West Lug

© Copyright 2019 by NuScale Power, LLC

{{

}}2(a),(c)

Figure K-87 In-Structure Response Spectra, Z Input, Node 49356, RXM-6 West Lug

© Copyright 2019 by NuScale Power, LLC

{{

}}2(a),(c)

Figure K-88 In-Structure Response Spectra, X Input, Node 49355, RXM-6 North Lug

© Copyright 2019 by NuScale Power, LLC

{{

}}2(a),(c)

Figure K-89 In-Structure Response Spectra, Y Input, Node 49355, RXM-6 North Lug

© Copyright 2019 by NuScale Power, LLC

{{

}}2(a),(c)

Figure K-90 In-Structure Response Spectra, Z Input, Node 49355, RXM-6 North Lug

© Copyright 2019 by NuScale Power, LLC

{{

}}2(a),(c)

Figure K-91 In-Structure Response Spectra, X Input, Node 49354, RXM-6 East Lug

© Copyright 2019 by NuScale Power, LLC

{{

}}2(a),(c)

Figure K-92 In-Structure Response Spectra, Y Input, Node 49354, RXM-6 East Lug

© Copyright 2019 by NuScale Power, LLC

{{

}}2(a),(c)

Figure K-93 In-Structure Response Spectra, Z Input, Node 49354, RXM-6 East Lug

© Copyright 2019 by NuScale Power, LLC

{{

}}2(a),(c)

Figure K-94 In-Structure Response Spectra, X Input, Node 43040, RXM-6 Top

© Copyright 2019 by NuScale Power, LLC

{{

}}2(a),(c)

Figure K-95 In-Structure Response Spectra, Y Input, Node 43040, RXM-6 Top

© Copyright 2019 by NuScale Power, LLC

{{

}}2(a),(c)

Figure K-96 In-Structure Response Spectra, Z Input, Node 43040, RXM-6 Top

© Copyright 2019 by NuScale Power, LLC

Appendix L. Example 4, Fluid Pressure Transfer Functions

The following plots have a title on the plot legend that consists of the node number followed by two letters. The first letter corresponds to the direction of ground motion or input. The second letter, ’P’ corresponds to pressure response. The top plot on each page corresponds to input in the X direction, the center plot corresponds to input in the Y direction, and the bottom plot corresponds to input in the Z direction.

X is East, Y is North and Z is up.

© Copyright 2019 by NuScale Power, LLC

{{

}}2(a),(c)

Figure L-1 Wingwall Pressure Transfer Functions at Node 87499

© Copyright 2019 by NuScale Power, LLC

{{

}}2(a),(c)

Figure L-2 Wingwall Pressure Transfer Functions at Node 95777

© Copyright 2019 by NuScale Power, LLC

{{

}}2(a),(c)

Figure L-3 Wingwall Pressure Transfer Functions at Node 87960

© Copyright 2019 by NuScale Power, LLC

{{

}}2(a),(c)

Figure L-4 Wingwall Pressure Transfer Functions at Node 96376

© Copyright 2019 by NuScale Power, LLC

{{

}}2(a),(c)

Figure L-5 Wingwall Pressure Transfer Functions at Node 89399

© Copyright 2019 by NuScale Power, LLC

{{

}}2(a),(c)

Figure L-6 Wingwall Pressure Transfer Functions at Node 97727

© Copyright 2019 by NuScale Power, LLC

Appendix M. Example 4, Fluid Pressure Time Histories

The following plots have a title on the plot legend that consists of the node number followed by two letters. The first letter corresponds to the direction of ground motion or input. The second letter, ’P’ corresponds to pressure response. The top plot on each page corresponds to input in the X direction, the center plot corresponds to input in the Y direction, and the bottom plot corresponds to input in the Z direction.

X is East, Y is North and Z is up.

© Copyright 2019 by NuScale Power, LLC

{{

}}2(a),(c)

Figure M-1 Wingwall Pressure Time Histories at Node 87499

© Copyright 2019 by NuScale Power, LLC

{{

}}2(a),(c)

Figure M-2 Wingwall Pressure Time Histories at Node 95777

© Copyright 2019 by NuScale Power, LLC

{{

}}2(a),(c)

Figure M-3 Wingwall Pressure Time Histories at Node 87960

© Copyright 2019 by NuScale Power, LLC

{{

}}2(a),(c)

Figure M-4 Wingwall Pressure Time Histories at Node 96376

© Copyright 2019 by NuScale Power, LLC

{{

}}2(a),(c)

Figure M-5 Wingwall Pressure Time Histories at Node 89399

© Copyright 2019 by NuScale Power, LLC

{{

}}2(a),(c)

Figure M-6 Wingwall Pressure Time Histories at Node 97727

© Copyright 2019 by NuScale Power, LLC

Appendix N. Example 4, Relative Displacement Transfer Functions

The following plots have a title on the plot legend that consists of the node number followed by two letters. The first letter corresponds to the direction of ground motion or input. The second letter corresponds to the response direction or output.

Results on a given page correspond to a common input direction, i.e. X, Y or Z. The top plot corresponds to output in the X direction, the center plot corresponds to output in the Y direction, and the bottom plot corresponds to output in the Z direction.

X is East, Y is North and Z is up.

© Copyright 2019 by NuScale Power, LLC

{{

}}2(a),(c)

Figure N-1 Relative Displacement TF, X Input, Node 120933, Northwest Corner on Top of Basemat

© Copyright 2019 by NuScale Power, LLC

{{

}}2(a),(c)

Figure N-2 Relative Displacement TF, Y Input, Node 120933, Northwest Corner on Top of Basemat

© Copyright 2019 by NuScale Power, LLC

{{

}}2(a),(c)

Figure N-3 Relative Displacement TF, Z Input, Node 120933, Northwest Corner on Top of Basemat

© Copyright 2019 by NuScale Power, LLC

{{

}}2(a),(c)

Figure N-4 Relative Displacement TF, X Input, Node 120978, Mid-Span of North Exterior Wall on Top of Basemat

© Copyright 2019 by NuScale Power, LLC

{{

}}2(a),(c)

Figure N-5 Relative Displacement TF, Y Input, Node 120978, Mid-Span of North Exterior Wall on Top of Basemat

© Copyright 2019 by NuScale Power, LLC

{{

}}2(a),(c)

Figure N-6 Relative Displacement TF, Z Input, Node 120978, Mid-Span of North Exterior Wall on Top of Basemat

© Copyright 2019 by NuScale Power, LLC

{{

}}2(a),(c)

Figure N-7 Relative Displacement TF, X Input, Node 121053, Northeast Corner on Top of Basemat

© Copyright 2019 by NuScale Power, LLC

{{

}}2(a),(c)

Figure N-8 Relative Displacement TF, Y Input, Node 121053, Northeast Corner on Top of Basemat

© Copyright 2019 by NuScale Power, LLC

{{

}}2(a),(c)

Figure N-9 Relative Displacement TF, Z Input, Node 121053, Northeast Corner on Top of Basemat

© Copyright 2019 by NuScale Power, LLC

{{

}}2(a),(c)

Figure N-10 Relative Displacement TF, X Input, Node 4914, RXM 1 Floor Node under Module

© Copyright 2019 by NuScale Power, LLC

{{

}}2(a),(c)

Figure N-11 Relative Displacement TF, Y Input, Node 4914, RXM 1 Floor Node under Module

© Copyright 2019 by NuScale Power, LLC

{{

}}2(a),(c)

Figure N-12 Relative Displacement TF, Z Input, Node 4914, RXM 1 Floor Node under Module

© Copyright 2019 by NuScale Power, LLC

{{

}}2(a),(c)

Figure N-13 Relative Displacement TF, X Input, Node 46054, RXM 6 Floor Node under Module

© Copyright 2019 by NuScale Power, LLC

{{

}}2(a),(c)

Figure N-14 Relative Displacement TF, Y Input, Node 46054, RXM 6 Floor Node under Module

© Copyright 2019 by NuScale Power, LLC

{{

}}2(a),(c)

Figure N-15 Relative Displacement TF, Z Input, Node 46054, RXM 6 Floor Node under Module

© Copyright 2019 by NuScale Power, LLC

{{

}}2(a),(c)

Figure N-16 Relative Displacement TF, X Input, Node 185505, Northwest Corner at El. 50’

© Copyright 2019 by NuScale Power, LLC

{{

}}2(a),(c)

Figure N-17 Relative Displacement TF, Y Input, Node 185505, Northwest Corner at El. 50’

© Copyright 2019 by NuScale Power, LLC

{{

}}2(a),(c)

Figure N-18 Relative Displacement TF, Z Input, Node 185505, Northwest Corner at El. 50’

© Copyright 2019 by NuScale Power, LLC

{{

}}2(a),(c)

Figure N-19 Relative Displacement TF, X Input, Node 182529, Mid-Span of West Slab along Grid Line RX-C at El. 50’

© Copyright 2019 by NuScale Power, LLC

{{

}}2(a),(c)

Figure N-20 Relative Displacement TF, Y Input, Node 182529, Mid-Span of West Slab along Grid Line RX-C at El. 50’

© Copyright 2019 by NuScale Power, LLC

{{

}}2(a),(c)

Figure N-21 Relative Displacement TF, Z Input, Node 182529, Mid-Span of West Slab along Grid Line RX-C at El. 50’

© Copyright 2019 by NuScale Power, LLC

{{

}}2(a),(c)

Figure N-22 Relative Displacement TF, X Input, Node 184359, Edge of Slab at Grid Line RX-4 at El. 50’

© Copyright 2019 by NuScale Power, LLC

{{

}}2(a),(c)

Figure N-23 Relative Displacement TF, Y Input, Node 184359, Edge of Slab at Grid Line RX-4 at El. 50’

© Copyright 2019 by NuScale Power, LLC

{{

}}2(a),(c)

Figure N-24 Relative Displacement TF, Z Input, Node 184359, Edge of Slab at Grid Line RX-4 at El. 50’

© Copyright 2019 by NuScale Power, LLC

{{

}}2(a),(c)

Figure N-25 Relative Displacement TF, X Input, Node 185174, Mid-Span of North Slab between Grid Lines RX-4 and RX-5 at El. 50’

© Copyright 2019 by NuScale Power, LLC

{{

}}2(a),(c)

Figure N-26 Relative Displacement TF, Y Input, Node 185174, Mid-Span of North Slab between Grid Lines RX-4 and RX-5 at El. 50’

© Copyright 2019 by NuScale Power, LLC

{{

}}2(a),(c)

Figure N-27 Relative Displacement TF, Z Input, Node 185174, Mid-Span of North Slab between Grid Lines RX-4 and RX-5 at El. 50’

© Copyright 2019 by NuScale Power, LLC

{{

}}2(a),(c)

Figure N-28 Relative Displacement TF, X Input, Node 185623, Northeast Corner at El. 50’

© Copyright 2019 by NuScale Power, LLC

{{

}}2(a),(c)

Figure N-29 Relative Displacement TF, Y Input, Node 185623, Northeast Corner at El. 50’

© Copyright 2019 by NuScale Power, LLC

{{

}}2(a),(c)

Figure N-30 Relative Displacement TF, Z Input, Node 185623, Northeast Corner at El. 50’

© Copyright 2019 by NuScale Power, LLC

{{

}}2(a),(c)

Figure N-31 Relative Displacement TF, X Input, Node 255527, Northwest Corner at El. 75’

© Copyright 2019 by NuScale Power, LLC

{{

}}2(a),(c)

Figure N-32 Relative Displacement TF, Y Input, Node 255527, Northwest Corner at El. 75’

© Copyright 2019 by NuScale Power, LLC

{{

}}2(a),(c)

Figure N-33 Relative Displacement TF, Z Input, Node 255527, Northwest Corner at El. 75’

© Copyright 2019 by NuScale Power, LLC

{{

}}2(a),(c)

Figure N-34 Relative Displacement TF, X Input, Node 255195, Mid-Span of North Slab between Grid Lines RX-4 and RX-5 at El. 75’

© Copyright 2019 by NuScale Power, LLC

{{

}}2(a),(c)

Figure N-35 Relative Displacement TF, Y Input, Node 255195, Mid-Span of North Slab between Grid Lines RX-4 and RX-5 at El. 75’

© Copyright 2019 by NuScale Power, LLC

{{

}}2(a),(c)

Figure N-36 Relative Displacement TF, Z Input, Node 255195, Mid-Span of North Slab between Grid Lines RX-4 and RX-5 at El. 75’

© Copyright 2019 by NuScale Power, LLC

{{

}}2(a),(c)

Figure N-37 Relative Displacement TF, X Input, Node 254481, Edge of East Slab along Grid Line RX-6 at El. 75’

© Copyright 2019 by NuScale Power, LLC

{{

}}2(a),(c)

Figure N-38 Relative Displacement TF, Y Input, Node 254481, Edge of East Slab along Grid Line RX-6 at El. 75’

© Copyright 2019 by NuScale Power, LLC

{{

}}2(a),(c)

Figure N-39 Relative Displacement TF, Z Input, Node 254481, Edge of East Slab along Grid Line RX-6 at El. 75’

© Copyright 2019 by NuScale Power, LLC

{{

}}2(a),(c)

Figure N-40 Relative Displacement TF, X Input, Node 332235, Northwest Corner of Exterior Wall at El 100’

© Copyright 2019 by NuScale Power, LLC

{{

}}2(a),(c)

Figure N-41 Relative Displacement TF, Y Input, Node 332235, Northwest Corner of Exterior Wall at El 100’

© Copyright 2019 by NuScale Power, LLC

{{

}}2(a),(c)

Figure N-42 Relative Displacement TF, Z Input, Node 332235, Northwest Corner of Exterior Wall at El 100’

© Copyright 2019 by NuScale Power, LLC

{{

}}2(a),(c)

Figure N-43 Relative Displacement TF, X Input, Node 331936, Mid-Span of North Slab between Grid Lines RX-4 and RX-5 at El 100’

© Copyright 2019 by NuScale Power, LLC

{{

}}2(a),(c)

Figure N-44 Relative Displacement TF, Y Input, Node 331936, Mid-Span of North Slab between Grid Lines RX-4 and RX-5 at El 100’

© Copyright 2019 by NuScale Power, LLC

{{

}}2(a),(c)

Figure N-45 Relative Displacement TF, Z Input, Node 331936, Mid-Span of North Slab between Grid Lines RX-4 and RX-5 at El 100’

© Copyright 2019 by NuScale Power, LLC

{{

}}2(a),(c)

Figure N-46 Relative Displacement TF, X Input, Node 331222, Edge of North Slab along Grid Line RX-4 at El 100’

© Copyright 2019 by NuScale Power, LLC

{{

}}2(a),(c)

Figure N-47 Relative Displacement TF, Y Input, Node 331222, Edge of North Slab along Grid Line RX-4 at El 100’

© Copyright 2019 by NuScale Power, LLC

{{

}}2(a),(c)

Figure N-48 Relative Displacement TF, Z Input, Node 331222, Edge of North Slab along Grid Line RX-4 at El 100’

© Copyright 2019 by NuScale Power, LLC

{{

}}2(a),(c)

Figure N-49 Relative Displacement TF, X Input, Node 331292, Edge of East Slab along Grid Line RX-6 at El 100’

© Copyright 2019 by NuScale Power, LLC

{{

}}2(a),(c)

Figure N-50 Relative Displacement TF, Y Input, Node 331292, Edge of East Slab along Grid Line RX-6 at El 100’

© Copyright 2019 by NuScale Power, LLC

{{

}}2(a),(c)

Figure N-51 Relative Displacement TF, Z Input, Node 331292, Edge of East Slab along Grid Line RX-6 at El 100’

© Copyright 2019 by NuScale Power, LLC

{{

}}2(a),(c)

Figure N-52 Relative Displacement TF, X Input, Node 352669, Northwest Corner of Exterior Wall at El 125’

© Copyright 2019 by NuScale Power, LLC

{{

}}2(a),(c)

Figure N-53 Relative Displacement TF, Y Input, Node 352669, Northwest Corner of Exterior Wall at El 125’

© Copyright 2019 by NuScale Power, LLC

{{

}}2(a),(c)

Figure N-54 Relative Displacement TF, Z Input, Node 352669, Northwest Corner of Exterior Wall at El 125’

© Copyright 2019 by NuScale Power, LLC

{{

}}2(a),(c)

Figure N-55 Relative Displacement TF, X Input, Node 351629, Northwest Corner of Bio Shield

© Copyright 2019 by NuScale Power, LLC

{{

}}2(a),(c)

Figure N-56 Relative Displacement TF, Y Input, Node 351629, Northwest Corner of Bio Shield

© Copyright 2019 by NuScale Power, LLC

{{

}}2(a),(c)

Figure N-57 Relative Displacement TF, Z Input, Node 351629, Northwest Corner of Bio Shield

© Copyright 2019 by NuScale Power, LLC

{{

}}2(a),(c)

Figure N-58 Relative Displacement TF, X Input, Node 352370, Mid-Span of North Slab at between Grid Lines RX-4 and RX-5 at El 125’

© Copyright 2019 by NuScale Power, LLC

{{

}}2(a),(c)

Figure N-59 Relative Displacement TF, Y Input, Node 352370, Mid-Span of North Slab at between Grid Lines RX-4 and RX-5 at El 125’

© Copyright 2019 by NuScale Power, LLC

{{

}}2(a),(c)

Figure N-60 Relative Displacement TF, Z Input, Node 352370, Mid-Span of North Slab at between Grid Lines RX-4 and RX-5 at El 125’

© Copyright 2019 by NuScale Power, LLC

{{

}}2(a),(c)

Figure N-61 Relative Displacement TF, X Input, Node 351696, Northeast Corner of Bio Shield

© Copyright 2019 by NuScale Power, LLC

{{

}}2(a),(c)

Figure N-62 Relative Displacement TF, Y Input, Node 351696, Northeast Corner of Bio Shield

© Copyright 2019 by NuScale Power, LLC

{{

}}2(a),(c)

Figure N-63 Relative Displacement TF, Z Input, Node 351696, Northeast Corner of Bio Shield

© Copyright 2019 by NuScale Power, LLC

{{

}}2(a),(c)

Figure N-64 Relative Displacement TF, X Input, Node 392329, Top of Roof at Grid Line RX-1

© Copyright 2019 by NuScale Power, LLC

{{

}}2(a),(c)

Figure N-65 Relative Displacement TF, Y Input, Node 392329, Top of Roof at Grid Line RX-1

© Copyright 2019 by NuScale Power, LLC

{{

}}2(a),(c)

Figure N-66 Relative Displacement TF, Z Input, Node 392329, Top of Roof at Grid Line RX-1

© Copyright 2019 by NuScale Power, LLC

{{

}}2(a),(c)

Figure N-67 Relative Displacement TF, X Input, Node 392378, Roof Slab between Grid Lines RX-4 and RX-5

© Copyright 2019 by NuScale Power, LLC

{{

}}2(a),(c)

Figure N-68 Relative Displacement TF, Y Input, Node 392378, Roof Slab between Grid Lines RX-4 and RX-5

© Copyright 2019 by NuScale Power, LLC

{{

}}2(a),(c)

Figure N-69 Relative Displacement TF, Z Input, Node 392378, Roof Slab between Grid Lines RX-4 and RX-5

© Copyright 2019 by NuScale Power, LLC

{{

}}2(a),(c)

Figure N-70 Relative Displacement TF, X Input, Node 394770, Northeast Corner of Roof Slab

© Copyright 2019 by NuScale Power, LLC

{{

}}2(a),(c)

Figure N-71 Relative Displacement TF, Y Input, Node 394770, Northeast Corner of Roof Slab

© Copyright 2019 by NuScale Power, LLC

{{

}}2(a),(c)

Figure N-72 Relative Displacement TF, Z Input, Node 394770, Northeast Corner of Roof Slab

© Copyright 2019 by NuScale Power, LLC

{{

}}2(a),(c)

Figure N-73 Relative Displacement TF, X Input, Node 8216, RXM-1 West Lug

© Copyright 2019 by NuScale Power, LLC

{{

}}2(a),(c)

Figure N-74 Relative Displacement TF, Y Input, Node 8216, RXM-1 West Lug

© Copyright 2019 by NuScale Power, LLC

{{

}}2(a),(c)

Figure N-75 Relative Displacement TF, Z Input, Node 8216, RXM-1 West Lug

© Copyright 2019 by NuScale Power, LLC

{{

}}2(a),(c)

Figure N-76 Relative Displacement TF, X Input, Node 8215, RXM-1 North Lug

© Copyright 2019 by NuScale Power, LLC

{{

}}2(a),(c)

Figure N-77 Relative Displacement TF, Y Input, Node 8215, RXM-1 North Lug

© Copyright 2019 by NuScale Power, LLC

{{

}}2(a),(c)

Figure N-78 Relative Displacement TF, Z Input, Node 8215, RXM-1 North Lug

© Copyright 2019 by NuScale Power, LLC

{{

}}2(a),(c)

Figure N-79 Relative Displacement TF, X Input, Node 8214, RXM-1 East Lug

© Copyright 2019 by NuScale Power, LLC

{{

}}2(a),(c)

Figure N-80 Relative Displacement TF, Y Input, Node 8214, RXM-1 East Lug

© Copyright 2019 by NuScale Power, LLC

{{

}}2(a),(c)

Figure N-81 Relative Displacement TF, Z Input, Node 8214, RXM-1 East Lug

© Copyright 2019 by NuScale Power, LLC

{{

}}2(a),(c)

Figure N-82 Relative Displacement TF, X Input, Node 1900, RXM-1 Top

© Copyright 2019 by NuScale Power, LLC

{{

}}2(a),(c)

Figure N-83 Relative Displacement TF, Y Input, Node 1900, RXM-1 Top

© Copyright 2019 by NuScale Power, LLC

{{

}}2(a),(c)

Figure N-84 Relative Displacement TF, Z Input, Node 1900, RXM-1 Top

© Copyright 2019 by NuScale Power, LLC

{{

}}2(a),(c)

Figure N-85 Relative Displacement TF, X Input, Node 49356, RXM-6 West Lug

© Copyright 2019 by NuScale Power, LLC

{{

}}2(a),(c)

Figure N-86 Relative Displacement TF, Y Input, Node 49356, RXM-6 West Lug

© Copyright 2019 by NuScale Power, LLC

{{

}}2(a),(c)

Figure N-87 Relative Displacement TF, Z Input, Node 49356, RXM-6 West Lug

© Copyright 2019 by NuScale Power, LLC

{{

}}2(a),(c)

Figure N-88 Relative Displacement TF, X Input, Node 49355, RXM-6 North Lug

© Copyright 2019 by NuScale Power, LLC

{{

}}2(a),(c)

Figure N-89 Relative Displacement TF, Y Input, Node 49355, RXM-6 North Lug

© Copyright 2019 by NuScale Power, LLC

{{

}}2(a),(c)

Figure N-90 Relative Displacement TF, Z Input, Node 49355, RXM-6 North Lug

© Copyright 2019 by NuScale Power, LLC

{{

}}2(a),(c)

Figure N-91 Relative Displacement TF, X Input, Node 49354, RXM-6 East Lug

© Copyright 2019 by NuScale Power, LLC

{{

}}2(a),(c)

Figure N-92 Relative Displacement TF, Y Input, Node 49354, RXM-6 East Lug

© Copyright 2019 by NuScale Power, LLC

{{

}}2(a),(c)

Figure N-93 Relative Displacement TF, Z Input, Node 49354, RXM-6 East Lug

© Copyright 2019 by NuScale Power, LLC

{{

}}2(a),(c)

Figure N-94 Relative Displacement TF, X Input, Node 43040, RXM-6 Top

© Copyright 2019 by NuScale Power, LLC

{{

}}2(a),(c)

Figure N-95 Relative Displacement TF, Y Input, Node 43040, RXM-6 Top

© Copyright 2019 by NuScale Power, LLC

{{

}}2(a),(c)

Figure N-96 Relative Displacement TF, Z Input, Node 43040, RXM-6 Top

© Copyright 2019 by NuScale Power, LLC

Appendix O. Example 4, Relative Displacement Time Histories

The following plots have a title on the plot legend that consists of the node number followed by two letters. The first letter corresponds to the direction of ground motion or input. The second letter corresponds to the response direction or output.

Results on a given page correspond to a common input direction, i.e. X, Y or Z. The top plot corresponds to output in the X direction, the center plot corresponds to output in the Y direction, and the bottom plot corresponds to output in the Z direction.

X is East, Y is North and Z is up.

© Copyright 2019 by NuScale Power, LLC

{{

}}2(a),(c)

Figure O-1 Relative Displacement TH, X Input, Node 120933, Northwest Corner on Top of Basemat

© Copyright 2019 by NuScale Power, LLC

{{

}}2(a),(c)

Figure O-2 Relative Displacement TH, Y Input, Node 120933, Northwest Corner on Top of Basemat

© Copyright 2019 by NuScale Power, LLC

{{

}}2(a),(c)

Figure O-3 Relative Displacement TH, Z Input, Node 120933, Northwest Corner on Top of Basemat

© Copyright 2019 by NuScale Power, LLC

{{

}}2(a),(c)

Figure O-4 Relative Displacement TH, X Input, Node 120978, Mid-Span of North Exterior Wall on Top of Basemat

© Copyright 2019 by NuScale Power, LLC

{{

}}2(a),(c)

Figure O-5 Relative Displacement TH, Y Input, Node 120978, Mid-Span of North Exterior Wall on Top of Basemat

© Copyright 2019 by NuScale Power, LLC

{{

}}2(a),(c)

Figure O-6 Relative Displacement TH, Z Input, Node 120978, Mid-Span of North Exterior Wall on Top of Basemat

© Copyright 2019 by NuScale Power, LLC

{{

}}2(a),(c)

Figure O-7 Relative Displacement TH, X Input, Node 121053, Northeast Corner on Top of Basemat

© Copyright 2019 by NuScale Power, LLC

{{

}}2(a),(c)

Figure O-8 Relative Displacement TH, Y Input, Node 121053, Northeast Corner on Top of Basemat

© Copyright 2019 by NuScale Power, LLC

{{

}}2(a),(c)

Figure O-9 Relative Displacement TH, Z Input, Node 121053, Northeast Corner on Top of Basemat

© Copyright 2019 by NuScale Power, LLC

{{

}}2(a),(c)

Figure O-10 Relative Displacement TH, X Input, Node 4914, RXM 1 Floor Node under Module

© Copyright 2019 by NuScale Power, LLC

{{

}}2(a),(c)

Figure O-11 Relative Displacement TH, Y Input, Node 4914, RXM 1 Floor Node under Module

© Copyright 2019 by NuScale Power, LLC

{{

}}2(a),(c)

Figure O-12 Relative Displacement TH, Z Input, Node 4914, RXM 1 Floor Node under Module

© Copyright 2019 by NuScale Power, LLC

{{

}}2(a),(c)

Figure O-13 Relative Displacement TH, X Input, Node 46054, RXM 6 Floor Node under Module

© Copyright 2019 by NuScale Power, LLC

{{

}}2(a),(c)

Figure O-14 Relative Displacement TH, Y Input, Node 46054, RXM 6 Floor Node under Module

© Copyright 2019 by NuScale Power, LLC

{{

}}2(a),(c)

Figure O-15 Relative Displacement TH, Z Input, Node 46054, RXM 6 Floor Node under Module

© Copyright 2019 by NuScale Power, LLC

{{

}}2(a),(c)

Figure O-16 Relative Displacement TH, X Input, Node 185505, Northwest Corner at El. 50’

© Copyright 2019 by NuScale Power, LLC

{{

}}2(a),(c)

Figure O-17 Relative Displacement TH, Y Input, Node 185505, Northwest Corner at El. 50’

© Copyright 2019 by NuScale Power, LLC

{{

}}2(a),(c)

Figure O-18 Relative Displacement TH, Z Input, Node 185505, Northwest Corner at El. 50’

© Copyright 2019 by NuScale Power, LLC

{{

}}2(a),(c)

Figure O-19 Relative Displacement TH, X Input, Node 182529, Mid-Span of West Slab along Grid Line RX-C at El. 50’

© Copyright 2019 by NuScale Power, LLC

{{

}}2(a),(c)

Figure O-20 Relative Displacement TH, Y Input, Node 182529, Mid-Span of West Slab along Grid Line RX-C at El. 50’

© Copyright 2019 by NuScale Power, LLC

{{

}}2(a),(c)

Figure O-21 Relative Displacement TH, Z Input, Node 182529, Mid-Span of West Slab along Grid Line RX-C at El. 50’

© Copyright 2019 by NuScale Power, LLC

{{

}}2(a),(c)

Figure O-22 Relative Displacement TH, X Input, Node 184359, Edge of Slab at Grid Line RX-4 at El. 50’

© Copyright 2019 by NuScale Power, LLC

{{

}}2(a),(c)

Figure O-23 Relative Displacement TH, Y Input, Node 184359, Edge of Slab at Grid Line RX-4 at El. 50’

© Copyright 2019 by NuScale Power, LLC

{{

}}2(a),(c)

Figure O-24 Relative Displacement TH, Z Input, Node 184359, Edge of Slab at Grid Line RX-4 at El. 50’

© Copyright 2019 by NuScale Power, LLC

{{

}}2(a),(c)

Figure O-25 Relative Displacement TH, X Input, Node 185174, Mid-Span of North Slab between Grid Lines RX-4 and RX-5 at El. 50’

© Copyright 2019 by NuScale Power, LLC

{{

}}2(a),(c)

Figure O-26 Relative Displacement TH, Y Input, Node 185174, Mid-Span of North Slab between Grid Lines RX-4 and RX-5 at El. 50’

© Copyright 2019 by NuScale Power, LLC

{{

}}2(a),(c)

Figure O-27 Relative Displacement TH, Z Input, Node 185174, Mid-Span of North Slab between Grid Lines RX-4 and RX-5 at El. 50’

© Copyright 2019 by NuScale Power, LLC

{{

}}2(a),(c)

Figure O-28 Relative Displacement TH, X Input, Node 185623, Northeast Corner at El. 50’

© Copyright 2019 by NuScale Power, LLC

{{

}}2(a),(c)

Figure O-29 Relative Displacement TH, Y Input, Node 185623, Northeast Corner at El. 50’

© Copyright 2019 by NuScale Power, LLC

{{

}}2(a),(c)

Figure O-30 Relative Displacement TH, Z Input, Node 185623, Northeast Corner at El. 50’

© Copyright 2019 by NuScale Power, LLC

{{

}}2(a),(c)

Figure O-31 Relative Displacement TH, X Input, Node 255527, Northwest Corner at El. 75’

© Copyright 2019 by NuScale Power, LLC

{{

}}2(a),(c)

Figure O-32 Relative Displacement TH, Y Input, Node 255527, Northwest Corner at El. 75’

© Copyright 2019 by NuScale Power, LLC

{{

}}2(a),(c)

Figure O-33 Relative Displacement TH, Z Input, Node 255527, Northwest Corner at El. 75’

© Copyright 2019 by NuScale Power, LLC

{{

}}2(a),(c)

Figure O-34 Relative Displacement TH, X Input, Node 255195, Mid-Span of North Slab between Grid Lines RX-4 and RX-5 at El. 75’

© Copyright 2019 by NuScale Power, LLC

{{

}}2(a),(c)

Figure O-35 Relative Displacement TH, Y Input, Node 255195, Mid-Span of North Slab between Grid Lines RX-4 and RX-5 at El. 75’

© Copyright 2019 by NuScale Power, LLC

{{

}}2(a),(c)

Figure O-36 Relative Displacement TH, Z Input, Node 255195, Mid-Span of North Slab between Grid Lines RX-4 and RX-5 at El. 75’

© Copyright 2019 by NuScale Power, LLC

{{

}}2(a),(c)

Figure O-37 Relative Displacement TH, X Input, Node 254481, Edge of East Slab along Grid Line RX-6 at El. 75’

© Copyright 2019 by NuScale Power, LLC

{{

}}2(a),(c)

Figure O-38 Relative Displacement TH, Y Input, Node 254481, Edge of East Slab along Grid Line RX-6 at El. 75’

© Copyright 2019 by NuScale Power, LLC

{{

}}2(a),(c)

Figure O-39 Relative Displacement TH, Z Input, Node 254481, Edge of East Slab along Grid Line RX-6 at El. 75’

© Copyright 2019 by NuScale Power, LLC

{{

}}2(a),(c)

Figure O-40 Relative Displacement TH, X Input, Node 332235, Northwest Corner of Exterior Wall at El 100’

© Copyright 2019 by NuScale Power, LLC

{{

}}2(a),(c)

Figure O-41 Relative Displacement TH, Y Input, Node 332235, Northwest Corner of Exterior Wall at El 100’

© Copyright 2019 by NuScale Power, LLC

{{

}}2(a),(c)

Figure O-42 Relative Displacement TH, Z Input, Node 332235, Northwest Corner of Exterior Wall at El 100’

© Copyright 2019 by NuScale Power, LLC

{{

}}2(a),(c)

Figure O-43 Relative Displacement TH, X Input, Node 331936, Mid-Span of North Slab between Grid Lines RX-4 and RX-5 at El 100’

© Copyright 2019 by NuScale Power, LLC

{{

}}2(a),(c)

Figure O-44 Relative Displacement TH, Y Input, Node 331936, Mid-Span of North Slab between Grid Lines RX-4 and RX-5 at El 100’

© Copyright 2019 by NuScale Power, LLC

{{

}}2(a),(c)

Figure O-45 Relative Displacement TH, Z Input, Node 331936, Mid-Span of North Slab between Grid Lines RX-4 and RX-5 at El 100’

© Copyright 2019 by NuScale Power, LLC

{{

}}2(a),(c)

Figure O-46 Relative Displacement TH, X Input, Node 331222, Edge of North Slab along Grid Line RX-4 at El 100’

© Copyright 2019 by NuScale Power, LLC

{{

}}2(a),(c)

Figure O-47 Relative Displacement TH, Y Input, Node 331222, Edge of North Slab along Grid Line RX-4 at El 100’

© Copyright 2019 by NuScale Power, LLC

{{

}}2(a),(c)

Figure O-48 Relative Displacement TH, Z Input, Node 331222, Edge of North Slab along Grid Line RX-4 at El 100’

© Copyright 2019 by NuScale Power, LLC

{{

}}2(a),(c)

Figure O-49 Relative Displacement TH, X Input, Node 331292, Edge of East Slab along Grid Line RX-6 at El 100’

© Copyright 2019 by NuScale Power, LLC

{{

}}2(a),(c)

Figure O-50 Relative Displacement TH, Y Input, Node 331292, Edge of East Slab along Grid Line RX-6 at El 100’

© Copyright 2019 by NuScale Power, LLC

{{

}}2(a),(c)

Figure O-51 Relative Displacement TH, Z Input, Node 331292, Edge of East Slab along Grid Line RX-6 at El 100’

© Copyright 2019 by NuScale Power, LLC

{{

}}2(a),(c)

Figure O-52 Relative Displacement TH, X Input, Node 352669, Northwest Corner of Exterior Wall at El 125’

© Copyright 2019 by NuScale Power, LLC

{{

}}2(a),(c)

Figure O-53 Relative Displacement TH, Y Input, Node 352669, Northwest Corner of Exterior Wall at El 125’

© Copyright 2019 by NuScale Power, LLC

{{

}}2(a),(c)

Figure O-54 Relative Displacement TH, Z Input, Node 352669, Northwest Corner of Exterior Wall at El 125’

© Copyright 2019 by NuScale Power, LLC

{{

}}2(a),(c)

Figure O-55 Relative Displacement TH, X Input, Node 351629, Northwest Corner of Bio Shield

© Copyright 2019 by NuScale Power, LLC

{{

}}2(a),(c)

Figure O-56 Relative Displacement TH, Y Input, Node 351629, Northwest Corner of Bio Shield

© Copyright 2019 by NuScale Power, LLC

{{

}}2(a),(c)

Figure O-57 Relative Displacement TH, Z Input, Node 351629, Northwest Corner of Bio Shield

© Copyright 2019 by NuScale Power, LLC

{{

}}2(a),(c)

Figure O-58 Relative Displacement TH, X Input, Node 352370, Mid-Span of North Slab at between Grid Lines RX-4 and RX-5 at El 125’

© Copyright 2019 by NuScale Power, LLC

{{

}}2(a),(c)

Figure O-59 Relative Displacement TH, Y Input, Node 352370, Mid-Span of North Slab at between Grid Lines RX-4 and RX-5 at El 125’

© Copyright 2019 by NuScale Power, LLC

{{

}}2(a),(c)

Figure O-60 Relative Displacement TH, Z Input, Node 352370, Mid-Span of North Slab at between Grid Lines RX-4 and RX-5 at El 125’

© Copyright 2019 by NuScale Power, LLC

{{

}}2(a),(c)

Figure O-61 Relative Displacement TH, X Input, Node 351696, Northeast Corner of Bio Shield

© Copyright 2019 by NuScale Power, LLC

{{

}}2(a),(c)

Figure O-62 Relative Displacement TH, Y Input, Node 351696, Northeast Corner of Bio Shield

© Copyright 2019 by NuScale Power, LLC

{{

}}2(a),(c)

Figure O-63 Relative Displacement TH, Z Input, Node 351696, Northeast Corner of Bio Shield

© Copyright 2019 by NuScale Power, LLC

{{

}}2(a),(c)

Figure O-64 Relative Displacement TH, X Input, Node 392329, Top of Roof at Grid Line RX-1

© Copyright 2019 by NuScale Power, LLC

{{

}}2(a),(c)

Figure O-65 Relative Displacement TH, Y Input, Node 392329, Top of Roof at Grid Line RX-1

© Copyright 2019 by NuScale Power, LLC

{{

}}2(a),(c)

Figure O-66 Relative Displacement TH, Z Input, Node 392329, Top of Roof at Grid Line RX-1

© Copyright 2019 by NuScale Power, LLC

{{

}}2(a),(c)

Figure O-67 Relative Displacement TH, X Input, Node 392378, Roof Slab between Grid Lines RX-4 and RX-5

© Copyright 2019 by NuScale Power, LLC

{{

}}2(a),(c)

Figure O-68 Relative Displacement TH, Y Input, Node 392378, Roof Slab between Grid Lines RX-4 and RX-5

© Copyright 2019 by NuScale Power, LLC

{{

}}2(a),(c)

Figure O-69 Relative Displacement TH, Z Input, Node 392378, Roof Slab between Grid Lines RX-4 and RX-5

© Copyright 2019 by NuScale Power, LLC

{{

}}2(a),(c)

Figure O-70 Relative Displacement TH, X Input, Node 394770, Northeast Corner of Roof Slab

© Copyright 2019 by NuScale Power, LLC

{{

}}2(a),(c)

Figure O-71 Relative Displacement TH, Y Input, Node 394770, Northeast Corner of Roof Slab

© Copyright 2019 by NuScale Power, LLC

{{

}}2(a),(c)

Figure O-72 Relative Displacement TH, Z Input, Node 394770, Northeast Corner of Roof Slab

© Copyright 2019 by NuScale Power, LLC

{{

}}2(a),(c)

Figure O-73 Relative Displacement TH, X Input, Node 8216, RXM-1 West Lug

© Copyright 2019 by NuScale Power, LLC

{{

}}2(a),(c)

Figure O-74 Relative Displacement TH, Y Input, Node 8216, RXM-1 West Lug

© Copyright 2019 by NuScale Power, LLC

{{

}}2(a),(c)

Figure O-75 Relative Displacement TH, Z Input, Node 8216, RXM-1 West Lug

© Copyright 2019 by NuScale Power, LLC

{{

}}2(a),(c)

Figure O-76 Relative Displacement TH, X Input, Node 8215, RXM-1 North Lug

© Copyright 2019 by NuScale Power, LLC

{{

}}2(a),(c)

Figure O-77 Relative Displacement TH, Y Input, Node 8215, RXM-1 North Lug

© Copyright 2019 by NuScale Power, LLC

{{

}}2(a),(c)

Figure O-78 Relative Displacement TH, Z Input, Node 8215, RXM-1 North Lug

© Copyright 2019 by NuScale Power, LLC

{{

}}2(a),(c)

Figure O-79 Relative Displacement TH, X Input, Node 8214, RXM-1 East Lug

© Copyright 2019 by NuScale Power, LLC

{{

}}2(a),(c)

Figure O-80 Relative Displacement TH, Y Input, Node 8214, RXM-1 East Lug

© Copyright 2019 by NuScale Power, LLC

{{

}}2(a),(c)

Figure O-81 Relative Displacement TH, Z Input, Node 8214, RXM-1 East Lug

© Copyright 2019 by NuScale Power, LLC

{{

}}2(a),(c)

Figure O-82 Relative Displacement TH, X Input, Node 1900, RXM-1 Top

© Copyright 2019 by NuScale Power, LLC

{{

}}2(a),(c)

Figure O-83 Relative Displacement TH, Y Input, Node 1900, RXM-1 Top

© Copyright 2019 by NuScale Power, LLC

{{

}}2(a),(c)

Figure O-84 Relative Displacement TH, Z Input, Node 1900, RXM-1 Top

© Copyright 2019 by NuScale Power, LLC

{{

}}2(a),(c)

Figure O-85 Relative Displacement TH, X Input, Node 49356, RXM-6 West Lug

© Copyright 2019 by NuScale Power, LLC

{{

}}2(a),(c)

Figure O-86 Relative Displacement TH, Y Input, Node 49356, RXM-6 West Lug

© Copyright 2019 by NuScale Power, LLC

{{

}}2(a),(c)

Figure O-87 Relative Displacement TH, Z Input, Node 49356, RXM-6 West Lug

© Copyright 2019 by NuScale Power, LLC

{{

}}2(a),(c)

Figure O-88 Relative Displacement TH, X Input, Node 49355, RXM-6 North Lug

© Copyright 2019 by NuScale Power, LLC

{{

}}2(a),(c)

Figure O-89 Relative Displacement TH, Y Input, Node 49355, RXM-6 North Lug

© Copyright 2019 by NuScale Power, LLC

{{

}}2(a),(c)

Figure O-90 Relative Displacement TH, Z Input, Node 49355, RXM-6 North Lug

© Copyright 2019 by NuScale Power, LLC

{{

}}2(a),(c)

Figure O-91 Relative Displacement TH, X Input, Node 49354, RXM-6 East Lug

© Copyright 2019 by NuScale Power, LLC

{{

}}2(a),(c)

Figure O-92 Relative Displacement TH, Y Input, Node 49354, RXM-6 East Lug

© Copyright 2019 by NuScale Power, LLC

{{

}}2(a),(c)

Figure O-93 Relative Displacement TH, Z Input, Node 49354, RXM-6 East Lug

© Copyright 2019 by NuScale Power, LLC

{{

}}2(a),(c)

Figure O-94 Relative Displacement TH, X Input, Node 43040, RXM-6 Top

© Copyright 2019 by NuScale Power, LLC

{{

}}2(a),(c)

Figure O-95 Relative Displacement TH, Y Input, Node 43040, RXM-6 Top

© Copyright 2019 by NuScale Power, LLC

{{

}}2(a),(c)

Figure O-96 Relative Displacement TH, Z Input, Node 43040, RXM-6 Top

© Copyright 2019 by NuScale Power, LLC

Appendix P. Example 4, RXM Lug Force Transfer Functions

The following plots have a title on the plot legend that consists of a Lug identifier followed by two letters. The first letter corresponds to the direction of ground motion or input. The second letter corresponds to the response direction or output.

X is East, Y is North and Z is up. The East and West Lugs resist motion in the Y or North-South Directions. The North Lugs resist motion in the X or East-West Directions. The top plot on each page corresponds to X direction input motion, the center plot corresponds to Y direction input motion, and the bottom plot corresponds to Z direction input motion.

© Copyright 2019 by NuScale Power, LLC

{{

}}2(a),(c)

Figure P-1 RXM #1 West Lug, Force Transfer Functions

© Copyright 2019 by NuScale Power, LLC

{{

}}2(a),(c)

Figure P-2 RXM #1 North Lug, Force Transfer Functions

© Copyright 2019 by NuScale Power, LLC

{{

}}2(a),(c)

Figure P-3 RXM #1 East Lug, Force Transfer Functions

© Copyright 2019 by NuScale Power, LLC

{{

}}2(a),(c)

Figure P-4 RXM #6 West Lug, Force Transfer Functions

© Copyright 2019 by NuScale Power, LLC

{{

}}2(a),(c)

Figure P-5 RXM #6 North Lug, Force Transfer Functions

© Copyright 2019 by NuScale Power, LLC

{{

}}2(a),(c)

Figure P-6 RXM #6 East Lug, Force Transfer Functions

© Copyright 2019 by NuScale Power, LLC

Appendix Q. Example 4, RXM Lug Force Time Histories

The following plots have a title on the plot legend that consists of a Lug identifier followed by two letters. The first letter corresponds to the direction of ground motion or input. The second letter corresponds to the response direction or output.

X is East, Y is North and Z is up. The East and West Lugs resist motion in the Y or North-South Directions. The North Lugs resist motion in the X or East-West Directions. The top plot on each page corresponds to X direction input motion, the center plot corresponds to Y direction input motion, and the bottom plot corresponds to Z direction input motion.

© Copyright 2019 by NuScale Power, LLC

{{

}}2(a),(c)

Figure Q-1 RXM #1 West Lug, Force Time Histories

© Copyright 2019 by NuScale Power, LLC

{{

}}2(a),(c)

Figure Q-2 RXM #1 North Lug, Force Time Histories

© Copyright 2019 by NuScale Power, LLC

{{

}}2(a),(c)

Figure Q-3 RXM #1 East Lug, Force Time Histories

© Copyright 2019 by NuScale Power, LLC

{{

}}2(a),(c)

Figure Q-4 RXM #6 West Lug, Force Time Histories

© Copyright 2019 by NuScale Power, LLC

{{

}}2(a),(c)

Figure Q-5 RXM #6 North Lug, Force Time Histories

© Copyright 2019 by NuScale Power, LLC

{{

}}2(a),(c)

Figure Q-6 RXM #6 East Lug, Force Time Histories

© Copyright 2019 by NuScale Power, LLC

Appendix R. Example 4, RXM Support Transfer Functions

The RXM base support section cuts have forces Fx, Fy and Fz along with moments Mx, My and Mz. The section cut plots have a title on the plot legend that consists of a cut identifier followed by two colon separated symbols. The first symbol corresponds to the direction of ground motion or input, X, Y or Z. The second symbol corresponds to the section cut force or moment.

X is East, Y is North and Z is up.

© Copyright 2019 by NuScale Power, LLC

{{

}}2(a),(c)

Figure R-1 Base Support for RXM 1, Force Fx TF

© Copyright 2019 by NuScale Power, LLC

{{

}}2(a),(c)

Figure R-2 Base Support for RXM 1, Force Fy TF

© Copyright 2019 by NuScale Power, LLC

{{

}}2(a),(c)

Figure R-3 Base Support for RXM 1, Force Fz TF

© Copyright 2019 by NuScale Power, LLC

{{

}}2(a),(c)

Figure R-4 Base Support for RXM 1, Moment Mx TF

© Copyright 2019 by NuScale Power, LLC

{{

}}2(a),(c)

Figure R-5 Base Support for RXM 1, Moment My TF

© Copyright 2019 by NuScale Power, LLC

{{

}}2(a),(c)

Figure R-6 Base Support for RXM 1, Moment Mz TF

© Copyright 2019 by NuScale Power, LLC

{{

}}2(a),(c)

Figure R-7 Base Support for RXM 6, Force Fx TF

© Copyright 2019 by NuScale Power, LLC

{{

}}2(a),(c)

Figure R-8 Base Support for RXM 6, Force Fy TF

© Copyright 2019 by NuScale Power, LLC

{{

}}2(a),(c)

Figure R-9 Base Support for RXM 6, Force Fz TF

© Copyright 2019 by NuScale Power, LLC

{{

}}2(a),(c)

Figure R-10 Base Support for RXM 6, Moment Mx TF

© Copyright 2019 by NuScale Power, LLC

{{

}}2(a),(c)

Figure R-11 Base Support for RXM 6, Moment My TF

© Copyright 2019 by NuScale Power, LLC

{{

}}2(a),(c)

Figure R-12 Base Support for RXM 6, Moment Mz TF

© Copyright 2019 by NuScale Power, LLC

Appendix S. Example 4, RXM Support Time Histories

The RXM base support section cuts have forces Fx, Fy and Fz along with moments Mx, My and Mz. The section cut plots have a title on the plot legend that consists of a cut identifier followed by two colon separated symbols. The first symbol corresponds to the direction of ground motion or input, X, Y or Z. The second symbol corresponds to the section cut force or moment.

X is East, Y is North and Z is up.

© Copyright 2019 by NuScale Power, LLC

{{

}}2(a),(c)

Figure S-1 Base Support for RXM 1, Force Fx Time Histories

© Copyright 2019 by NuScale Power, LLC

{{

}}2(a),(c)

Figure S-2 Base Support for RXM 1, Force Fy Time Histories

© Copyright 2019 by NuScale Power, LLC

{{

}}2(a),(c)

Figure S-3 Base Support for RXM 1, Force Fz Time Histories

© Copyright 2019 by NuScale Power, LLC

{{

}}2(a),(c)

Figure S-4 Base Support for RXM 1, Moment Mx Time Histories

© Copyright 2019 by NuScale Power, LLC

{{

}}2(a),(c)

Figure S-5 Base Support for RXM 1, Moment My Time Histories

© Copyright 2019 by NuScale Power, LLC

{{

}}2(a),(c)

Figure S-6 Base Support for RXM 1, Moment Mz Time Histories

© Copyright 2019 by NuScale Power, LLC

{{

}}2(a),(c)

Figure S-7 Base Support for RXM 6, Force Fx Time Histories

© Copyright 2019 by NuScale Power, LLC

{{

}}2(a),(c)

Figure S-8 Base Support for RXM 6, Force Fy Time Histories

© Copyright 2019 by NuScale Power, LLC

{{

}}2(a),(c)

Figure S-9 Base Support for RXM 6, Force Fz Time Histories

© Copyright 2019 by NuScale Power, LLC

{{

}}2(a),(c)

Figure S-10 Base Support for RXM 6, Moment Mx Time Histories

© Copyright 2019 by NuScale Power, LLC

{{

}}2(a),(c)

Figure S-11 Base Support for RXM 6, Moment My Time Histories

© Copyright 2019 by NuScale Power, LLC

{{

}}2(a),(c)

Figure S-12 Base Support for RXM 6, Moment Mz Time Histories

© Copyright 2019 by NuScale Power, LLC

Enclosure 3:

Affidavit of Zackary W. Rad, AF-1119-67982

NuScale Power, LLC
1100 NE Circle Blvd., Suite 200 Corvallis, Oregon 97330 Office 541.360-0500 Fax 541.207.3928
www.nuscalepower.com

NuScale Power, LLC

AFFIDAVIT of Zackary W. Rad

I, Zackary W. Rad, state as follows:

(1) I am the Director of Regulatory Affairs of NuScale Power, LLC (NuScale), and as such, I have been specifically delegated the function of reviewing the information described in this Affidavit that NuScale seeks to have withheld from public disclosure, and am authorized to apply for its withholding on behalf of NuScale

(2) I am knowledgeable of the criteria and procedures used by NuScale in designating information as a trade secret, privileged, or as confidential commercial or financial information. This request to withhold information from public disclosure is driven by one or more of the following:

(a) The information requested to be withheld reveals distinguishing aspects of a process (or component, structure, tool, method, etc.) whose use by NuScale competitors, without a license from NuScale, would constitute a competitive economic disadvantage to NuScale.

(b) The information requested to be withheld consists of supporting data, including test data, relative to a process (or component, structure, tool, method, etc.), and the application of the data secures a competitive economic advantage, as described more fully in paragraph 3 of this Affidavit.

(c) Use by a competitor of the information requested to be withheld would reduce the competitor's expenditure of resources, or improve its competitive position, in the design, manufacture, shipment, installation, assurance of quality, or licensing of a similar product.

(d) The information requested to be withheld reveals cost or price information, production capabilities, budget levels, or commercial strategies of NuScale.

(e) The information requested to be withheld consists of patentable ideas.

(3) Public disclosure of the information sought to be withheld is likely to cause substantial harm to NuScale's competitive position and foreclose or reduce the availability of profit-making opportunities. The accompanying topical report reveals distinguishing aspects about the method by which NuScale develops its improvements in frequency domain soil-structure-fluid interaction analysis methodology.

NuScale has performed significant research and evaluation to develop a basis for this methodology and has invested significant resources, including the expenditure of a considerable sum of money.

The precise financial value of the information is difficult to quantify, but it is a key element of the design basis for a NuScale plant and, therefore, has substantial value to NuScale.

If the information were disclosed to the public, NuScales competitors would ha ve access to the information without purchasing the right to use it or having been required to undertake a similar expenditure of resources. Such disclosure would constitute a misappropriation of NuScales intellectual property, and would deprive NuScale of the opportunity to exercise its competitive advantage to seek an adequate return on its investment.

(4) The information sought to be withheld is in the enclosed topical report titled "Improvements in Frequency Domain Soil-Structure-Fluid Interaction Analysis." The enclosure contains the designation "Proprietary" at the top of each page containing proprietary information. The information considered by NuScale to be proprietary is identified within double braces, "{{ }}" in the document.

(5) The basis for proposing that the information be withheld is that NuScale treats the information as a trade secret, privileged, or as confidential commercial or financial information. NuScale relies upon the exemption from disclosure set forth in the Freedom of Information Act ("FOIA"), 5 USC § 552(b)(4), as well as exemptions applicable to the NRC under 10 CFR §§ 2.390(a)(4) and 9.17(a)(4).

(6) Pursuant to the provisions set forth in 10 CFR § 2.390(b)(4), the following is provided for consideration by the Commission in determining whether the information sought to be withheld from public disclosure should be withheld:

(a) The information sought to be withheld is owned and has been held in confidence by NuScale.

(b) The information is of a sort customarily held in confidence by NuScale and, to the best of my knowledge and belief, consistently has been held in confidence by NuScale. The procedure for approval of external release of such information typically requires review by the staff manager, project manager, chief technology officer or other equivalent authority, or the manager of the cognizant marketing function (or his delegate), for technical content, competitive effect, and determination of the accuracy of the proprietary designation. Disclosures outside NuScale are limited to regulatory bodies, customers and potential customers and their agents, suppliers, licensees, and others with a legitimate need for the information, and then only in accordance with appropriate regulatory provisions or contractual agreements to maintain confidentiality.

(c) The information is being transmitted to and received by the NRC in confidence.

(d) No public disclosure of the information has been made, and it is not available in public sources. All disclosures to third parties, including any required transmittals to NRC, have been made, or must be made, pursuant to regulatory provisions or contractual agreements that provide for maintenance of the information in confidence.

(e) Public disclosure of the information is likely to cause substantial harm to the competitive position of NuScale, taking into account the value of the information to NuScale, the amount of effort and money expended by NuScale in developing the information, and the difficulty others would have in acquiring or duplicating the information. The information sought to be withheld is part of NuScales technology that provides NuScale with a competitive advantage over other firms in the industry. NuScale has invested significant human and financial capital in developing this technology and NuScale believes it would be difficult for others to duplicate the technology without access to the information sought to be withheld.

I declare under penalty of perjury that the foregoing is true and correct. Executed on November 19, 2019.

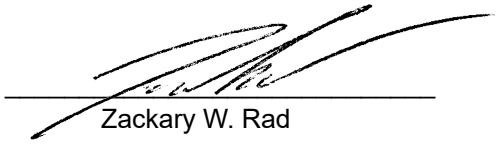

Zackary W. Rad